

Global model studies on the distribution and composition of potential atmospheric ice nuclei

Dissertation
der Fakultät für Physik der
Ludwig-Maximilians-Universität München

vorgelegt von Dipl.-Phys. Valentina Aquila
aus Genua, Italien

München, 9. Oktober 2009

1. Gutachter: Prof. Dr. Robert Sausen
2. Gutachter: Prof. Dr. George Craig

Tag der mündlichen Prüfung: 11. Dezember 2009

Abstract

Black carbon (BC) and mineral dust particles are among the most important atmospheric aerosol types forming ice crystals by heterogeneous nucleation, the so called potential ice nuclei (PIN). When emitted, most BC and dust particles are externally mixed with other aerosol compounds. Through coagulation with other particles and condensation of gases, externally mixed particles gain a liquid coating and are, therefore, transferred to an internal mixture. This ageing process is essential for the direct and indirect effect of BC and dust particles on the climate, since the coating changes their radiative and hygroscopic properties and consequently their cloud activation ability and lifetime. Moreover, laboratory studies have shown that a liquid coating influences the freezing properties of the particles and hence their behavior as ice nuclei. Due to large computational resources required, global climate models mostly parameterize the particle ageing by using estimated turnover times rather than simulating the ageing processes explicitly.

In the present study the population of PIN in the global upper troposphere and lowermost stratosphere (UTLS) is characterized. To reach this goal the new aerosol model ECHAM5/MESSy-MADEsoot is developed. The aerosol module MADEsoot is able to simulate separately BC and dust particles in their different states of mixing (internally or externally mixed) and BC and dust free aerosols, as well as the relevant ageing processes of externally mixed particles. MADEsoot is implemented in the global climate model ECHAM5/MESSy. The resulting system is evaluated with aircraft and surface measurements and performs well both in the boundary layer and in the UTLS. ECHAM5/MESSy-MADEsoot (E5/M-MADEsoot) is the only existing model able to resolve the mixing state of BC and dust particles while giving a reliable representation of the UTLS.

E5/M-MADEsoot is applied to characterize the PIN through their number and mass concentration, composition and mixing state. The results of this study show that PIN contribute only up to 0.7% to the total aerosol number concentration in the UTLS. At surface level PIN contribute between 10% and 50% to the total aerosol number concentration, where the highest values are reached over the major emission areas. Nearly all PIN in the UTLS are internally mixed with soluble material, while only up to the 3% of PIN is externally mixed. E5/M-MADEsoot allows also for the investigation of the ageing process of BC and dust particles and for the determination of its timescale, showing that the ageing process is mainly driven by the condensation of vapor. The timescale of the ageing process is calculated with E5/M-MADEsoot to be around some hours at surface level and some days in the UTLS, but shows a high geographical variability, especially in the boundary layer and in the lower troposphere. The timescale of the ageing process shows also a less pronounced seasonality, with higher values in winter and lower in summer.

Kurzfassung

Globale Modellstudien zur Verteilung und Zusammensetzung potentieller atmosphärischer Eiskerne

Ruß- und Mineralstaubpartikel gehören zu den wichtigsten atmosphärischen Aerosolspezies, die Eiskristalle durch heterogene Nukleation bilden können, die so genannten potentiellen Eiskerne. Ruß- und Mineralstaubpartikel werden meist in einer externen Mischung mit anderen Aerosolspezies emittiert. Nach ihrer Emission können die extern gemischten Partikel durch Koagulation mit anderen Partikeln oder durch Kondensation von Gasen mit einer flüssigen Hülle beschichtet werden und folglich intern gemischt sein. Dieser Alterungsprozess ist sehr wichtig für den direkten und indirekten Effekt von Ruß- und Mineralstaubpartikeln auf das Klima, da die flüssige Hülle die optischen und hygroskopischen Eigenschaften der Partikel ändert und daher auch ihre Lebenszeit und ihre Fähigkeit als Wolkenkondensationskern zu dienen. Außerdem zeigen Laborstudien, dass sich eine flüssige Hülle auf die Gefriereigenschaften der Partikel und daher auf ihr Verhalten als Eiskern auswirken kann. Wegen des großen Rechenzeitbedarfes globaler Klimamodelle wird die Alterung der Partikel nur selten explizit simuliert, stattdessen wird sie oft durch eine feste Transformationszeit parametrisiert.

In dieser Arbeit werden die potentiellen Eiskerne der globalen oberen Troposphäre und unteren Stratosphäre (UTLS, aus dem Englischen *upper troposphere - lowermost stratosphere*) charakterisiert. Um dieses Ziel zu erreichen, wurde das Aerosolmodell ECHAM5/MESSEy-MADEsoot (E5/M-MADEsoot) entwickelt. Das Aerosolmodul MADEsoot kann Ruß- und Mineralstaubpartikel in ihren verschiedenen Mischungszuständen (intern oder extern gemischt) sowie die Partikel, die weder Ruß noch Mineralstaub enthalten, getrennt simulieren. Dies erlaubt dann die relevanten Alterungsprozesse von extern gemischten Ruß- und Mineralstaubpartikeln mit MADEsoot explizit zu simulieren. Das neu entwickelte Modell wurde mit Flugzeug- und Bodenmessungen evaluiert. Es zeigt sich eine gute Übereinstimmung mit Beobachtungen sowohl in der Grenzschicht als auch in der UTLS. E5/M-MADEsoot ist derzeit das einzige globale Modell, das den Mischungszustand von Ruß- und Mineralstaubpartikeln auflösen kann und eine gute Beschreibung der UTLS erlaubt.

E5/M-MADEsoot wurde hier angewendet, um sowohl die Anzahl- und Masskonzentration, als auch die Zusammensetzung und den Mischungszustand der potentiellen Eiskerne zu beschreiben. Es zeigt sich, dass die potentiellen Eiskerne in der UTLS nur bis zu 0.7% zur gesamten Aerosolanzahlkonzentration beitragen. Bodennah liegt ihr Beitrag bei 10%-50%, wobei die maximalen Werte über den Hauptemissionsregionen erreicht werden. In der UTLS sind nur bis zu 3% der potentiellen Eiskerne extern gemischt. E5/M-MADEsoot ermöglicht auch die Untersuchung der Alterungsprozesse von Ruß- und Mineralstaubpartikeln und die Bestimmung ihrer Zeitskala. Die Simulationen zeigen, dass die Alterung hauptsächlich durch Kondensation von Gasen verursacht wird. Die mit E5/M-MADEsoot berechnete Zeitskala des Alterungsprozesses beträgt einige Stunden am Boden und einige Tage in der UTLS, aber zeigt eine hohe räumliche Abhängigkeit, besonders in der Grenzschicht und der unteren Troposphäre. Die Zeitskala zeigt eine geringere saisonale Abhängigkeit, mit höheren Werten im Winter und niedrigeren im Sommer.

Contents

Abstract	i
Kurzfassung	iii
1 Introduction	1
1.1 The scientific problem	1
1.2 State of the art of global aerosol-climate modeling	5
1.3 Aim of the thesis	7
1.4 Structure of the thesis	7
2 Atmospheric aerosol	9
2.1 Characterization of atmospheric aerosol	9
2.1.1 Particle size and concentration	9
2.1.2 Chemical composition	10
2.1.3 What is it meant by black carbon and dust?	11
2.1.4 Morphology	11
2.2 Sources of aerosol: emissions, coagulation and nucleation	12
2.3 Sinks of aerosols: dry and wet deposition, coagulation and ageing	13
2.4 The role of aerosols in cloud formation	14
2.5 The climate effects of aerosol	15
3 The aerosol model: MADEsoot	17
3.1 Description of the aerosol population	17
3.2 Representation of aerosol microphysics	22
3.2.1 Gas/aerosol partitioning	23
3.2.2 Condensation of sulfuric acid and organic material	25
3.2.3 Nucleation of new particles	26
3.2.4 Particle coagulation	26
3.2.5 Particle growth	31
3.2.6 Ageing of black carbon and dust particles	32
4 The three-dimensional model: ECHAM5/MESSy-MADEsoot	35
4.1 The starting point: ECHAM5/MESSy-MADE	35
4.2 Modifications for modeling the upper troposphere	36
4.3 Implementation of MADEsoot in ECHAM5/MESSy	40
4.3.1 Sources of aerosols	40
4.3.2 Activation of aerosol particles	43
4.3.3 Effect of aerosol on radiation	44
4.3.4 Scavenging by ice and rain and evaporation of droplets	44
4.3.5 Dry deposition	45

5	Reference simulation and model evaluation	47
5.1	Model set-up	47
5.2	Evaluation	48
5.2.1	Vertical profiles of aerosol mass concentrations	49
5.2.2	Vertical profiles of aerosol number concentrations	51
5.2.3	Surface measurements	53
5.2.4	Comparison of the mixing state of black carbon particles	57
5.3	Conclusions	58
6	Characterization of sub-micrometer aerosol and potential ice nuclei	61
6.1	Characterization of the sub-micrometer aerosol	61
6.1.1	Number concentration	61
6.1.2	The size distribution of the global aerosol	65
6.1.3	Chemical composition	66
6.1.4	Burden and life time of atmospheric aerosol	69
6.1.5	Comparison with ECHAM5/MESSy-MADE	72
6.2	Characterization of the potential ice nuclei	73
6.2.1	Number concentration	73
6.2.2	Size distribution	78
6.2.3	Chemical composition of the coating	79
6.2.4	Thickness of the coating	79
6.3	Ageing of black carbon and dust particles	82
6.3.1	Effectiveness of the single ageing processes	83
6.3.2	Transformation time of externally mixed black carbon and dust	90
7	Summary and outlook	97
A	Prognostic equations	103
A.1	Prognostic equations in MADE	103
A.2	Prognostic equations in MADEsoot	105
B	Technical details	109
B.1	Calculation of the condensation coefficients	109
B.2	Calculation of the coagulation rate	110
C	Chemical reactions	113
C.1	The chemical mechanism of MECCA	113
C.2	The chemical mechanism of SCAV	114
D	Acronyms	117
	Bibliography	121
	Acknowledgments	131

Chapter 1

Introduction

1.1 The scientific problem

With the beginning of the industrialized era the composition of the atmosphere has changed substantially due to anthropogenic emissions. Industry, road, air and sea traffic, house heating, land management: these are only a few examples of all the human activities that cause emissions of large amounts of chemicals in the atmosphere (*Olivier et al.*, 2002). Extensive research has been focusing for long time on the chemistry of the atmospheric gas components, developing comprehensive models able to quantify the influence of man-made gas emissions on the climate (*Harvey et al.*, 1997). The level of confidence in the knowledge of the greenhouse gases climate effect is such to convince policy makers to undertake measures for their limitation, as in the Montreal (*UNEP*, 2006) and Kyoto (*UNFCCC*, 2008) protocols in 1987 and 1997, respectively. The anthropogenic contribution, however, does not modify only the gas components of the atmosphere, but also the atmospheric aerosol, i.e. the suspension of particulate matter in the atmosphere: Land management activities such as deforestation or intensive farming destabilize the surface to wind erosion and increase the amount of soil dust risen into the atmosphere. Fuel combustion processes produce massive amounts of sulfate, particulate organic matter and black carbon particles that change the proportion of the aerosol compounds in the atmosphere (*Dentener et al.*, 2006; *Kloster et al.*, 2008).

Effect of atmospheric aerosol on climate. Fig. 1.1 provides the estimation of the radiative forcing¹ (RF) of the different forcing agents for 2005 (*Forster et al.*, 2007) published by the Intergovernmental Panel on Climate Change (IPCC), the international committee of scientists that periodically reviews the state of the art of climate research. The radiative forcing is a measure of the influence that a change in a component of the atmosphere induces on the radiation budget, and therefore on the temperature, of the Earth-atmosphere system: a positive radiative forcing corresponds to a warming, a negative one to a cooling. On the global scale, changes in aerosol concentrations cause a large negative contribution to the total radiative forcing, comparable to the effect of the changes in long-lived greenhouse gas concentrations, but the uncertainty on this estimation is the largest among all the forcing agents. There are still many open questions concerning the effect of changes in aerosol loading, and any contribution to the subject may lead to important steps forward to understand the human-induced changes of climate.

The effect of aerosol on the Earth-atmosphere system is a rather complex issue. Besides

¹From *Forster et al.* (2007): “Radiative forcing is a measure of how the energy balance of the Earth-atmosphere system is influenced when factors that affect climate are altered. Radiative forcing is usually quantified as the rate of energy change per unit area of the globe as measured at the top of the atmosphere, and is expressed in units of Watts per m². ”

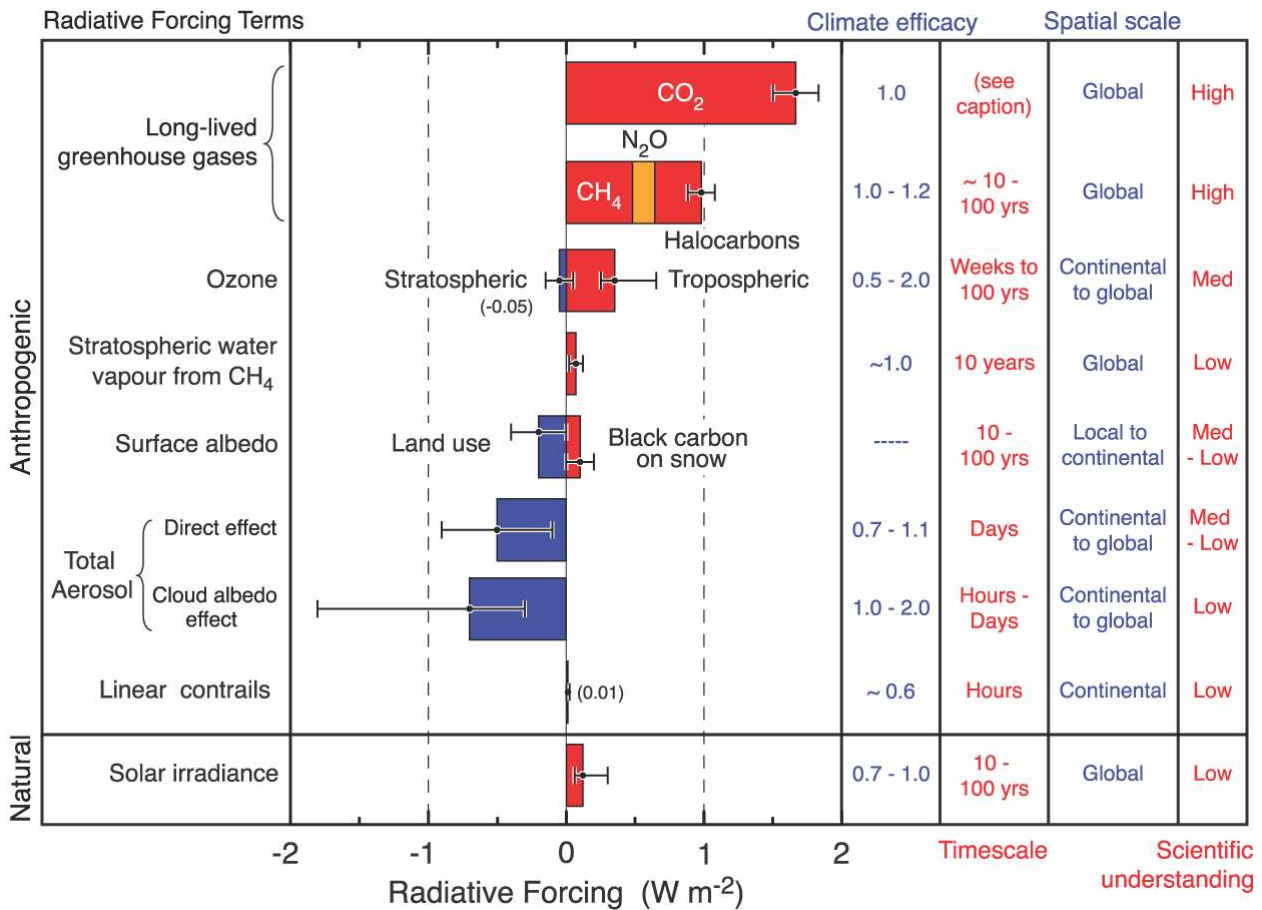


Figure 1.1: Global average radiative forcing estimates and uncertainties in 2005, relative to year 1750. No CO₂ time scale is given in column 4, as its removal from the atmosphere involves a range of processes that can span long time scales, and thus cannot be expressed accurately with a narrow range of lifetime values. Figure from *Forster et al.* (2007).

the direct absorption and scattering of solar radiation, atmospheric aerosol indirectly affect the climate by changing the properties of clouds (*Lohmann and Feichter, 2005*). Aerosol particles, or, more simply, aerosols, foster the condensation of cloud droplets, making the existence of clouds possible at all. Their ability to initiate clouds and changing the properties of the resulting cloud, as well as their interaction with radiation, depend not only on the mass of aerosols, but also on their size and their number concentration. A climate model aiming to investigate the aerosol climate effect cannot avoid keeping track of these parameters. This poses new challenges compared to the study of the gaseous species, whose effect is mainly determined by their mass concentration in the air. Furthermore the variability of the concentration of aerosols, on the geographical and temporal scales, is very high, making the calculation of a global aerosol radiative forcing an excessive simplification: Even if the aerosol radiative forcing is negative on the global scale, there may be regions or seasons where its sign is positive.

Anthropogenic contribution to the atmospheric aerosol. *Dentener et al.* (2006) have developed inventories of the emissions of aerosol species (black carbon, dust, particulate organic matter and sulfate) for the pre-industrial era, identified with the year 1750, and for the year 2000. The data for the pre-industrial era result from an extrapolation done on the basis of changes in population, crop production and wood consumption. While the emissions of dust are supposed to stay roughly the same, the increase of the emitted amount of other

species due to the anthropogenic contribution is dramatic. The emissions of particulate organic matter have increased from 33.5 to 66.1 Tg per year, the emissions of sulfur dioxide (SO_2), of which roughly 25% is converted to liquid sulfate (SO_4^{2-}), have increased from 30.2 to 142 Tg per year and those of black carbon from 1.41 Tg per year to 7.7 Tg per year, a fivefold increase.

Black carbon, also called soot, is a strongly light-absorbing carbon compound that is the result of any kind of combustion processes: while its natural emissions are bound only to wildfires, every human activity where combustion processes are involved implies the emission of soot. The anthropogenic emission of soot differs from the natural ones not only in the amount, but also in the kind of particles emitted: while black carbon particles from wildfires are quite large, with a diameter of around 100 nanometers and more, those from fuel combustion are smaller, with a diameter of some 10 nm. Such small particles can accumulate more easily in the lungs and are more harmful for human health (*WHO*, 2003). Additionally, the massive man-made injection of small soot particles changes the size distribution of atmospheric soot aerosols, modifying their influence on clouds and their effect on climate in a way that is still to be investigated.

Potential atmospheric ice nuclei. Black carbon and other insoluble particles (mainly mineral dust) can foster the formation of ice crystals at lower supersaturation than those needed for a liquid particle to freeze (*DeMott et al.*, 1999, 2003; *Sassen et al.*, 2003; *Möhler et al.*, 2006; *Kanji et al.*, 2008). The solid, insoluble particles initiating the nucleation of an ice crystal are called ice nuclei. However, only a small fraction of the insoluble particles actually act as ice nuclei, therefore all insoluble particles that can potentially initiate ice nucleation are called potential ice nuclei. The number concentration of the potential ice nuclei is a crucial factor: If ice crystals nucleate rather around insoluble particles than around the soluble ones, which are much more abundant in the atmosphere, the available water vapor will more likely form fewer and larger ice crystals around the insoluble particles than more and smaller ones out of the liquid phase, as schematically depicted in Fig. 1.2. As for warm clouds, formed by liquid water droplets, the number and size of the ice crystals influences the optical properties of cirrus clouds. A relevant region for the formation of cirrus is the upper troposphere and lowermost stratosphere (UTLS), at around 10 km altitude, where the conditions are favorable to the ice nucleation. Black carbon and dust particles emitted at surface are transported to the UTLS by the ascending air masses. Additionally, air traffic injects black carbon particles directly at this altitude. *Hendricks et al.* (2004) have shown that aviation can cause a regional increase in the black carbon particle number concentration of more than 30% at this altitude in areas with high flight density. The air traffic sector has experienced such a dramatic growth in the last decades, and there are currently no indications of a slowdown, that its influence on the climate deserves intensive investigation.

Lohmann (2002b) discussed the hypothesis that anthropogenic soot particles can modulate the indirect aerosol effect in mixed-phase clouds, i.e. clouds containing both liquid and ice particles. She claims that an increase in the number concentration of hydrophilic black carbon particles, assuming that they efficiently act as ice nuclei, can lead to an increase of precipitation via the ice phase. As a consequence, the cloud fraction would decrease thus allowing more short-wave radiation to be absorbed in the surface-atmosphere system. The number concentration of potential ice nuclei is the critical parameter to determine whether this effect may counteract the other indirect aerosol effects.

Mixing state of potential ice nuclei. There is another issue that makes the description of aerosols even more complex: Besides the geographical distribution, the seasonal variation, the mass and the number concentrations and the size distribution, also the mixing state

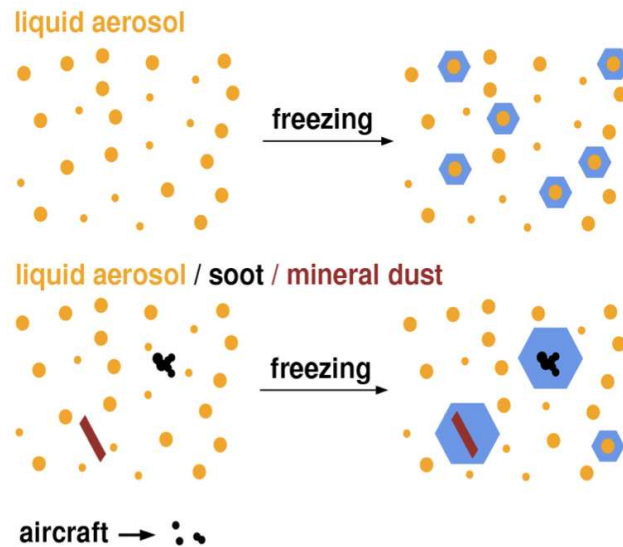


Figure 1.2: Schematic representation of homogeneous (above) and heterogeneous (below) freezing. The presence of insoluble particles (ice nuclei) fosters the formation of ice crystals limiting their number concentration. Figure by Johannes Hendricks.

of black carbon and dust particles influences their interaction with the Earth-atmosphere system. Black carbon and dust particles may be externally mixed, i.e. appear as homogeneous particles composed only by one species, or internally mixed, i.e. each particle contains black carbon and/or dust together with other species. This is the case, for instance, for a particle composed of an insoluble core of black carbon or dust surrounded by a coating of soluble material. Freshly emitted particles are mainly in an external mixture, but, during their life, condensation of vapor and coagulation with soluble particles may transfer them to an internal mixture (*Kotzick and Niessner, 1999; Weingartner et al., 1997, 2000*). Initially insoluble aerosols can be activated to form cloud droplets once they are transformed in an internal mixture with soluble material (*Khalizov et al., 2009*), therefore internally mixed insoluble particles will be more efficiently removed by rain than the externally mixed ones (*Hitzenberger et al., 2001; Zuberi et al., 2005*).

Different studies, both experimental and theoretical, have shown that the presence of a soluble coating changes the ability of black carbon of absorbing solar radiation (*Jacobson, 2001; Schnaiter et al., 2005; Bond et al., 2006; Shiraiwa et al., 2008; Naoe et al., 2009*). Other studies have focused on the potential of black carbon and dust particles to act as ice nuclei, and reached contradictory results: some studies conducted on black carbon particles under cirrus conditions have concluded that a soluble coating may enhance the ability of black carbon to act as ice nuclei (*DeMott et al., 1999*), others that it may make the heterogeneous nucleation of ice crystals less efficient (*Möhler et al., 2005, 2008*). *Hoose et al.* (2008) have investigated the effect of a soluble coating on dust particles, concluding that coating with soluble material can lead to quasi-deactivation of dust ice nuclei in mixed-phase clouds.

Scientific objectives. Fig. 1.3 shows the radiative forcing from aviation for 1992 and 2000 (*Sausen et al., 2005*). The present knowledge of the influence of aircraft emissions on the concentration of ice nuclei and of their ability of nucleating ice particles is too poor to provide a reliable estimate of cirrus cloud coverage induced by soot from aviation (*Sausen et al., 2005*). Potentially, however, the RF from aviation-induced cirrus could be as large as the RF from all other forcing agents. More experimental and theoretical studies are required to characterize the ice nuclei population and the relation between aerosols and ice clouds,

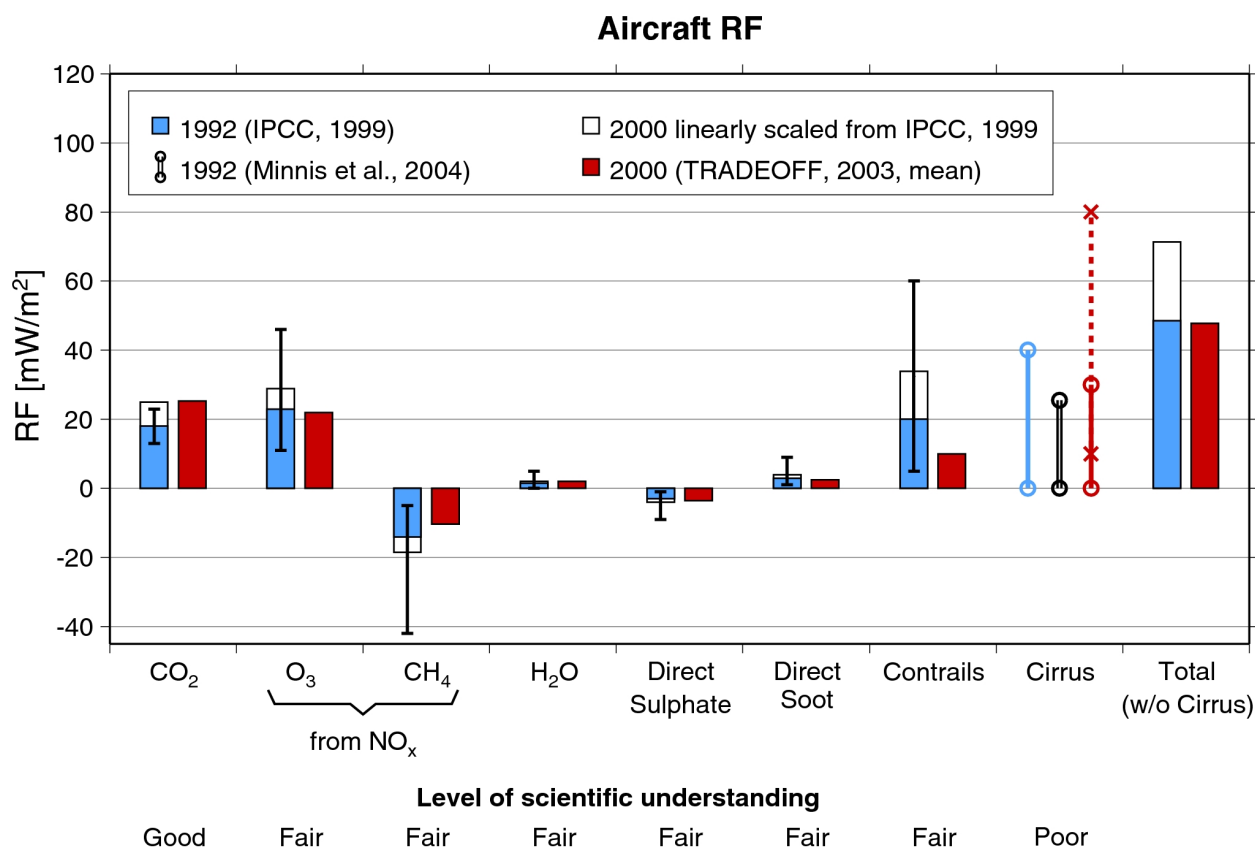


Figure 1.3: Radiative forcing from aviation for 1992 and 2000, based on *Penner et al. (1999)* and on the results of the TRADEOFF project (*Sausen et al., 2005*). The whiskers denote the 2/3 confidence intervals introduced by *Penner et al. (1999)*. The lines with the circles at the end display different estimates for the possible range of RF from aviation induced cirrus clouds. The value calculate by *Minnis et al. (2004)* is also reported. In addition the dashed line with the crosses at the end denote an estimate of the range for RF from aviation induced cirrus. The total does not include the contribution from cirrus clouds. The figure is taken from *Sausen et al. (2005)*.

in order to provide an estimation of the climate effect of aviation and of cirrus clouds in general. It is important to quantify which fraction of the atmospheric aerosol is contributed by potential ice nuclei. Furthermore, the mixing state and the size distribution of the potential ice nuclei has to be determined as one of the first steps in the investigation of the effects of ice nuclei on clouds and climate.

1.2 State of the art of global aerosol-climate modeling

The simplest way of treating aerosols in global models is to prescribe a standard climatology for the aerosol distribution, as it was done in the standard version of the global climate model ECHAM4 (*Roeckner et al., 1996*) and in the original ECHAM5 (*Roeckner et al., 2003*). A fixed climatology does not allow for feedbacks from any atmospheric process to the aerosol distribution, so that changes in weather or climate cannot induce modifications of the aerosol population. A better simulation of the interaction between aerosol and atmosphere is obtained with the introduction of an online representation of aerosols, i.e. the coupling between aerosol and atmospheric processes as dynamics, chemistry, radiation and cloud formation. *Feichter et al. (1996)*, for instance, introduced the coupling between aerosols and sulfate

chemistry in ECHAM in order to simulate the formation of sulfate aerosols. The full life cycle of sulfate aerosols was represented in the model, which was later on extended with dust, organic carbon, black carbon and sea salt (*Lohmann et al.*, 1999). *Adams et al.* (1999) extended the Goddard Institute for Space Studies General Circulation Model (GISS GCM II-prime) with sulfate, nitrate, ammonium and water, and *Koch et al.* (1999) with black carbon. *Chin et al.* (2000) developed the Georgia Tech/Goddard Global Ozone Chemistry Aerosol Radiation and Transport (GOCART) model which is driven by the meteorological data from the Goddard Earth Observing System Data Assimilation System (GEOS DAS) for the simulation of the global sulfuric cycle. Other examples of aerosol models coupled to global climate models can be found in *Textor et al.* (2006).

However, most of these models were capable only of simulating the aerosol mass, but neither the number concentration nor the size distribution. Methods to simulate these variables were developed and applied first within regional models, as for instance the Regional Particulate Model RPM (*Binkowski and Shankar*, 1995) and the European Air pollution Dispersion model EURAD coupled with the two moment (mass and number) Modal Aerosol Dynamics model for Europe MADE (*Ackermann et al.*, 1998). Nevertheless these methods were too expensive for applications in global climate models. With the increase in computer capacities, attempts have been made also on the global scale. *Adams and Seinfeld* (2002) incorporated the Two-Moment Aerosol Sectional (TOMAS) model in the GISS GCM II-prime to simulate also the number concentration and the microphysics of aerosols, though limited to sulfate aerosols. *Lauer et al.* (2005, 2007) coupled the microphysical aerosol model MADE to ECHAM4 and to ECHAM5 in the MESSy framework (*Jöckel et al.*, 2005). *Vignati and Wilson* (2004) and *Stier et al.* (2005) developed the two-moment (mass and number) microphysical aerosol module HAM and implemented it in ECHAM5. Recently *Ayash et al.* (2008) implemented the sectional Canadian Aerosol Module (CAM) into the Third Generation Canadian Climate Center General Circulation Model (CCC GCM III).

Although these models represent the aerosol mass and number concentrations, they represent the mixing state of the aerosol components in a very simplified manner. Some models treat aerosols as completely internally mixed (*Adams et al.*, 1999), others as externally mixed (*Chin et al.*, 2000), and some track separately hydrophobic, i.e. externally mixed, and hydrophilic, i.e. internally mixed, black carbon, while assuming a fixed turnover rate from the external into the internal mixture. *Lauer et al.* (2005), *Lohmann et al.* (1999) and *Koch* (2001) assume for this transfer an exponential decay with an e-folding time of 24, 40 and 43 hours respectively.

Only a few models resolve the mixing state of black carbon particles by simulating the ageing processes explicitly: *Jacobson* (2001) developed a model that differentiates between the two states of mixing, and even among particles with different core to shell thickness ratio. However, this model is computationally too expensive to be used for long term global climate simulations. The aerosol model MADRID-BC (*Oshima et al.*, 2009) can simulate changes in the black carbon mixing state resulting from condensation and evaporation processes, but up to now it has not been implemented in any regional nor global model. KAMM/DRAIS-MADEsoot (*Riemer et al.*, 2004) is a regional model that can simulate mass and number concentration of soluble aerosol, of internally mixed and of externally mixed black carbon particles.

Among the global aerosol climate models the only ones able to resolve the mixing-state of BC particles are ECHAM5/HAM (*Stier et al.*, 2005) and GISS-ModelE/MATRIX (*Bauer et al.*, 2008). HAM makes a distinction between internally and externally mixed black carbon and dust, but cannot predict which fraction of the total aerosol is free from any insoluble component. MATRIX can simulate an aerosol population composed by soluble particles, externally and internally mixed black carbon and externally and internally mixed

dust. Additionally the internally mixed particles are divided depending on the different insoluble to soluble mass ratio. However, the model does not perform well when compared to measurements, especially above the boundary layer. The mass concentration of black carbon, for instance, which is particularly relevant in the investigation of ice nuclei, is systematically too large when compared to the vertical profiles by *Schwarz et al.* (2006) and *Schwarz et al.* (2008b).

A global aerosol climate model that could be the appropriate tool to investigate the population of potential ice nuclei is still missing. Such a model needs to be able to simulate the composition, mass concentration, number concentration and size distribution of aerosol, and, additionally, to determine the mixing state of the potential ice nuclei and the fraction of the total aerosol population that they represent. Such a model must perform well not only in the boundary layer, but also in the UTLS. Furthermore, this must be accomplished while keeping the computational demand low enough to allow for long-term climate simulations.

1.3 Aim of the thesis

To reduce the uncertainty of the climate effect of cirrus clouds, a more detailed knowledge of the ice nucleation potential of atmospheric aerosol is needed. This work aims to provide a detailed characterization of atmospheric aerosol, with particular focus on the population of potential ice nuclei in the upper troposphere and lowermost stratosphere on the global scale. The behavior of aerosol in the atmosphere is dependent on its mass and number concentration, chemical composition, size distribution and mixing state. The aim is to quantify the global characteristics of all these parameters.

To reach this goal a new aerosol model is developed. This aerosol model is able to describe the life cycle of aerosols resolving all the above mentioned parameters, while keeping the needed computational resources to a level low enough to allow for global climate simulations. In this model, the mass concentration, number concentration and chemical composition are simulated separately for soluble particles, externally mixed black carbon and dust as well as black carbon and dust particles in an internal mixture with soluble material.

This aerosol model is implemented in the global climate model ECHAM5/MESSy. The new model system is applied to the characterization of the global aerosol and of the atmospheric ice nuclei. The model system performs well compared to measurements both in the boundary layer and in the UTLS, which is the region of interest for the description of the ice nuclei population.

With the model developed in this work the number concentration of the potential ice nuclei is explicitly calculated. For the first time it can be determined which fraction of the total aerosol number concentration is composed by potential ice nuclei. Furthermore the mixing state of the potential ice nuclei is investigated, determining the mass and number concentrations of the potential ice nuclei in each state of mixing and the amount of soluble material that constitutes the coating of the internally mixed black carbon and dust particles. With this unique model it is possible to provide a robust representation of the aerosol population at all altitudes and to study the interaction between aerosols and warm, mixed and ice clouds.

1.4 Structure of the thesis

The second chapter of this work presents a short overview of the atmospheric aerosol, its main characteristics and its life cycle. It provides the necessary theoretical knowledge and the definitions of the fundamental concepts needed in this work.

The model developed in this thesis is described in the third and fourth chapters: Chapter 3 describes the mixing-state resolving aerosol microphysical model, MADEsoot, and Chapter 4 the global climate model ECHAM5-MESSy, and the implementation of MADEsoot within it. Chapter 4 also presents the modification introduced in ECHAM5/MESSy during this work to reach a better representation of the UTLS.

The evaluation of ECHAM5/MESSy-MADEsoot with experimental data is reported in Chapter 5. Chapter 6 presents the studies done with the newly developed model system to characterize aerosols and potential ice nuclei and to investigate the transfer of black carbon and dust particles from the external into the internal mixture.

The conclusions of this study and an outlook to possible future investigations are provided in Chapter 7.

Chapter 2

Atmospheric aerosol

Aerosol is defined as a suspension of particles, liquid and/or solid, in gases. People refer to aerosol with many different terms, as dust, smoke, mist, haze, soot or smog, reflecting the huge variety of origin and composition that aerosol particles, simply referred to as aerosols, have and the impression they have made on humans from early times (*Friedlander, 2000*). Dust usually refers to solid particles produced by disintegration processes, smoke is composed of smaller particles from condensing vapor, mist and haze denote a suspension of liquid droplets in humid or dry air respectively, soot refers to small carbon particles generated in fuel combustions, smog is used for aerosols with anthropogenic origin.

2.1 Characterization of atmospheric aerosol

The most important properties determining the behavior of aerosol particles are size, number concentration and chemical composition. These are the main parameters that allow for a description of the life cycle of aerosols and for the determination of their properties, e.g. their optical or hygroscopic properties.

2.1.1 Particle size and concentration

The diameters of aerosol particles span orders of magnitude from 1 nm to 100 μm , corresponding to a variation in mass of 15 orders of magnitude. Particles of the size of some nanometers are, for instance, freshly nucleated sulfate particles, while the largest particles are usually windblown dust, pollen, plant fragments and sea salt. Particles smaller than 2.5 μm , particularly important in health studies, are usually referred to as fine, and particles larger than 2.5 μm as coarse. The lives of fine and coarse particles are in general quite independent from each other (*Whitby, 1978*).

The aerosol population can be roughly divided into modes: the nucleation mode, that comprises particles with diameter up to 10 nm, the Aitken mode, for particles with diameter between 10 nm and 0.1 μm , the accumulation mode, for particles between 0.1 μm and 2.5 μm , and the coarse mode, for particles larger than 2.5 μm . The definition of diameter, however, is straightforward only for spherical particles, may be liquid droplets or nuclei surrounded by a thick liquid coating, but it is not for solid crystal fragment or agglomerate. To characterize the size of such particles the equivalent diameter is often used, which is the diameter of a spherical particle that would have the same behavior with respect to the property of interest. The most common equivalent diameters are the aerodynamic diameter and the mobility diameter: The aerodynamic diameter is defined as the diameter of a unit density sphere with the same terminal settling velocity of the measured particle, while the mobility diameter is the diameter of a spherical particle having the same mobility of the

Region	Mass [$\mu\text{g}/\text{m}^3$]	Percentage Composition				
		BC	OC	NH_4^+	NO_3^-	SO_4^{2-}
Remote	4.8	0.3	11	7	3	22
Non-urban continental	15	5	24	11	4	37
Urban	32	9	31	8	6	28

Table 2.1: Typical mass concentration and composition of fine tropospheric aerosol as resulting from measurements (*Heintzenberg, 1989; Seinfeld and Pandis, 2006*).

particle under consideration, where the mobility is defined as the ratio between the velocity of the particle and the force to which the particle is subjected. The model used in this work assumes that all particles are spherical, using the mass equivalent diameter, i.e. the diameter of a spherical particle with the same mass of the observed one.

The transfer of energy and mass between the particle and the carrier gas depends on the relation between the size of the particle and the mean free path of the surrounding gas molecules. The dimensionless number used to describe the regime of the particle with respect to the fluid is the Knudsen number Kn , defined as $2\lambda/D_p$, where λ is the mean free path of the gas molecules and D_p the diameter of the particle. λ depends on the molecular density of the gas. It is about $0.065 \mu\text{m}$ in air for normal temperature $T = 293 \text{ K}$ and pressure $P = 1013 \text{ hPa}$ and molecular density $2.5 \times 10^{19} \text{ molecules}/\text{cm}^3$, calculated through the ideal gas relationship (*Friedlander, 2000*). The two asymptotic cases for $\text{Kn} = 0$ and $\text{Kn} \rightarrow \infty$ are called near-continuum and free molecular regime respectively. The treatment of the transition between the two regimes is a very complex topic.

While the nucleation and the Aitken modes account for the largest part of the total aerosol number, the accumulation and the coarse modes provide the major contributions to the total aerosol mass. Particles smaller than $1 \mu\text{m}$ usually have number concentrations in the range from 10 to thousands particles/ cm^3 , while particles larger than $1 \mu\text{m}$ are generally found at concentrations of less than 1 particle/ cm^3 (*Seinfeld and Pandis, 2006*).

2.1.2 Chemical composition

Stratospheric and tropospheric aerosol are significantly different. Since the main sources of aerosol particles are not uniformly located at surface, and since the aerosol residence time in the troposphere is generally low, the concentration and composition of tropospheric aerosol is very inhomogeneous. Tropospheric aerosol is mainly composed by sulfate (SO_4^{2-}), ammonium (NH_4^+), nitrate (NO_3^-), sodium (Na), chloride (Cl^-), trace metals, carbonaceous material both as black (BC, see Sec. 2.1.3) and organic carbon (OC), crustal elements and water. While crustal element and sea salt make up the major part of the coarse fraction, the dry mass of the fine fraction of tropospheric aerosol is mainly composed by sulfate, ammonium, nitrate, BC and OC. Tab. 2.1 reports the mass concentration and composition of fine tropospheric aerosol.

Stratospheric aerosol is more homogeneous than tropospheric aerosol and mainly composed of sulfuric acid. Stratospheric aerosol is frequently perturbed by volcanic eruptions, which inject large amount of sulfur dioxide (SO_2) in the lower stratosphere. The eruption of Mt. Pinatubo in June 1991, the largest in the 20th century, injected 30 Tg of aerosol mass in the stratosphere and led to enhanced stratospheric aerosol levels for over two year (*Seinfeld and Pandis, 2006*). Due to the inefficiency of stratospheric sinks, stratospheric aerosols have a very long residence time, allowing for a long range transport that results in

an efficient mixing of the stratospheric layer.

2.1.3 What is it meant by black carbon and dust?

As pointed out by *Bond et al.* (2006), the nomenclature used for carbonaceous particles is quite confusing. Usually, the term *black carbon* refers to the strongly light absorbing component of carbonaceous aerosol. The less absorbing part is generally called *organic carbon*, subsuming with this term a very broad spectrum of compounds.

Strongly-absorbing carbon is often called elemental carbon or soot: *Elemental carbon* identifies in atmospheric chemistry the carbonaceous material that does not volatilize below a certain temperature, usually about 550°C, even though a more correct name for the material defined through this operative definition would be *refractory carbon*. *Soot* generally refers to any light-absorbing, combustion-generated carbonaceous material, and in this meaning is used by the Intergovernmental Panel on Climate Change (IPCC). In this work the term black carbon will be employed, as the most widely used among climate modelers.

The term dust is used in this work as a catchall term for all different species that may be found in soil dust, i.e. mainly quartz, clays, calcite, gypsum and iron oxides.

2.1.4 Morphology

As already mentioned, aerosol particles are not always spherical. Dust particles originated by wind erosion, for instance, often have a highly irregular shape. Freshly emitted soot appears usually as chains of small particles. Through condensation of vapor or coagulation with other particles a coating of soluble material can form at the soot surface, and the chain-like particles contract assuming a shape more similar to a sphere, that they maintain also when the coating evaporates (*Zhang et al.*, 2008; *Saathoff et al.*, 2003), as shown in Fig. 2.1.

The distribution of strongly-absorbing and less-absorbing material inside a single particle is important for the optical properties of aerosols. The idealized case in which the aerosol population is composed by a heterogeneous ensemble of homogeneous particles is called *external mixture*, while the expression *internal mixture* is used to describe any occurrence of multiple species in the same particles. The term internal mixture, however, does not define completely the state of mixing of the aerosol population: it may describe a homogeneous population of homogeneous particles, where all species are perfectly mixed with the others inside each particle at a molecular level, or it may refer to a particle that is internally heterogeneous, having for instance a core of black carbon surrounded by a shell of less absorbing material. These idealized cases are illustrated Fig. 2.2. The review by *Bond and Bergstrom* (2006) gives a very complete overview on the influence of the state of mixing of black carbon on the aerosol optical properties. This work focuses on the characterization of the hygroscopic behavior of black carbon and dust particles: in this respect an internally mixed black carbon or dust particle is meant as a particle with an insoluble core and a shell of soluble material (Fig. 2.2c). Externally mixed black carbon and dust particles are considered hydrophobic, internally mixed ones hydrophilic. However, the optical properties of aerosol are here calculated assuming that aerosol particles are an homogeneous internal mixture (Fig. 2.2b). This assumption simplify the coupling with radiation and reduces the computational demand of the model.

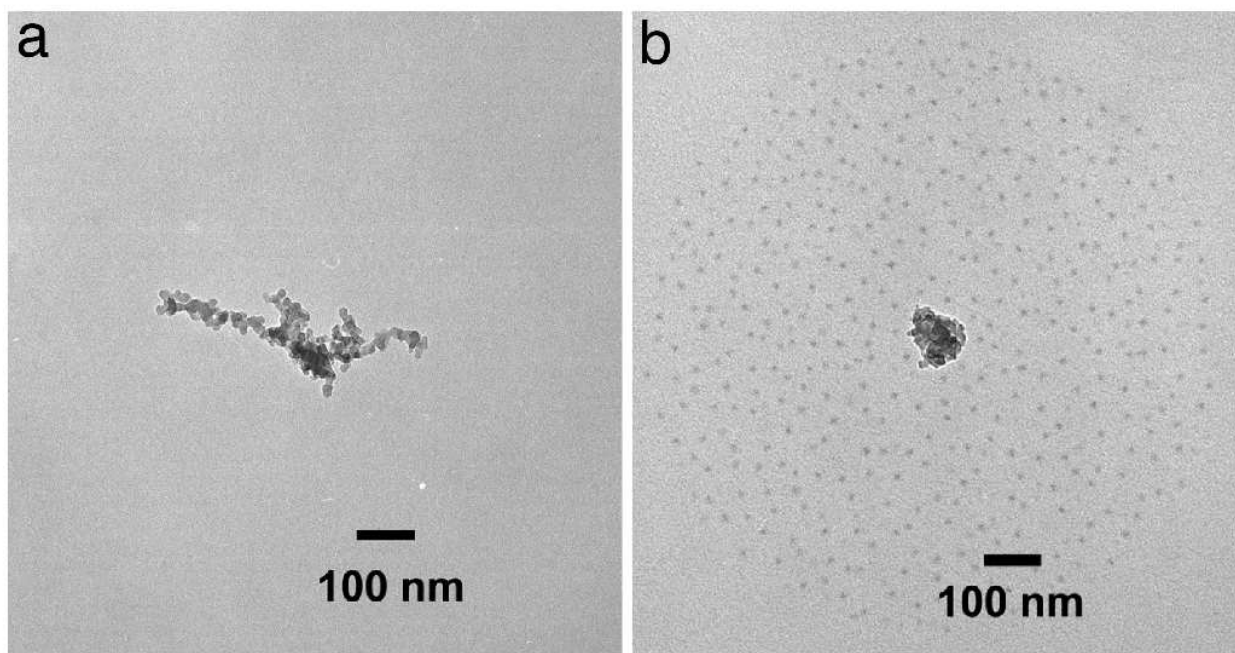


Figure 2.1: Images of soot particles taken with a transmission electron microscope (TEM). (a) Fresh soot particle. (b) Soot particle after exposure to H_2SO_4 vapor. The cloud of small droplets surrounding the soot particle corresponds to the H_2SO_4 that was shaken off the coated soot particle because of the impact against the TEM grid. The picture was taken from *Zhang et al.* (2008).

2.2 Sources of aerosol: emissions, coagulation and nucleation

Aerosols are emitted directly (*primary aerosol*) or form via the oxidation of precursor gases (*secondary aerosol*). Primary aerosols arise in the atmosphere from natural sources, such as desert wind-born dust, sea spray, volcanoes and natural fires, or from anthropogenic activities, such as combustion of fossil fuels, e.g. by industry or traffic. Secondary aerosols are produced by the gas-to-particle conversion of low volatile species, which results from the oxidation of precursor gases. These low volatile species may then condense on preexisting particles, modifying the optical, physical and chemical properties of their surface. If not enough surface is available, they may nucleate to new fine particles with diameter between 3 and 4 nm (*Weber et al.*, 1997). *Condensation* is a source mainly of aerosol mass, while *nucleation* to new particles increases the number concentration of the aerosol population and only slightly the mass concentration. Especially in the upper troposphere lowermost stratosphere (UTLS) the contribution of nucleation to the number concentration of aerosol can be of substantial magnitude. On the other hand, the freshly nucleated particles are so small that the contribution of single nucleation events to the total aerosol mass is almost negligible.

Important precursor gases are SO_2 , dimethyl sulfide ($\text{DMS} = (\text{CH}_3)_2\text{S}$) and H_2S , that, after reacting with OH radicals, give sulfuric acid (H_2SO_4), which may condense or nucleate into sulfate (SO_4^{2-}). Other precursor gases are nitrogen oxide (NO_X , corresponding to the sum of NO and NO_2), which can be oxidized into nitric acid (HNO_3), ammonia (NH_3) and several organic compounds. A significant fraction of HNO_3 and NH_3 can be present in the aerosol phase in the form of nitrate (NO_3^-) and ammonium (NH_4^+), respectively. In the same way volatile organic compounds (VOC), a term that broadly refers to any organic compound

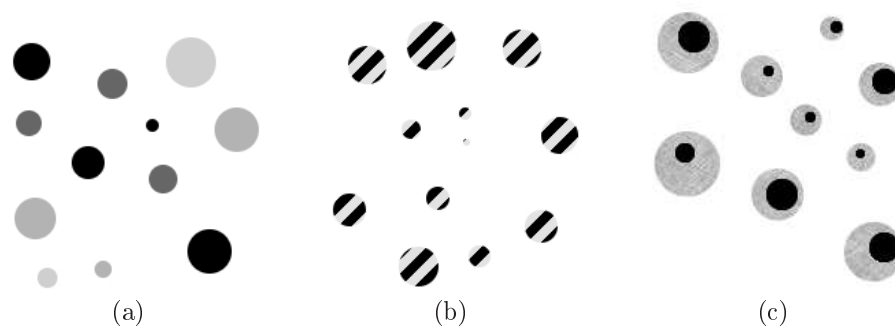


Figure 2.2: Idealized relationships between absorbing and non-absorbing material. (a) External mixture, i.e. a heterogeneous population of internally homogeneous particles containing only one compound; (b) Internal mixture as homogeneous population of internally homogeneous particles containing more than one compound; (c) Internal mixture as heterogeneous population of internally heterogeneous particles. Figure by *Bond and Bergstrom* (2006).

that evaporate readily under normal conditions, can be transformed to condensable species by photodissociation.

About 10% of global atmospheric aerosol mass is generated by human activity. This aerosol fraction is concentrated in the immediate vicinity or downwind of sources (*Chin et al.*, 2009). The major anthropogenic sources of aerosols and precursor gases are urban and industrial emissions, domestic fire and other combustion products, smoke from agricultural burning and soil dust created by any land management activity (e.g. overgrazing, deforestation, draining of inland water bodies and farming) that destabilizes the surface to wind erosion. Most of the natural sources of aerosol mass are wind-driven, like the erosion of the crust, the raising of dust from the desert and the raising of sea salt from the sea surface into the atmosphere. Next to the wind-driven ones, important natural sources of aerosols are wildfire and volcanic activities. DMS is produced by marine phytoplankton on the sea surface, and organic compounds are emitted by plants.

2.3 Sinks of aerosols: dry and wet deposition, coagulation and ageing

Aerosol particles are eventually removed from the atmosphere due to direct settling to the Earth's surface by dry or wet deposition. The expression *dry deposition* refers to the removal processes that do not involve any precipitation event. Besides *sedimentation*, which is the accumulation of particles at surface because of gravity, an important sink is also the impact of aerosols against a surface following the Brownian motion of a particle. This is what is properly called *deposition*. Sedimentation is particularly effective on coarse particles, deposition on particles with diameter smaller than $1 \mu\text{m}$ (*Seinfeld and Pandis*, 2006).

Wet deposition, or scavenging, indicates removal processes involving precipitation (snow or rain). Aerosol particles can be incorporated in a precipitating particle in different ways: A cloud droplet may incorporate an aerosol particle after the collision due to the aerosol Brownian motion or to the sedimentation of the cloud particle (*impact scavenging*), or the cloud particle may form around an aerosol particle (*nucleation scavenging*), which is then defined as activated (see Sec. 2.4). The mechanisms of wet deposition are often called in-cloud and below-cloud scavenging, referring to where the process takes place rather than to the process itself. In-cloud scavenging comprises both nucleation and impact scavenging, while below-cloud scavenging can take place only through impact scavenging. These definitions

are not employed in this work, since the adopted scavenging parameterization depends on the process itself and not on where it takes place.

Strictly speaking, the term sink is applied to the processes that remove aerosol mass from the atmosphere. In a more general sense, it may be used also for those processes, as coagulation, that conserve the aerosol mass in the atmosphere but lower its number concentration. *Coagulation* is the process for which two aerosol particles stick together after colliding, forming a single particle. It is particularly effective when the particles involved have very different size, while its efficiency is minimum between particles of the same size. The term sink may also be used for those processes that cause a loss of particles in a specific aerosol state, as e.g. the transformation of particles from externally to internally mixed. In this case the transformation, called *ageing*, is a sink for externally mixed particles.

2.4 The role of aerosols in cloud formation

Aerosol are essential for the formation of clouds, since cloud droplets form in the atmosphere through condensation of supersaturated water vapor on aerosol particles (heterogeneous nucleation). The formation of cloud droplets is highly favored by the presence of soluble aerosols. As extensively explained by *Andreae and Rosenfeld (2008)*, the homogeneous nucleation of supersaturated water vapor, i.e. the condensation of water molecules without a foreign condensation nucleus, would require the initial formation of very small droplets. Due to the Kelvin effect, over such small droplets the equilibrium vapor pressure is extremely high (*Pruppacher and Klett, 2000*): This makes homogeneous nucleation possible only at very high supersaturation values. However, the equilibrium vapor pressure over a solution is much lower than that over pure water (the Raoult effect), making the formation of cloud droplets over soluble particles easier. Depending on supersaturation, the Köhler theory of cloud droplet formation predicts for each dry soluble particle size and composition a critical wet particle size. Particle larger than this critical size are said activated and grows spontaneously into droplets. The aerosols that can potentially induce the formation of cloud droplets are called cloud condensation nuclei (CCN).

Ice particles can form in the atmosphere via homogeneous or heterogeneous freezing. For homogeneous freezing to take place, i.e. for ice particles to nucleate directly out of the liquid phase, temperature lower than -36°C are required (*Rosenfeld and Woodley, 2000*). Heterogeneous freezing, i.e. freezing in the presence of an insoluble particle, can occur at temperatures well above those typical for homogeneous freezing. The insoluble particles initiating the freezing are called ice nuclei (IN). Such IN particles may be dust, soot, organic or metallic particles, mixed or not with soluble material, and are generally present in the atmosphere at concentrations of 0.01 particles/ cm^3 , which is orders of magnitudes lower than the typical aerosol number concentrations (*Andreae and Rosenfeld, 2008*). The heterogeneous freezing of an ice particles can take place through different processes. When the freezing process is initiated by an ice nucleus immersed in a supercooled cloud droplet, we speak about immersion freezing. Impact freezing refers to the freezing process initiated from outside, when the supercooled cloud droplet collides with an ice nuclei. The case of a liquid layer condensing on the ice nucleus and subsequently freezing is called condensation freezing, and the case of ice growth directly on the dry ice nucleus is called deposition freezing. The relative importance of the different nucleation modes is still unclear (*Hoose et al., 2008*).

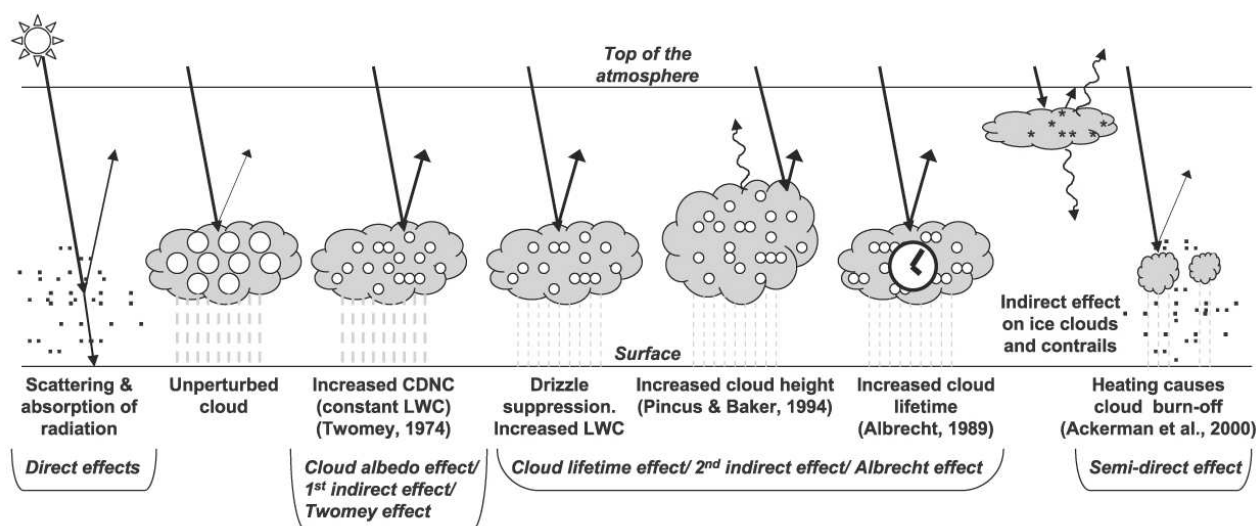


Figure 2.3: Aerosol effect on climate. Figure from *Forster et al.* (2007)

2.5 The climate effects of aerosol

Besides the possible effects that aerosol can have on human health when concentrated near the surface (e.g. *WHO* (2003)), aerosol also affects the radiation balance of the atmosphere, as schematically illustrated in Fig. 2.3. First, aerosols scatter and absorb the short-wave solar radiation (direct effect), causing a brightening of the planet when viewed from space. Second, acting as CCN, they modify the microphysical properties of clouds and their amount and lifetime (indirect effect). Finally, absorbing aerosol warms the atmosphere changing the atmospheric stability, and this is thought to suppress cloudiness (semi-direct effect, *Ackerman et al.* (2000)). A detailed review of the aerosol indirect effect is given by *Lohmann and Feichter* (2005). The cloud albedo effect is related to the number of cloud droplets inside the cloud: A higher number of aerosols, i.e. of CCN, with respect to the unperturbed case leads, keeping constant the cloud liquid water content, to more and smaller cloud droplets, and therefore to an increase in the reflected solar radiation (cloud albedo effect or first indirect effect, *Twomey* (1977)). An increase of aerosols is also supposed to decrease the precipitation efficiency thereby prolonging the cloud lifetime (cloud lifetime effect or second indirect effect, *Pincus and Baker* (1994); *Albrecht* (1989)). *Lohmann* (2002b) has hypothesized also another kind of indirect effect caused by hydrophilic black carbon particles in mixed clouds. She claims that, if no potential ice nuclei are present, more aerosols lead to less precipitation, a prolongation of the lifetime of clouds and an increase of the cloud fraction. On the other hand, if the aerosol is composed by a sufficient number of potential ice nuclei, more ice particles can be formed at the expenses of the droplets, since in favorable conditions ice crystals grow more rapidly than droplets. This leads to a situation with some large ice crystals and less small liquid droplets, implying a higher precipitation rate via the ice phase and a decrease of the cloud fraction (glaciation indirect aerosol effect), hence more solar radiation can be absorbed by the Earth-atmosphere system and the temperature increases.

The overall impact of aerosol is an increase in Earth's reflectance, leading to a reduction of sunlight reaching the Earth's surface and consequently producing a net climate cooling. The estimates of the magnitudes of these effects given by the different climate models, however, are very different and there is a very large uncertainty on the net radiative forcing of aerosol (*Forster et al.*, 2007). Furthermore, the aerosol spatial and temporal distribution

is highly heterogeneous, so that the magnitude and even the sign of their climate effects vary immensely with location and season (*Chin et al.*, 2009).

Chapter 3

The aerosol model: MADEsoot

A global climate model simulates the atmosphere using a three dimensional grid. The physical and chemical processes take place in each box of the grid, and quantities like mass and number concentration are transported between neighboring boxes due to advective, diffusive and convective transport.

The first stage of the development of the new model happens at the level of the box model: thanks to the much smaller computational resources needed, many tests can be performed to check if the model is robust in the whole range of possible values of the model variables and parameters. Once tested, the box model is implemented in the three dimensional one, previously modified to give a good description of the region of interest.

This chapter presents the box version of the aerosol model MADEsoot and its representation of the aerosol dynamics and chemistry. Chapter 4 introduces the three dimensional model ECHAM5/MESSy, the modifications done to simulate the upper troposphere-lowermost stratosphere, and the implementation of MADEsoot in it.

MADEsoot is a model for aerosol dynamics that allows for simulations of distribution and composition of the atmospheric aerosol. Following the concept that *Riemer et al.* (2003) implemented in the frame of a regional model for the south-west part of Germany, MADEsoot enhances the Modal Aerosol Dynamics Model for Europe MADE, developed as a part of the European Air Pollution Dispersion model system (EURAD) by *Ackermann et al.* (1998). The core of MADE goes up to the the Regional Particulate Model (RPM) of *Binkowski and Shankar* (1995), that used a modal representation of aerosol dynamics (*Whitby et al.*, 1991) for studies in the northern American region. MADE was coupled to the general circulation model ECHAM4 (*Lauer et al.*, 2005; *Lauer and Hendricks*, 2006), and later to ECHAM5 in the framework of the Earth model system MESSy (*Jöckel et al.*, 2005; *Lauer et al.*, 2007). This second version has been used as the basis for the development of ECHAM5/MESSy-MADEsoot.

3.1 Description of the aerosol population

Aerosol models generally represent the size distribution of aerosol by means of sectional or moment-based methods. The sectional method (*Adams and Seinfeld*, 2002; *Jacobson*, 2001) divides the size domain into bins and calculates the number concentration in each size bin. It is the most general method, because it explicitly calculates the aerosol size distribution instead of making assumptions on its shape. It is very accurate when a large number of size bins is used, but, on the other hand, it is computationally very expensive. The moment-based methods keep tracks of the moments of the aerosol size distribution instead of tracking the distribution itself. Moment-based methods are the quadrature method of moments (QMOM) (*McGraw*, 1997) and the modal method (*Whitby and McMurry*, 1997). QMOM calculates

the aerosol properties and their evolution from the moments of the distribution without requiring the knowledge of the distribution itself, while the modal method describes the aerosol population through one or more lognormal size distributions, whose parameters are derived from the moments. This is the method adopted in this work, and is explained in details in the following.

MADE. The aerosol model MADE, in the version described by *Lauer et al. (2007)*, is the starting point for the development of MADEsoot. MADE describes the aerosol population through three modes, depending on the particle size, under the assumption that all particles are spherical and internally mixed. The three modes are:

- an Aitken mode, for particles with diameter between about 10 nm and 100 nm and composed of SO_4^{2-} , NH_4^+ , NO_3^- , particulate organic matter (POM), H_2O , black carbon (BC) and sea salt (SS);
- an accumulation mode, for particles with diameter between about 100 nm and $1\mu\text{m}$, composed of SO_4^{2-} , NH_4^+ , NO_3^- , POM, H_2O , BC, SS and mineral dust (DU);
- a coarse mode, for particles with diameter larger than about $1\mu\text{m}$, composed of H_2O , DU and SS.

In the Aitken and in the accumulation mode two mass tracers are used to keep track of the mass of hydrophilic and hydrophobic BC. The transfer from the hydrophobic to the hydrophilic is assumed to be an exponential decay with e-folding time of one day (see Sec. 3.2.6). Mineral dust is assumed to be hydrophobic. A detailed description of MADE is presented in *Lauer et al. (2005)* and *Lauer and Hendricks (2006)*. Since MADE focuses on the characterization of sub-micrometer aerosols, whose evolution is quite independent of coarse mode particles (*Whitby, 1978*), the coarse mode has no interaction with the smaller modes.

MADEsoot. The aerosol model MADEsoot maintains the assumption of spherical particles, but makes a distinction between internally and externally mixed BC and sub-micrometer dust. Internally and externally mixed BC and dust particles are assumed to be hydrophilic and hydrophobic, respectively. The aerosol population is described through seven modes:

- an Aitken mode (akn_{sol}) for internally mixed soluble particles with diameter between about 10 nm and 100 nm. akn_{sol} particles are composed of SO_4^{2-} , NH_4^+ , NO_3^- , POM, H_2O , SS;
- an accumulation mode (acc_{sol}) for internally mixed soluble particles with diameter between about 100 nm and $1\mu\text{m}$. acc_{sol} particles are composed of the same species as akn_{sol} ;
- an Aitken mode (akn_{ext}) for externally mixed BC particles with diameter between about 10 nm and 100 nm;
- an accumulation mode (acc_{ext}) for externally mixed BC and dust particles with diameter between about 100 nm and $1\mu\text{m}$;
- an Aitken mode (akn_{mix}) for internally mixed BC and dust particles, i.e. BC and dust particles covered by a coating of soluble material, with diameter between about 10 nm and 100 nm. The coating is composed of the species present in akn_{sol} ;

- an accumulation mode (acc_{mix}) for internally mixed BC and dust particles with diameter between about 100 nm and $1\mu\text{m}$. The coating is composed of the species present in acc_{sol} ;
- a coarse mode (cor) containing particles with diameter larger than about $1\mu\text{m}$ and composed of H_2O , SS and dust.

As in MADE, the coarse mode does not interact with the Aitken and the accumulation modes. The chemical composition of the individual modes in MADE and in MADEsoot is summarized in Tab. 3.1

Through coagulation between different modes and condensation of soluble material, externally mixed BC and dust particles gain a cover of soluble material and, if the coating is sufficiently large, are transferred to an internal mixture. In MADEsoot this ageing process corresponds to the transfer of the mass and number concentration from the externally mixed modes to the internally mixed ones, as explained in detail in Sec. 3.2.6.

Mathematical aspects. The particle number concentration $n(D)$ within each mode is represented as a function of the diameter D by a log-normal distribution:

$$n(D) = \frac{dN}{dD} = \frac{N_t}{\sqrt{2\pi} D \ln \sigma_g} \exp\left(-\frac{(\ln D - \ln D_g)^2}{2 \ln^2 \sigma_g}\right), \quad (3.1)$$

where N_t is the total number concentration of the mode, D_g the median diameter and σ_g the standard deviation of the mode. N_t , D_g and σ_g completely determine each mode. The number of particles with diameter smaller than \bar{D} is given by the integral of Eq. [3.1] between 0 and \bar{D} and is equal to:

$$N(\bar{D}) = \frac{N_t}{2} + \frac{N_t}{2} \operatorname{erf}\left(\frac{\ln(\bar{D}/D_g)}{\sqrt{2} \ln \sigma_g}\right), \quad (3.2)$$

where the error function $\operatorname{erf}(z)$ is defined as

$$\operatorname{erf}(z) = \frac{2}{\sqrt{\pi}} \int_0^z e^{-\eta^2} d\eta \quad (3.3)$$

with $\operatorname{erf}(0) = 0$ and $\operatorname{erf}(\infty) = 1$.

The surface and volume distribution corresponding to a log-normal number distribution are also log-normal. From Eq. [3.1] the surface distribution $n_S(D)$ can be written for spherical particles as

$$\begin{aligned} n_S(D) &= \pi D^2 n(D) = \\ &= \frac{N_t}{\sqrt{2\pi} D \ln \sigma_g} \pi \exp[2 \ln D_g + 2 \ln^2 \sigma_g] \exp\left[-\frac{[\ln D - (\ln D_g + 2 \ln^2 \sigma_g)]^2}{2 \ln^2 \sigma_g}\right], \end{aligned} \quad (3.4)$$

which is a log-normal distribution with standard deviation σ_g and median diameter given by

$$\ln D_{g(S)} = \ln D_g + 2 \ln^2 \sigma_g. \quad (3.5)$$

Likewise the volume distribution $n_V(D)$

$$\begin{aligned} n_V(D) &= \frac{\pi}{6} D^3 n(D) = \\ &= \frac{N_t}{\sqrt{2\pi} D \ln \sigma_g} \frac{\pi}{6} \exp\left[3 \ln D_g + \frac{9}{2} \ln^2 \sigma_g\right] \exp\left[-\frac{[\ln D - (\ln D_g + 3 \ln^2 \sigma_g)]^2}{2 \ln^2 \sigma_g}\right] \end{aligned} \quad (3.6)$$











MADE								
Mode	Species							
	SO_4^{2-}	NH_4^+	NO_3^-	POM	H_2O	SS	BC	DU
akn 	×	×	×	×	×	×	×	
acc 	×	×	×	×	×	×	×	×
cor 					×	×		×
MADEsoot								
Mode	Species							
	SO_4^{2-}	NH_4^+	NO_3^-	POM	H_2O	SS	BC	DU
akn _{sol} 	×	×	×	×	×	×		
acc _{sol} 	×	×	×	×	×	×		
akn _{ext} 	×	×	×	×	×	×	×	
acc _{ext} 	×	×	×	×	×	×	×	×
akn _{mix} 	×	×	×	×	×	×	×	
acc _{mix} 	×	×	×	×	×	×	×	×
cor 					×	×		×

Table 3.1: Chemical composition of the modes in MADE and in MADEsoot. POM stands for particulate organic matter, BC for black carbon, DU for mineral dust and SS for sea salt; akn_{sol} and acc_{sol} indicate the soluble Aitken and accumulation modes, akn_{ext} and acc_{ext} the modes for externally mixed BC and dust, akn_{mix} and acc_{mix} the modes for internally mixed BC and dust, cor the coarse mode.

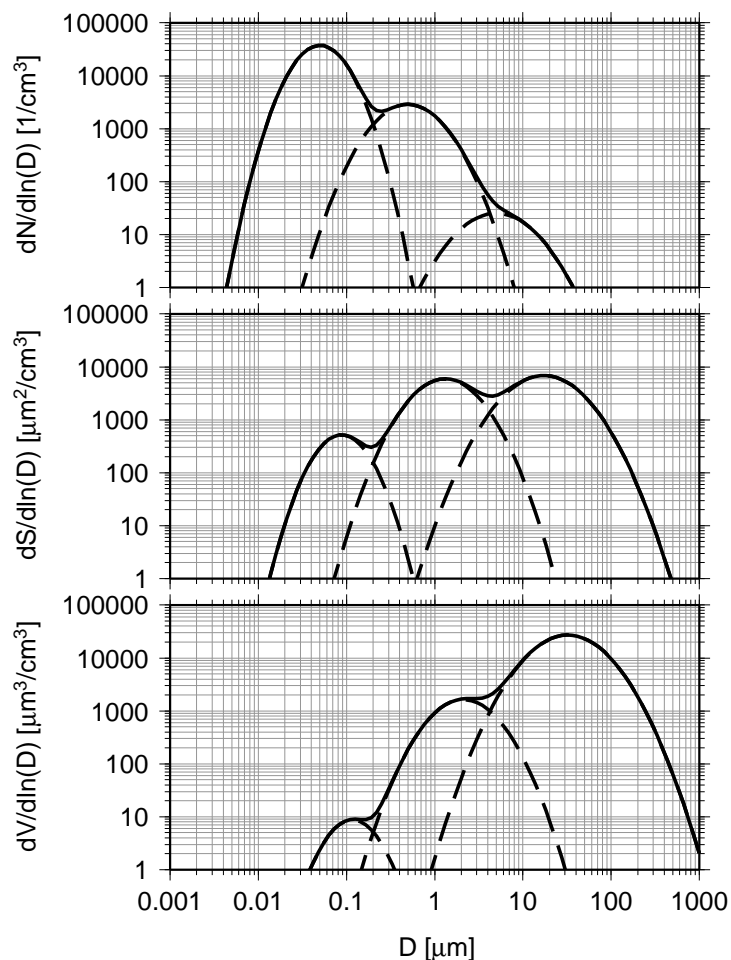


Figure 3.1: Number, surface and volume distribution of three log-normal modes in the range of atmospheric Aitken, accumulation and coarse modes. The median diameters are 50 nm, 0.5 μm and 5 μm , the total number concentrations 50000 cm^{-3} , 5000 cm^{-3} and 50 cm^{-3} and the standard deviations 1.7, 2.0 and 2.2, respectively.

is log-normally distributed with standard deviation σ_g and median diameter given by

$$\ln D_{g(V)} = \ln D_g + 3 \ln^2 \sigma_g. \quad (3.7)$$

Fig. 3.1 shows the number, surface and volume distribution of three log-normal modes in the typical range of the atmospheric Aitken, accumulation and coarse modes. While the Aitken mode gives the larger contribution to the number concentration, the coarse mode dominates the volume distribution.

In MADEsoot the standard deviation of the modes is fixed and set to 1.7, 2.0 and 2.2 for the Aitken, accumulation and coarse modes, respectively, therefore only two parameters, N_t and D_g , are needed to characterize the modes. However, solving the equations directly for the diameter D_g is not simple, therefore MADEsoot solves those for the 0th and 3rd moment, which allow to characterize the mode as N_t and D_g do. The k^{th} moment $M^{(k)}$ of

a distribution is defined as

$$\begin{aligned}
 M^{(k)} &= \int_{-\infty}^{+\infty} D^k n(\ln D) d(\ln D) \\
 &= \int_0^{+\infty} D^{k-1} n(D) dD \\
 &= N_t D_g^k \exp\left(\frac{k^2}{2} \ln^2 \sigma_g\right),
 \end{aligned} \tag{3.8}$$

where the last equivalence is true if $n(D)$ is a log-normal distribution. In particular, $M^{(0)}$ and $M^{(3)}$ are related to total number N_t and total volume V_t of the mode:

$$M^{(0)} = N_t, \tag{3.9}$$

$$M^{(3)} = \frac{6}{\pi} V_t. \tag{3.10}$$

From Eq. 3.8 and Eq. 3.9 the median diameter of the mode is equal to

$$D_g = \frac{M^{(3)}}{M^{(0)} e^{\frac{9}{2} \ln^2 \sigma_g}} \tag{3.11}$$

The prognostic variables of the model are the 0th moments of the modes, corresponding to their total number concentrations, and the mass concentrations of the single species present in each mode. This sums up to 21 prognostic variables in MADE, and to 52 in MADEsoot. The number of the prognostic variables in MADEsoot is given by the number concentrations of the seven modes plus the mass concentrations of the chemical species in each mode, which are six in akn_{sol} , six in acc_{sol} , seven in akn_{ext} , eight in acc_{ext} , seven in akn_{mix} , eight in acc_{mix} and three in the coarse mode.

3.2 Representation of aerosol microphysics

The aerosol processes simulated in MADE and in MADEsoot are the following:

- gas/aerosol partitioning, which is the partitioning between nitric acid (HNO_3) and ammonia (NH_3) in the gas phase and their salts in the liquid phase, i.e. nitrate (NO_3^-) and ammonium (NH_4^+), and the partitioning between the gas and particulate phase of water;
- condensation of sulfuric acid (H_2SO_4) and organic material on preexisting aerosols;
- nucleation of H_2SO_4 in fresh aerosol particles;
- coagulation, which consists in the coagulation between two particles belonging to the same mode (intramodal coagulation) or between two particles belonging to two different mode (intermodal coagulation);

MADEsoot, as most aerosol models, uses the operator splitting approach, i.e. treats the microphysical processes independently within each time step. The succession of the processes is chosen depending on their typical time scale. Gas/aerosol partitioning is assumed to act as first, followed by condensation, nucleation and coagulation. These processes change the aerosol mass and number concentration, which can result in variations of the median diameters of the respective mode. In this way the Aitken mode can grow into the size range of the accumulation mode. If this happens, the aerosol model assigns a part of the mass and number concentration of the Aitken mode to the accumulation mode:

- particle growth from the Aitken modes into the accumulation modes.

Furthermore, gas/aerosol partitioning, condensation and coagulation create a coating on externally mixed BC and dust particles which may transform them in an internal mixture. MADEsoot, but not MADE, simulates also this ageing process:

- ageing of BC and dust particles from external to internal mixture (only in MADEsoot).

These processes determine the evolution of the prognostic variables. The prognostic equations for the number concentration of each mode are

$$\frac{\partial N_i}{\partial t} = R(N_i) + \frac{\partial N_i^{\text{nucl}}}{\partial t} + \frac{\partial N_i^{\text{coag}}}{\partial t} + \frac{\partial N_i^{\text{growth}}}{\partial t} + \frac{\partial N_i^{\text{ageing}}}{\partial t}, \quad (3.12)$$

$$\frac{\partial N_{\text{cor}}}{\partial t} = R(N_{\text{cor}}), \quad (3.13)$$

where $i = \text{akn}, \text{acc}$ in MADE and $i = \text{akn}_{\text{sol}}, \text{acc}_{\text{sol}}, \text{akn}_{\text{ext}}, \text{acc}_{\text{ext}}, \text{akn}_{\text{mix}}, \text{acc}_{\text{mix}}$ in MADEsoot. $R(N_i)$ represents the change in the number concentration of the mode i due to transport, emissions, dry and wet deposition. These processes are not included in the aerosol model, but are simulated in the three-dimensional system ECHAM5/MESSy-MADE(soot) by other sub-models (see Ch. 4). $\partial N_i/\partial t^{\text{nucl}}$, $\partial N_i/\partial t^{\text{coag}}$ and $\partial N_i/\partial t^{\text{growth}}$ corresponds to the change in the number concentration due to nucleation of H_2SO_4 , coagulation, and growth of the Aitken mode into the accumulation mode size range, respectively. The terms $\partial N_i/\partial t^{\text{ageing}}$, which are present only in MADEsoot, describe the ageing of BC and dust particles, i.e. the transfer of particles from akn_{ext} and acc_{ext} to akn_{mix} and acc_{mix} .

The prognostic equations for the mass concentration of the species in each mode are

$$\frac{\partial C_{x,i}}{\partial t} = R(C_{x,i}) + \frac{\partial C_{x,i}^{\text{nucl}}}{\partial t} + \frac{\partial C_{x,i}^{\text{g/p}}}{\partial t} + \frac{\partial C_{x,i}^{\text{coag}}}{\partial t} + \frac{\partial C_{x,i}^{\text{cond}}}{\partial t} + \frac{\partial C_{x,i}^{\text{growth}}}{\partial t} + \frac{\partial C_{x,i}^{\text{ageing}}}{\partial t} \quad (3.14)$$

$$\frac{\partial C_{x,\text{cor}}}{\partial t} = R(C_{x,\text{cor}}) \quad (3.15)$$

where x identifies the species in each mode (Tab. 3.1), and i the mode, as for Eq. [3.12]. $R(C_{x,i})$ represents the change in the mass concentration of the species x in the mode i due to transport, emissions, dry and wet deposition and chemistry. Besides the terms describing the change in the mass concentration due to nucleation, coagulation, growth and ageing, which are included also in Eq. [3.12], Eq. [3.14] includes also the terms $\partial C_{x,i}/\partial t^{\text{g/p}}$ and $\partial C_{x,i}/\partial t^{\text{cond}}$, which describe the changes in the mass concentration of NO_3^- , NH_4^+ and H_2O due to mass exchange between gas and particles and the increase in SO_4^{2-} and POM mass due to condensation of gases, respectively. As in Eq. [3.12], $\partial C_{x,i}/\partial t^{\text{ageing}}$ is present only in MADEsoot. Intramodal coagulation does not affect the mass concentration in the mode. The explicit equations for each prognostic variable are shown in App. A.

The treatment of these processes in MADE and MADEsoot is described in the following. The description focuses on the modification introduced in MADE related to the new ability of MADEsoot to simulate the different mixing states of aerosols. A detailed description of the approach used by MADE is provided by Lauer (2005) and Lauer *et al.* (2005).

3.2.1 Gas/aerosol partitioning

The partitioning between gas and particulate phase of water, gaseous nitric acid (HNO_3) and ammonia (NH_3) and their particle phase, nitrate (NO_3^-) and ammonium (NH_4^+) respectively, is calculated using the computationally efficient equilibrium model EQSAM (Metzger *et al.*, 2002a,b). The basic concept of EQSAM is that the activities of atmospheric aerosol species,

when in equilibrium with the ambient air, are governed by the relative humidity (RH), allowing for a parameterization of single solute molalities and activity coefficients only dependent on the type of solute and RH. The two main assumptions of EQSAM are that aerosols are internally mixed and that the system is in thermodynamical equilibrium. *Meng and Seinfeld (1996)* have shown that the equilibration time of relevant aerosol species in atmospheric conditions is typically of the order of minutes, reaching one hour at low relative humidity. The assumption of thermodynamic equilibrium is therefore feasible in global climate models, where the time step is typically between 0.5 and 1 hour.

In order to reduce computational costs, EQSAM defines four different domains, depending on the abundance of sulfate with respect to sodium, ammonium, potassium, calcium and magnesium. In each domain, several parameters are defined. One parameter is, for instance, the stoichiometric coefficient of ammonium, which is used to determine the amount of available ammonia after the neutralization of the total sulfate. Additionally, each concentration domain is divided into sub-domains, defined through the comparison between RH and relative humidity of deliquescence (RHD). Depending on whether RH is larger or smaller than RHD, the partitioning is done between gas and liquid or between gas and solid aerosol.

MADE. Since the equilibrium time is shorter for smaller than for larger particles (*Meng and Seinfeld, 1996*), MADE applies EQSAM first to the Aitken mode, and subsequently to the accumulation mode. The mass concentrations of SO_4^{2-} , NO_3^- , NH_4^+ and sea salt in the Aitken mode is given as input to EQSAM, together with the gas concentration of NH_3 and HNO_3 . The output is the new concentration of aerosol water, NO_3^- and NH_4^+ in the Aitken mode. The same procedure is applied afterwards to the accumulation modes, taking as input the concentrations of NH_3 and HNO_3 which are left from the first call of EQSAM. After EQSAM has been called, the concentration of the species $x = \text{NH}_4^+, \text{NO}_3^-, \text{H}_2\text{O}$ in the mode $i = \text{akn}$, acc is

$$C_{x,i}(t + \Delta t) = M_{x,i}^{\text{EQSAM}}(C_{\text{SO}_4^{2-},i}(t), C_{\text{NO}_3^-,i}(t), C_{\text{NH}_4^+,i}(t), C_{\text{SS},i}(t), RH), \quad (3.16)$$

where M_x^{EQSAM} is the output concentration of the species x calculated by EQSAM.

MADEsoot. Since the size order of the three MADEsoot Aitken modes is not fixed, it is not possible to set a priori if EQSAM has to be called first for akn_{sol} , akn_{ext} or akn_{mix} . The same problem occurs in the case of the accumulation mode. Therefore, in MADEsoot the EQSAM input concentrations of SO_4^{2-} , NO_3^- , NH_4^+ and sea salt are the total concentrations summed over the three respective modes. The output concentrations of aerosol water, NO_3^- , NH_4^+ is then divided among the three modes proportionally to the concentration of soluble material before EQSAM was called. This is done first for the three Aitken mode and afterwards for the three accumulation mode.

$$C_{x,i}^{\text{EQSAM}}(t + \Delta t) = M_{x,\gamma}^{\text{EQSAM}}(C_{\text{SO}_4^{2-},\gamma}(t), C_{\text{NO}_3^-,\gamma}(t), C_{\text{NH}_4^+,\gamma}(t), C_{\text{SS},\gamma}(t), RH) \times \frac{C_{\text{SO}_4^{2-},i}(t) + C_{\text{NO}_3^-,i}(t) + C_{\text{NH}_4^+,i}(t) + C_{\text{SS},i}(t)}{\sum_{i=1}^3 C_{\text{SO}_4^{2-},i}(t) + C_{\text{NO}_3^-,i}(t) + C_{\text{NH}_4^+,i}(t) + C_{\text{SS},i}(t)} \quad (3.17)$$

where, if $\gamma = \text{akn}$, $i = \text{akn}_{\text{sol}}, \text{akn}_{\text{ext}}, \text{akn}_{\text{mix}}$ and, if $\gamma = \text{acc}$, $i = \text{acc}_{\text{sol}}, \text{acc}_{\text{ext}}, \text{acc}_{\text{mix}}$. The index x refers to the species, with $x = \text{NH}_4, \text{NO}_3^-, \text{H}_2\text{O}$, and $M_{x,\text{akn}}^{\text{EQSAM}}$ is the output concentration of the species x calculated by EQSAM. A certain amount of NO_3^- , NH_4^+ and water mass is assigned also to the externally mixed modes, concurring to increase their coating.

The terms corresponding to the gas/particle equilibrium in the prognostic equations Eq. [3.14] are

$$\frac{\partial C_{\text{NO}_3^-,i}^{\text{g/p}}}{\partial t} = \frac{C_{\text{NO}_3^-,i}^{\text{EQSAM}}(t + \Delta t) - C_{\text{NO}_3^-,i}(t)}{\Delta t} \quad (3.18)$$

$$\frac{\partial C_{\text{NH}_4^+,i}^{\text{g/p}}}{\partial t} = \frac{C_{\text{NH}_4^+,i}^{\text{EQSAM}}(t + \Delta t) - C_{\text{NH}_4^+,i}(t)}{\Delta t} \quad (3.19)$$

$$\frac{\partial C_{\text{H}_2\text{O},i}^{\text{g/p}}}{\partial t} = \frac{C_{\text{H}_2\text{O},i}^{\text{EQSAM}}(t + \Delta t) - C_{\text{H}_2\text{O},i}(t)}{\Delta t} \quad (3.20)$$

$$\frac{\partial C_{\text{SO}_4^{2-},i}^{\text{g/p}}}{\partial t} = \frac{\partial C_{\text{POM},i}^{\text{g/p}}}{\partial t} = \frac{\partial C_{\text{SS},i}^{\text{g/p}}}{\partial t} = \frac{\partial C_{\text{BC},i}^{\text{g/p}}}{\partial t} = \frac{\partial C_{\text{DU},i}^{\text{g/p}}}{\partial t} = 0 \quad (3.21)$$

3.2.2 Condensation of sulfuric acid and organic material

The growth of the aerosol mass due to condensation of sulfuric acid and organic vapor is explicitly calculated by MADE and by MADEsoot. The mass concentration of sulfuric acid gas evolves following the analytic solution of the equation

$$\frac{dC_{\text{H}_2\text{SO}_4}(t)}{dt} = P - L \cdot C_{\text{H}_2\text{SO}_4}(t), \quad (3.22)$$

where P is the production rate of H_2SO_4 in the gas phase and L is the loss due to condensation. The amount of condensing sulfuric acid ΔC^{cond} can be calculated from Eq. [3.22] and is equal to

$$\begin{aligned} \Delta C^{\text{cond}} &= \Delta C_{\text{H}_2\text{SO}_4} - \Delta C^{\text{production}} \\ &= \left(\frac{P}{L} - C_{\text{H}_2\text{SO}_4}(t_0) \right) (1 - e^{-L\Delta t}) - P\Delta t. \end{aligned} \quad (3.23)$$

The calculation of the loss coefficient L is shown in App. B.1. ΔC^{cond} is divided among the aerosol modes proportionally to the third moment growth coefficients $G_i^{(3)} = \partial M_i^{(3)} / \partial t$, where i is the index of the mode. The coefficients $G_i^{(3)}$ are calculated as the harmonic mean between the free-molecular and near-continuum regimes, and depend on the first and second momentum of the modes, on the sticking coefficients of H_2SO_4 , on the mean molecular velocity and on the diffusion coefficient. The complete expression of the condensation coefficients is derived in App. B.1.

The condensation of organic material is calculated in the same way. The amount of condensing gas C_{SOA} , however is provided to the aerosol module as an external field rather than derived by an equation as Eq. [3.22].

The terms in the prognostic equations relative to the condensation of sulfuric acid and organic compounds are the following:

MADE.

$$\frac{\partial C_{\text{SO}_4^{2-},i}^{\text{cond}}}{\partial t} = \frac{G_i^{(3)}}{G_{\text{akn}}^{(3)} + G_{\text{acc}}^{(3)}} \frac{\Delta C^{\text{cond}}}{\Delta t}, \quad (3.24)$$

$$\frac{\partial C_{\text{POM},i}^{\text{cond}}}{\partial t} = \frac{G_{\text{SOA},i}^{(3)}}{G_{\text{SOA, akn}}^{(3)} + G_{\text{SOA, acc}}^{(3)}} \frac{C_{\text{SOA}}}{\Delta t}. \quad (3.25)$$

MADEsoot.

$$\frac{\partial C_{\text{SO}_4^{2-},i}^{\text{cond}}}{\partial t} = \frac{G_i^{(3)}}{\sum_{j=1}^6 G_j^{(3)}} \frac{\Delta C^{\text{cond}}}{\Delta t}, \quad (3.26)$$

$$\frac{\partial C_{\text{POM},i}^{\text{cond}}}{\partial t} = \frac{G_{\text{SOA},i}^{(3)}}{\sum_{j=1}^6 G_{\text{SOA},j}^{(3)}} \frac{C_{\text{SOA}}}{\Delta t}. \quad (3.27)$$

3.2.3 Nucleation of new particles

The binary nucleation of water and sulfuric acid is parameterized following *Vehkamäki et al.* (2002). The nucleation rate of new particles J is parameterized by temperature, relative humidity and concentration of sulfuric acid in the gas phase. The H_2SO_4 concentration used to parameterize J is the amount left in the gas phase after condensation has taken place.

The parameterization of *Vehkamäki et al.* (2002) is valid in the temperature range of 190.15 - 300.15 K, in the relative humidity range of 0.01%-100% and in the sulfuric acid concentration range of $10^4 - 10^{11}$ particles/cm³. The resulting nucleation rate is in the range of $10^{-7} - 10^{10}$ particles/(cm³s). The mass production corresponding to the nucleation rate J is calculated assuming that the freshly nucleated particles are log-normally distributed with wet median diameter of 3.5 nm (*Weber et al.*, 1997) and standard deviation of the Aitken mode. The sulfate mass $m_{3.5}$ contained in a sphere with wet diameter 3.5 nm is calculated as a function of the relative humidity fitting experimental data. The nucleation of new particles can give a large contribution to the number of particles in the Aitken mode, but rarely increase substantially the mass concentration of the mode, given the small diameter of the freshly nucleated particles (*Lauer and Hendricks*, 2006).

MADE. The freshly nucleated particles are assigned to the Aitken mode.

$$\frac{\partial N_{\text{akn}}^{\text{nucl}}}{\partial t} = J(T, \text{RH}, C_{\text{H}_2\text{SO}_4}), \quad (3.28)$$

$$\frac{\partial C_{\text{SO}_4^{2-}, \text{akn}}^{\text{nucl}}}{\partial t} = J(T, \text{RH}, C_{\text{H}_2\text{SO}_4}) m_{3.5}(\text{RH}) e^{\frac{9}{2} \ln^2 \sigma_{\text{akn}}}. \quad (3.29)$$

MADEsoot. The freshly nucleated particles are assigned to the BC and dust free Aitken mode.

$$\frac{\partial N_{\text{akn}_{\text{sol}}}^{\text{nucl}}}{\partial t} = J(T, \text{RH}, C_{\text{H}_2\text{SO}_4}), \quad (3.30)$$

$$\frac{\partial C_{\text{SO}_4^{2-}, \text{akn}_{\text{sol}}}^{\text{nucl}}}{\partial t} = J(T, \text{RH}, C_{\text{H}_2\text{SO}_4}) m_{3.5}(\text{RH}) e^{\frac{9}{2} \ln^2 \sigma_{\text{akn}_{\text{sol}}}}. \quad (3.31)$$

3.2.4 Particle coagulation

Coagulation is the process of collision of aerosol particles and the subsequent creation of a larger particle. This process conserves the total mass of the coagulating particles, but lowers the number concentration, shifting the aerosol population towards larger diameters. A complete description of the coagulation process is very complicated and requires large computational resources. The problem considerably simplifies if one considers only coagulation due to Brownian motion, ignoring the motion produced by other forces as the hydrodynamic, electromagnetic and gravitational forces, and assumes that the aerosol distribution keeps log-normal after the coagulation process (*Binkowski and Shankar*, 1995). The coagulation rates are calculated for spherical particles, following *Binkowski and Shankar* (1995),

as a function of the median diameter of the coagulating modes. They are higher between particles with different diameters than between particles of the same size. The coagulation rates $C_{i,j}^{(k)}$ describe the changing rate of the moment k of the mode l due to the coagulation between the mode i and j

$$C_{ij}^{(k)} = \left. \frac{\partial M_l^{(k)}}{\partial t} \right]_{i,j}. \quad (3.32)$$

Their calculation is shown in App. B.2.

MADE and MADEsoot describe bimodal coagulation of particles belonging to the same mode (intramodal coagulation) or to two different modes (intermodal coagulation). Both aerosol models assume that particles resulting from intramodal coagulation belong to the same mode of the coagulating particles, therefore intramodal coagulation is simulated in a very similar way in MADE and in MADEsoot. On the other hand, the simulation of intermodal coagulation is very different, given the higher number of possible coagulation events. Tab. 3.2 shows all possible coagulation events in MADE and in MADEsoot and the destination of the particles resulting from each coagulation process.

MADE. MADE assumes that the coagulation between an Aitken mode particle and an accumulation mode particle results in an accumulation mode particle, while the coagulation between particles belonging to the same mode results in a particle that still belongs to the same mode. This implies that the intramodal coagulation lowers the number concentration of both modes but leaves the mass concentration unchanged, while the intermodal coagulation lowers the Aitken mode number and mass concentration and increases the accumulation mode mass concentration, but not its number concentration. The coagulation terms in the prognostic equations Eq. [3.12] for the number concentrations are

$$\frac{\partial N_{\text{akn}}^{\text{coag}}}{\partial t} = -C_{\text{akn, akn}}^{(0)} - C_{\text{akn, acc}}^{(0)} \quad (3.33)$$

$$\frac{\partial N_{\text{acc}}^{\text{coag}}}{\partial t} = -C_{\text{acc, acc}}^{(0)} \quad (3.34)$$

The coagulation terms for the mass concentrations in Eq. 3.14 are related to the changing rate of the third momentum





$$\frac{\partial C_{x,\text{akn}}^{\text{coag}}}{\partial t} = -\frac{1}{M_{\text{akn}}^{(3)}} \frac{\partial M_{\text{akn}}^{(3)}}{\partial t} C_{x,\text{akn}} = -\frac{C_{\text{akn, acc}}^{(3)}}{M_{\text{akn}}^{(3)}} C_{x,\text{akn}} \quad (3.35)$$

$$\frac{\partial C_{x,\text{acc}}^{\text{coag}}}{\partial t} = -\frac{\partial C_{x,\text{akn}}^{\text{coag}}}{\partial t} = \frac{C_{\text{akn, acc}}^{(3)}}{M_{\text{akn}}^{(3)}} C_{x,\text{akn}}, \quad (3.36)$$

where the sign of the coagulation rate $C_{i,j}^{(k)}$ is explicitly written.

MADEsoot. The simulation of the intermodal coagulation is more complicated in MADEsoot than in MADE. Besides shifting the modes towards larger values of the median diameter, BC and dust free particles may coagulate with BC and dust containing particles, and externally mixed particles may coagulate with particles containing enough soluble material to transform them in an internal mixture. When such coagulation events take place and the amount of soluble material contained in the coagulation modes is large enough, the resulting particle is assigned to the internally mixed modes containing BC and dust, otherwise to the externally mixed modes. The criterion to define a particle as internally mixed is explained in Sec. 3.2.6.

MADE

	akn 	acc 
akn 	akn	acc
acc 		acc

MADEsoot













	akn_{sol} 	acc_{sol} 	akn_{ext} 	acc_{ext} 	akn_{mix} 	acc_{mix} 
akn_{sol} 	akn _{sol}	acc _{sol}	akn _{mix} OR akn _{ext}	acc _{mix} OR acc _{ext}	akn _{mix}	acc _{mix}
acc_{sol} 		acc _{sol}	acc _{mix} OR akn _{ext}	acc _{mix} OR acc _{ext}	acc _{mix}	acc _{mix}
akn_{ext} 			akn _{ext}	acc _{ext}	akn _{mix} OR akn _{ext}	acc _{mix} OR akn _{ext}
acc_{ext} 				acc _{ext}	acc _{mix} OR acc _{ext}	acc _{mix} OR acc _{ext}
akn_{mix} 					akn _{mix}	acc _{mix}
acc_{mix} 						acc _{mix}

Table 3.2: Intermodal and intramodal coagulation events in MADE and in MADEsoot. The first row and the first column report the coagulating modes, and the body of the table the destination of each coagulation event.

The coagulation term in the prognostic equation for the the number concentration of the mode l is given by

$$\frac{\partial N_l^{\text{coag}}}{\partial t} = C_{l,l}^{(0)} + C_{i,j}^{(0)}. \quad (3.37)$$

$C_{l,l}^{(0)}$ describes the intramodal coagulation events, hence it is always negative. $C_{i,j}^{(0)}$, on the other hand, can be positive, negative or equal to 0. If i , j and l are different from each other, $C_{i,j}^{(0)}$ is positive. This is for instance the case of an externally mixed BC or dust particle coagulating with a soluble one to give an internally mixed particle with BC and dust. If

$i = l$ or $j = l$, $C_{i,j}^{(0)}$ can be negative or equal to zero, depending on l being mode that loses or receives the resulting particle, respectively. $C_{i,j}^{(0)}$ is symmetric with respect to switching i and j . Writing explicitly the terms of Eq. [3.37], the prognostic equations for the number concentrations of the soluble modes are

$$\frac{\partial N_{\text{akn}_{\text{sol}}}^{\text{coag}}}{\partial t} = -C_{\text{akn}_{\text{sol}},\text{akn}_{\text{sol}}}^{(0)} \quad (3.38)$$

$$-C_{\text{akn}_{\text{sol}},\text{acc}_{\text{sol}}}^{(0)} - C_{\text{akn}_{\text{sol}},\text{akn}_{\text{ext}}}^{(0)} - C_{\text{akn}_{\text{sol}},\text{acc}_{\text{ext}}}^{(0)} - C_{\text{akn}_{\text{sol}},\text{akn}_{\text{mix}}}^{(0)} - C_{\text{akn}_{\text{sol}},\text{acc}_{\text{mix}}}^{(0)},$$

$$\frac{\partial N_{\text{acc}_{\text{sol}}}^{\text{coag}}}{\partial t} = -C_{\text{acc}_{\text{sol}},\text{acc}_{\text{sol}}}^{(0)} \quad (3.39)$$

$$-C_{\text{acc}_{\text{sol}},\text{akn}_{\text{ext}}}^{(0)} - C_{\text{acc}_{\text{sol}},\text{acc}_{\text{ext}}}^{(0)} - C_{\text{acc}_{\text{sol}},\text{akn}_{\text{mix}}}^{(0)} - C_{\text{acc}_{\text{sol}},\text{acc}_{\text{mix}}}^{(0)},$$

where the sign of the coagulation coefficients is explicitly written. All the possible coagulation events lower the number concentrations of the soluble modes.

The result of a coagulation event involving an externally mixed mode is not always assigned to the same mode. The coagulation between akn_{sol} and akn_{ext} , for instance, can give a particle in akn_{mix} or in akn_{ext} , depending on the ratio of soluble to insoluble mass involved in the coagulation process. The number concentration of akn_{sol} becomes lower in both cases, while the number concentration of akn_{ext} becomes lower in the first case and stays the same in the second case. In the following the prognostic equations for the modes containing BC and dust are explicitly written. For each coagulation event whose resulting mode is not fixed, the two possible terms are written: The upper term in the curly bracket corresponds to the case where the resulting particle is internally mixed, the lower to the case where it is externally mixed. Each term corresponds to a different coagulation event.

$$\frac{\partial N_{\text{akn}_{\text{ext}}}^{\text{coag}}}{\partial t} = -C_{\text{akn}_{\text{ext}},\text{akn}_{\text{ext}}}^{(0)} + \left\{ \begin{array}{l} -C_{\text{akn}_{\text{sol}},\text{akn}_{\text{ext}}}^{(0)} \\ 0 \end{array} \right. + \left\{ \begin{array}{l} -C_{\text{acc}_{\text{sol}},\text{akn}_{\text{ext}}}^{(0)} \\ 0 \end{array} \right. \quad (3.40)$$

$$-C_{\text{akn}_{\text{ext}},\text{acc}_{\text{ext}}}^{(0)} + \left\{ \begin{array}{l} -C_{\text{akn}_{\text{ext}},\text{akn}_{\text{mix}}}^{(0)} \\ 0 \end{array} \right. + \left\{ \begin{array}{l} -C_{\text{akn}_{\text{ext}},\text{acc}_{\text{mix}}}^{(0)} \\ 0 \end{array} \right. ,$$

$$\frac{\partial N_{\text{acc}_{\text{ext}}}^{\text{coag}}}{\partial t} = -C_{\text{acc}_{\text{ext}},\text{acc}_{\text{ext}}}^{(0)} + \left\{ \begin{array}{l} -C_{\text{akn}_{\text{sol}},\text{acc}_{\text{ext}}}^{(0)} \\ 0 \end{array} \right. + \left\{ \begin{array}{l} -C_{\text{acc}_{\text{sol}},\text{acc}_{\text{ext}}}^{(0)} \\ 0 \end{array} \right. \quad (3.41)$$

$$+ \left\{ \begin{array}{l} -C_{\text{acc}_{\text{ext}},\text{akn}_{\text{mix}}}^{(0)} \\ 0 \end{array} \right. + \left\{ \begin{array}{l} -C_{\text{acc}_{\text{ext}},\text{acc}_{\text{mix}}}^{(0)} \\ 0 \end{array} \right. ,$$

There are no coagulation events that increase the number concentrations of the externally mixed modes. On the other hand the number concentrations of the internally mixed modes with BC and dust can increase following the coagulation of externally mixed BC and dust with soluble particles.

$$\frac{\partial N_{\text{akn}_{\text{mix}}}^{\text{coag}}}{\partial t} = -C_{\text{akn}_{\text{mix}},\text{akn}_{\text{mix}}}^{(0)} + \left\{ \begin{array}{l} +C_{\text{akn}_{\text{sol}},\text{akn}_{\text{ext}}}^{(0)} \\ 0 \end{array} \right. - C_{\text{acc}_{\text{sol}},\text{akn}_{\text{mix}}}^{(0)} \quad (3.42)$$

$$+ \left\{ \begin{array}{l} 0 \\ -C_{\text{akn}_{\text{ext}},\text{akn}_{\text{mix}}}^{(0)} \end{array} \right. - C_{\text{acc}_{\text{ext}},\text{akn}_{\text{mix}}}^{(0)} - C_{\text{akn}_{\text{mix}},\text{acc}_{\text{mix}}}^{(0)},$$

$$\frac{\partial N_{\text{acc}_{\text{mix}}}^{\text{coag}}}{\partial t} = -C_{\text{acc}_{\text{mix}},\text{acc}_{\text{mix}}}^{(0)} + \left\{ \begin{array}{l} +C_{\text{akn}_{\text{sol}},\text{acc}_{\text{ext}}}^{(0)} \\ 0 \end{array} \right. + \left\{ \begin{array}{l} +C_{\text{acc}_{\text{sol}},\text{akn}_{\text{ext}}}^{(0)} \\ 0 \end{array} \right. + \left\{ \begin{array}{l} +C_{\text{acc}_{\text{sol}},\text{acc}_{\text{ext}}}^{(0)} \\ 0 \end{array} \right. \quad (3.43)$$

$$+ C_{\text{acc}_{\text{sol}},\text{akn}_{\text{mix}}}^{(0)} + \left\{ \begin{array}{l} 0 \\ -C_{\text{akn}_{\text{ext}},\text{acc}_{\text{mix}}}^{(0)} \end{array} \right. + \left\{ \begin{array}{l} +C_{\text{acc}_{\text{ext}},\text{akn}_{\text{mix}}}^{(0)} \\ 0 \end{array} \right. + \left\{ \begin{array}{l} 0 \\ -C_{\text{acc}_{\text{ext}},\text{acc}_{\text{mix}}}^{(0)} \end{array} \right. .$$

The changing rate of the mass concentration of the species x in the mode l due to coagulation is

$$\frac{\partial C_{x,l}}{\partial t}^{\text{coag}} = \sum_{i,j} \frac{C_{i,j}^{(3)}}{M_i^{(3)}} C_{x,i} \equiv \sum_{i,j} K_x^{i,j}, \quad (3.44)$$

where i and j identifies the coagulating modes in events where the mode l is involved, as coagulating mode or as outcome of the event. Since the intramodal coagulation does not change the mass of the mode, the changing rate of $M_l^{(3)}$ depends only on intermodal coagulation. $C_{i,j}^{(3)}$ is not symmetric with respect to switching i and j . If the particles resulting from the coagulation between the mode i and j are assigned to the mode k , then $C_{i,j}^{(3)}$ is related to the moment that is transferred from the mode i to the mode k , and $C_{j,i}^{(3)}$ to the moment transferred from the mode j to the mode k . $K_x^{i,j}$ is the mass of the species x which is transferred from the mode i . If $i = l$, $K_x^{i,j}$ is negative or equal to zero.

Writing explicitly the sign of the single terms, the terms in the prognostic equations for the mass concentrations of the soluble modes are

$$\frac{\partial C_{x,\text{akn}_{\text{sol}}}}{\partial t}^{\text{coag}} = -K_x^{\text{akn}_{\text{sol}},\text{acc}_{\text{sol}}} - K_x^{\text{akn}_{\text{sol}},\text{akn}_{\text{ext}}} - K_x^{\text{akn}_{\text{sol}},\text{acc}_{\text{ext}}} - K_x^{\text{akn}_{\text{sol}},\text{akn}_{\text{mix}}} - K_x^{\text{akn}_{\text{sol}},\text{acc}_{\text{mix}}} \quad (3.45)$$

$$\frac{\partial C_{x,\text{acc}_{\text{sol}}}}{\partial t}^{\text{coag}} = +K_x^{\text{akn}_{\text{sol}},\text{acc}_{\text{sol}}} - K_x^{\text{acc}_{\text{sol}},\text{akn}_{\text{ext}}} - K_x^{\text{acc}_{\text{sol}},\text{acc}_{\text{ext}}} - K_x^{\text{acc}_{\text{sol}},\text{akn}_{\text{mix}}} - K_x^{\text{acc}_{\text{sol}},\text{acc}_{\text{mix}}} \quad (3.46)$$

As for the prognostic equations for the number concentrations, the terms describing the coagulation events involving an externally mixed mode depend on the amount of soluble material involved. The upper term in the curly brackets is valid in case the resulting particle is internally mixed, the lower if it is externally mixed.

$$\frac{\partial C_{x,\text{akn}_{\text{ext}}}}{\partial t}^{\text{coag}} = \left\{ \begin{array}{l} -K_x^{\text{akn}_{\text{ext}},\text{akn}_{\text{sol}}} \\ +K_x^{\text{akn}_{\text{sol}},\text{akn}_{\text{ext}}} \end{array} \right\} + \left\{ \begin{array}{l} -K_x^{\text{akn}_{\text{ext}},\text{acc}_{\text{sol}}} \\ +K_x^{\text{acc}_{\text{sol}},\text{akn}_{\text{ext}}} \end{array} \right\} - K_x^{\text{akn}_{\text{ext}},\text{acc}_{\text{ext}}} \quad (3.47)$$

$$+ \left\{ \begin{array}{l} -K_x^{\text{akn}_{\text{ext}},\text{akn}_{\text{mix}}} \\ +K_x^{\text{akn}_{\text{mix}},\text{akn}_{\text{ext}}} \end{array} \right\} + \left\{ \begin{array}{l} -K_x^{\text{akn}_{\text{ext}},\text{acc}_{\text{mix}}} \\ +K_x^{\text{acc}_{\text{mix}},\text{akn}_{\text{ext}}} \end{array} \right\}$$

$$\frac{\partial C_{x,\text{acc}_{\text{ext}}}}{\partial t}^{\text{coag}} = \left\{ \begin{array}{l} -K_x^{\text{acc}_{\text{ext}},\text{akn}_{\text{sol}}} \\ +K_x^{\text{akn}_{\text{sol}},\text{acc}_{\text{ext}}} \end{array} \right\} + \left\{ \begin{array}{l} -K_x^{\text{acc}_{\text{ext}},\text{acc}_{\text{sol}}} \\ +K_x^{\text{acc}_{\text{sol}},\text{acc}_{\text{ext}}} \end{array} \right\} + K_x^{\text{akn}_{\text{ext}},\text{acc}_{\text{ext}}} \quad (3.48)$$

$$+ \left\{ \begin{array}{l} -K_x^{\text{acc}_{\text{ext}},\text{akn}_{\text{mix}}} \\ +K_x^{\text{akn}_{\text{mix}},\text{acc}_{\text{ext}}} \end{array} \right\} + \left\{ \begin{array}{l} -K_x^{\text{acc}_{\text{ext}},\text{acc}_{\text{mix}}} \\ +K_x^{\text{acc}_{\text{mix}},\text{acc}_{\text{ext}}} \end{array} \right\}$$

If the resulting particle is externally mixed, the number concentration of the involved externally mixed mode does not change, but its mass concentration does. The prognostic

equations for the internally mixed modes with BC and dust are

$$\frac{\partial C_{x,\text{akn}_{\text{mix}}}}{\partial t}^{\text{coag}} = \begin{cases} +K_x^{\text{akn}_{\text{sol}},\text{akn}_{\text{ext}}} + K_x^{\text{akn}_{\text{ext}},\text{akn}_{\text{sol}}} & + K_x^{\text{akn}_{\text{sol}},\text{akn}_{\text{mix}}} - K_x^{\text{akn}_{\text{mix}},\text{acc}_{\text{sol}}} \\ 0 \end{cases} \quad (3.49)$$

$$\begin{aligned} & + \begin{cases} +K_x^{\text{akn}_{\text{ext}},\text{akn}_{\text{mix}}} & - K_x^{\text{akn}_{\text{mix}},\text{acc}_{\text{ext}}} - K_x^{\text{akn}_{\text{mix}},\text{acc}_{\text{mix}}} \\ -K_x^{\text{akn}_{\text{mix}},\text{akn}_{\text{ext}}} \end{cases} \\ \frac{\partial C_{x,\text{acc}_{\text{mix}}}}{\partial t}^{\text{coag}} & = \begin{cases} +K_x^{\text{akn}_{\text{sol}},\text{acc}_{\text{ext}}} + K_x^{\text{acc}_{\text{ext}},\text{akn}_{\text{sol}}} & + K_x^{\text{akn}_{\text{sol}},\text{acc}_{\text{mix}}} \\ 0 \end{cases} \quad (3.50) \\ & + \begin{cases} +K_x^{\text{acc}_{\text{sol}},\text{akn}_{\text{ext}}} + K_x^{\text{akn}_{\text{ext}},\text{acc}_{\text{sol}}} & + \begin{cases} +K_x^{\text{acc}_{\text{sol}},\text{acc}_{\text{ext}}} + K_x^{\text{acc}_{\text{ext}},\text{acc}_{\text{sol}}} \\ 0 \end{cases} \\ 0 \end{cases} \\ & + K_x^{\text{akn}_{\text{mix}},\text{acc}_{\text{sol}}} + K_x^{\text{acc}_{\text{sol}},\text{acc}_{\text{mix}}} + \begin{cases} +K_x^{\text{akn}_{\text{ext}},\text{acc}_{\text{mix}}} \\ -K_x^{\text{acc}_{\text{mix}},\text{akn}_{\text{ext}}} \end{cases} \\ & + \begin{cases} +K_x^{\text{acc}_{\text{ext}},\text{akn}_{\text{mix}}} + K_x^{\text{akn}_{\text{mix}},\text{acc}_{\text{ext}}} & + \begin{cases} +K_x^{\text{acc}_{\text{ext}},\text{acc}_{\text{mix}}} \\ -K_x^{\text{acc}_{\text{mix}},\text{acc}_{\text{ext}}} \end{cases} + K_x^{\text{akn}_{\text{mix}},\text{acc}_{\text{mix}}} \\ 0 \end{cases} \end{aligned}$$

3.2.5 Particle growth

Condensation of vapor and coagulation with other particles increase the volume of individual aerosol particles, and therefore shift the modes toward larger diameters. Since the evolution of the Aitken and of the accumulation mode are calculated independently, the diameter of the Aitken mode can grow into the size range of the accumulation mode. If this happens, a fraction of the Aitken mode containing large particles is transferred to the accumulation mode. To achieve this, the aerosol model transfer to the accumulation mode the number concentration of the Aitken mode particles with diameter larger than D_n , where D_n is the intersection diameter between the Aitken and accumulation mode number distributions (Fig. 3.2). In the same way, the mass concentration of the Aitken mode particles with diameter larger than D_V , where D_V is the intersection diameter between the Aitken and accumulation mode volume distributions, is transferred to the accumulation mode. The number and mass of the particles with diameter larger than D_n or D_V is calculated by means of Eq. [3.2] This operation is called mode merging.

MADE. A part of the number and mass concentration of the Aitken mode is transferred to the accumulation mode. From Eq. [3.2],

$$\frac{\partial N_{\text{akn}}}{\partial t}^{\text{growth}} = -\frac{\partial N_{\text{acc}}}{\partial t}^{\text{growth}} = -\frac{N_{\text{akn}}(D > D_n)}{\Delta t}, \quad (3.51)$$

$$\frac{\partial C_{x,\text{akn}}}{\partial t}^{\text{growth}} = -\frac{\partial C_{x,\text{acc}}}{\partial t}^{\text{growth}} = -\frac{C_{x,\text{akn}}(D > D_V)}{\Delta t}, \quad (3.52)$$

MADEsoot. The merging between the Aitken and the accumulation mode applies only to modes with the same mixing state, i.e. akn_{sol} merges with acc_{sol} , akn_{ext} with acc_{ext} and

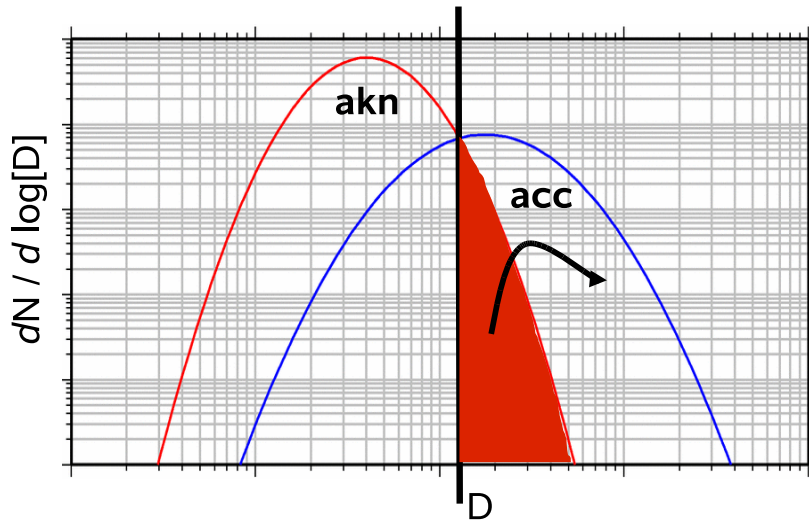


Figure 3.2: Model representation of the merging between Aitken and accumulation modes.

akn_{mix} with acc_{mix} .

$$\frac{\partial N_{\text{akn}_{\text{sol}}}}{\partial t}^{\text{growth}} = -\frac{\partial N_{\text{acc}_{\text{sol}}}}{\partial t}^{\text{growth}} \quad (3.53)$$

$$\frac{\partial N_{\text{akn}_{\text{ext}}}}{\partial t}^{\text{growth}} = -\frac{\partial N_{\text{acc}_{\text{ext}}}}{\partial t}^{\text{growth}} \quad (3.54)$$

$$\frac{\partial N_{\text{akn}_{\text{mix}}}}{\partial t}^{\text{growth}} = -\frac{\partial N_{\text{acc}_{\text{mix}}}}{\partial t}^{\text{growth}} \quad (3.55)$$

$$\frac{\partial C_{x,\text{akn}_{\text{sol}}}}{\partial t}^{\text{growth}} = -\frac{\partial C_{x,\text{acc}_{\text{sol}}}}{\partial t}^{\text{growth}} \quad (3.56)$$

$$\frac{\partial C_{x,\text{akn}_{\text{ext}}}}{\partial t}^{\text{growth}} = -\frac{\partial C_{x,\text{acc}_{\text{ext}}}}{\partial t}^{\text{growth}} \quad (3.57)$$

$$\frac{\partial C_{x,\text{akn}_{\text{mix}}}}{\partial t}^{\text{growth}} = -\frac{\partial C_{x,\text{acc}_{\text{mix}}}}{\partial t}^{\text{growth}} \quad (3.58)$$

3.2.6 Ageing of black carbon and dust particles

Coagulation and condensation of gases on externally mixed particles create a coating around externally mixed BC and dust particles, and can therefore transfer them to an internal mixture (e.g. *Okada et al. (2005)*; *Moteki et al. (2007)*). Also photochemical reactions can contribute to the ageing of externally mixed BC particles, transforming the surface from being hydrophobic to hydrophilic. *Weingartner et al. (1997)* show that ageing through photochemical reactions is mostly less efficient than the ageing through coagulation or condensation, while *Kotzick and Niessner (1999)* state that oxidation of ozone could be more important than coagulation in the change of the hygroscopic behavior. However, *Kotzick and Niessner (1999)* use a quite high ozone concentration compared to usual tropospheric values. MADEsoot simulates explicitly the condensation of SO_4^{2-} and organic material (Sec. 3.2.2), inter-modal coagulation (Sec. 3.2.4) and heterogeneous nucleation of condensable compound (Sec. 3.2.1).

MADE. MADE does not simulate explicitly the ageing of black carbon and dust particles and, in the handling of the microphysical processes, does not keep track separately of

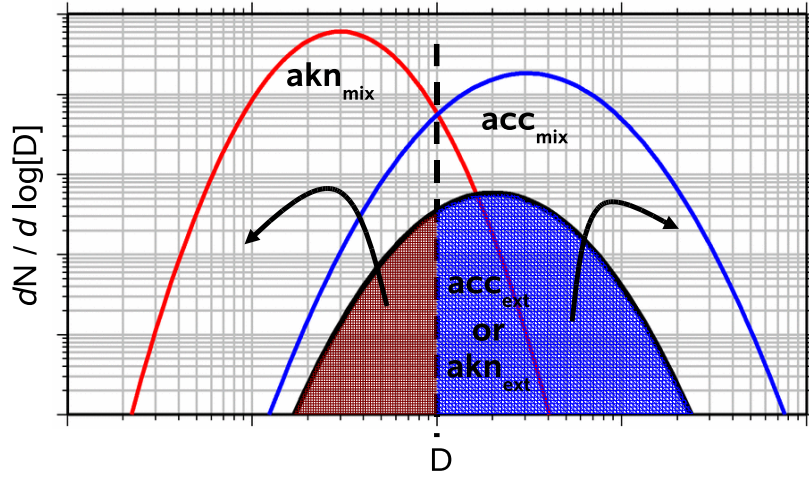


Figure 3.3: Model representation of the ageing of the externally mixed modes.

externally and internally mixed BC and dust. However, while dust is supposed to be completely hydrophobic, MADE assumes for BC an exponential decay from the hydrophobic into the hydrophilic state, here used as synonym of externally and internally mixed, respectively. Technically, MADE uses two different tracers for the mass concentration of BC, one for each state of mixing. Before the aerosol microphysics is simulated, the ageing is calculated as

$$M_{\text{BC}_{\text{ext}},i}(t + \delta t) = M_{\text{BC}_{\text{ext}},i}(t)(1 - e^{-\Delta t/\tau}), \quad (3.59)$$

$$M_{\text{BC}_{\text{int}},i}(t + \delta t) = M_{\text{BC}_{\text{int}},i}(t) + M_{\text{BC}_{\text{ext}},i}(t)e^{-\Delta t/\tau}, \quad (3.60)$$

where the e-folding time τ is arbitrarily set to one day. The mass of hydrophobic and hydrophilic BC are then added up, and the aerosol microphysics is calculated for the total BC. The number concentration of the modes is not affected.

MADEsoot. Given the new modes available in MADEsoot, which allow to keep track of externally and internally mixed BC and dust during the calculation of aerosol microphysics, MADEsoot simulates explicitly the ageing of BC and dust. After all aerosol processes have been simulated, MADEsoot calculates the amount of soluble mass (SO_4^{2-} , NH_4^+ , NO_3^- , POM, H_2O , SS) in each externally mixed mode i . If it is larger than a critical fraction x of the total mass of the mode i , where x is a free parameter of the mode, the mass and the number concentrations of the mode i are transferred to the internally mixed Aitken and accumulation modes with black carbon and dust. To achieve this the diameter D at which the number distribution of akn_{mix} intersects that of acc_{mix} is calculated, and the aged externally mixed particles with diameter larger than D , obtained by means of Eq. [3.2], are assigned to acc_{mix} , the others to akn_{mix} (Fig. 3.3). This is a step process, since it does not act as long as the ratio of soluble to total mass in the externally mixed mode i is lower than x . When the mass ration exceeds x , the whole externally mixed mode is transferred to the internally mixed ones. Therefore if there is no ageing the relative terms in the prognostic equations are 0. Defining for each externally mixed mode i the ratio r_i of soluble material as

$$r_i = \frac{m_i^{\text{sol}}}{m_i^{\text{tot}}}, \quad (3.61)$$

the ageing terms in the prognostic equations are

$$\frac{\partial N_{\text{akn}_{\text{sol}}}}{\partial t}^{\text{ageing}} = \frac{\partial C_{x,\text{akn}_{\text{sol}}}}{\partial t}^{\text{ageing}} = 0 \quad (3.62)$$

$$\frac{\partial N_{\text{acc}_{\text{sol}}}}{\partial t}^{\text{ageing}} = \frac{\partial C_{x,\text{acc}_{\text{sol}}}}{\partial t}^{\text{ageing}} = 0 \quad (3.63)$$

$$\begin{aligned} \frac{\partial N_{\text{akn}_{\text{mix}}}}{\partial t}^{\text{ageing}} &= \begin{cases} 0 & \text{if } r_{\text{akn}_{\text{ext}}} < x \\ \frac{1}{\Delta t} N_{\text{akn}_{\text{ext}}} (d < D) & \text{if } r_{\text{akn}_{\text{ext}}} \geq x \end{cases} \\ &+ \begin{cases} 0 & \text{if } r_{\text{acc}_{\text{ext}}} < x \\ \frac{1}{\Delta t} N_{\text{acc}_{\text{ext}}} (d < D) & \text{if } r_{\text{acc}_{\text{ext}}} \geq x \end{cases} \end{aligned} \quad (3.64)$$

$$\begin{aligned} \frac{\partial N_{\text{acc}_{\text{mix}}}}{\partial t}^{\text{ageing}} &= \begin{cases} 0 & \text{if } r_{\text{akn}_{\text{ext}}} < x \\ \frac{1}{\Delta t} N_{\text{akn}_{\text{ext}}} (d \geq D) & \text{if } r_{\text{akn}_{\text{ext}}} \geq x \end{cases} \\ &+ \begin{cases} 0 & \text{if } r_{\text{acc}_{\text{ext}}} < x \\ \frac{1}{\Delta t} N_{\text{acc}_{\text{ext}}} (d \geq D) & \text{if } r_{\text{acc}_{\text{ext}}} \geq x \end{cases} \end{aligned} \quad (3.65)$$

$$\begin{aligned} \frac{\partial C_{x,\text{akn}_{\text{mix}}}}{\partial t}^{\text{ageing}} &= \begin{cases} 0 & \text{if } r_{\text{akn}_{\text{ext}}} < x \\ \frac{1}{\Delta t} C_{x,\text{akn}_{\text{ext}}} (d < D) & \text{if } r_{\text{akn}_{\text{ext}}} \geq x \end{cases} \\ &+ \begin{cases} 0 & \text{if } r_{\text{acc}_{\text{ext}}} < x \\ \frac{1}{\Delta t} C_{x,\text{acc}_{\text{ext}}} (d < D) & \text{if } r_{\text{acc}_{\text{ext}}} \geq x \end{cases} \end{aligned} \quad (3.66)$$

$$\begin{aligned} \frac{\partial C_{x,\text{acc}_{\text{mix}}}}{\partial t}^{\text{ageing}} &= \begin{cases} 0 & \text{if } r_{\text{akn}_{\text{ext}}} < x \\ \frac{1}{\Delta t} C_{x,\text{akn}_{\text{ext}}} (d \geq D) & \text{if } r_{\text{akn}_{\text{ext}}} \geq x \end{cases} \\ &+ \begin{cases} 0 & \text{if } r_{\text{acc}_{\text{ext}}} < x \\ \frac{1}{\Delta t} C_{x,\text{acc}_{\text{ext}}} (d \geq D) & \text{if } r_{\text{acc}_{\text{ext}}} \geq x \end{cases} \end{aligned} \quad (3.67)$$

As a consequence of the aging process, the mass and number concentrations of the externally mixed modes are set to 0.

The parameter x can be chosen depending on the aerosol properties to investigate. *Bond et al.* (2006) studied from a theoretical point of view the influence of a soluble shell on the radiative properties of an aerosol particle, finding very different values of the absorption amplification for different shell to core ratios. *Weingartner et al.* (1997) and *Khalizov et al.* (2009) presented experimental studies on the hygroscopic properties of externally and internally mixed BC, and set to 10% the fraction of soluble mass in a particle beyond which the particles show a more hygroscopic behavior. In the present study three simulations have been performed, with $x=5\%$, 10% and 50% , respectively. For each of them the evaluation tests shown in Ch. 5 have been performed. The concentration of total BC and dust have not shown sensible variations among the three runs. More details about these studies are reported in Sec. 6.1.4.

Chapter 4

The three-dimensional model: ECHAM5/MESSy-MADEsoot

The global climate model used in this work is the ECHAM5/MESSy system (E5/M). ECHAM5 (version 5.3.01) is the general circulation model (GCM), responsible for the movement of air masses, the transport of the tracers as e.g. the mass of the chemical species and the number concentration of the modes, and for the atmospheric physics as radiation or precipitation. The interface MESSy (version 1.4), on the other hand, couples the processes, which are simulated by the different sub-models, to each other and to the GCM.

In this chapter the global aerosol-chemistry model E5/M-MADE, which is the starting point of the the implementation of MADEsoot in a global climate model, is presented, as well as the modifications that were introduced to obtain a better description of the aerosol concentrations in the upper troposphere-lowermost stratosphere (UTLS), and also the implementation of the aerosol box model MADEsoot in E5/M is described.

4.1 The starting point: the ECHAM5/MESSy-MADE aerosol-chemistry model

The ECHAM5/MESSy model is a numerical chemistry and climate simulation system that includes sub-models to describe physical and chemical processes of the troposphere and middle atmosphere (*Jöckel et al.*, 2006). The model was extended with the aerosol module MADE by *Lauer et al.* (2007).

ECHAM5 (*Roeckner et al.*, 2003) is the atmospheric general circulation model developed at the Max Planck Institute for Meteorology, Hamburg. The first version of ECHAM was developed following the weather prediction model of the European Center for Medium Range Weather Forecasts (ECMWF).

ECHAM5 is a spectral model based on the so called primitive equations, i.e. the differential equations for momentum, temperature and moisture. The prognostic variables are vorticity, divergence, temperature, specific humidity and logarithm of the surface pressure. Except for the specific humidity, that is calculated in the grid point space, the prognostic variables are represented in the spectral space by a truncated series of spherical harmonics. The standard truncations used in ECHAM5 are at 21, 31, 42, 63, 85, 106 and 159 harmonics, and the chosen truncation determines the horizontal resolution of the model. The horizontal resolution used in this work is T42, which corresponds to a grid of 64 cells along the latitude and 128 along the longitude, with a cell width of approximately $2.8^\circ \times 2.8^\circ$.

The atmosphere up to 10 hPa is divided vertically in non-equidistant levels with a hybrid vertical representation that follows the orography close to the surface and flattens the UTLS. The pressure at each level boundary is defined through the two constant hybrid parameters A and B as a function of the surface pressure p_s as

$$p_k = A_k + B_k p_s, \quad (4.1)$$

$$A_0 = B_{N_{lev}+1} = A_{N_{lev}+1} = 0, \quad B_0 = 1, \quad (4.2)$$

where the index $k = N_{lev} + 1$ refers to the upper boundary of the upper level, and $k = 0$ to the lower boundary of the lower level. The possible vertical resolution are 19, 41, 39 and 90 levels. In this work the vertical resolution L19 was chosen, which is precise enough for the studies here performed and keeps low the amount of computational time required. The time step of the model is dependent on the chosen horizontal and vertical resolution to fulfill the Courant-Friedrich-Lewy (CFL) criterion, a condition for the numerical solution of partial equations. The CFL criterion applied to this model prescribes that the time step must be shorter than the time for an air parcel to travel adjacent grid points. The standard ECHAM5 time step for the resolution T42L19 is 30 minutes, but it has been set here to 24 minutes in order to reach a higher model stability.

MESSy is the acronym for Modular Earth Sub-model System (*Jöckel et al.*, 2005, 2006), developed at the Max-Planck-Institute for Chemistry, Mainz. MESSy is the link between the sub-models and the base model, ECHAM5 in this case, and among the sub-models themselves. MESSy is composed by four levels:

- the Base Model Layer, which comprises the GCM;
- the Base Model Interface Layer, which is responsible for the control of the sub-models, for the transfer of data to and from the sub-models, and for the model output;
- the Sub-Models Interface Layer, which handles the internal data transformation in each sub-model and the sub-model specific procedures as the call of subroutines;
- the Sub-model Core Layer, which consists of the box models of each sub-model and can be used independently from the other layers.

The sub-models used in this work are listed in Tab. 4.1. Those relevant for aerosol dynamics and chemistry are presented in Sec. 4.3, apart from MADEsoot that has been described in detail in Ch. 3. The version of MESSy used in this work is the version 1.4.

MADE has been briefly described in Sec 3.1. The aerosol processes are simulated by MADE in a similar way as MADEsoot does. A detailed description of MADE is presented in *Lauer et al.* (2005) and *Lauer and Hendricks* (2006).

4.2 Modifications for modeling the upper troposphere

The studies conducted with E5/M-MADE in *Lauer et al.* (2007) aimed to quantify the impact of ocean-going ships on aerosols. They focused on the aerosol concentrations in the boundary layer, where the model had been rigorously evaluated and performs well. On the other hand, the vertical profile of the aerosol concentration calculated with E5/M-MADE showed a deficiency in the UTLS above 500 hPa, a region where the formation of ice particles is particularly evident. Since this study focuses on the concentration of ice nuclei, the

Sub-model	Function	Reference
CONVECT	Original ECHAM5 convection schema	<i>Tiedtke (1989); Nordeng (1994)</i>
CVTRANS	Transport of tracers caused by convection	<i>Tost (2006)</i>
DRYDEP	gas phase and aerosols dry deposition	<i>Kerkweg et al. (2006a)</i>
H2O	Initialization of H ₂ O in the stratosphere and mesosphere from satellite observations and feedback with specific humidity	<i>Lelieveld et al. (2007)</i>
JVAL	Calculation of photolysis rate coefficients	<i>Landgraf and Crutzen (1998)</i>
LNOX	Production of NO _x by lightening	<i>Price and Rind (1992)</i>
MADE	Aerosol microphysics	<i>Lauer et al. (2005)</i>
MADEsoot	Aerosol microphysics	this study
MECCA	Tropospheric and stratospheric chemistry	<i>Sander et al. (2005)</i>
OFFLEM	Offline emissions	<i>Kerkweg et al. (2006b)</i>
ONLEM	Online emissions	<i>Kerkweg et al. (2006b)</i>
RAD4ALL	Original ECHAM5 radiation model	<i>Roeckner et al. (2003)</i>
SCAV	Wet deposition and liquid phase chemistry	<i>Tost et al. (2006)</i>
SEDI	Sedimentation of aerosols	<i>Kerkweg et al. (2006a)</i>
TNUDGE	Nudging of tracers	<i>Kerkweg et al. (2006b)</i>
TROPOP	Calculation of the altitude of the tropopause	-
Cloud	Cloud physics	<i>Lohmann (2002a)</i>

Table 4.1: List of the sub-models that has been used in this work. The sub-model responsible for cloud physics has been developed by *Lohmann (2002a)* and is not included in the standard ECHAM5/MESSy 1.4.

performance of the model in that region had been improved before implementing the new aerosol sub-model MADEsoot.

To obtain a reliable description of the aerosol population in the UTLS, the model had to be modified in particular in the depiction of the cloud scavenging processes, i.e. the uptake of aerosols by cloud droplets or ice crystals through the collision between aerosols and falling cloud particles or through the nucleation of new cloud particles around them. Scavenging is described in E5/M by the sub-model SCAV (*Tost et al., 2006*).

Scavenging of aerosols by ice crystals. The version of SCAV included in the standard E/M-v1.4 describes separately the uptake of aerosol particles by liquid water droplets and by ice particles, but the amount of aerosol that is washed out is weighted in both case with the rain flux. If scav_i and scav_w are the scavenging coefficients for ice and water respectively, the total scavenging coefficient is the sum of the two

$$\text{scav}_{tot} = \text{scav}_i + \text{scav}_w. \quad (4.3)$$

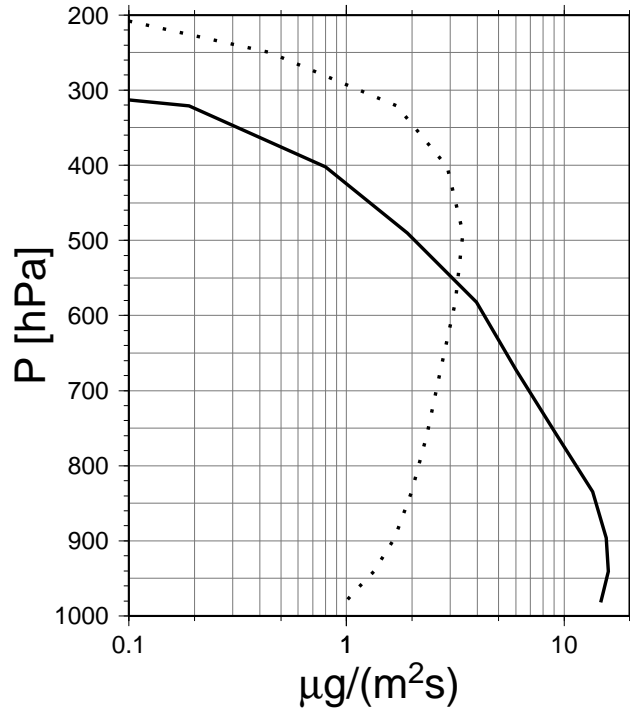


Figure 4.1: Vertical profile of the globally averaged rain (solid line) and snow (dotted line) precipitation rate, for a global average of a two years simulation with E5/M-MADE.

The concentration of interstitial aerosol, i.e. the aerosol that has not been taken up by cloud particles, is

$$c(t + \Delta t) = c(t) e^{-\text{scav}_{tot}\Delta t}, \quad (4.4)$$

and the concentration of scavenged aerosol, i.e. the aerosol that has been taken up by cloud droplets but not yet washed out, is

$$c_{\text{scav}} = c(t) - c(t + \Delta t). \quad (4.5)$$

The amount of the aerosol that is washed out is obtained multiplying the scavenged aerosol by the rain formation rate f_r

$$c_{\text{washed out}} = c_{\text{scav}} \times f_r. \quad (4.6)$$

If the snow flux is negligible with respect to the rain flux, as it mostly happens in the lower troposphere, this simplification does not cause any problem; in the UTLS, however, the snow flux is larger than the rain flux, as shown in Fig.4.1, and this simplification is not acceptable.

The modified version of SCAV developed in this study takes into account both the snow and the rain fluxes and provides a description of the wash out of aerosols through the uptake by ice particles suitable also for the UTLS. The amount of aerosol that is scavenged by ice crystals and by cloud droplets is calculated separately:

$$c_{\text{scav. ice}} = c(t) (1 - e^{\text{scav}_i\Delta t}) \quad (4.7)$$

$$c_{\text{scav. liquid}} = c(t) (1 - e^{\text{scav}_l\Delta t}), \quad (4.8)$$

and the amount of aerosols that is removed by precipitation is calculated taking into account both the rain and the snow formation rate f_r and f_s :

$$c_{\text{washed out}} = c_{\text{scav. ice}} \times f_s + c_{\text{scav. liquid}} \times f_r. \quad (4.9)$$

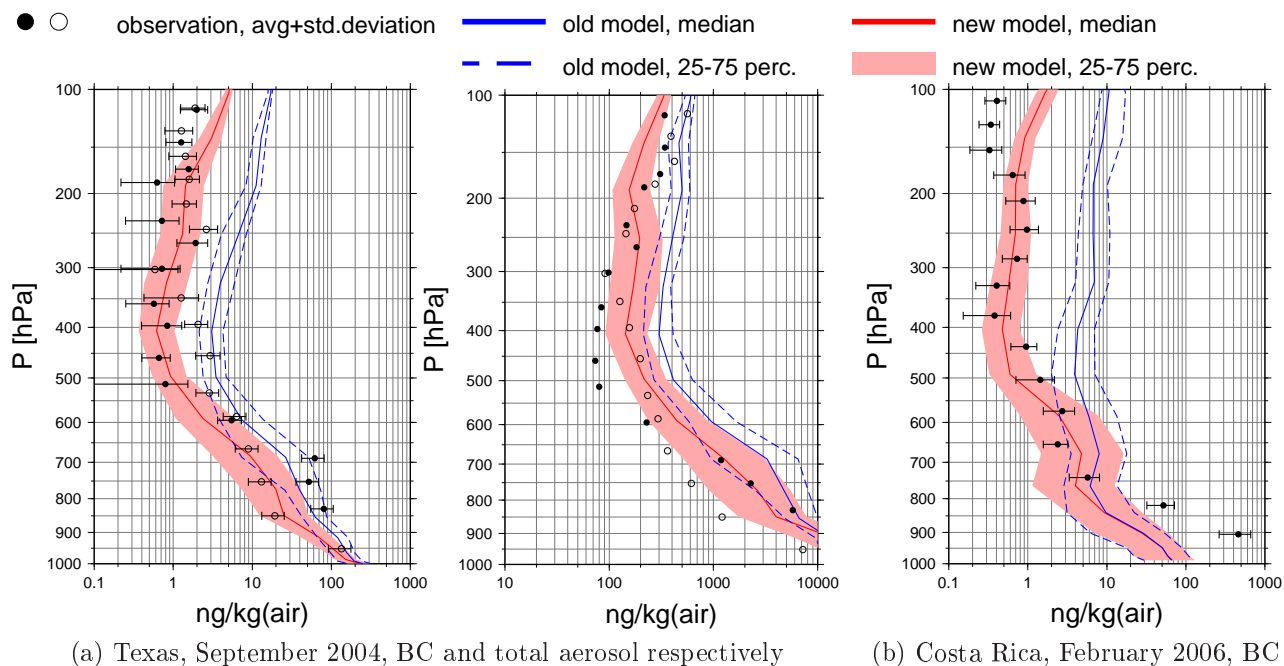


Figure 4.2: Vertical profile of BC and total aerosol mass concentrations simulated by ECHAM5/MESSy-MADE before and after the modification introduced to apply the model to the UTLS. The experimental data are from *Schwarz et al.* (2006, 2008b). Solid and open circles correspond to two different flights.

Ice scavenging in convective clouds. SCAV simulates the uptake of aerosol particles by liquid water droplets through nucleation and impact scavenging with two different parameterizations. On the contrary, the distinction between impact and nucleation scavenging is not done for ice scavenging, which is simply parameterized by assuming that 5% of the given aerosol is taken up by ice particles, both in stratiform and in convective clouds. Assuming higher supersaturation, the ice scavenging coefficient in convective clouds is here set to 90% (*Ekman et al.*, 2004).

Ice scavenging by heterogeneous freezing. To simulate the higher ability of BC and dust particles to act as ice nuclei (*Seinfeld and Pandis*, 2006), different ice scavenging parameters for hydrophilic and hydrophobic species were introduced. According to *Verheggen et al.* (2007) and fitting the vertical profile of BC and total aerosol presented in *Schwarz et al.* (2006, 2008b), it is assumed here that the aerosol fraction that is scavenged by ice in stratiform clouds is 10% for the mass of BC and dust and 5% for all other tracers. Only 5% of the number concentration is scavenged by ice. This brings to an inconsistency in the treatment of the number concentration, since MADE does not allow to simulate which number fraction of particles contains BC or dust. This inconsistency will be resolved with the implementation of MADEsoot.

Fig.4.2 shows the vertical profile of BC and total aerosol mass concentration calculated with the original and the modified version of E5/M-MADE, compared to airborne measurements. The experimental data were taken with a single particle soot photometer during a campaign over Texas in November 2004 (*Schwarz et al.*, 2006) and over Costa Rica in February 2006 (*Schwarz et al.*, 2008b). The version of E5/M-MADE developed in this work has been evaluated also with data from other campaigns, whose results are not reported here. The results of these evaluations are shown in Ch. 5 for E5/M-MADEsoot, that has been developed starting from this version of E5/M-MADE.

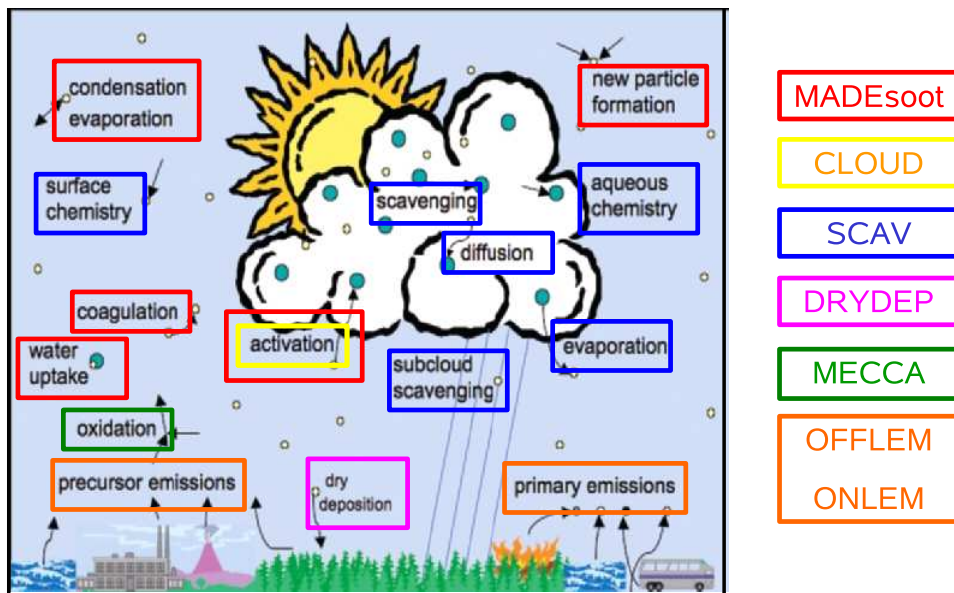


Figure 4.3: Atmospheric processes relevant for aerosol and relative sub-models. Modified from *Ghan and Schwartz (2007)*.

4.3 Implementation of MADEsoot in the global model ECHAM5/MESSy

Aerosols are emitted directly (primary aerosol) or form via the oxidation of precursor gases (secondary aerosol). The relative humidity of air and the availability of condensable species controls the particle growth or evaporation. Between clouds and aerosols there is a mutual interaction: the uptake of aerosols by cloud particles followed by cloud evaporation can alter particle properties, and at the same time aerosols can serve as cloud condensation nuclei or ice nuclei for new cloud particle formation. Dry deposition and scavenging by precipitation eventually remove aerosols from the atmosphere. The major processes controlling the life cycle of atmospheric aerosols and the sub-models that describe them in E5/M-MADEsoot are shown in Fig. 4.3. The implementation of the box model of MADEsoot in the three-dimensional model requires the coupling between the aerosol sub-model and the sub-models responsible for those processes, and the modification of those sub-models to account for the new features of MADEsoot that were not present in MADE. Fig. 4.4 presents a schematic representation of E5/M-MADEsoot.

4.3.1 Sources of aerosols

The emissions of aerosols and gases in the atmosphere are described by the sub-models OFFLEM and ONLEM. OFFLEM is responsible for the offline emissions, i.e. external fields that are provided as input to E5/M, while ONLEM handles the online emissions, i.e. the emissions whose amount is calculated by the model itself depending on meteorological conditions. The data set for the offline aerosol emissions used in this work is the inventory defined for the AeroCom Experiment “B” (*Dentener et al., 2006*), that prescribes typical emission values for the year 2000.

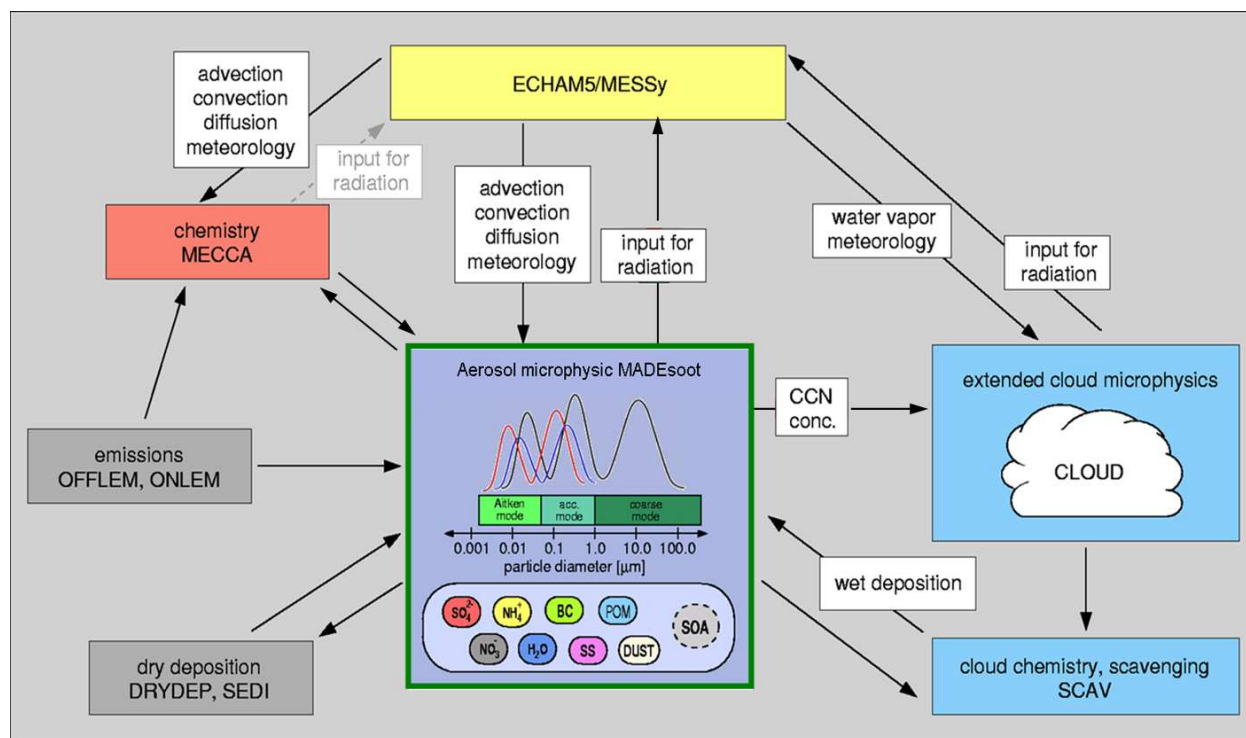


Figure 4.4: Schematic representation of the model system ECHAM5/MESSy-MADEsoot. Picture by Axel Lauer (modified).

Primary Emissions

The aerosol species emitted in E5/M-MADEsoot are SO_4^{2-} , black carbon, particulate organic matter (POM), dust and sea salt. In E5/M-MADE these species had to be split only among three modes, while in E5/M-MADEsoot this has to be done among seven modes. The emitted soluble aerosol that were assigned in E5/M-MADE to the Aitken mode are to be split between the Aitken modes with BC and the one without BC, and the emitted BC is to be split between the internally and the externally mixed BC modes. The same has to be done for the emissions that were assigned by E5/M-MADE to the accumulation mode. The emissions assigned to the coarse mode are the same in E5/MESSy-MADE and E5/M-MADEsoot.

The assignment of the emissions to the respective mode is not part of the global model, it has to be done separately before starting the simulation. E5/M-MADE(soot) reads files where the emissions are already divided among the modes.

Black carbon. The sources of BC included here are large scale biomass burning, biofuel and fossil fuel combustion. BC emissions are split between the internally and the externally mixed modes, assuming that 80% of the emitted BC is in an external mixture and the remaining 20% in an internal mixture. BC from biofuel and biomass burning is assigned to the accumulation mode, BC from fossil fuel to the Aitken mode. BC emissions from large scale fire are based on the Global Fire Emission Database (GFED) inventory (*van der Werf et al.*, 2004) and are an average of the values between 1997 and 2002. They are injected between the surface and 6 km altitude, depending on the kind of fire and the latitude where it takes place. Bio and fossil fuel BC emissions, from the Speciated Particulate Emissions Wizard (SPEW) inventory for 1996 (*Bond et al.*, 2004), are emitted at surface level.

SO_4^{2-} . Sulfur from volcanic, shipping, traffic, off-road, biomass burning and domestic sources is emitted as SO_2 (97.5%) and particulate SO_4^{2-} (2.5%). 50% of the SO_4^{2-} emitted by volcanic sources is assigned to the Aitken mode and 50% to the accumulation mode, SO_4^{2-} from biomass burning is assigned to the accumulation mode and SO_4^{2-} from all other sources to the Aitken mode. The amount of particulate SO_4^{2-} assigned to the internally mixed modes with BC and dust is the minimum needed to define the 20% of the emitted BC mass as internally mixed, according to the definition explained in Sec. 3.2.6. If not enough SO_4^{2-} is available, the missing mass is taken from the emitted POM. Bio and fossil fuel sulfur emissions are from *Cofala et al.* (2005), except those from shipping which follow the Emission Database for Global Atmospheric Research (EDGARv3.2 FT2000¹, *Olivier et al.* (2005)) and are injected at surface level. Volcanic sulfur emissions data are based on the GEIA inventory (*Andres and Kasgnoc*, 1998) and are injected at different altitudes.

Particulate organic matter. POM is emitted by the same sources as BC. As BC, POM from biofuel and biomass burning is assigned to the accumulation mode, POM from fossil fuel to the Aitken mode. For the splitting between the modes with or without BC, see the paragraph about SO_4 emissions. for the injection altitude and the database used, see the paragraph about BC.

Dust. Emissions of dust are based on simulations with near surface winds of the year 2000 generated by the NASA Goddard Earth Observing System Data Assimilation System (GEOS DAS). 98.6% of the emitted dust is assigned to the coarse mode and the remaining 1.4% to the externally mixed accumulation mode. No dust is assigned to the internally mixed accumulation mode, since the major emission regions of dust are poor of soluble material, and the lifetime of externally mixed dust particles is comparatively long (*Zhang et al.*, 2003). An online calculation of dust emissions, that is also allowed by the model, is not used here, since the diameter of the resulting dust particles is larger than the typical coarse mode of MADEsoot.

Sea Salt. Sea salt emissions are calculated online by the sub-model ONLEM, depending on the wind speed and on the sea fraction and ice coverage of the grid cell (*Ganzeveld et al.*, 2006). The emissions are assigned to the accumulation and coarse modes following *Guelle et al.* (2001).

The set of emissions provided by the AeroCom Experiment B includes the mass concentrations of all species described above and, additionally, the number concentration of the emitted dust. When only the mass is available, a log normal size distribution has to be assumed to calculate the number concentrations. The assumed distribution of the emissions assigned to the Aitken and to the accumulation modes have standard deviation equal to 1.8 and median diameter of 0.03 μm and 0.08 μm , respectively.

Emissions of precursor gases

Secondary aerosols result from the change of phase following oxidation of precursor gases as dimethyl sulfide (DMS), SO_2 , NO_x , NH_3 and organic gases. The chemistry sub-model MECCA calculates the reaction rates of the oxidation processes of DMS, SO_2 and NO_x . These processes give as product HNO_3 and H_2SO_4 , whose condensation, together with the

¹<http://www.mnp.nl/edgar>

condensation of NH_3 and organic gases, is calculated by MADEsoot as explained in Sec. 3.2.1 and Sec. 3.2.2.

DMS. Oceanic DMS emissions are calculated online by ONLEM from the 10m wind speed and a climatology of the ocean water DMS concentration (*Ganzeveld et al.*, 2006). Terrestrial DMS, much smaller than oceanic DMS, is emitted offline following *Spiro et al.* (1992).

SO_2 . SO_2 emissions have already been described in the paragraph about particulate SO_4 emissions. Besides the sources that have been mentioned for SO_4 , SO_2 is emitted from industry and power plants. These emissions are injected between 100 and 300 m.

NO_x The adopted NO_x emissions are those described in *Ganzeveld et al.* (2006) but with shipping emissions from EDGAR3.2 FT2000 *Olivier et al.* (2005) instead of those from *Eyring et al.* (2005), in order to be consistent with the shipping emissions used in the AeroCom experiment. Additionally the DLR inventory (*Schmitt and Brunner*, 1997) is used for NO emissions from air traffic, and NO_x from lightening is calculated online by the sub-model LNOX following *Price and Rind* (1992).

NH_3 NH_3 emissions are the standard MESSy emissions described in *Ganzeveld et al.* (2006).

Condensable organic gases. The production of condensable organic gases, whose condensation into secondary organic aerosol (SOA) is calculated by MADE, is from the AeroCom data set. They are based on the assumption that 15% of natural terpene emissions form SOA. SOA forms on short time scales, therefore SOA precursors emissions are assumed to condense instantaneously onto pre-existing aerosol particles and their transport and chemistry is neglected.

4.3.2 Activation of aerosol particles

The microphysics of clouds is simulated with the model developed by *Lohmann* (2002a). This cloud model is not included in the standard E5/M, and has been implemented in it by *Lauer et al.* (2007). This cloud microphysical model solves prognostic equations not only for cloud liquid water and cloud ice, as the standard E5/M sub-model CLOUD does, but also for the number concentration of cloud droplets and ice crystals. The cloud microphysics parameterized by the sub-model used in this work includes (*Lohmann et al.*, 1999; *Lohmann and Kärcher*, 2002): growth of cloud droplets through condensation, growth of ice crystal through deposition of water vapor, homogeneous and heterogeneous freezing of cloud droplets, auto-conversion of cloud droplets and ice crystals to rain and snow respectively, aggregation of ice crystals, accretion of cloud droplets to rain and of ice crystals and cloud droplets to snow, evaporation of liquid water and rain and sublimation and melting of cloud ice and snow.

The number concentration of cloud condensation nuclei (CCN) is calculated according to *Abdul-Razzak and Ghan* (2000) as a function of the diameter of the modes, and is provided to the cloud sub-model. Externally mixed BC and dust particles cannot act as CCN, but, since MADE cannot simulate their number concentration, they cannot be excluded from the simulation of the activation process. The number of CCN is therefore calculated over the total Aitken mode and accumulation mode number concentration. On the other hand, this can be done in MADEsoot, which can simulate how many BC and dust particles are

internally mixed and how many externally mixed. In E5/M-MADEsoot the number of CCN is calculated only over the number concentration of the soluble modes and of the internally mixed BC and dust modes (akn_{sol} , acc_{sol} , akn_{mix} and acc_{mix}).

4.3.3 Effect of aerosol on radiation

The aerosol optical properties are calculated by MADEsoot in the Sub-Models Interface Layer (see Sec. 4.1) and read by the E5/M radiation sub-model RAD4ALL. In analogy to MADE, MADEsoot calculates the refraction index of an internal mixture as the average of the refractive index of each component, weighted with its relative volume (*Ouimette and Flagan, 1982*).

The refractive index and the wet radius of each mode are used to identify the extinction cross section, single scattering albedo and asymmetry factor of the particles in previously generated look-up tables, which have been calculated by *Lauer et al. (2007)* for Mie scattering using the libRadtran code (*Mayer and Kylling, 2005*). The aerosol optical thickness is the sum of the optical thickness of each mode, which is calculated by multiplying the extinction cross section of each mode by the respective particle number concentration, integrated along a vertical layer. The procedure to calculate the aerosol optical properties is the same in E5/M-MADE and E5/M-MADEsoot.

4.3.4 Scavenging by ice and rain and evaporation of droplets

As mentioned in Sec. 4.2, SCAV uses different parameterization for impact and nucleation scavenging. Since externally mixed BC and dust particles are not efficient as cloud condensation nuclei, only internally mixed BC and dust particles can be scavenged through nucleation scavenging. On the other hand impact scavenging acts in the same way on all aerosol types.

ECHAM5/MESSy-MADE. E5/M-MADE uses two different tracers for the mass concentration of externally and internally mixed BC (Sec 3.2.6), but not for their number concentrations. This brings to an inconsistency in the simulation of nucleation scavenging: while only the mass of the internally mixed BC is scavenged through nucleation scavenging, the same cannot be done for its number concentration. To at least parameterize the loss in the aerosol number concentration, it is assumed by E5/M-MADE to be affected by the nucleation scavenging proportionally to the mass of internally mixed BC present in the mode, assuming that the internally and externally mixed BC particles are homogeneously distributed over the size distribution. Dust is not removed at all through nucleation scavenging.

ECHAM5/MESSy-MADEsoot. In E5/M-MADEsoot nucleation scavenging is applied only to the hydrophilic particles (akn_{sol} and acc_{sol} , akn_{mix} and acc_{mix}), and not to the hydrophobic ones (akn_{ext} and acc_{ext}). In contrast to MADE, MADEsoot allows for a consistent parameterization of the mass and of the number concentration, since the number concentrations of the BC and dust containing particles and of the BC and dust free particles are simulated independently.

Furthermore, different ice scavenging parameters for soluble and insoluble particles were introduced in E5/M-MADEsoot to simulate the higher ability of BC and dust particles to act as ice nuclei (*Seinfeld and Pandis, 2006*). It is assumed here that 5% of the soluble modes (akn_{sol} and acc_{sol}) and 10% of the insoluble BC and dust-containing modes (akn_{ext} , acc_{ext} , akn_{mix} and acc_{mix}) is scavenged by ice in stratiform clouds. These fractions are applied both to the number and to the mass concentrations.

The aerosols taken up by a cloud particle tend to compact together and, once the cloud droplets or ice crystals evaporates, a larger particle is released in the atmosphere. To simulate this process in the model, the Aitken mode particles that have been taken up by cloud particles disappear and their mass is transferred to the accumulation mode.

Moreover, a droplet that has nucleated around an accumulation mode soluble particle can scavenge an Aitken mode particle containing BC. When this happens, the mass of the soluble particle have to be transferred to the internally mixed accumulation mode with BC and dust. If the BC containing particle is externally mixed, than also its mass has to be transferred to the internally mixed modes, and the number concentration of the internally mixed mode will increase. If the BC containing particle is internally mixed, the number concentration of the internally mixed mode is unchanged. The scavenged externally mixed BC and dust are assumed to be aged after the evaporation of the cloud particle, and are transferred to the internally mixed modes. This process, together with condensation and coagulation, concurs to the ageing of externally mixed BC and dust aerosols.

The number concentration $N_{\text{transferred}}$ of soluble particles that is contaminated by BC and dust is calculated from the number concentrations of the particles that are taken up by cloud droplets. if $N_{\text{transferred}}$ is lower than the number concentration of the soluble accumulation mode N_{accsol} , this fraction is equal to

$$N_{\text{transferred}} = \frac{N_{\text{accsol}}}{N_{\text{accTot}}} (N_{\text{akn}_{\text{mix}}} + N_{\text{akn}_{\text{ext}}}). \quad (4.10)$$

If $N_{\text{transferred}} > N_{\text{accsol}}$, all soluble particles are transferred to the internally mixed accumulation mode with BC and dust and $N_{\text{transferred}} = N_{\text{accsol}}$. Eq. [4.10] assumes that only accumulation mode particles can be activated, and that during the ageing process the externally mixed BC particles in the Aitken mode are homogeneously distributed to the accumulation mode particles.

4.3.5 Dry deposition

The dry deposition of aerosols is simulated by the sub-models DRYDEP and SEDI (*Kerkweg et al.*, 2006a), which consider the role of sedimentation, turbulence, impaction and Brownian diffusion. The dry deposition velocity is calculated as a function of the wet radius and mass of the particles, that are read by DRYDEP from the output of E5/M-MADEsoot. Dry deposition is simulated exactly as in E5/M-MADE.

Chapter 5

Reference simulation and model evaluation

5.1 Model set-up

The resolution used in the reference study is T42L19, corresponding to a horizontal grid of around $2.5^\circ \times 2.5^\circ$ and 19 vertical levels. A simulation with 41 vertical level has also been conducted: Since the aerosol concentrations have not shown relevant differences from those calculated using 19 vertical levels, and taking into account that the computational time needed by L41 is twice longer than the one needed by L19, the lower vertical resolution has been used. The species present in each mode are those reported in Tab. 3.1, except for sea salt (SS) that is present only in the accumulation (acc_{sol} , acc_{mix} and acc_{ext}) and in the coarse modes, given the typical large size of SS particles.

The model results shown in this chapter and in Chapter 6, unless otherwise specified, are based on 11 years simulation runs. Since the aerosol concentrations are initialized to zero at each simulation start, the first simulated year is needed as spin-up, and is not included in the statistics (Fig. 5.1). The emissions and boundary conditions are typical for the year 2000. Sea surface temperature and ice cover fraction are based on the climatological mean of the Hadley Center data set (*Rayner et al.*, 2003) over the period 1995-2004. The emissions of trace gases, except for SO_2 and dimethylsulfate (DMS), are chosen according to the EDGARv3.2-FT2000 inventory, as described in *Ganzeveld et al.* (2006). SO_2 and aerosol emissions (except SS) are those used for the AeroCom Experiment B (*Textor et al.*, 2007) as described in *Dentener et al.* (2006) (see Sec. 4.3.1). Sea DMS and SS emissions are

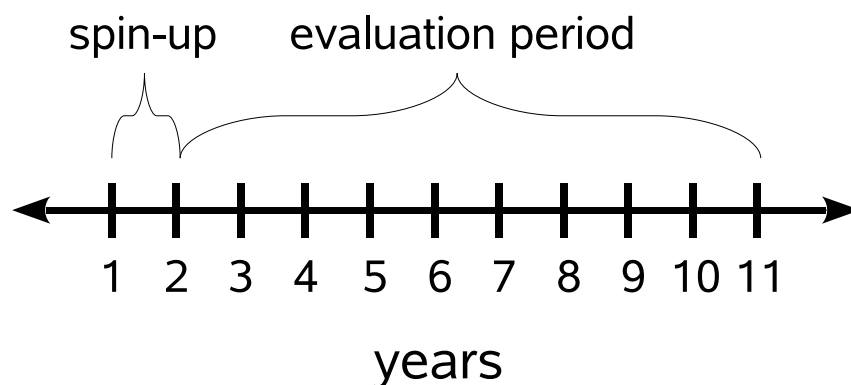


Figure 5.1: Timescale of the simulations performed in this work.

Masses (Tg/yr)		Particle number (particles/yr)	
SO ₂	139.0831	akn _{sol}	5.0218623×10^{28}
SO ₄	1.978900	acc _{sol}	1.0561161×10^{28}
BC	8.191910	akn _{mix}	4.1863800×10^{27}
POM	27.93921	acc _{mix}	1.5737092×10^{27}
DU	1675.207	akn _{ext}	1.5169698×10^{28}
SS	online	acc _{ext}	6.0365568×10^{26}
		cor	4.6387304×10^{26}

Table 5.1: Emitted burdens of the aerosol species.

calculated online. Tab. 5.1 summarizes the emitted global amount of the aerosol species.

The mass fraction x of soluble material in the externally mixed BC and dust modes (akn_{ext} and acc_{ext}) which is required to define them as internally mixed (see Sec. 3.2.6) has been set in the reference run to 10%, following *Zhang et al.* (2008) and *Weingartner et al.* (1997). The sensitivity of the aerosol concentrations to changes in the value of x have been investigated by running two additional simulations with x equal to 5% and 50%, and all the evaluation comparisons shown in the following have been repeated for each of these tests. The most relevant results of these studies are shown in Sec. 6.1.3. The simulation with $x = 5\%$ was also used to compare the time scale of the ageing process with *Riemer et al.* (2004) (see Sec. 6.3.2).

The chemistry implemented in the adopted model version is a basic tropospheric chemistry including sulfur chemistry (DMS, SO₂). The complete list of chemical reactions calculated by MECCA (gas phase chemistry) and SCAV (liquid phase chemistry and heterogeneous chemistry) is reported in App. C.

Before starting the first production run, the model set-up has been tuned relatively to the radiation balance, acting on the parameters that are not well known, as e.g. those for the conversion of cloud particles into rain or snow. Modifying these parameters in the range of reasonable values, it is possible to obtain a long (LCF) and short wave cloud forcing (SCF) close to experimental data. The reference values are summarized in *Lohmann et al.* (2007). The adopted values of cloud forcing used are the ones derived from Earth Radiation Budget Experiment (ERBE) observation by *Kiehl and Trenberth* (1997), equal to -50 W/m² for SCF and 30 W/m² for LCF. However, LCF estimates from the TOVS satellites only amount to 22 W/m² (*Suskind et al.*, 1997; *Scott et al.*, 1999). The set of parameters chosen for the reference simulation led to a simulated LCF equal to 30 W/m² and SCF equal to -57 W/m² as the best compromise. The other variables that have been checked for the setting of the set of chosen parameters are reported in Tab. 5.2. The value of the vertically integrated cloud ice simulated by E5/M-MADEsoot is much lower than the observation. The uncertainty on the observation data of the vertically integrated ice, however, is very high, therefore the choice of the tuning parameters was not much oriented to get a good agreement of this quantity with the experimental data.

5.2 Evaluation

The evaluation of a global climate model with observations is a necessary but delicate issue. Observations are always influenced by the particular meteorological conditions of the time they are taken and by single events, as large forest fires that may occur during the period

	Unity	E5/M-MADEsoot	Observations
Vertically integrated cloud ice	[g/m ²]	8.0	26.7
Vertically integrated cloud liquid water	[g/m ²]	53	50-84
Vertically integrated water vapor	[kg/m ²]	26.3	25.1
Cloud cover	[%]	69	62-67
Total precipitation rate	[mm/day]	2.94	2.74
Short wave cloud forcing	[W/m ²]	-57	-50
Long wave cloud forcing	[W/m ²]	31	22-30

Table 5.2: Annual global mean values used for the setting of the tuning parameters. The reference observation data are those used by *Lohmann et al.* (2007).

of measurements. Furthermore, a global model cannot correctly reproduce subscale effects that can influence the observations. If, for instance, measurements are taken close to a city, the observed aerosol concentration will likely be very high and will show a large variability depending on the station being upwind or downwind of the city.

Therefore the observations suitable for the evaluation of a climate model should possibly cover large regions or long periods of time, to decouple the results from the meteorological conditions occurring during the campaign and from any geographical local effect. These requirements are close to be satisfied by e.g. aircraft campaigns, that are flown over very large areas, and by long series of surface measurements, that can be collected over several years.

5.2.1 Vertical profiles of aerosol mass concentrations

The vertical profiles of the simulated aerosol concentrations have been compared with measurements taken with an airborne Single Particle Soot Photometer (SP2) over Texas by *Schwarz et al.* (2006) in November 2004, over Costa Rica during the CR-AVE (*Schwarz et al.*, 2008b) and TC4 campaigns¹ (*Spackman et al.*, manuscript in preparation, 2009) in February 2006 and August 2007 respectively, and over northern Europe during the CIRRUS campaign (*Baumgardner et al.*, 2008) in November 2006. Fig. 5.2 shows the comparison between simulated and measured mass concentrations of BC, total aerosol and particles with no detectable BC. The average of the concentrations and the relative standard deviation are not always the best indication of the variability of the data, since the distributions can be non-Gaussian and strongly asymmetric. When available, medians and percentiles have also been plotted. For clarity, only positive standard deviations are drawn for the simulated concentrations as well as for the CIRRUS data.

The simulated vertical profiles were obtained from climatological means of the aerosol concentrations for the month the campaign took place. In the case of the Texas campaign and of CIRRUS, the exact profiles of the flights were available: The simulated concentrations have been calculated only on the grid box crossed by the flight, projecting the flight profiles on the E5/M-MADEsoot grid. In the case of TC4 and CR-AVE only the boundaries of the examined region were known and the simulated profiles have been calculated over a rectangular region containing the flight trajectory (85°W-79.5°W, 2°N-10°N for TC4 and 85°W-79°W, 1°S-11°N for CR-AVE). The experimental data are averaged over 1-km bins.

¹The data sets of these three campaigns are publicly available through the NASA archive at <http://espoarchive.arc.nasa.gov/archive/arcs/>

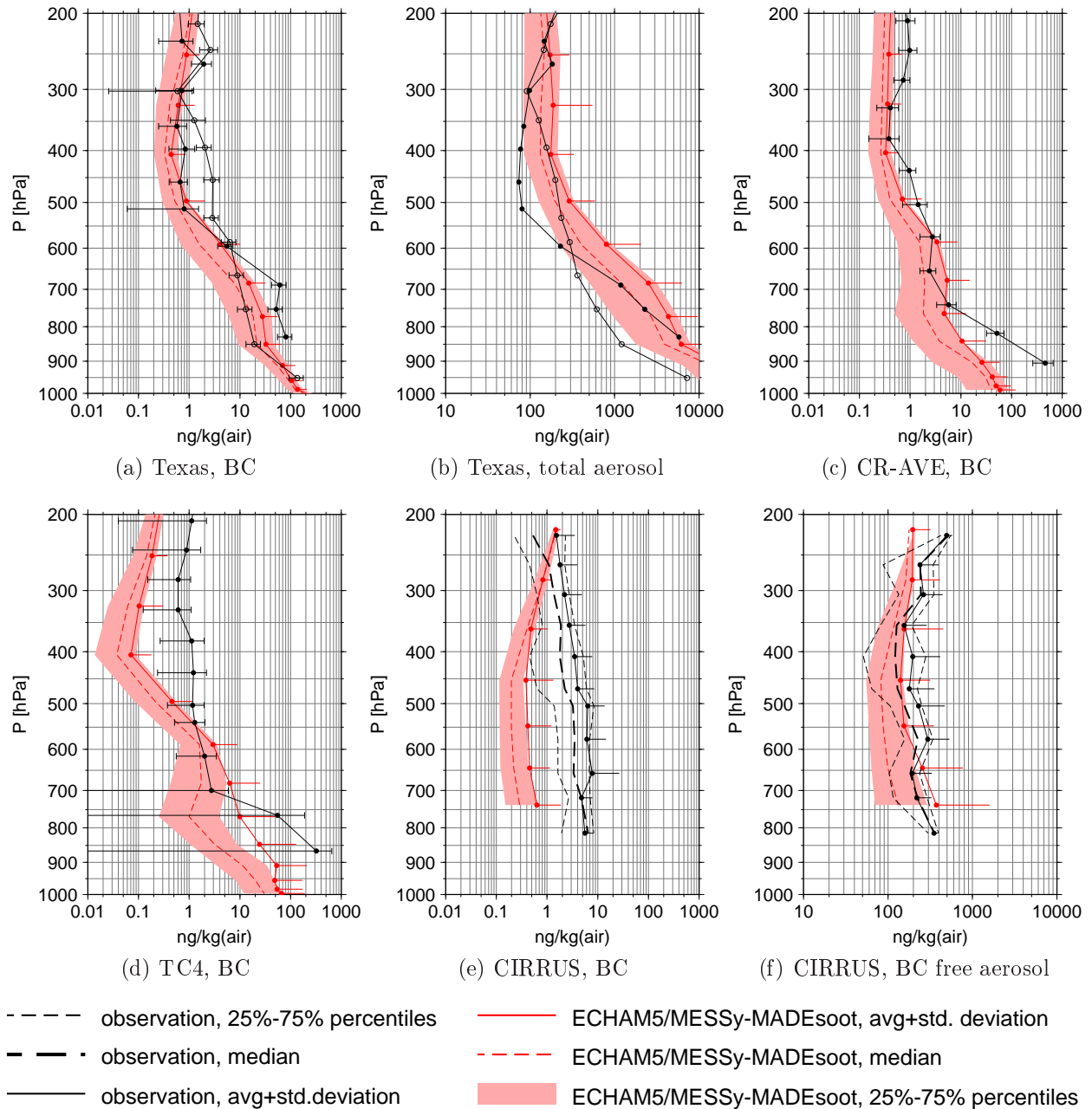


Figure 5.2: Comparison of the vertical profile of BC, total aerosol and BC free aerosol mass concentrations simulated by E5/M-MADEsoot and measured by *Schwarz et al.* (2006, 2008b) and *Baumgardner et al.* (2008). Open and solid circles in the Texas campaign correspond to two different flights. The CIRRUS observations were strongly influenced by some values which are much larger or much smaller than the others, therefore the average and the standard deviations are not the best tool to make a statistic of the data. For strongly asymmetric set of data the median and 25%-75% percentiles, which are also shown as dashed lines, are more suitable for a comparison. The average and standard deviations are also shown, but for clarity only on the positive side.

The simulated profiles are in good agreement with the experimental data. In the case of the TC4 campaign (Fig. 5.2d) the simulated BC mass concentration is one order of magnitude lower than the measurements at most altitudes. This could be due to the high convective cloud coverage that the model reproduces in August over Costa Rica, which may amplify the modifications implemented in the model for ice scavenging in convective clouds

(see Sec. 4.2).

The experimental profiles of the CIRRUS campaign refer to clear sky conditions, therefore the statistics of the simulated concentrations has been calculated including only those grid boxes where the cloud cover is lower than 1%. The campaign took place over Europe between 50° N and 70° N: This region shows a strong latitudinal gradient in the aerosol concentrations that makes a precise knowledge of the history of the measured air masses important for meaningful comparison between simulations and observations. While the simulated BC vertical profile is lower than the measured one, the profile of the BC free mass is in very good agreement with the experimental data. This discrepancy may be related to the fact that the sources of BC free particles are more homogeneously distributed over the observed area with respect to BC sources, which are mainly concentrated in the southern part of the observed region. Therefore the concentration of BC particles is more related to the meteorological conditions and to the trajectory of the air masses. This makes the simulation of their concentration with a global climate model quite difficult, given the rough resolution of the model. Furthermore, the distribution of the BC sources in Europe presents a very large regional variability, which cannot be represented in the large model grid boxes. BC free aerosol is mainly composed by secondary aerosol species (Sec. 6.1.3): Secondary aerosol is less dependent on the sources, since the precursor gases can be transported over long distances before they are transformed in aerosol. With increasing height, indeed, the correlation between aerosol concentration and sources becomes smaller and the simulated and observed BC concentrations closer.

5.2.2 Vertical profiles of aerosol number concentrations

The vertical profile of the aerosol number concentrations has been compared with observations taken during several campaigns. As for the aerosol mass concentrations, when available median and percentiles have been used.

Fig. 5.3 shows the comparison between E5/M-MADEsoot with the vertical structure calculated by *Clarke and Kapustin (2002)* between 70°S and 70°N over the Pacific ocean. The observed profiles refer to the data taken during the GLOBE-2 (May 1990), ACE-1 (November 1995) and PEM-Tropics A (September 1996) and B (March 1999) campaigns, using an ultrafine condensation nuclei (UCN) counter to detect particles with diameter between 0.003 and 3.0 μm . The data set covers a very large geographical region (the whole Pacific ocean), as well as different seasons and years and is very suitable for a comparison with a global climate model. The simulated vertical profiles were calculated over climatological means of the months during which the observation were taken (March, May, September and November). The agreement between simulated and observed concentrations is very good. The observed profiles are nearly always inside the variability values of the model. The tests performed with the different values of the fraction x of soluble material that define BC as hydrophilic have shown very similar vertical profiles. Even though the value of x influences the efficiency of the scavenging of BC and dust particles, the number concentrations of BC and dust particles is so much lower than the one of soluble aerosols that the vertical profiles have shown no sensitivity to changes of x (see Sec. 6.1.3).

The observations shown in Fig. 5.4a and 5.4b were taken as part of the INCA project (*Minikin et al., 2003*) during nine flights starting from Prestwick, Scotland, in October 2000 and ten flights from Punta Arenas, Chile, in March and April 2000. Fig. 5.4c refers to the measurements by *Petzold et al. (2002)* taken during the LACE campaign, that took place over the area of Berlin (13.5°-14.5°E, 51.5°-52.7°N) in August 1998. Since the aerosol concentrations were measured only during the takeoff and landing phase of the flights, the simulated profile are calculated over the grid box containing the airport (4.5°W, 55.5°N for

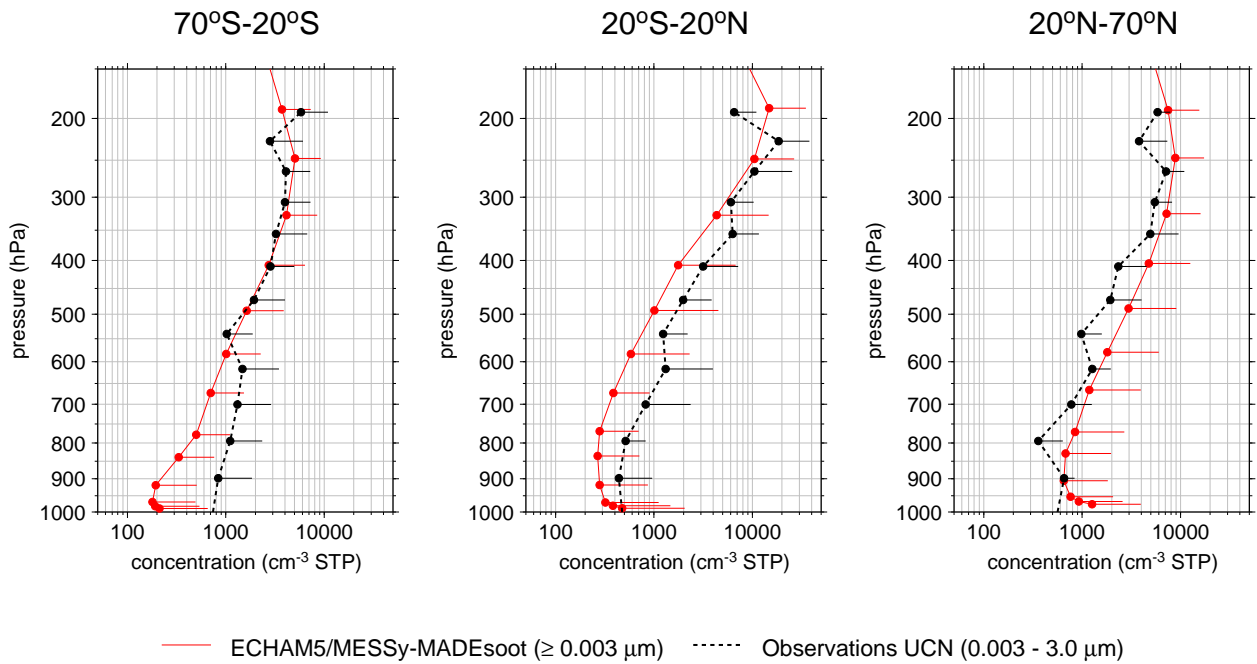


Figure 5.3: Comparison of the vertical profile of the aerosol number concentration simulated by E5/M-MADEsoot and extracted from measurements by *Clarke and Kapustin (2002)* over the Pacific ocean. The plot shows average and standard deviation, only positive for clarity.

Prestwick and 71.1°W, 53°S for Punta Arenas).

The agreement between modeled and observed profiles is particularly good in the case of Fig. 5.4b and of Fig. 5.4c, while Fig. 5.4a shows an underestimation in the modeled median number concentration below 600 hPa and an overestimation above the same level. However, the regions between the values of 25% and 75% percentiles of the measured and simulated data overlap between 850 hPa and 350 hPa. The model slightly underestimates the number concentration measured during the LACE campaign at all altitudes up to 350 hPa (Fig. 5.4c), but there is a very good agreement between model and observation in the UTLS, region of interest of this work.

Fig. 5.5 shows a comparison of the modeled and observed size distributions at different altitudes during the LACE campaign, reaching an overall good agreement. In the boundary layer, where the aerosol population is mainly influenced by the emissions, the model shows an underestimation of particles smaller than 50 nm and an overestimation of particles between 0.4 μm and 2 μm . The two figures referring to the boundary layer show the limitation of the modal approach: The number concentration of the experimental data has a clear trimodal behavior, which cannot be reproduced by MADEsoot, since the simulated coarse mode contains only sea salt and dust, species that are not abundant in the area of the campaign. If the simulated accumulation mode particles grow in the range of the coarse mode, they shift the median diameter of the whole accumulation mode toward larger values. However, even the observed coarse mode is inside the variability of the model.

In the lower free troposphere (4 km) the simulated median number concentration is lower than the measured one, but all flights fall inside the large variability of the model. The model does not reproduce the peak around 0.3 μm detected during three of the flights. These peaks may be due to meteorological conditions with a particularly inefficient scavenging of aerosols, a process that acts mainly on accumulation modes particles.

Above 6 km altitude the model overestimates the number of particles with diameter smaller than 0.1 μm . In that region the nucleation of small H_2SO_4 particles is more important

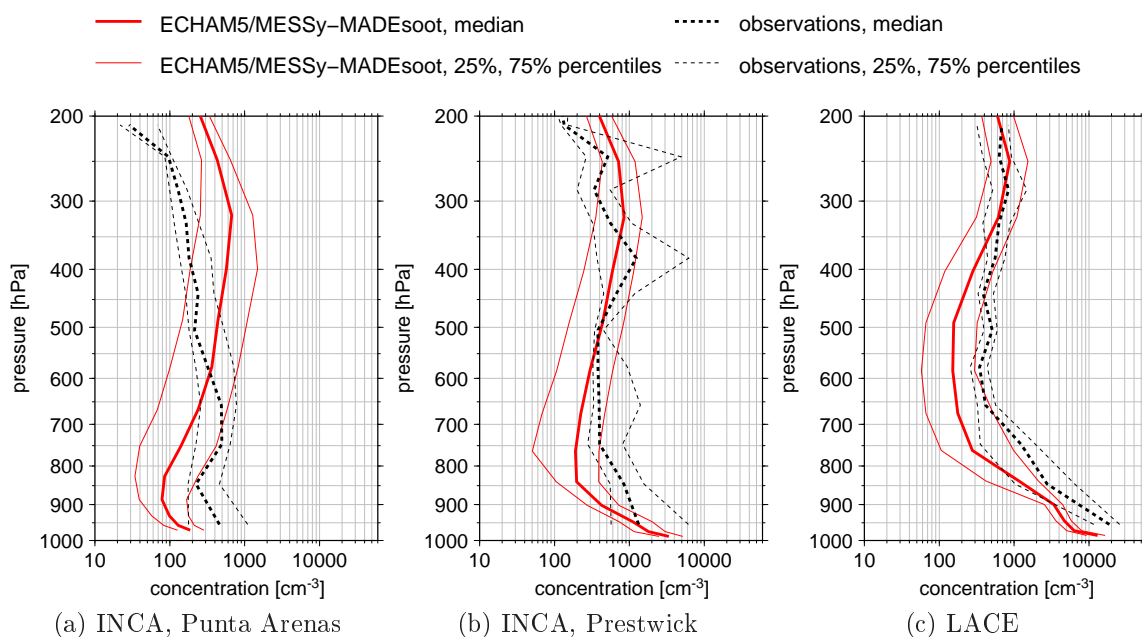


Figure 5.4: Comparison of the vertical profile of the aerosol number concentration simulated by E5/M-MADEsoot and measured by *Minikin et al.* (2003) during INCA over Punta Arenas (Chile) in March-April 2000 and over Prestwick (Scotland) in October 2000 (Fig. 5.4a and Fig. 5.4b), and by *Petzold et al.* (2002) during LACE over north Europe in August 1998 (Fig. 5.4c).

than in the boundary layer, where the higher concentration of background aerosol favors the condensation of sulfuric acid. Since the very small freshly nucleated particles are assigned to the Aitken mode, its median diameter is shifted towards smaller values. The introduction of a nucleation mode in MADEsoot would represent an improvement in the representation of the size distribution of the sub-micrometer aerosol.

5.2.3 Surface measurements

The mass concentration of BC simulated by E5/M-MADEsoot has been compared with several surface measurements from all over the world, as shown in Fig. 5.6. For each observational data set, the average of the modeled concentration is calculated over the climatological mean of the relative months in the model box where the corresponding station is located. The observations considered are the same of *Chung and Seinfeld* (2002), *Cooke et al.* (1999), *Köhler et al.* (2001), *Lioussé et al.* (1996) and *Takemura et al.* (2000). Additionally, measurements by the Interagency Monitoring of Protected Visual Environments (IMPROVE) network² are used for North America. The map of Fig. 5.7 projects the location of the measurement stations over the T42 grid of the model, and shows which stations are included in each region.

The ratio between modeled and observed BC concentration is between 1:10 and 10:1 nearly everywhere. The comparison shows that the model underestimates the BC mass concentration in the Pacific area. While the emissions of BC in the other five regions are mainly due to fossil fuel combustion, as in North America, Southeast Asia and Europe, or biomass burning, as in Africa and South America, the only emissions source of BC in the Pacific Ocean is due to shipping. Since this signal is small (*Eyring et al.*, 2005), the concentrations of BC represent background BC resulting from long-range transport. On the

²<http://vista.cira.colostate.edu/improve/>

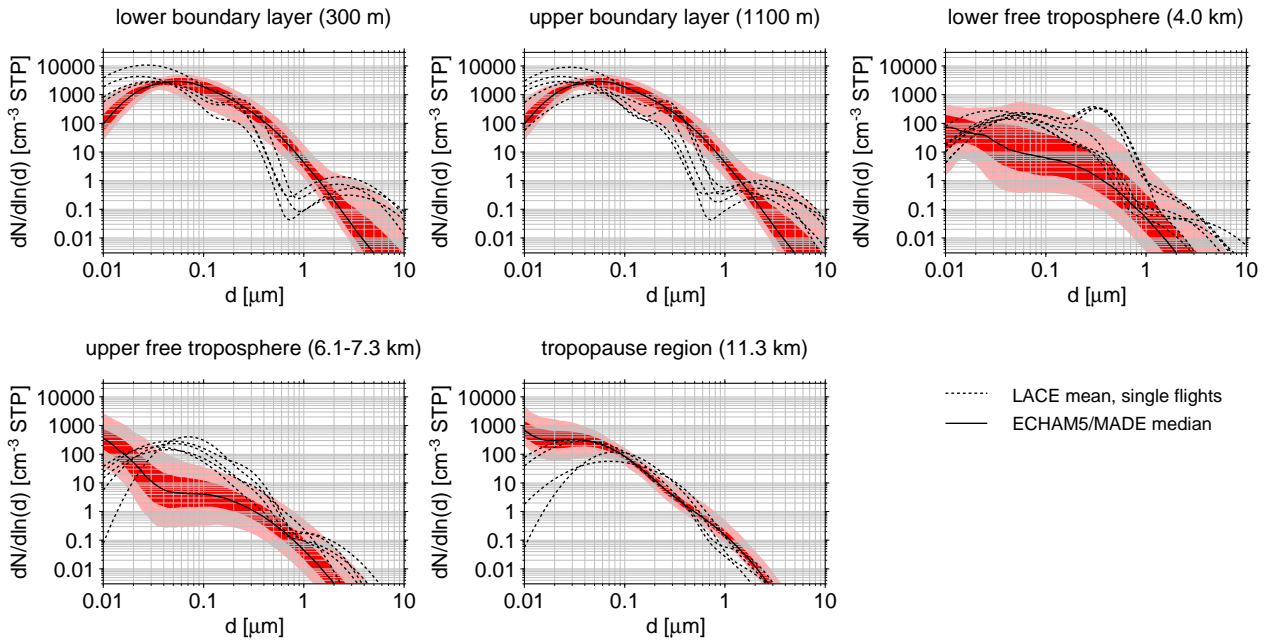


Figure 5.5: Modeled and observed size distributions at different altitude levels. The shaded areas represent the 5%, 25%, 75% and 95% percentiles. Measurements by *Petzold et al.* (2002) during the LACE campaign over northern Europe. The distributions are relative to the dry diameter. The simulated size distribution is calculated for each August output time step in the model box relative to the region of the campaign. The so calculated size distributions are then discretized and the median and the percentile are calculated in each size bin.

long time scale of this transport the parameterization of the sinks of BC, that focused on the sinks in the UTLS, may be too effective at surface level.

The simulated mass concentrations of BC, OC, SO₄ and NO₃ have been compared with surface measurements from the IMPROVE network, an extensive long term monitoring program started in 1985 to establish the visibility and aerosol conditions in the National Parks and Wilderness Areas in the USA. Each station participating in the IMPROVE project collects the total PM_{2.5} (particles with diameter smaller than 2.5 μm) and PM₁₀ (particles with diameter smaller than 10 μm) mass concentrations and, for PM_{2.5}, the mass concentrations of sulfate, nitrate, chloride, BC and organic carbon (OC) twice a week, each time over a 24 hours long period.

The total SO₄, NO₃, BC and POM mass concentrations simulated by E5/M-MADEsoot in the lower vertical level have been compared with the corresponding IMPROVE data taken between 1995 and 2005 for PM_{2.5}. The simulated mass concentration of POM has been divided by the factor 1.4 (*Dentener et al.*, 2006) to compare it with the observed OC concentration, since POM includes not only OC, but also other species as oxygen and water.

Fig. 5.8 shows the results of the comparison. The order of magnitude and the patterns of the concentrations of the four species are similar to the experimental data in nearly the whole region. For each species the normalized mean error (NME) and the normalized mean

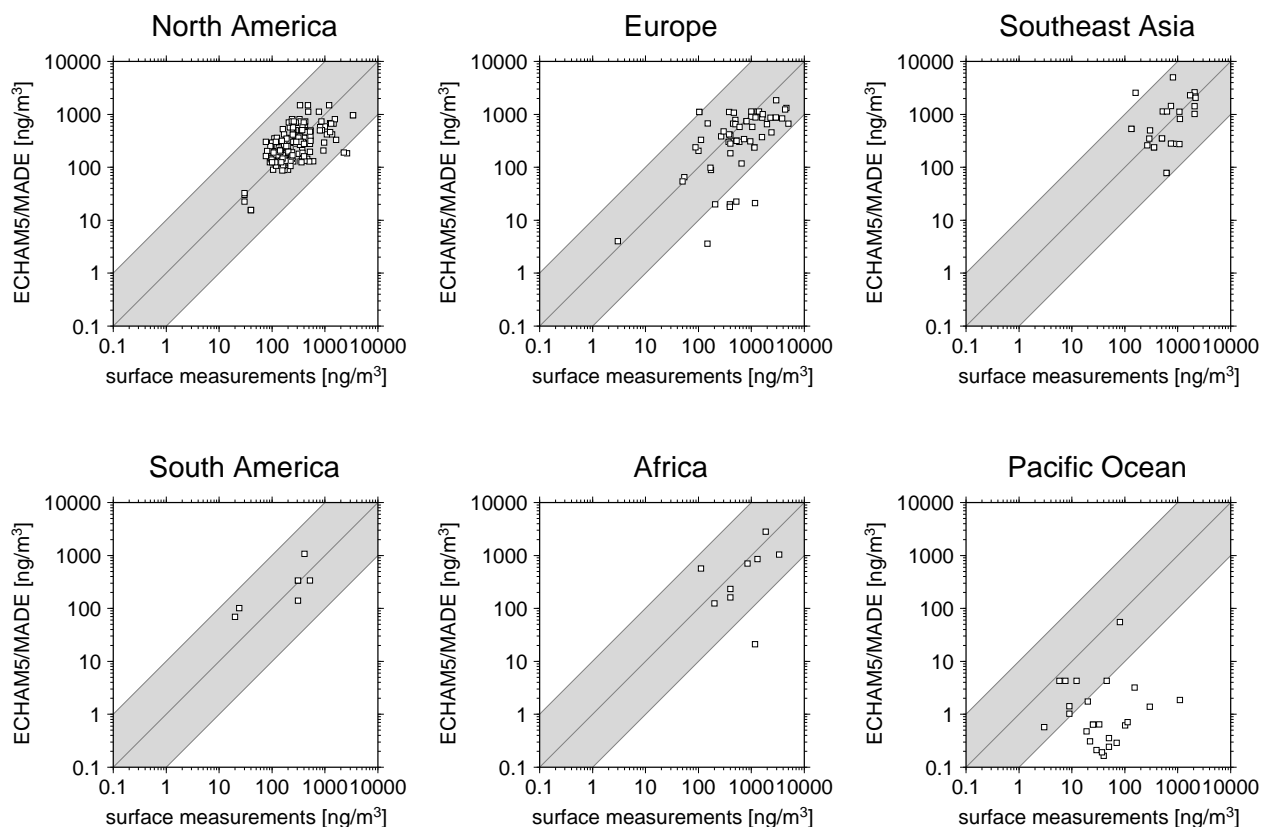


Figure 5.6: Comparison between modeled and observed BC mass concentrations at surface for different regions of the world. Each point corresponds to a measurement site. The shaded region indicates the area where the ratio between measurements and model results is within the range of 1:10 and 10:1.

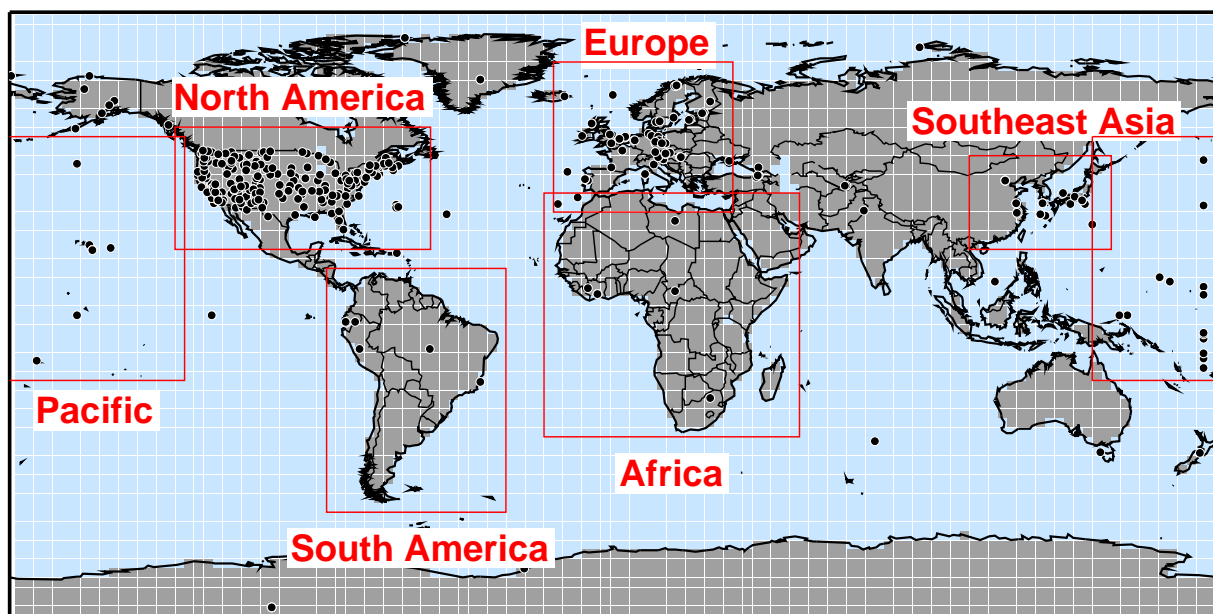


Figure 5.7: Distribution of the measurements stations taken into account for the comparison of Fig. 5.6, projected on the T42 grid.

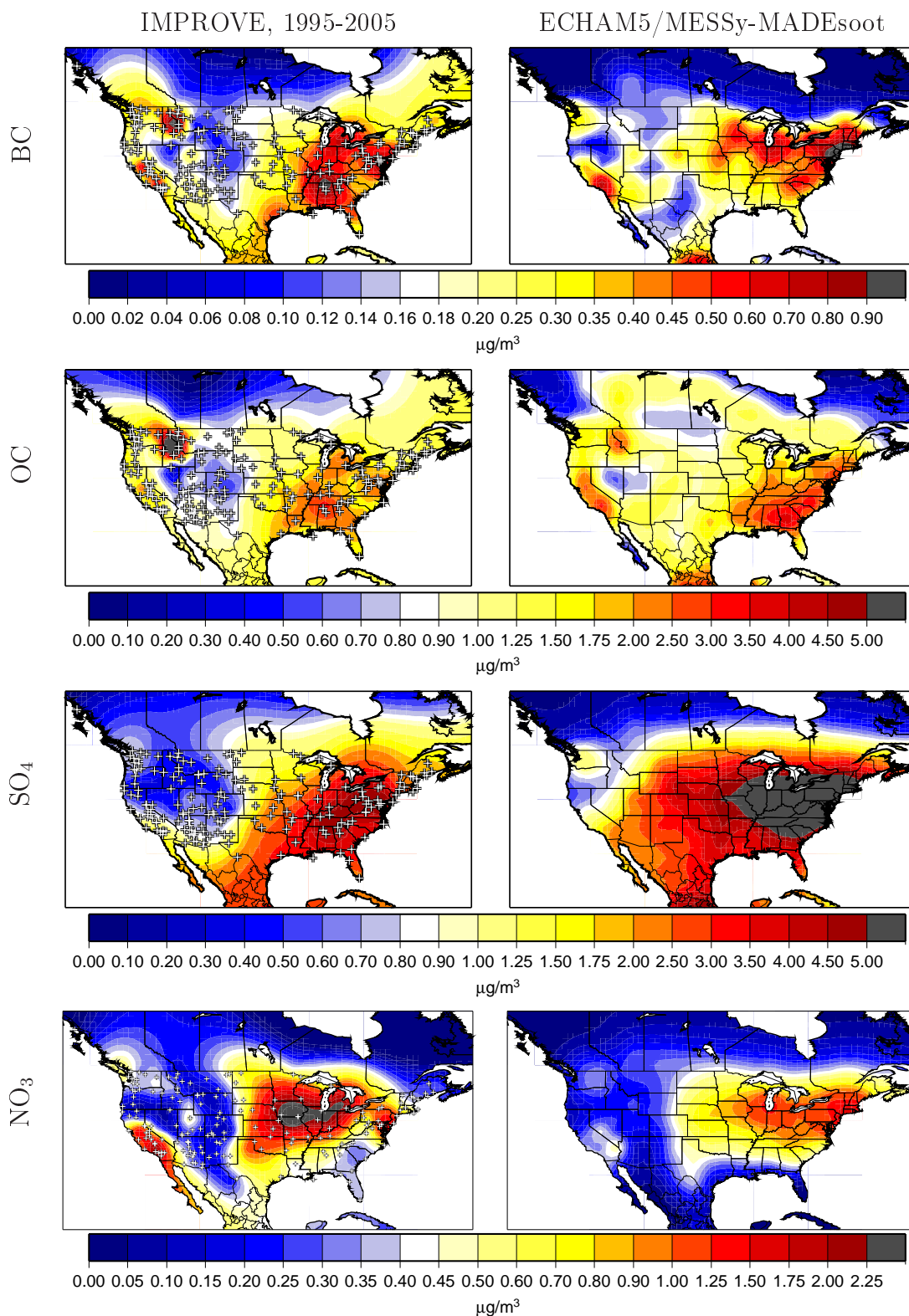


Figure 5.8: Comparison between the climatological annual mean of BC, OC, SO₄ and NO₃ in PM_{2.5} from observations by the IMPROVE network (left hand side) and E5/M-MADEsoot (right hand side). The crosses indicate the measurement sites.

Species	NME	NMB
BC	44.9%	-6.2%
OC	34.9%	-3.3%
SO ₄	82.6%	+77.0%
NO ₃	55.5%	-28.1%

Table 5.3: Normalized mean error and normalized mean bias of the mass concentrations simulated with E5/M-MADEsoot with respect to the IMPROVE data set.

bias (NMB) have been calculated. These are defined as

$$\text{NME} = \frac{\sum_{i=1}^N |\text{Model}_i - \text{Observation}_i|}{\sum_{i=1}^N \text{Observation}_i} \cdot 100, \quad (5.1)$$

$$\text{NMB} = \frac{\sum_{i=1}^N \text{Model}_i - \text{Observation}_i}{\sum_{i=1}^N \text{Observation}_i} \cdot 100, \quad (5.2)$$

$$(5.3)$$

where i is an index running over the grid boxes containing at least one measurement station, and Model_i and Observation_i are the averages of the simulated and observed concentrations in the grid box i . If one grid box contains more than one station, Observation_i represents the mean among those stations. NME gives an estimation of the mean relative difference between simulations and observations, while NMB estimates the direction of the bias, being positive (negative) if the simulated concentrations are larger (smaller) than the observed ones. The number of grid boxes N containing at least one station is 96. Tab. 5.3 reports the NME and NMB for each analyzed species.

The pattern of the mass concentrations of each species is well reproduced by the model, particularly those of BC and OC, where even the isolated maximum between north Idaho and west Montana is reproduced (Fig. 5.8, first and second panels). The maximum, probably due to very strong forest fires that took place in year 2000 in the region, can be reproduced by the model thanks to the used BC and OC emissions from biomass burning from the satellite based GFED database, that includes also that strong fire season.

The model overestimates the concentration of SO₄ with respect to IMPROVE measurements. This is probably due to the fact that the IMPROVE measurement stations are in natural parks, where the air is particularly clean. Since the major sources of sulfate are industrial and domestic emissions (*Dentener et al.*, 2006), the interpolation over the whole USA obtained from the IMPROVE data set is probably biased toward low sulfate values.

5.2.4 Comparison of the mixing state of black carbon particles

Not many observations about the mixing state of BC particles are available, since not many measurements technique are capable to resolve the mixing state of aerosol. *Schwarz et al.* (2008b) presented data taken during the CR-AVE campaign with the SP2 which show the number fraction of internally mixed BC particles at different altitudes. The comparison between simulated and observed BC mixing state is quite complicated for several reasons. The BC mixing state is not directly measured, but is calculated from measurements of the optical properties of the detected particles. This implies that the number fraction of internally mixed BC given by *Schwarz et al.* (2008b) depends on some assumptions they make. Furthermore, the mixing state of BC particles can be determined from SP2 data only

for particles with a BC core in the size range of 100-250 nm, roughly corresponding to a small slice of the MADEsoot accumulation mode. Since the simulated aerosol distribution has a fixed log-normal shape, discrepancies in the simulated and observed number concentration within a particle size window could mean that the simulated particle number is incorrect or that the simulated particles are slightly too small or too large. Furthermore, the SP2 size window refers to the size of the BC cores, while the size distributions simulated by MADEsoot refer to the size of the whole particles, composed by core and coating. Comparing only the mixing state of the simulated accumulation mode would not be correct, since it contains also particles with BC cores out of the SP2 detection window. Moreover the simulated number concentration in the accumulation mode includes also the number concentration of dust particles.

To allow at least for a qualitative comparison, a simulation has been performed where only accumulation mode BC particles have been emitted, i.e. no Aitken mode BC particles and no dust particles. This comparison cannot be quantitative, since the atmosphere reproduced by such a simulation is not realistic. The formation of clouds, for instance, could be different, the aerosol effect on radiation and even the ageing of accumulation mode BC, since it does not suffer the competition of Aitken mode BC. However, it can help to understand if the simulation of the ageing process is effective enough. In this simulation the fraction of soluble material needed to define a BC particle as internally mixed (Sec. 3.2.6) is set to 50%, since this is the amount needed by the SP2 to detect the soluble coating (*J. Schwarz*, personal communications, 2008).

Fig. 5.9 shows the vertical profiles of the number fraction of internally mixed BC particles, as calculated by *Schwarz et al.* (2008b) from the SP2 measurements and simulated by E5/M-MADEsoot. Both profiles show that large fractions of BC particles near the tropopause are internally mixed. Up to 5 km altitude the fraction of internally mixed BC particles calculated from SP2 measurements scatter over a large range of values. This is probably related to the variability of the sources, which influences strongly the lower altitudes. While the simulated fractions growths with height, the profile calculated from the SP2 data presents lower fractions between 5 and 15 km. There, however, the statistical uncertainty of the values is high, due to the low number of BC particles detected.

5.3 Conclusions

The model system E5/M-MADEsoot performs well in the boundary layer and in the UTLS. Especially in the UTLS, the region of interest for the formation of ice clouds, the agreement between E5/M-MADEsoot results and measurements is particularly good. The aerosol size distribution is well reproduced at all altitudes and the horizontal distributions of the single chemical species is in reasonable good agreement with observations. Only a few measurements are available for the evaluation of the mixing state of BC and dust particles. However, the results of *Schwarz et al.* (2008b) and the simulations lead to similar conclusions about the mixing state of black carbon. Overall, the model is robust enough to be employed for the study of global aerosol and in particular of the potential ice nuclei in the UTLS.

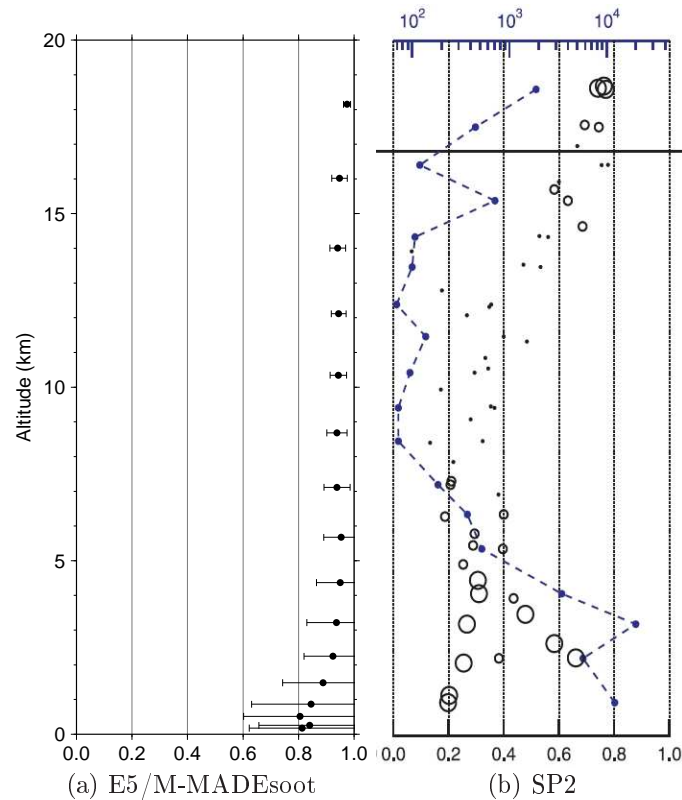


Figure 5.9: Number fraction of internally mixed BC particles as (a) simulated by E5/M-MADEsoot (average and standard deviation) and (b) calculated by *Schwarz et al.* (2008b) from SP2 measurements. In (b) each symbol corresponds to a 1-km average from one flight with the symbol diameter roughly proportional to its statistical confidence; large, medium and small symbols correspond to $< 5\%$, $< 10\%$ and $< 25\%$ statistical uncertainty, respectively. The blue dashed line (top scale) shows the number of BC particles detected in each altitude level. The horizontal black line marks the tropopause.

Chapter 6

Characterization of sub-micrometer aerosol and potential ice nuclei

The model E5/M-MADEsoot allows for the simulation of the size distribution, concentration, mixing state and chemical composition of the global atmospheric aerosol, and in particular of the potential ice nuclei (PIN). This chapter reports the analysis of the simulation evaluated in Chapter 5 in order to provide a detailed characterization of global aerosol and PIN. Furthermore the results of the different studies that have been conducted with E5/M-MADEsoot are shown, with the purpose of investigating the ageing processes of externally mixed BC and dust particles and the time scale of their transformation into an internal mixture. Since this study focuses on the sub-micrometer aerosol, the results are shown only for the Aitken and the accumulation modes.

6.1 Characterization of the sub-micrometer aerosol

The following sections show the horizontal distribution and zonal mean of the annual mean number concentrations, the chemical composition and the size distribution of each mode describing the sub-micrometer aerosol, i.e. the three Aitken and the three accumulation modes. The results shown refer to annual means. Similar studies have been conducted with other global aerosol-climate models, e.g. *Adams et al. (1999)*; *Easter et al. (2004)*; *Lauer and Hendricks (2006)*; *Bauer et al. (2008)*, and have led to similar results.

6.1.1 Number concentration

This section presents the global distribution of the particle number concentration at surface level, that is mainly driven by the emissions, and the corresponding zonal mean vertical distribution. Fig. 6.1 shows the number concentrations of the two BC and dust free modes, akn_{sol} and acc_{sol} . Different scale are used for akn_{sol} and for acc_{sol} . In the northern hemisphere (NH) the order of magnitude of the number concentration of akn_{sol} at surface level is similar to the one of acc_{sol} . In the southern hemisphere (SH) over the continents the number concentration of the accumulation mode is one order of magnitude larger than that of the Aitken mode. This is due to the fact that the major sources of Aitken mode particles, related to industry and fossil fuel burning, are mainly located in the NH, especially over the United States, Europe, India and China, as clearly shown in the pattern of the concentrations. In these regions, the number concentration of soluble particles can reach 10^4 particles/cm³. Accumulation mode particles, on the other hand, form following the growth of Aitken mode particles and, additionally, are emitted by biomass burning. The high accumulation mode

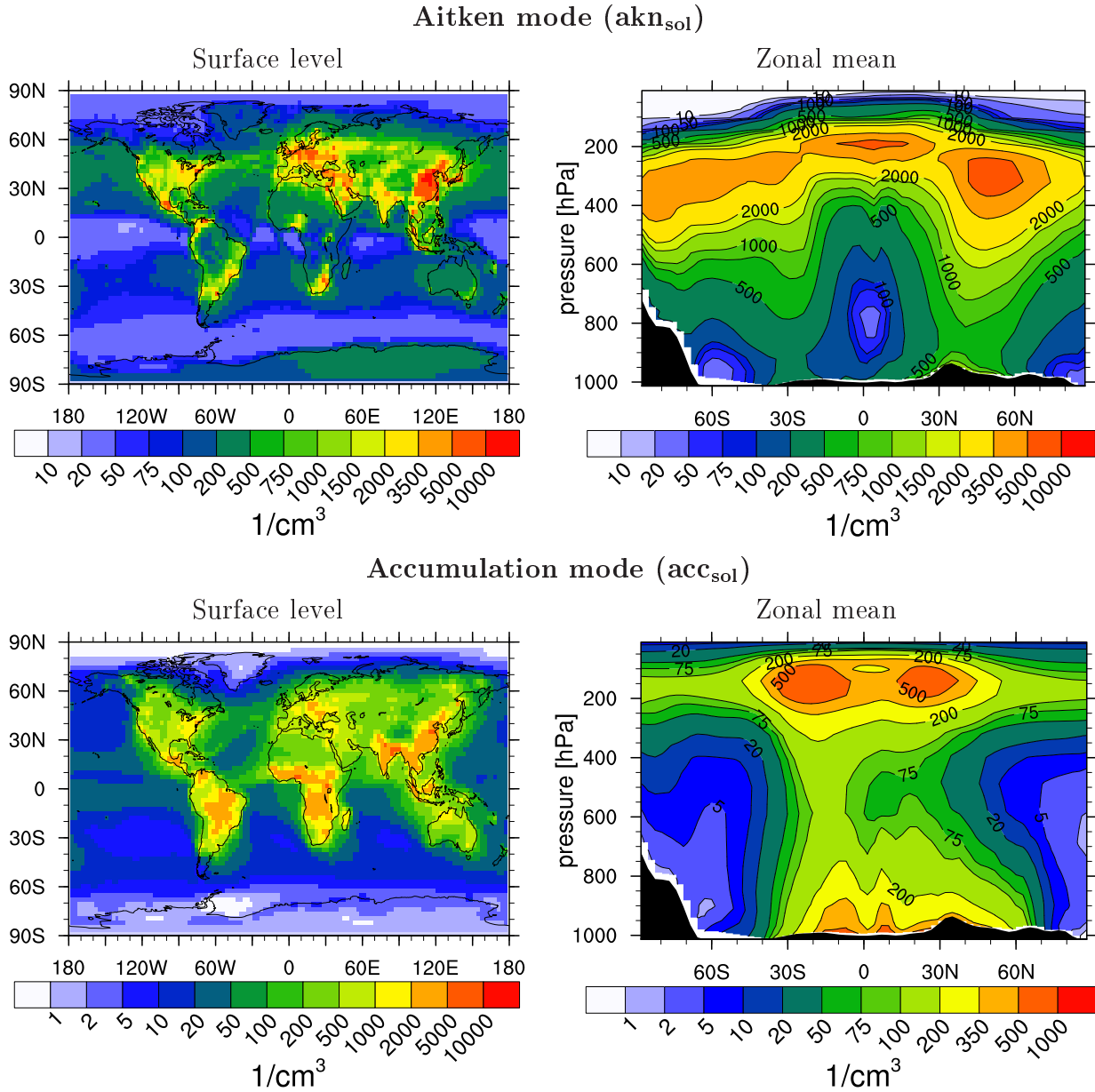


Figure 6.1: Horizontal distribution at surface level and zonal mean vertical distribution of the annual mean number concentration of the totally soluble Aitken (upper panels) and accumulation (lower panels) mode particles. Note the different scale between akn_{sol} and acc_{sol} .

number concentrations in the SH originate from biomass burning, while the growth of particles from the Aitken mode causes the high values of the NH, of the same order of magnitude of the Aitken mode number concentration.

The lowest values of the number concentration are reached over the oceans, both in the Aitken and in the accumulation mode. The emissions from shipping are concentrated in the NH and in the Indian Ocean, and they are the origin of the areas where the number concentration of akn_{sol} is between 200 and 500 particles/ cm^3 . Over the remaining parts of the oceans no primary Aitken mode particles are emitted, since in the model set up used in this work sea salt is present only in the accumulation and coarse modes. However, the oceans are a source of DMS, that can be transformed into secondary aerosols. The accumulation mode receives the contribution of wind-driven sea salt emissions over the ocean.

The number concentration of the Aitken mode decreases up to 800 hPa, reaching zonal

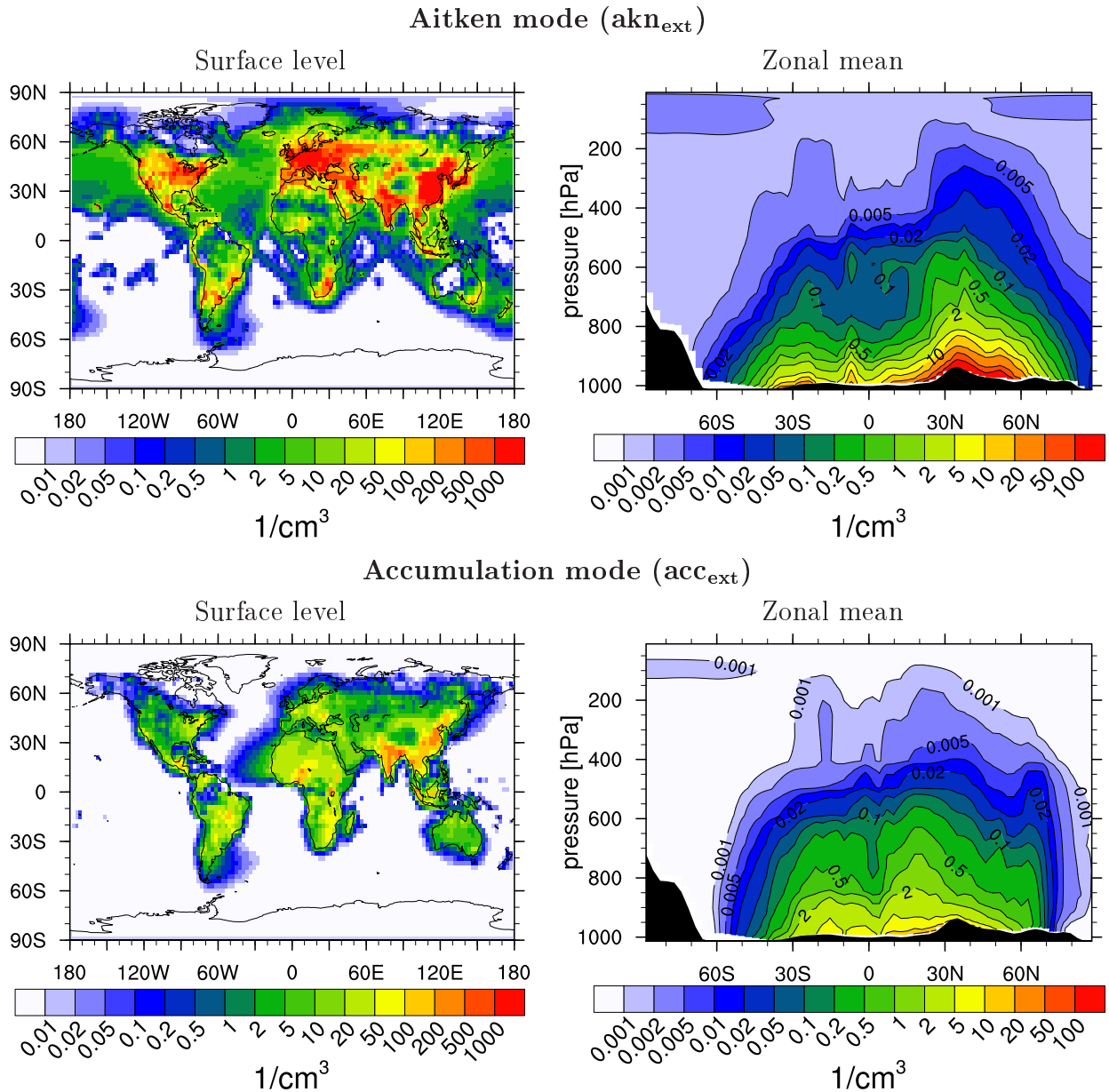


Figure 6.2: Horizontal distribution at surface level and zonal mean vertical distribution of the annual mean number concentration of the externally mixed BC and dust particles in the Aitken and accumulation mode.

mean minimum concentrations between 20 and 50 particles/cm³ at the equator and between 500 and 750 particles/cm³ at mid-latitude in the NH. Above 800 hPa the Aitken mode number concentration grows again up to 5000 particles/cm³ at 200 hPa. This is caused by the nucleation of sulfuric acid particles, favored by the low temperature and by the lack of particle surface available for the condensation of H₂SO₄.

The zonal mean of the accumulation mode shows a decrease in the number of particles up to 500 hPa, reaching minimum values between 2 and 5 particles/cm³ in the polar regions and between 100 and 200 particles/cm³ in the southern tropical region. Between 500 hPa and 100 hPa the accumulation mode number concentration increases up to 500 particles/cm³. This maximum is related to the high number concentration of the Aitken mode particles, that, growing, are transferred to the accumulation mode, and to the low efficiency of the sinks at this altitude. The sink processes of the number concentration are dry deposition, wet deposition, intermodal and intramodal coagulation, where intermodal coagulation is the

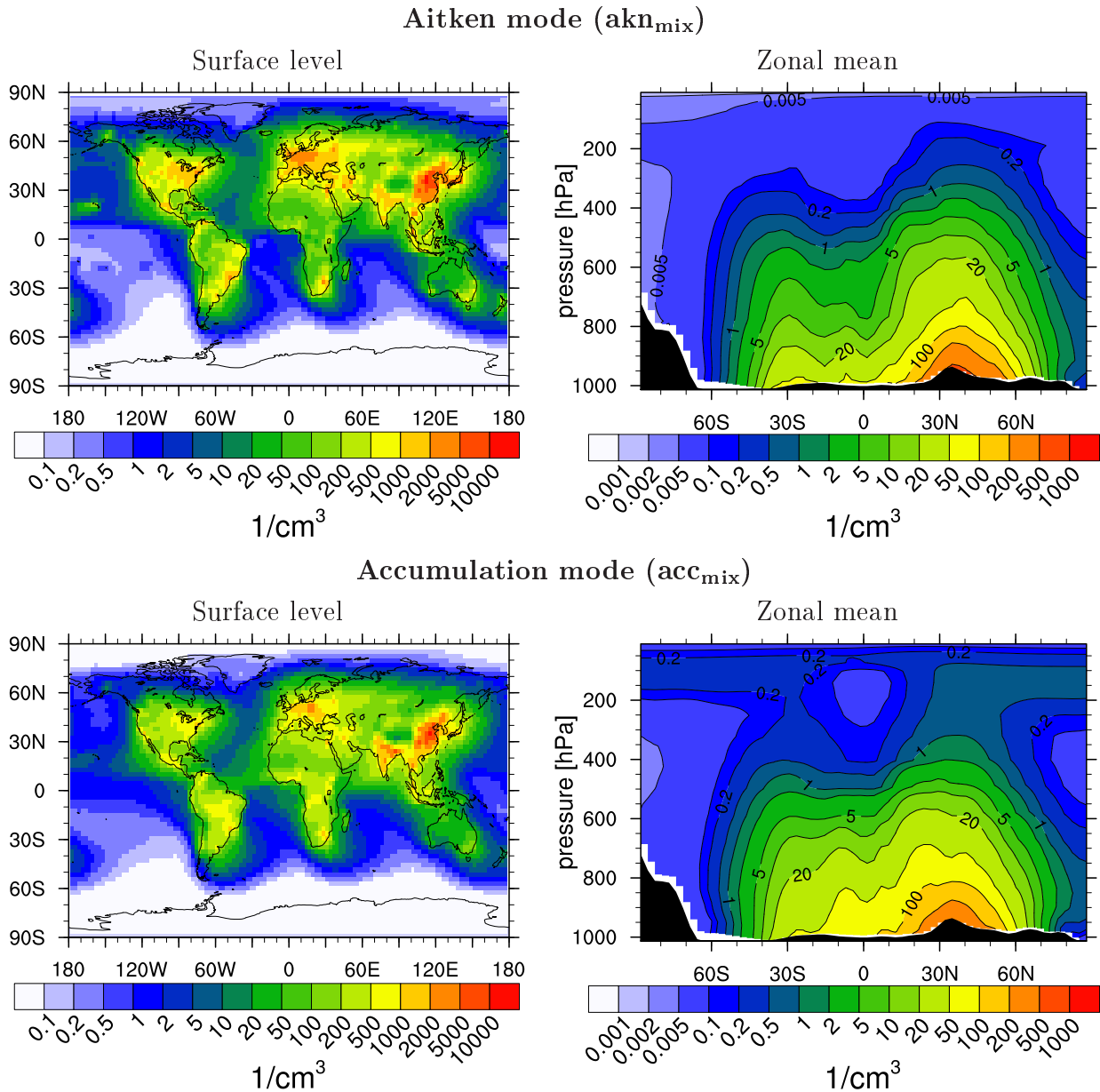


Figure 6.3: Horizontal distribution at surface level and zonal mean vertical distribution of the annual mean number concentration of the internally mixed BC and dust particles in the Aitken and accumulation mode.

most effective process for Aitken mode particles and wet deposition for accumulation mode particles (*Lauer and Hendricks, 2006*).

Furthermore, the pattern of the number concentration of the Aitken mode shows the trajectory of the air masses: raising in the tropical belt, the air descends again at about $30^\circ N$ and $30^\circ S$ latitude, transporting the Aitken mode particles originated in the UTLS downwards. In their movement towards the surface, the particles are growing and the number concentration is diminishing again, until the updraft of the particles emitted at surface compensates the decrease and the value of the number concentration grows again.

Fig. 6.2 shows the number concentrations of the externally mixed BC and dust particles in the Aitken and accumulation modes (akn_{ext} and acc_{ext}). At surface level the emission regions can be clearly identified: the maximum number concentration of akn_{ext} , which contains only BC from fossil fuel combustion (industry, traffic and house heating) is located over the industrialized regions. In the SH, the number concentration of the externally mixed Aitken

mode BC particles is particularly high in the areas of Rio de Janeiro and Buenos Aires in South America and over South Africa, areas with a higher density of industry and population. The shipping routes are visible across the oceans. No dust is present in the Aitken mode, hence the low values over the Sahara.

Important sources of accumulation mode BC are biomass burning, corresponding to the maximum over South America and Sub-Saharan Africa, and biofuel, especially over India and eastern China. Dust particles are emitted over the deserts. Given their large dimension, however, they do not contribute to the number concentration of the accumulation mode as significantly as they do to the mass.

The zonal means of the externally mixed modes decrease strongly with altitude, due to the efficient transformation into an internal mixture. While dust is emitted only at the surface, BC can be emitted also at higher level. In particular the emissions from wild-land fires over Canada and Asia north of 60° N are injected in the model up to 6 km altitude, causing the isolated peak with concentration between 0.005 and 0.05 particles/cm³ visible at that latitude in the number concentration of the accumulation mode.

Fig. 6.3 shows the number concentrations of the Aitken and accumulation modes with internally mixed BC and dust particles (akn_{mix} and acc_{mix}). The emission areas show higher concentrations, but are not as well defined as in the pattern of the number concentration of the externally mixed modes (Fig. 6.2), since only 20% of the emitted BC and no fraction of dust is supposed to be injected in the atmosphere as internally mixed. The largest part of the internally mixed modes with BC and dust derives from the ageing of externally mixed BC and dust particles, which can be transported away from the emission regions before the ageing process takes place. The number concentrations of akn_{mix} and acc_{mix} decrease with altitude. Above 400 hPa the concentration of the accumulation mode stays constant at mid-latitudes between 0.2 and 1 particles/cm³, since the main sink process of the accumulation mode, the wet deposition, is not efficient at such height due to the low cloud cover. In the tropics, instead, the many high clouds and the efficient wash-out in convective clouds causes the loss of aerosol.

6.1.2 The size distribution of the global aerosol

The median number size distribution of the global aerosol, including the coarse mode, is shown in Fig. 6.4 at different altitudes. The soluble modes akn_{sol} and acc_{sol} dominate the number concentration at all altitude levels. The median diameter of akn_{sol} is around 0.02 μm in the boundary layer and decreases with altitude up to 3 nm in the tropopause region. Since freshly nucleated H_2SO_4 particles are assumed by E5/M-MADEsoot to have a wet diameter of 3.5 nm, this leads to the conclusion that the diameter of the soluble Aitken mode is driven in the tropopause region by nucleation. The hydrophilic BC and dust Aitken mode akn_{mix} has the same sink processes as akn_{sol} , but, contrary to akn_{sol} does not receive a direct contribution from the freshly nucleated particles, and keeps at all altitude a diameter larger than 20 nm. The introduction of a nucleation mode into the model could give an even better representation of the aerosol size distribution, even though the agreement with experimentally measured aerosol size distributions is already good (Fig. 5.5). The diameter of acc_{sol} is roughly one order of magnitude larger than the diameter of the Aitken mode at all altitude levels analyzed.

Fig 6.5 shows the aerosol size distribution in the lower boundary layer (around 300 m altitude) over the regions defined in Fig. 5.7 of Chapter 5. The size distribution of the soluble aerosol, mainly coincident with the total size distribution, is relatively similar over the industrialized areas, Europe, North America and South-East Asia. There the externally mixed Aitken mode has much larger number concentration than the accumulation mode,

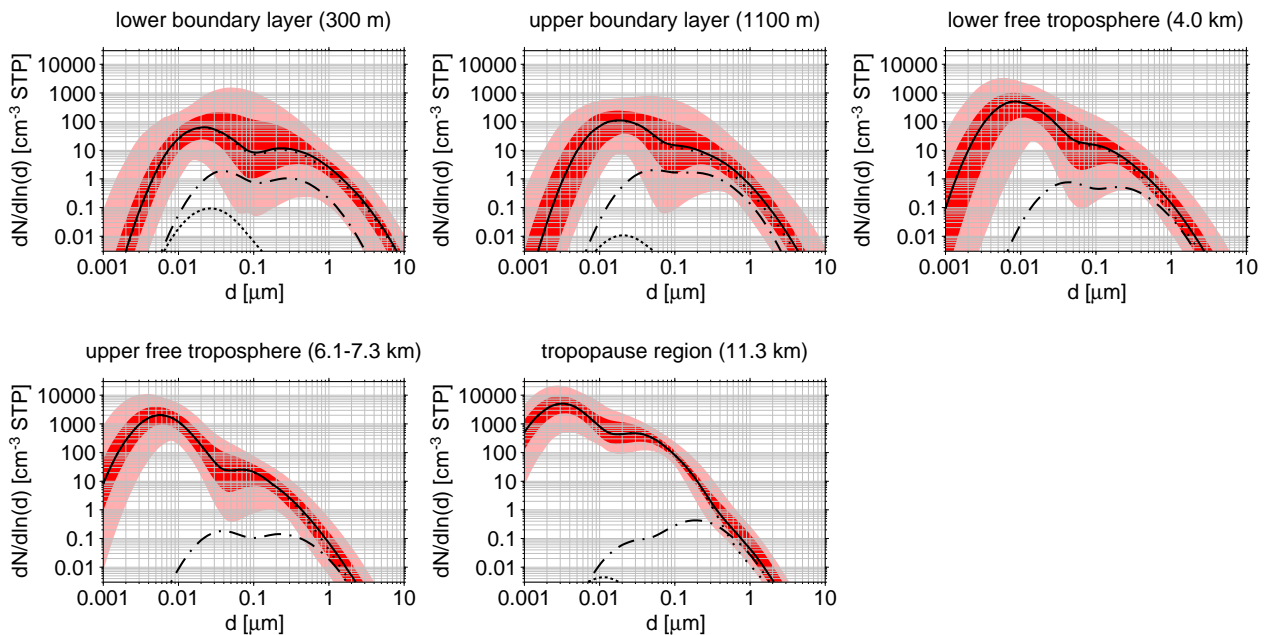


Figure 6.4: Size distribution of global aerosol number concentration (solid line), of the soluble modes akn_{sol} and acc_{sol} (dotted), of the internally mixed BC and dust modes akn_{mix} and acc_{mix} (dot-dashed) and of the externally mixed BC and dust modes akn_{ext} and acc_{ext} (short-dashed). The black lines represent the median values, the shadowed areas the 5%, 25%, 75% and 95% percentiles. Using the climatological monthly means of the diameter and the number concentration of the modes, the size distribution in each grid box and for each time step is calculated (64 boxes along the latitude \times 128 boxes along the longitude \times 12 months). Such size distributions are then discretized and the median and the percentile are calculated in each size bin.

driven by the emissions from fossil fuel combustion. In particular South-East Asia shows the highest concentration of BC and dust containing particles, of the same order of magnitude of the concentration of soluble particles. Over the Pacific Ocean externally mixed black carbon is limited to the Aitken mode, since the only BC emissions are the small particles from shipping. In Africa the number concentration of the externally mixed Aitken and accumulation modes are similar, since the emissions of particles in these modes are mainly driven by BC from biomass burning and mineral dust from the Sahara desert, both in the accumulation mode range.

6.1.3 Chemical composition

The chemical composition of the simulated total aerosol is depicted in Fig. 6.6, Fig 6.7 and Fig 6.8 as annual means. The horizontal distributions at surface level and the vertical distribution of the zonal means are shown.

Fig. 6.6 shows the mass concentration of the aerosol species that are emitted only as primary aerosol, i.e. BC, dust and sea salt. The shown concentration of BC include all modes where BC is present (akn_{ext} , acc_{ext} , akn_{mix} and acc_{mix}), while the concentrations of dust and sea salt include only the fraction in the accumulation mode, i.e. acc_{ext} and acc_{mix} for dust and acc_{sol} , acc_{ext} and acc_{mix} for sea salt. The emission regions are clearly defined in the distribution of all species. BC is concentrated over industrialized areas and over areas with strong biomass burning, dust over the deserts, and sea salt over the oceans. The emission regions of dust are quite isolated from the emission regions of BC. While over the

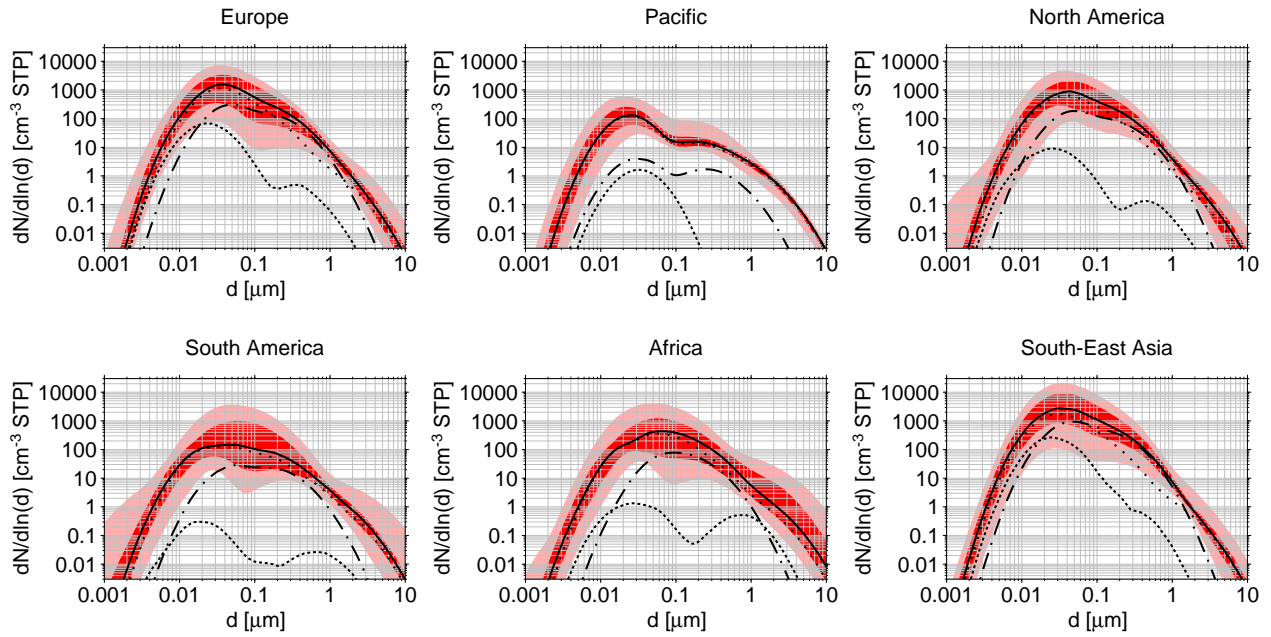


Figure 6.5: Size distribution of total aerosol number concentration (solid line), of the soluble modes akn_{sol} and acc_{sol} (dotted), of the internally mixed BC and dust modes akn_{mix} and acc_{mix} (dot-dashed) and of the externally mixed BC and dust modes akn_{ext} and acc_{ext} (short-dashed) at surface level. The plotted regions are those defined in Fig. 5.7. The black lines are the median values, the shadowed areas the 5%, 25%, 75% and 95% percentiles. See Fig 6.4 for details about the calculation of the distributions.

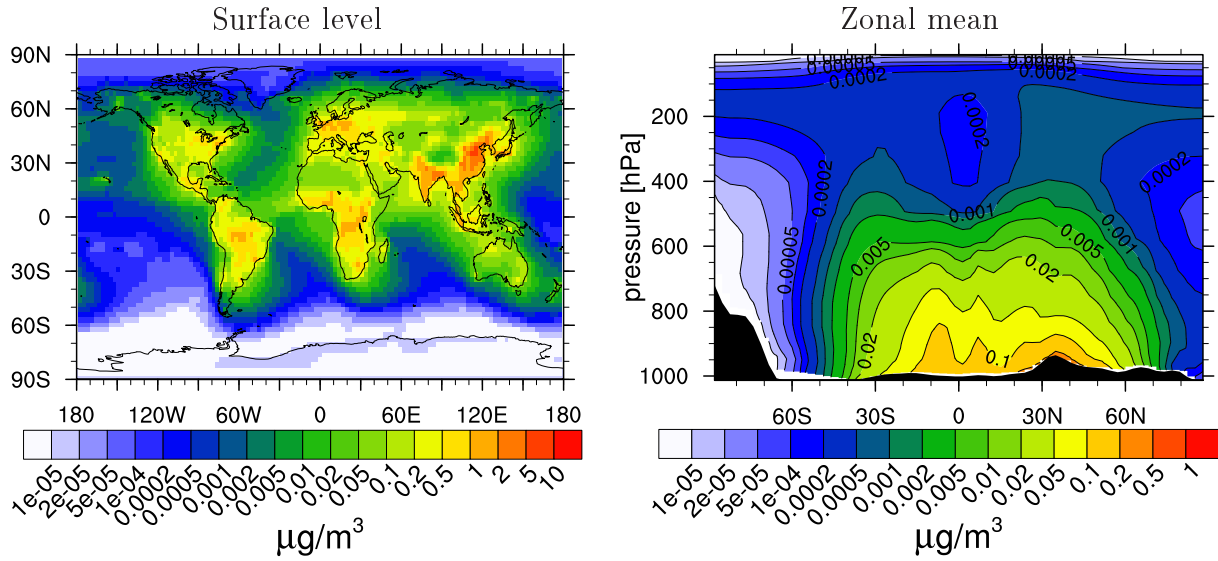
oceans sea salt is nearly everywhere the most abundant species, over the continents it is mostly negligible in comparison with the other species. Over the Atlantic ocean between the Equator and the $30^\circ N$ the wind coming from Africa carries a large amount of wind-borne dust and BC generated by biomass burning, so that their concentration over that area is higher than the sea salt one.

The mass concentration of all species becomes smaller with increasing altitude. The concentration of sea salt decreases very rapidly, decreasing of two order of magnitude between the surface and 800 hPa. Such decrease is related to the large size of sea salt particles, which let them be efficiently removed by wet deposition. The vertical profile of the zonal mean of dust shows a large asymmetry between the NH and the SH, related to the asymmetric location of the emission regions. This asymmetry is visible at all altitude, showing that the exchange of air masses between the NH and the SH is quite low.

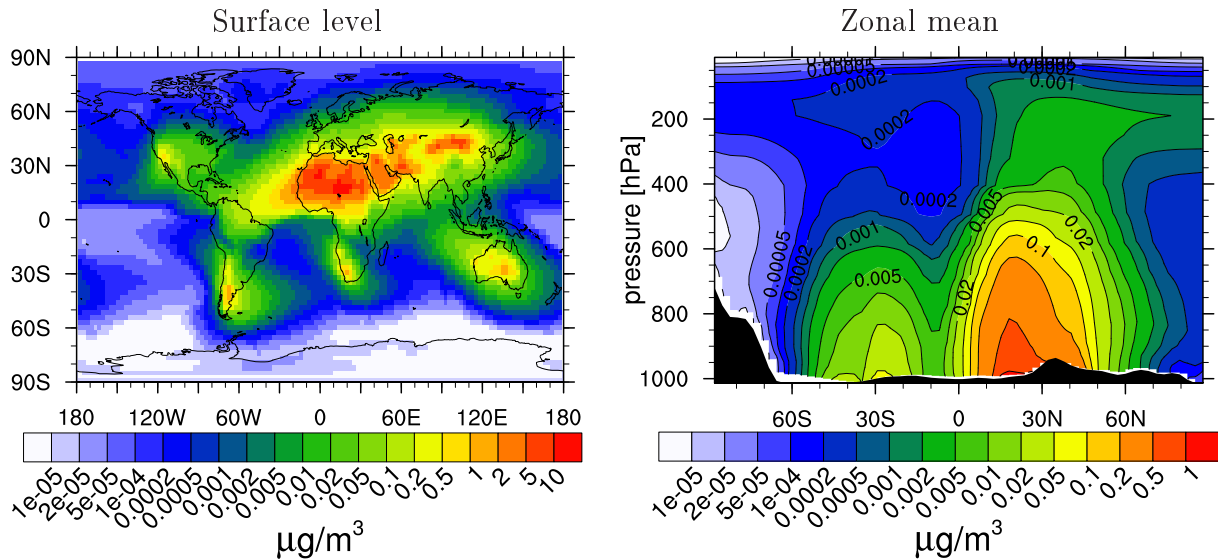
Fig. 6.7 shows the mass concentrations of the secondary aerosol species, NH_4^+ and NO_3^- . The pattern of these species is less influenced by the location of the emission regions, since the precursor gases can be transported over large distances before they are transformed into aerosol particles. As for primary aerosol (Fig. 6.6), the concentrations of all species of Fig. 6.7 decrease with altitude.

Fig. 6.8 shows the mass concentrations of particulate organic matter (POM) and sulfate (SO_4^{2-}). These two species are emitted both as primary and as secondary aerosol. POM shows high concentrations especially in the southern hemisphere, related to the strong emissions from biomass burning. Particularly interesting in the UTLS is the lack of high SO_4^{2-} concentrations around 300 hPa: Even if the nucleation of sulfuric acid vapor is very efficient at that altitude (Fig. 6.1), the mass of the freshly nucleated particles is too small for the formation of a local maximum in the mass concentration.

Black carbon



Dust



Sea salt

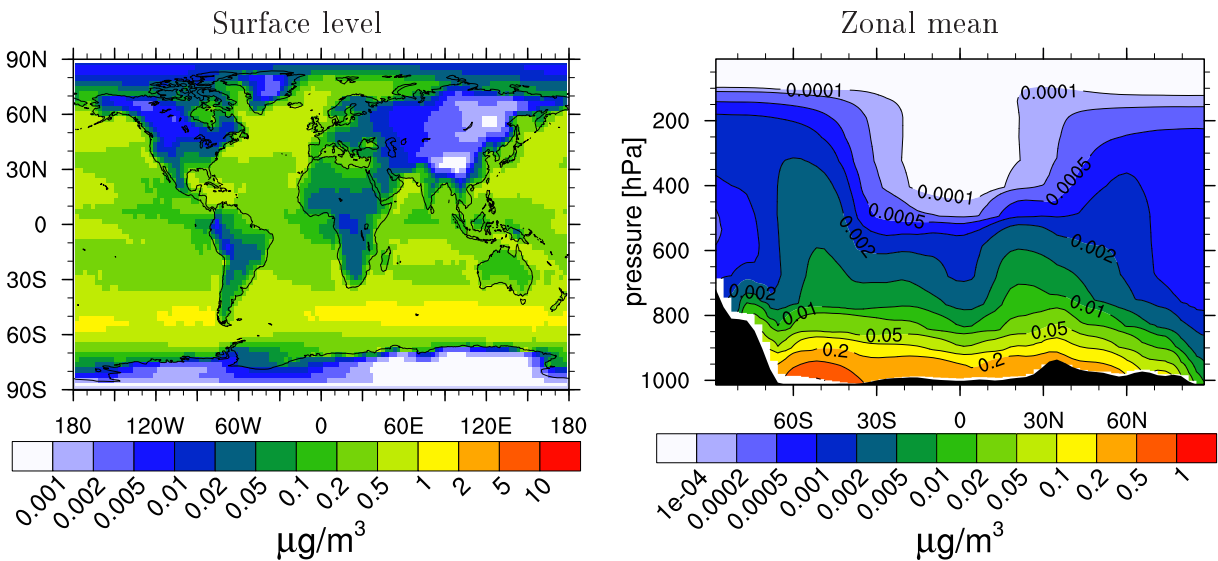


Figure 6.6: Horizontal distribution at surface level and zonal mean vertical distribution of the simulated aerosol annual mean mass concentration of black carbon (BC), dust and sea salt. These species are emitted only as primary aerosol particles. The shown dust and sea salt concentrations do not include the coarse mode.

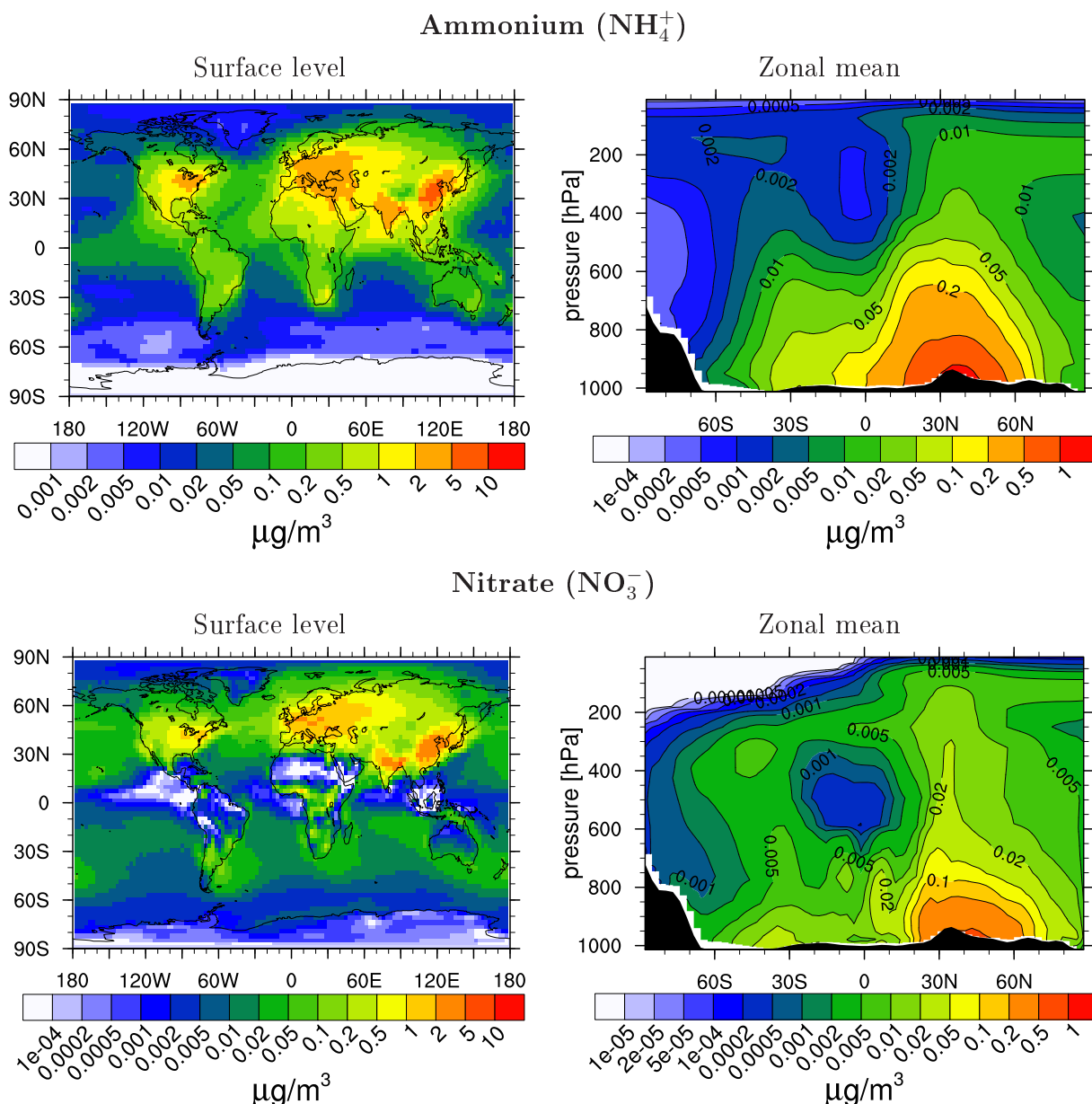


Figure 6.7: Horizontal distribution at surface level and zonal mean vertical distribution of the simulated aerosol annual mean mass concentration of NH_4^+ and NO_3^- . These species form after the oxidation of precursor gases.

6.1.4 Burden and life time of atmospheric aerosol

The most abundant aerosol species in the sub-micrometer range is SO_4^{2-} . In the simulation discussed above the average global burden of SO_4^{2-} is equal to 1.4 Tg, followed by NH_4^+ (0.4 Tg), POM (0.7 Tg), dust (0.2 Tg in the accumulation modes, but 8.3 Tg if the coarse mode dust is included), NO_3^- (0.1 Tg), SS (0.1 Tg in the accumulation modes, 2.5 Tg including the coarse mode) and BC (0.1 Tg). These burdens are consistent with those simulated by ECHAM5/MESy-MADE and by the other global aerosol model based on the GCM ECHAM, ECHAM5/HAM (*Stier et al., 2005; Kloster et al., 2008*) (Tab. 6.1). *Textor et al. (2007)* present a statistic of the global burden of SO_4^{2-} , POM, dust, SS and BC based on the values simulated by the different model participating in the AeroCom project to assess the influence of emissions on aerosol properties in global models. They calculated for SO_4^{2-} a burden equal to $2.1 \pm 21\%$ Tg, for POM to $1.3 \pm 18\%$ Tg, and for BC to $0.2 \pm 26\%$ Tg.

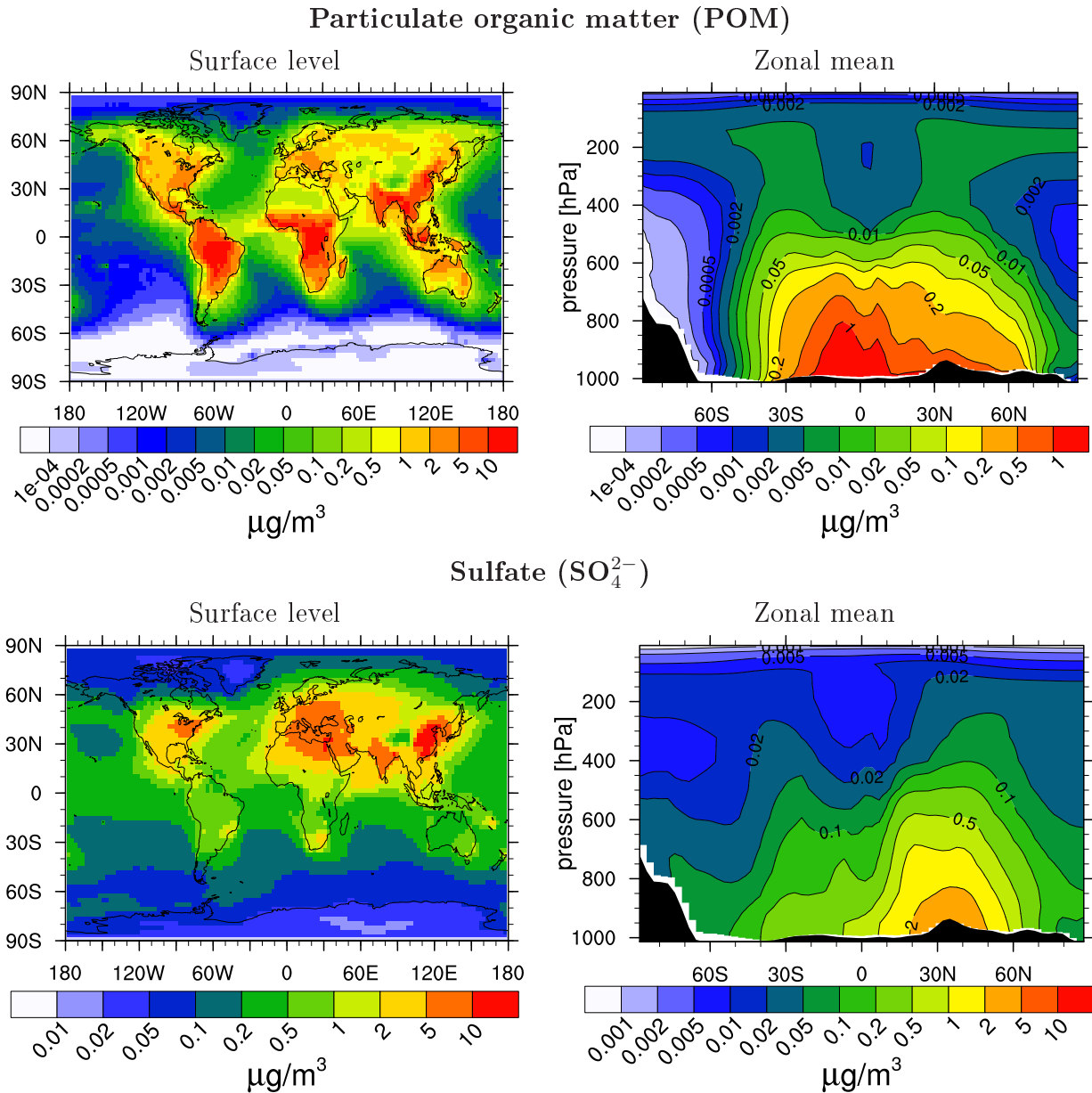


Figure 6.8: Horizontal distribution at surface level and zonal mean vertical distribution of the simulated aerosol annual mean mass concentration of particulate organic matter (POM) and sulfate (SO_4^{2-}). These species are emitted as primary and secondary aerosol.

The values of the sea salt and dust burdens cannot be compared, since their mass is mainly in the coarse mode, which is treated in a simplified way in E5/M-MADEsoot. Furthermore SS is here emitted online. In general, the burdens simulated by E5/M-MADEsoot are lower than the values of *Textor et al.* (2007). The statistics calculated by *Textor et al.* (2007) is strongly influenced by some models which simulate very high burdens. When compared to measurements, as for instance in *Schwarz et al.* (2006), the models based on the GCM ECHAM do not show a deficiency in the concentration of aerosol. The lower SO_4^{2-} burden simulated by E5/M-MADEsoot with respect to *Textor et al.* (2007) may be due to a different representation of the sulfur cycle in the chemistry module, since SO_4^{2-} originates predominantly from oxidation of the precursor gases. Additionally, the statistics of *Textor et al.* (2007) for the sulfuric cycle is based only on three models. POM is mainly emitted in the tropics, where the convective cloud coverage is high. The lower POM burden may be related to the high efficiency of scavenging in convective clouds simulated by E5/M-MADEsoot. The

Species	Global burden [Tg]			
	E5/M-MADEsoot	E5/M-MADE	E5/HAM	AeroCom
Sulfate	1.4	1.4	0.8	2.1
BC	0.1	0.1	0.1	0.2
POM	0.7	0.7	1.0	1.3
SS	2.5	2.9	10.5	12.7
DU	8.3	7.8	8.3	21.3

Table 6.1: Global burden of the aerosol sulfate, black carbon (BC), particulate organic matter (POM), sea salt (SS) and dust (DU) simulated by ECHAM5/MESSy-MADEsoot, ECHAM5/MESSy-MADE, ECHAM5/HAM (*Stier et al., 2005*) and by the AeroCom project (*Textor et al., 2007*) (annual average). The AeroCom values refer to the average among the models participating to the project. The version of E5/M-MADE here considered includes the modifications introduced in the parameterization of the scavenging process, as described in Sec. 4.2.

lower value of the BC burden is probably to be attributed to the fast ageing that MADEsoot simulates (see Sec. 6.3).

The average residence time of an aerosol species can be estimated, assuming that sources and sinks are in equilibrium, as

$$\text{residence time [days]} = \frac{\text{burden [Tg]}}{\text{sources[Tg/days]}}. \quad (6.1)$$

The residence time of externally mixed BC and dust particles depends directly on the definition of internal mixture (Sec. 3.2.6), since besides dry deposition and impact scavenging, also the ageing into the internal mixture is a sink. Indirectly, also the total mass of BC and dust is dependent on the chosen definition of internal mixture, because nucleation scavenging acts only on hydrophilic particles. In addition to the reference run, where a soluble fraction of $x = 10\%$ of the total mass of the mode is required for the transformation of externally mixed particles to internally mixed, two simulations have been performed with $x = 5\%$ and $x = 50\%$. The residence time of externally mixed BC and dust particles varies strongly with x (Tab. 6.2), ranging from 3.2 hours with $x = 5\%$ to nearly 18 hours with $x = 50\%$ for BC and from 57 hours with $x = 5\%$ to 138 hours with $x = 50\%$ for mineral dust. While the increase of the residence time relative to the reference run is very large for the externally mixed modes, the residence times of the total mass of BC and dust is not as sensitive to changes in x . Even though the mass of BC and dust that cannot be scavenged through nucleation scavenging is much higher, the total amount of BC and of dust stay roughly the same.

Tab. 6.2 shows that BC is transformed into an internal mixture faster than dust. This is reasonable, since dust particles are larger than BC from biomass burning (Fig. 6.5), and therefore require a larger coating to be transform into an internal mixture. Furthermore the regions with high mass concentration of dust, i.e. the deserts, are characterized by low humidity (water is the main component of the coating, as shown in Sec. 6.2.3) low concentrations of other soluble aerosols, with which dust particles could coagulate, and low concentrations of SO_2 , which could be transformed into SO_4^{2-} and condense over the externally mixed dust particles. On the contrary, the sources of BC are also sources of SO_4^{2-} . Also Fig. 6.12b leads to the same conclusion.

x	Residence time [days]			Global Burden [$10^{-3}\cdot\text{Tg}$]		
	5%	10%	50%	5%	10%	50%
ext. mixed BC	0.14	0.21 (+50%)	0.78 (+457%)	2.46	3.94	14.0
total BC	3.31	3.43 (+4%)	3.54 (+7%)	74.4	76.4	79.5
ext. mixed dust	2.39	3.49 (+46%)	5.73 (+139%)	69.1	98.4	165
total dust	7.23	7.46 (+3%)	8.03 (+11%)	209	212	232

Table 6.2: Residence time and average global burden of the sub-micrometer BC and mineral dust in the reference run ($x = 10\%$) and in two additional simulations with different definition of internal mixture (Sec. 3.2.6). In parenthesis is the increase of the residence time relative to the run with $x = 5\%$.

6.1.5 Comparison with ECHAM5/MESSy-MADE

The version of E5/M-MADE considered for the comparison with E5/M-MADEsoot includes the modification introduced in the parameterization of the scavenging process, as described in Sec. 4.2. The residence time of BC and dust calculated with E5-M/MADEsoot are shorter than those calculated with the version of E5/M-MADE. E5/M-MADE simulates a residence time of around four days for BC and of around 10 days for dust, while E5/M-MADEsoot of around 3.5 days and 7.5 days respectively. The longer residence time in E5/M-MADE indicates that the scavenging, which is influenced by the arbitrary assumption about the splitting between hydrophobic and hydrophilic BC, is less effective than in E5-M/MADEsoot. This suggests that the transformation time of 1 day used by MADE for the ageing of BC is too long, as confirmed in Sec. 6.3.2. The difference between the residence time of dust is larger than the one between the residence time of BC since MADE assumes dust to be totally hydrophobic and therefore underestimates its wet removal. Tab. 6.3 shows the burden of the different aerosol species in E5/M-MADE and in E5/M-MADEsoot. The burden of dust is lower in E5/M-MADEsoot, compatible with the lower residence time simulated. The burden of the other species, except sea salt, are similar. The largest mass of the soluble species is contained in the soluble modes, and they are only to a certain extent influenced by the modifications introduced by MADEsoot. Sea salt is difficult to compare, since it is dependent on the simulated meteorology.

	Global burden [Tg]	
	MADE	MADEsoot
BC	0.09	0.08
DU	0.31	0.21
SO ₄ ²⁻	1.35	1.35
NH ₄ ⁺	0.38	0.37
NO ₃ ⁻	0.14	0.12
POM	0.72	0.71
SS	0.18	0.13

Table 6.3: Global burden of all aerosol species in ECHAM5/MESSy-MADE and in ECHAM5/MESSy-MADEsoot (annual average). The burdens of dust and sea salt refer only to the accumulation mode.

6.2 Characterization of the potential ice nuclei

In the present study, the term potential ice nuclei (PIN) refers to particles containing BC or dust, either internally or externally mixed, in the Aitken and accumulation mode. For a more detailed discussion on the formation of ice crystals see Chapter 2. The magnitude of the number concentration is an important parameter for the characterization of PIN, since, in the case of heterogeneous freezing, it may limit the number of ice crystals in cirrus clouds, changing their microphysical properties.

In this section the number concentration of PIN is discussed, together with their mass concentration and size distribution, and the chemical composition of the coating of the internally mixed BC and dust particles in the sub-micrometer modes. Dust is also present in the coarse mode, but, since the number concentration of the coarse mode particles is typically one or two orders of magnitude lower than the concentration of the Aitken and of the accumulation mode, ranging from 10^{-2} to 10^{-1} particles/cm³ at 300 hPa, it does not contribute significantly to the number concentration of potential IN. All horizontal distributions are shown at 300 hPa, typical altitude where cirrus form at mid-latitudes.

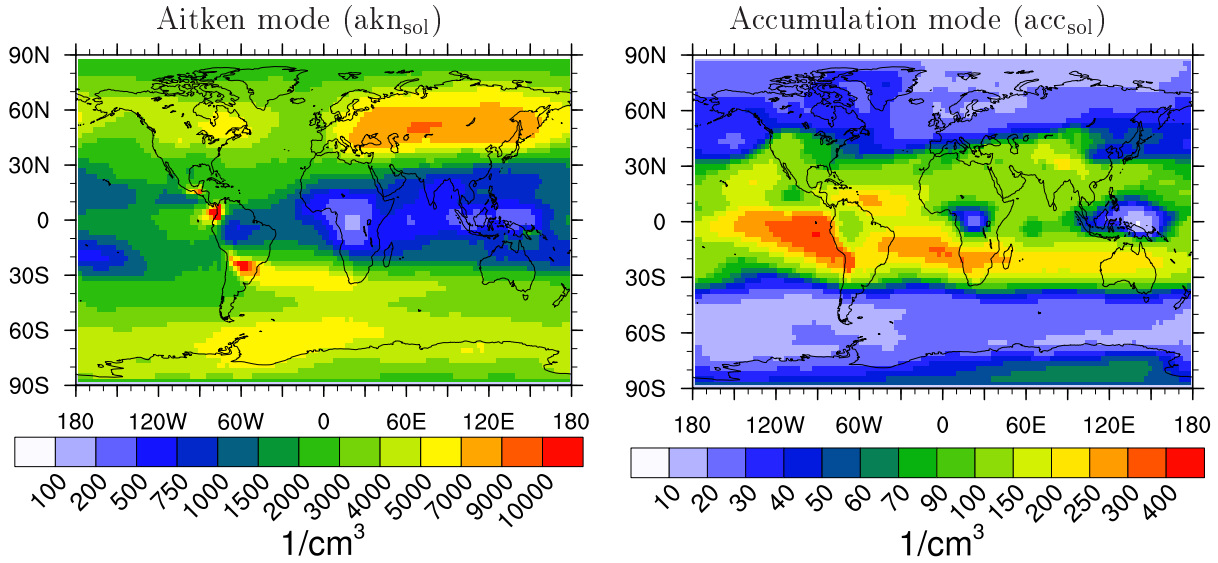
Similar studies about potential IN have not been performed to date. Models have not yet been applied to explicitly calculate the number and size distribution of PIN and of the BC and dust free particles nor the mixing state of PIN. *Hendricks et al.* (2004, 2005) applied the ECHAM4 GCM (*Roeckner et al.*, 1996) to investigate the increase in the number concentration of PIN at 250 hPa due to air traffic with respect to the background number concentration. Since ECHAM4 simulates only the mass concentration of BC, these studies have to make assumptions about the ageing of the ice nuclei and their size distribution, in order to estimate the number concentration of PIN. They assume that all BC and dust particles from surface measurements show a constant size distribution. They further simulate two different scenarios for the aircraft emissions. In the first scenario the BC number-to-mass ratio is not affected by particle ageing, in the second this ratio is lowered by effective ageing processes. The results presented in the following can be compared to the number concentration of PIN from surface sources calculated by *Hendricks et al.* (2005), which is between 1 and 5 particle/cm³ over the northern hemisphere and large part of the southern hemisphere, between 0.5 and 1 particle/cm³ over the southern Pacific ocean and between 0.2 and 0.5 particle/cm³ over Antarctica.

6.2.1 Number concentration

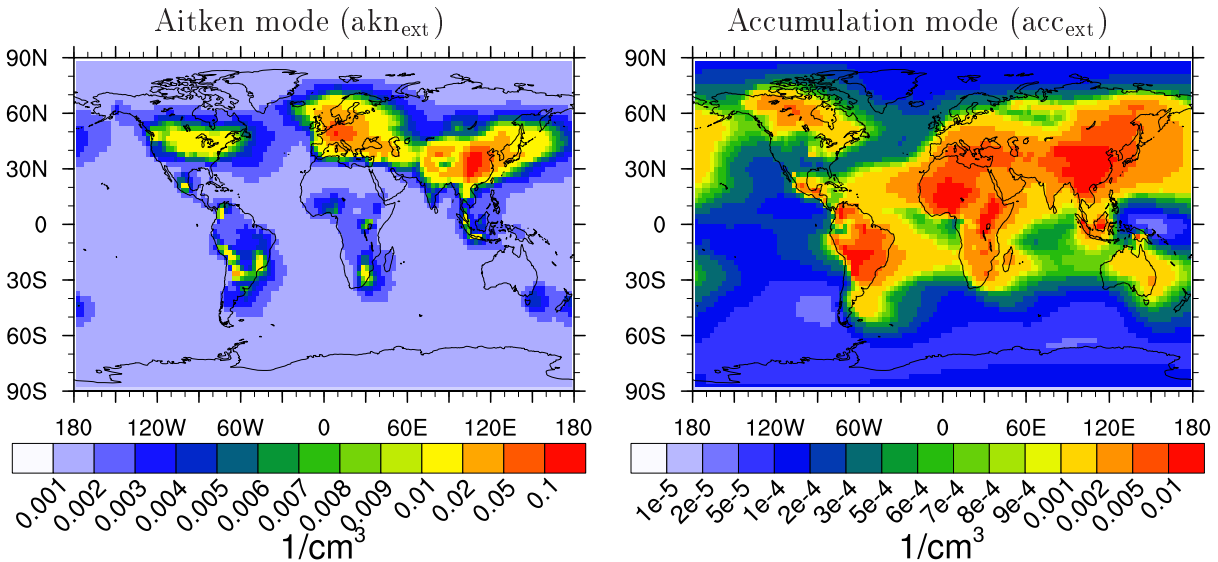
Fig. 6.9 shows the number concentration of each mode at 300 hPa. The emission areas can be recognized, but are much less pronounced than at surface layer (Fig. 6.1, Fig. 6.2, Fig. 6.3). The residence time of the species in the UTLS is much longer than in the boundary layer, allowing the air to become well mixed and less bound to the location of the emissions. The soluble modes have by far the highest number concentration at all altitudes, being the order of magnitude of the number concentration of akn_{sol} nearly everywhere 10^3 particles/cm³. While in the tropical region the nucleation of sulfuric acid particles is most efficient around 200 hPa (Fig. 6.1), at latitudes northern of 30°N and southern of 30°S this happens at 300 hPa. In Fig. 6.9, indeed, a belt with a lower particle concentration, between 750 and 1500 particles/cm³, is clearly visible in the tropical area, while the extra-tropical values are higher than 2000 particles/cm³.

The number concentration of acc_{sol} is one or two orders of magnitude lower than the one of akn_{sol} . Furthermore, the pattern is inverse with respect to akn_{sol} : the number concentration of acc_{sol} has its maximum in the tropical belt and presents lower values at higher latitudes. This is related to the distribution of the sources of the Aitken and the accumulation mode

Soluble Modes



Externally mixed BC and dust



Internally mixed BC and dust

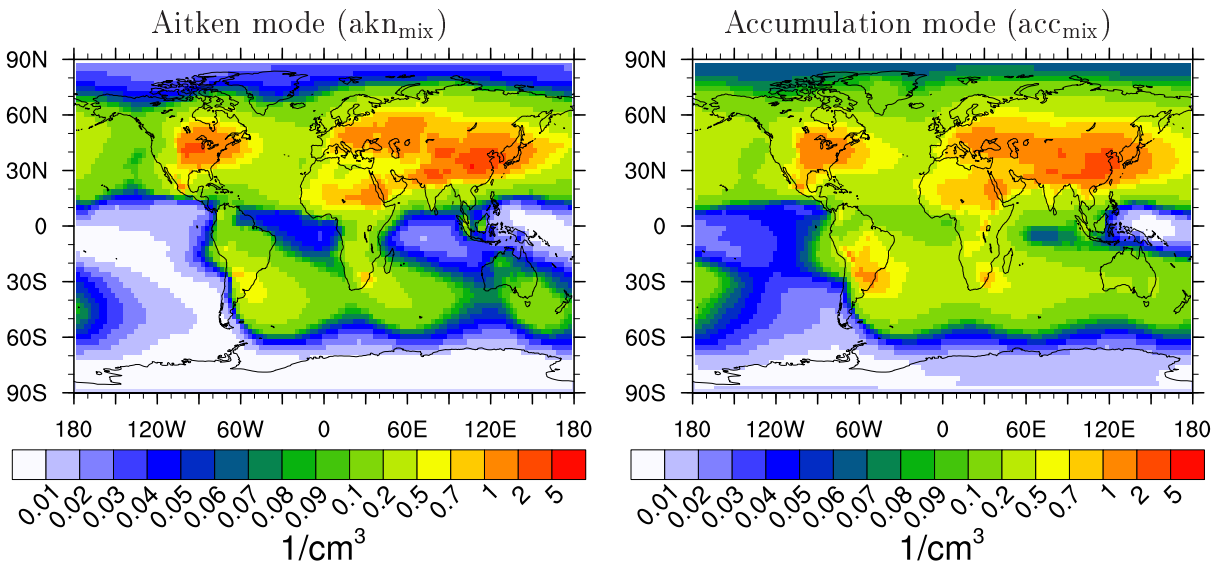


Figure 6.9: Annual mean horizontal distribution of the number concentration of the sub-micrometer modes at 300 hPa. The two soluble modes are depicted in the first row, the externally mixed BC and dust modes in the second row and the internally mixed ones in the last. Note the different scales of the plots.

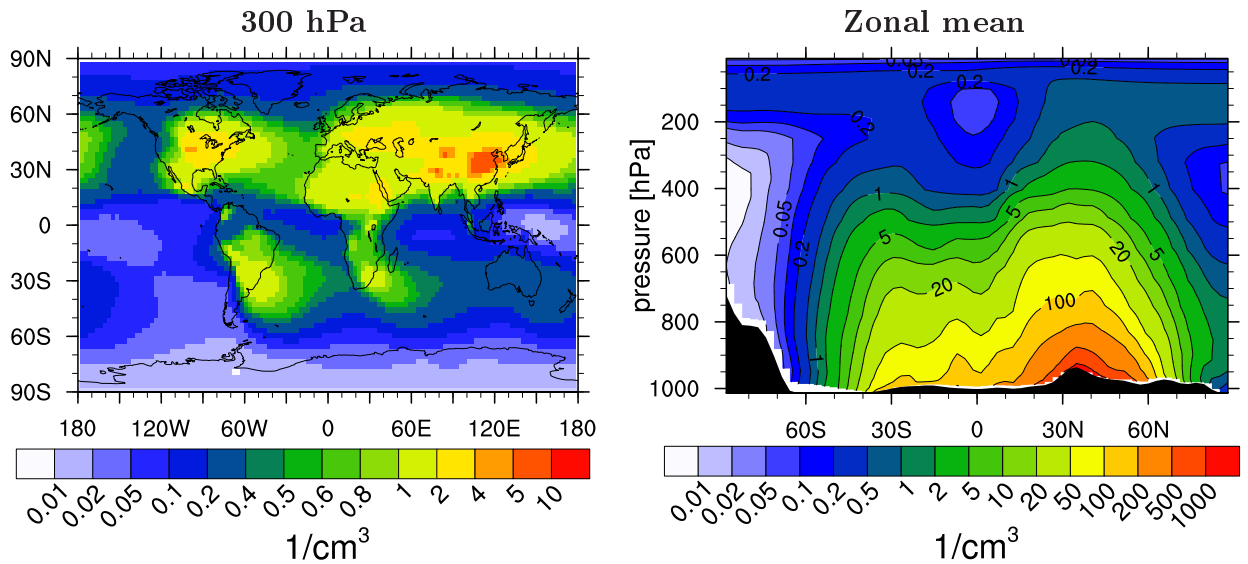
particles, together with the convective transport that carries accumulation mode particles to the UTLS in the tropics. The externally mixed modes show the lowest concentrations among the modes: there are no sources of externally mixed particles apart from the emissions of primary aerosols, which are limited at altitudes up to 300 m for akn_{ext} and up to 6 km for acc_{ext} . Even in the areas with the highest concentrations, however, the absolute number concentration of acc_{ext} is very low and never exceeds 0.05 particles/cm³. The concentration of internally mixed BC and dust particles is also much lower than the one of soluble particles, but higher than the one of the externally mixed modes, since akn_{mix} and acc_{mix} receive constantly particles from akn_{ext} and acc_{ext} due to the ageing of the externally mixed particles.

At 300 hPa altitude the total concentration of PIN (Fig. 6.10a, left) varies between 10⁻² particles/cm³ over the Pacific ocean to about 10 particles/cm³ over the major emissions regions. The sub-micrometer PIN contribute only a very small fraction to the total aerosol number concentration (Fig. 6.10b, left): Over the largest part of the globe, PIN represent between the 0.01% and the 0.1% of the total aerosol number concentration, reaching the maximum value of 0.5% over Africa, India and China. The possibility of calculating this fraction is one of the features of MADEsoot that is not available in any other global aerosol model. Between 0.1% and 1% of the IN is externally mixed at 300 hPa (Fig. 6.10c, left), with a maximum fraction of 10% over Indonesia. This maximum corresponds to a minimum in the total aerosol concentration, hence it is mainly caused by a lack of soluble and mixed aerosol, rather than by high emissions.

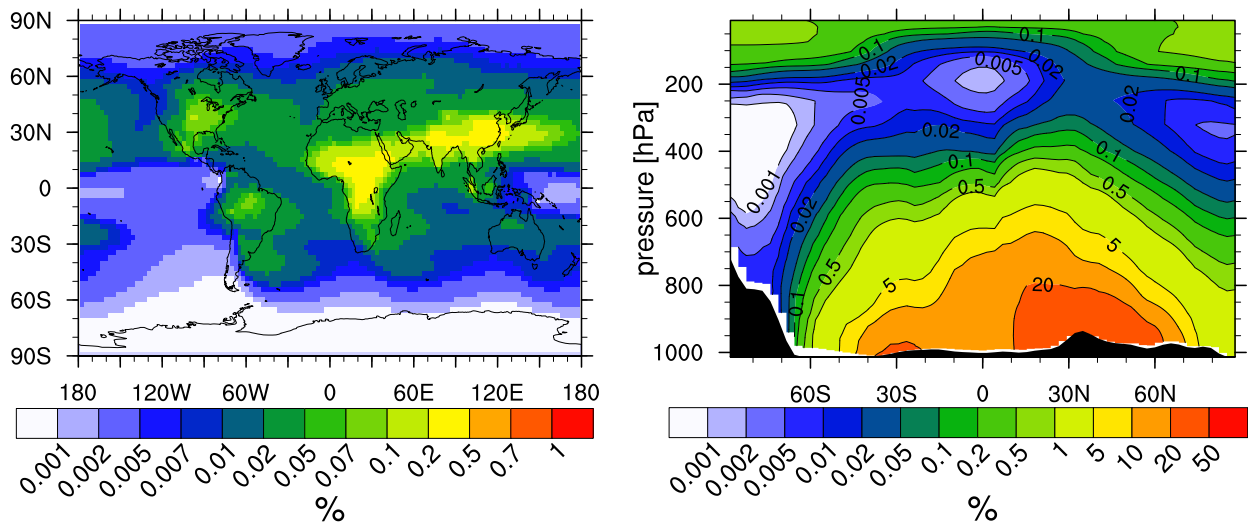
The vertical profile of the IN number concentration shows a decrease with altitude (Fig. 6.10a, right). The increase in the PIN fraction (Fig. 6.10b, right) above 200 hPa is tied to the decrease of soluble aerosol show in Fig. 6.1. The minimum at the equator at 200 hPa is related to the extremely high number concentration in the akn_{sol} . The same area presents a maximum in the fraction of the externally mixed BC and dust particles (Fig. 6.10c, right), related to the fact that, even if they are many, the freshly nucleated soluble particles are too small to be an efficient ageing agent.

The fraction of PIN that is externally mixed at 300 hPa (Fig. 6.10c, left) reaches the highest values in areas with low concentration of PIN: The blue areas in Fig. 6.10a correspond indeed to the red areas of Fig. 6.10c. This shows that, where the sinks are efficient in removing BC and dust from the atmosphere, they act mainly on the internally mixed particles, affecting at a lower extent the externally mixed ones. The zonal mean of the externally mixed PIN fraction (Fig. 6.10c, right) presents quite a complicated pattern: The boundary layer, up to 850 hPa, shows the highest fraction of externally mixed insoluble particles, obviously influenced by BC and dust emitted at surface. Above the boundary layer the fraction of externally mixed PIN is higher than 1% only in the Antarctic region, at the Equator and north of 60° N. The higher values above Antarctica are related to the low PIN concentration that characterizes the region, the ones northern of 60°N are due to the wildfires in boreal Canada and Eurasia that inject BC in the atmosphere up to 6 km (~ 400 hPa), and the ones at the equator correspond to the very fast updraft due to convection that characterizes the equatorial belt, which brings the emitted particles very fast to higher altitudes. These particles are then descending following the atmospheric circulation at latitudes around 30°N and 30°S, as discussed in Sec. 6.1.1 in the description of Fig. 6.1. During their transport, the externally mixed particles age and are transferred into an internal mixture, and their fraction decreases until it reaches 0.1%. The areas with the lowest fraction of externally mixed insoluble particles, around 500 hPa in the northern and between 500 and 700 in the southern hemisphere, are the ones where the updraft of air from the surface containing fresh externally mixed particles meets the aged air masses originating from the UTLS.

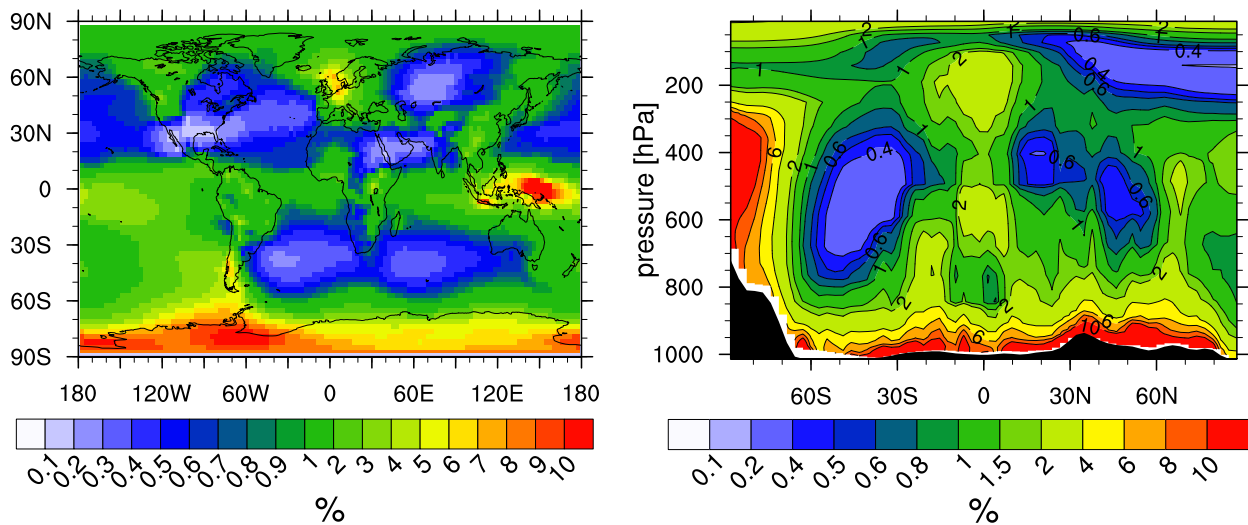
The fraction of externally mixed BC and dust particles near the Earth's surface is shown separately for the two modes in Fig. 6.11. Excluding the deserts, where ageing is particularly



(a) Total number concentration of potential ice nuclei (PIN)



(b) PIN over the total aerosol number concentration



(c) Externally mixed PIN over total number of PIN

Figure 6.10: Fig. 6.10a shows the horizontal distribution at 300 hPa and the vertical distribution of the zonal mean of the number concentration of potential ice nuclei (annual mean). Fig. 6.10b shows the fraction of the total aerosol particles which is contributed by PIN. Fig. 6.10c presents the fraction of the PIN that is externally mixed.

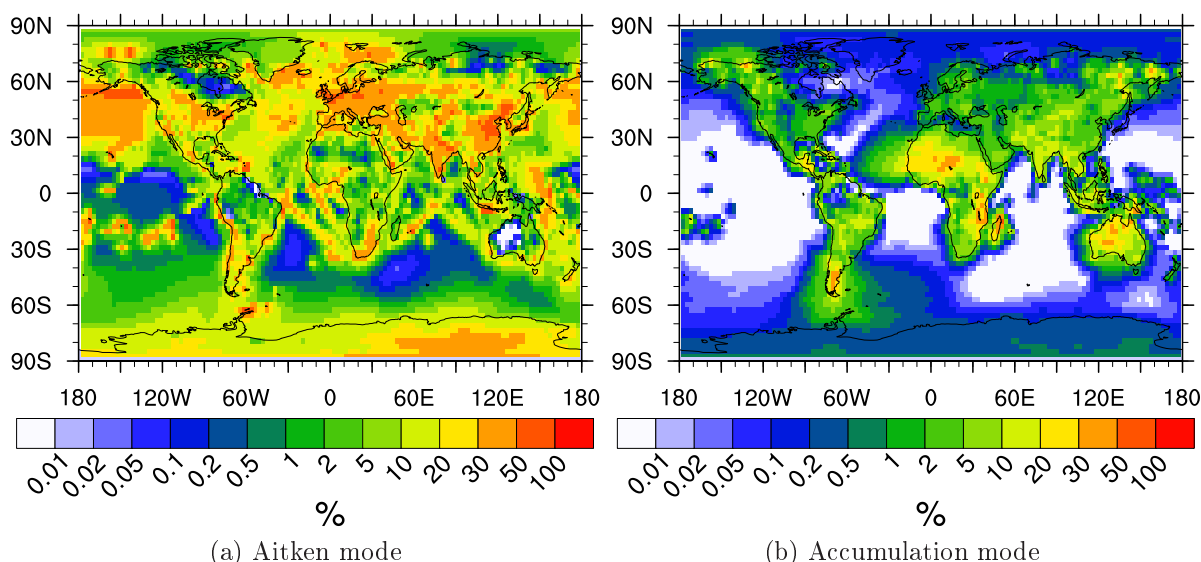
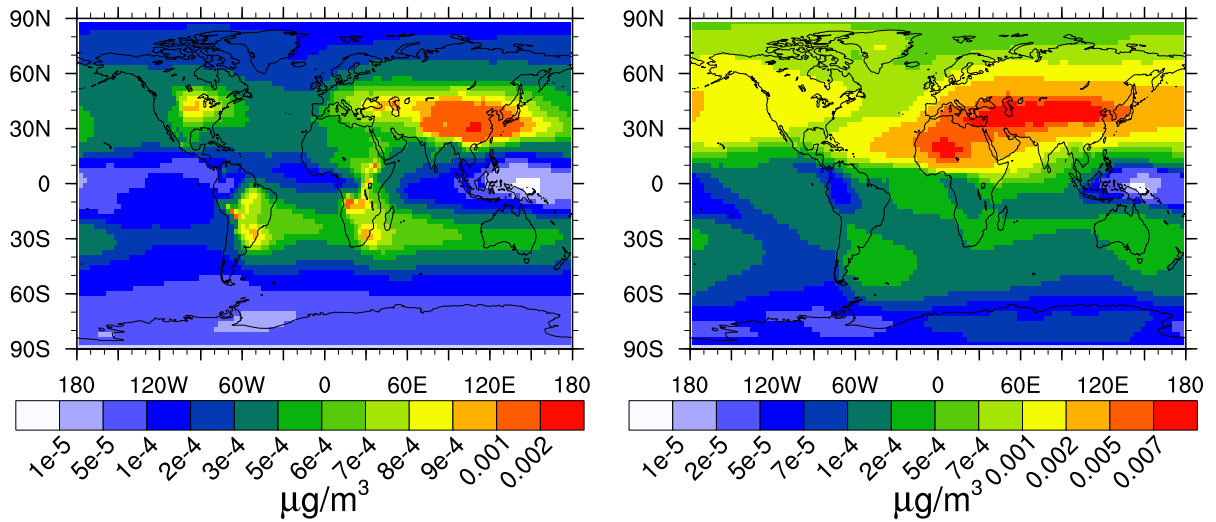


Figure 6.11: Horizontal distribution of the annual mean number fraction of potential IN that is externally mixed in the Aitken and in the accumulation mode at surface level.

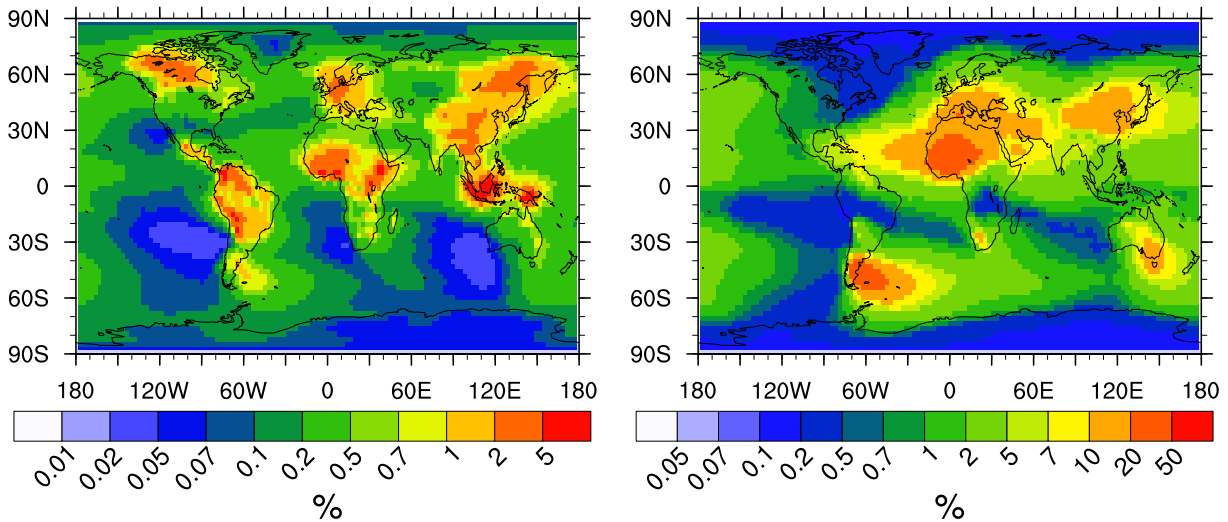
inefficient because of the lack of ageing agents, the Aitken mode presents a higher fraction of externally mixed particles with respect to the accumulation mode. Between 10% and 50% of the Aitken mode particles (Fig. 6.11a) is externally mixed at surface in areas characterized by high emission levels, whereas for the accumulation mode particles (Fig. 6.11b) the fraction ranges only between 0.1% and 10%. Since the coagulation coefficient is maximum when the diameter of the coagulating particles are different, the ageing through coagulation of the externally mixed Aitken mode BC particles (akn_{ext}) takes place mainly with accumulation mode particles (acc_{sol} and acc_{mix}). The resulting internally mixed BC particles are assigned to the accumulation mode acc_{mix} (see Tab. 3.2 in Ch.3), causing the higher fraction of externally mixed particles in the Aitken mode with respect to the accumulation mode. The externally mixed PIN fraction at surface level has very different pattern with respect to the one at 300 hPa (Fig. 6.10c), where the distribution is much more homogeneous.

Fig. 6.12 shows the individual mass concentrations of BC and dust (Fig. 6.12a) and the fraction of this mass that is externally mixed (Fig. 6.12b) at 300 hPa. While the number concentration of IN is higher in the northern hemisphere than in the southern one (Fig. 6.10a), the magnitude of the mass concentration of BC is similar in both hemispheres: This is due to the fact that the number concentration is dominated by small BC particles originated by fuel combustion processes, concentrated in the NH. The mass concentration, on the other hand, receives similar contributions from the small BC particles from fuel combustion and from the large ones from biomass burning, the main source in the SH. The fraction of externally mixed BC is lower than the one of externally mixed dust, for which the time scale of ageing is longer (see Sec. 6.3.2). Dust sources are indeed located where ageing is not particularly efficient. Additionally, the emissions of dust are supposed to be totally externally mixed, while 20% of BC mass is assumed to be internally mixed already at the time of the emission.

The number concentration of PIN simulated here is similar to the one *Hendricks et al.* (2004, 2005) calculated assuming fixed size distributions for the different PIN types. Over the Pacific ocean, however, the number concentration they calculated is lower than the one simulated by E5/M-MADEsoot.



(a) Total BC (left) and dust (right) mass concentration at 300 hPa



(b) Fraction of externally mixed BC (left) and dust (right) mass at 300 hPa

Figure 6.12: Horizontal distribution of the annual mean mass concentration of potential ice nuclei. a) BC and dust particles both externally and internally mixed. b) Fraction of the mass concentration of PIN that is externally mixed. All distribution are shown for 300 hPa level. Note the different scale of the plots.

6.2.2 Size distribution of the potential ice nuclei

Fig. 6.13, which is a detail of Fig. 6.4, shows the global median size distribution of particles containing BC and dust. The number concentration of the externally mixed BC and dust particles is clearly dominated by the Aitken mode, with median diameter of around $0.01 \mu\text{m}$ at 300 hPa. The median diameter of the externally mixed modes does not grow with altitude, because a sensible growth in size implies ageing and transfer into the internal mixture. On the contrary, the median diameter decreases slightly with altitude: This may be related to the simulated mode merging (see Sec. 3.2.5), which assigns the larger tail of the Aitken mode to the accumulation mode, when the median diameter of the Aitken mode becomes larger than 30 nm. The Aitken mode median diameter is then shifted toward smaller values.

Fig. 6.14 shows the size distribution of potential ice nuclei at 300 hPa level over different regions. The externally mixed accumulation mode has nearly disappeared at 300 hPa in all

shown regions except over South-East Asia. A large fraction of the internally mixed PIN in the Aitken mode have grown sufficiently to be transferred into the accumulation mode, and the number concentrations of the two modes at this altitude are similar. The differences among the regions are not as strong as at surface level (Fig. 6.5), owing to the homogeneity of the UTLS. As at surface level, the highest number concentration of particles containing black carbon, internally or externally mixed, occurs over South-East Asia.

6.2.3 Chemical composition of the coating of the internally mixed potential ice nuclei

Depending on the chemical composition of the coating, the freezing properties of the ice nuclei may be different. *Möhler et al.* (2008) have found that a coating of organic material may suppress the heterogeneous ice nucleation potential of atmospheric mineral particles, while *DeMott et al.* (1999) have shown that the sulfuric acid coating of Degussa soot particles lowers the freezing threshold. On the other hand, *Möhler et al.* (2005) have found that a sulfuric acid coating over soot increases the ice saturation ratio required for ice nucleation. The analysis of the internally mixed BC and dust modes gives information about the chemical composition of the coating of the particles. The main component of the coating is water (Fig. 6.15). Up to 200 hPa water represents more than 50% of the mass of coating in both the Aitken and the accumulation mode. The water fraction decreases to values of less than 5% in the higher levels.

Fig. 6.16, Fig. 6.17, Fig. 6.18 and Fig. 6.19 show the chemical composition of the dry mass of the coating, i.e. excluding the water component, for the internally mixed Aitken and accumulation mode, respectively. The zonal mean of Fig. 6.17 shows that the coating of the Aitken mode akn_{mix} is mainly composed by NH_4^+ and SO_4^{2-} . In the northern hemisphere and on a large part of the southern one NH_4^+ represents more than the 50% of the dry mass of the coating of the internally mixed BC particles in the Aitken mode. Above 300 hPa in the southern hemisphere the fraction of NH_4^+ decreases to 20%, substituted by an increase in the SO_4^{2-} fraction from around the 20% to the 50%. In contrast, above 200 hPa in the northern hemisphere the most abundant species, together with NH_4^+ , is NO_3^- , while SO_4^{2-} represents less than the 5% of the coating mass. POM constitutes in NH and at mid latitudes in SH less than 10% of the coating mass. Between the equator and 30°S the POM fraction of the coating increases strongly and reaches 50% at 400 hPa. Here the major sources of POM are located (Fig. 6.6), and a strong convective updraft frequently occurs. The sharp gradient between the southern tropic region and the northern one is due the low air mixing between the two hemispheres.

The fraction of SO_4^{2-} in the coating of the internally mixed accumulation mode with BC and dust is higher than in the Aitken mode (Fig. 6.18 and Fig. 6.19), since the freshly nucleated small SO_4^{2-} particles coagulate rather with the larger BC and dust particles than with the small ones (see Sec. 3.2.4). SO_4^{2-} is the major component of the coating in the southern hemisphere, while NH_4^+ dominates in the northern hemisphere. NO_3^- represents everywhere less than the 20% of the coating mass, mostly less than the 10%. Sea salt is everywhere negligible, with the exception of the region between 30°S and 60°S, where it amounts up to 40% at surface level.

6.2.4 Thickness of the coating of the internally mixed potential ice nuclei

The heterogeneous formation of ice crystals can take place through different processes, as explained in Sec. 2.4. Depending on the morphology of the PIN, some of these freezing

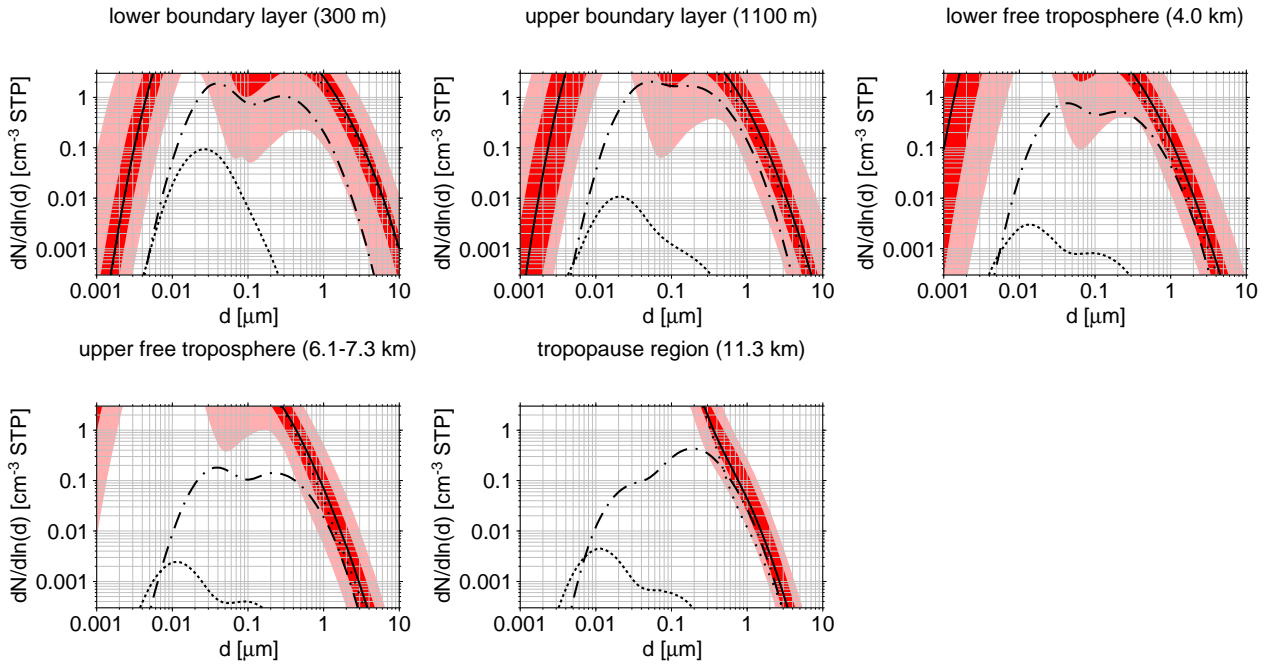


Figure 6.13: Detail of Fig. 6.4 to show the global size distribution of the potential ice nuclei. The size distribution of akn_{mix} and acc_{mix} is the dot-dashed line, the one of akn_{ext} and acc_{ext} is the short-dashed line.

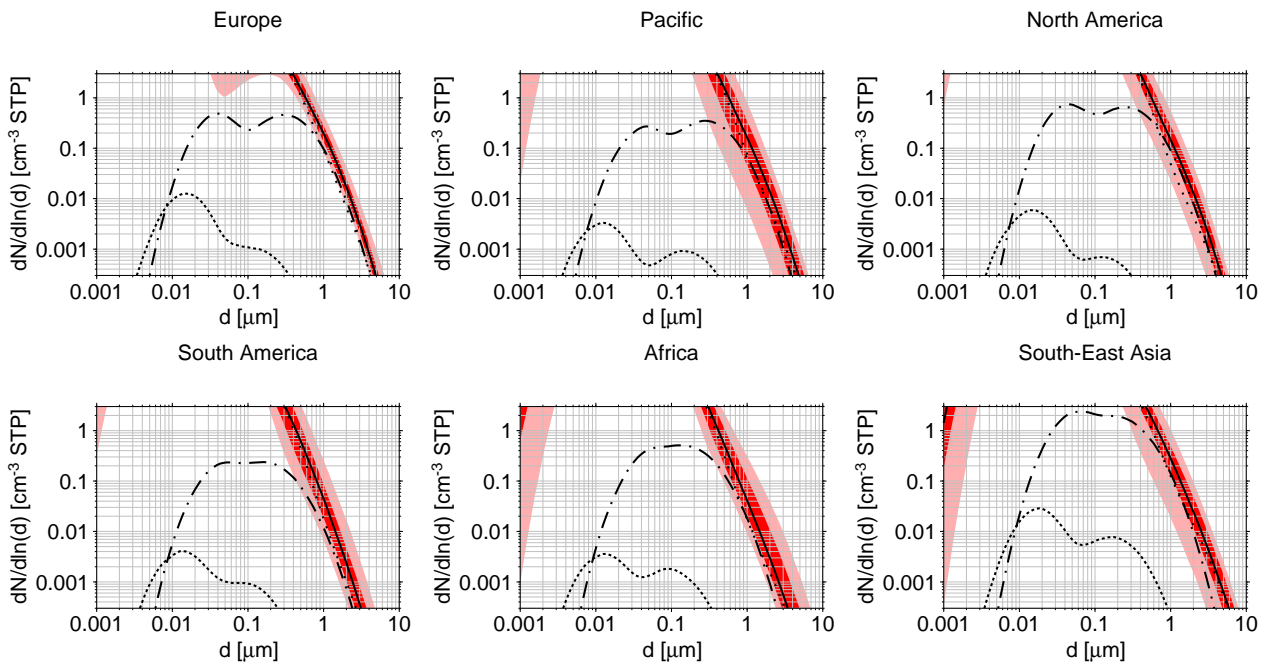


Figure 6.14: Size distribution of the potential ice nuclei at 300 hPa over different regions. The plotted regions are those defined in Fig. 5.7. The size distribution of akn_{mix} and acc_{mix} is the dot-dashed line, the one of akn_{ext} and acc_{ext} is the short-dashed line.

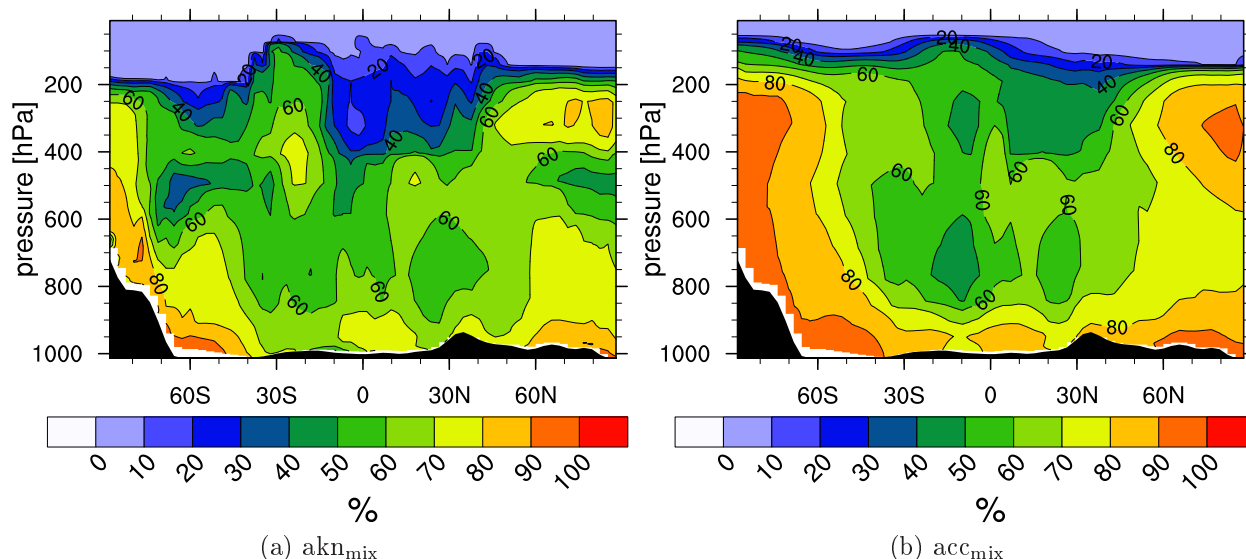


Figure 6.15: Annual zonal mean vertical distribution of the fraction of the coating mass of internally mixed BC and dust particles that consists of water.

mechanisms may be favored with respect to the others. The presence of a large number of internally mixed PIN with a thick coating may suggest that immersion freezing is favored, while deposition freezing may be favored if the PIN population presents mainly particles with thin coating. However, more experimental studies are needed to prove the correlation between the favored freezing mechanism and the thickness of the coating.

Fig. 6.20 and Fig. 6.21 shows the ratio between the mass of the soluble material and the mass of BC and dust in the akn_{mix} and acc_{mix} modes, respectively. A value of 1 means that the depicted mode contains the same amount of soluble and insoluble material. The horizontal distribution at 300 hPa and the vertical distribution of the zonal mean is shown for each of the two modes. Since the modal approach does not keep track of the size distribution of the BC and dust cores, the shown results may not represent any existing particles. In each mode, keeping fixed the number of particles and the soluble to insoluble mass ratio, both the case of particles with thin cores and large coating and the case of particles with a large core and thin coating are equally possible. However, this study gives indication about the typical coating of an average aerosol population.

The mass ratio of soluble to insoluble material in the Aitken mode (Fig. 6.20a) show a less homogeneous pattern compared to the accumulation mode (Fig. 6.21a). Particles are removed from akn_{mix} not only when they are removed from the atmosphere, as in the case of acc_{mix} , but also when they grow into the accumulation mode size range. The area between the equator and 30°S is characterized by high concentration of accumulation mode particles (especially POM) originated by biomass burning. The frequent coagulation between the externally mixed Aitken mode BC particles and the soluble accumulation mode particles causes the ageing of the externally mixed BC and at the same time the transfer to the accumulation mode.

Fig. 6.21a presents a band between the equator and 30°S where the soluble mass in the accumulation mode is mainly up to three times the insoluble mass. The vertical distribution of the zonal mean shows that the amount of soluble material mixed with black carbon and dust grows with the latitude. The low values above 200 hPa are caused by the transport of particles with small soluble fraction from the equator and by the slow ageing at that altitude. Overall, the mass of the soluble species is never lower than the mass of BC and dust in the accumulation mode.

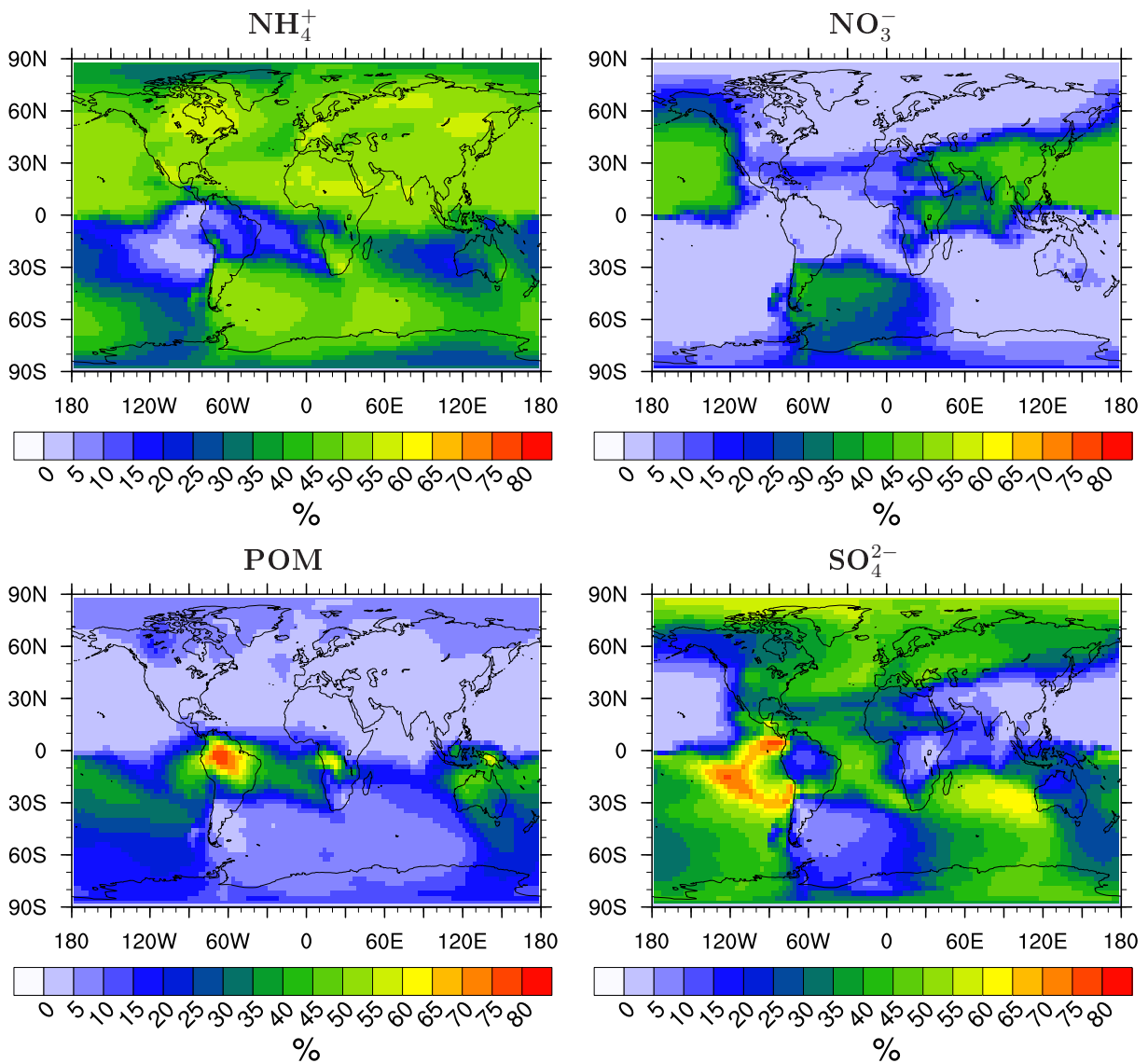


Figure 6.16: Horizontal distribution at 300 hPa of the annual mean chemical composition of the dry mass present in the internally mixed BC particles coating in the Aitken mode (akn_{mix}).

6.3 Ageing of black carbon and dust particles

As explained in detail in Sec. 3.2.6 and Sec. 4.3.4, E5/M-MADEsoot can explicitly simulate the ageing of externally mixed BC and dust particles to an internal mixture due to coagulation with other particles containing soluble material, condensation of sulfuric acid vapor and cloud processing.

In most global aerosol models the transformation of BC and dust from the external into the internal mixture is simulated, in a very simplified way, assuming a fixed turnover rate. In MADE, for instance, the externally mixed BC is assumed to decay exponentially into an internal mixture following

$$c_{\text{ext BC}}(t) = c_{\text{ext BC}}(t_0)e^{-\frac{1}{\tau}(t-t_0)}, \quad (6.2)$$

with an e-folding time τ arbitrarily assumed to be 1 day. The same decay law is used by *Lohmann et al.* (1999) and *Koch* (2001), who assume an e-folding time of around 1.8

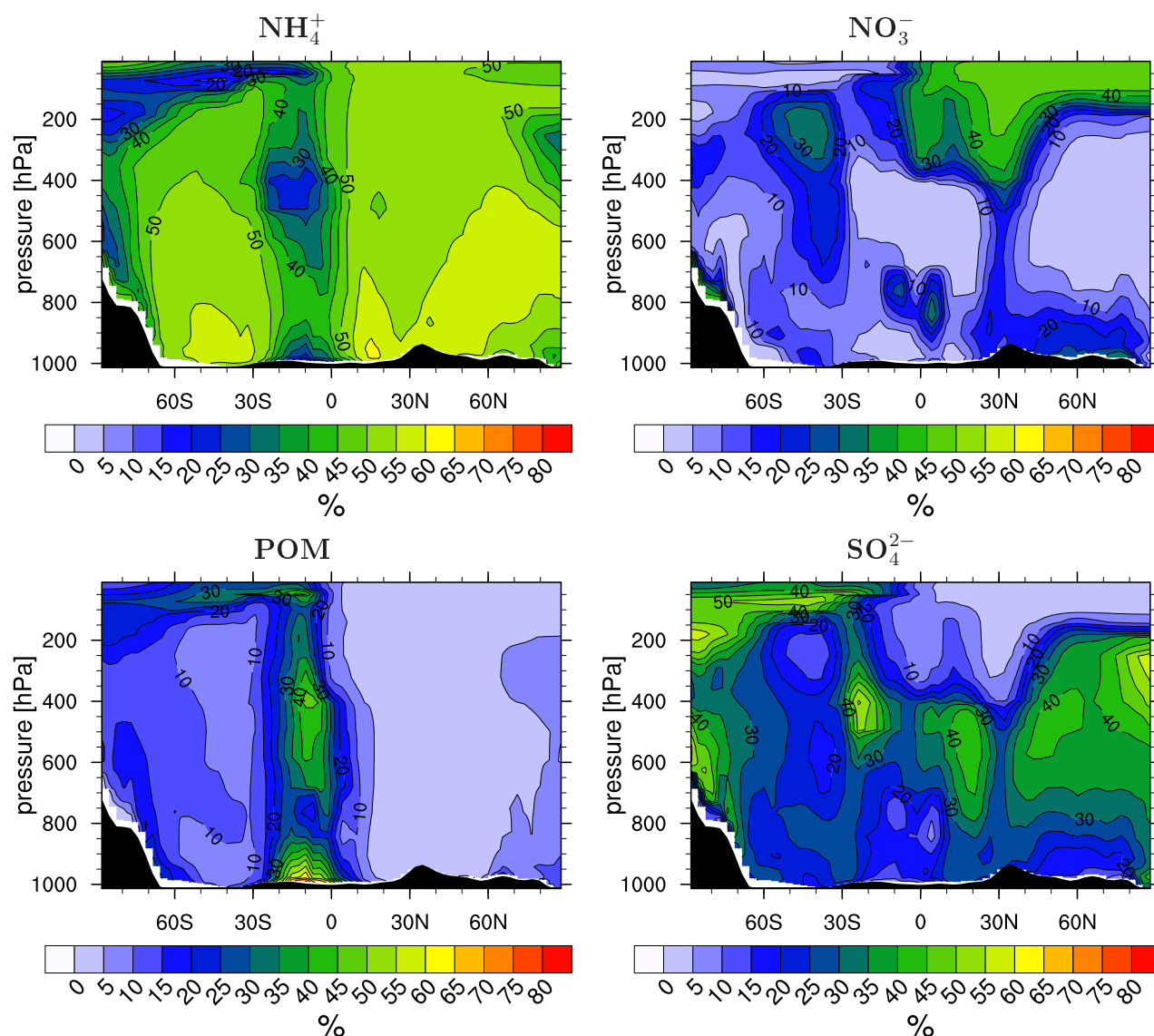


Figure 6.17: Vertical distribution of the annual zonal mean chemical composition of the dry mass of the coating present in the internally mixed BC particles coating in the Aitken mode (akn_{mix}).

days. The number fraction of hydrophilic particles is assumed to be proportional to their hydrophilic mass fraction. Dust is supposed by MADE to be always hydrophobic. The studies conducted with MADEsoot and here described allows to prove if this e-folding time is reasonable.

6.3.1 Effectiveness of the single ageing processes on the mixing state of black carbon and dust

The influence of condensation, coagulation and cloud processing on the mixing state of black carbon and dust particles have been investigated in this work by mean of three sensitivity simulations which are discussed here:

- COAG: the intermodal coagulation is the only ageing process. The condensation of sulfuric acid vapor takes place only on soluble particles and on internally mixed BC and

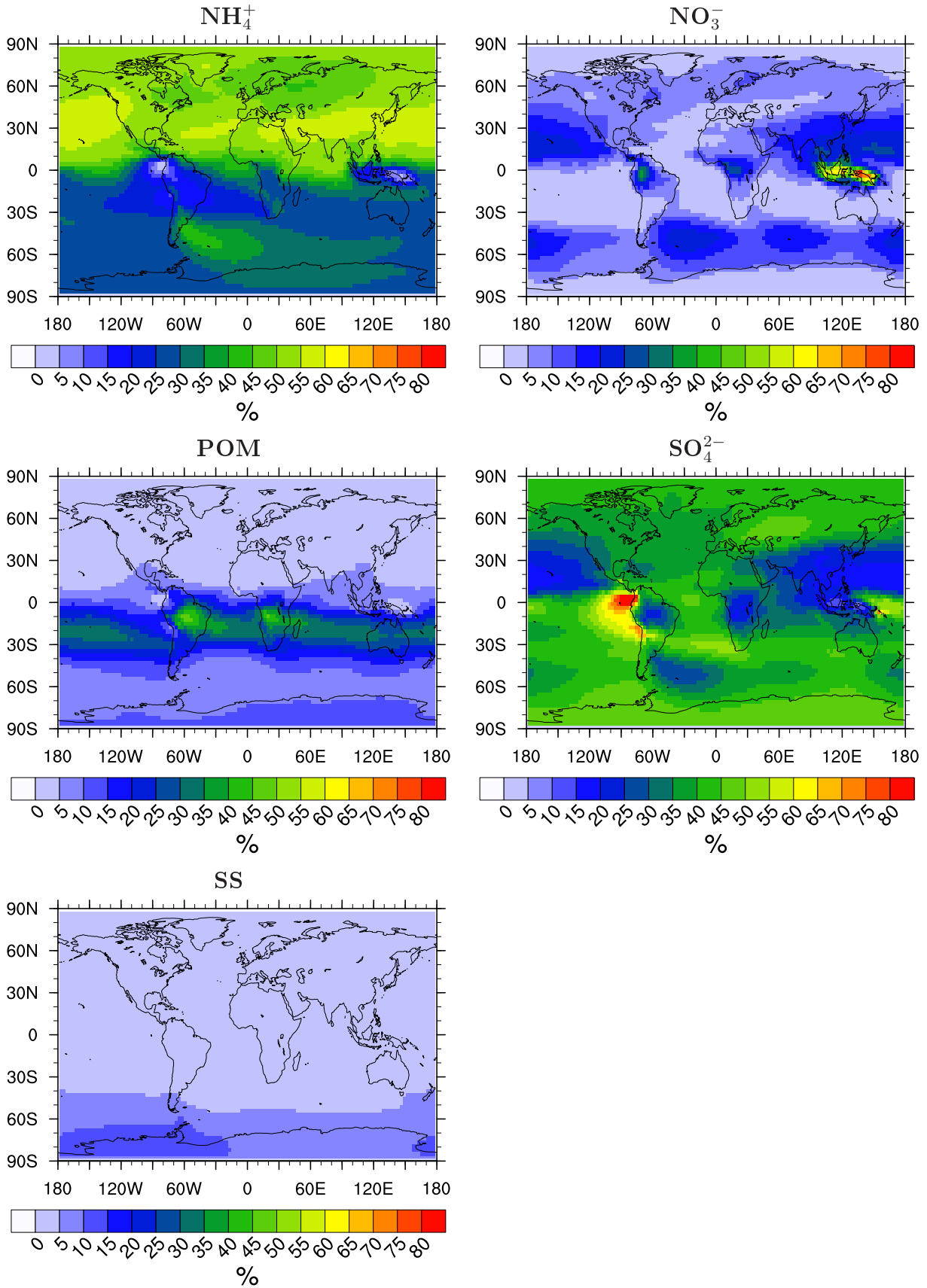


Figure 6.18: Horizontal distribution at 300 hPa of the annual mean chemical composition of the dry mass present in the internally mixed BC and dust particles coating in the accumulation mode (acc_{mix}).

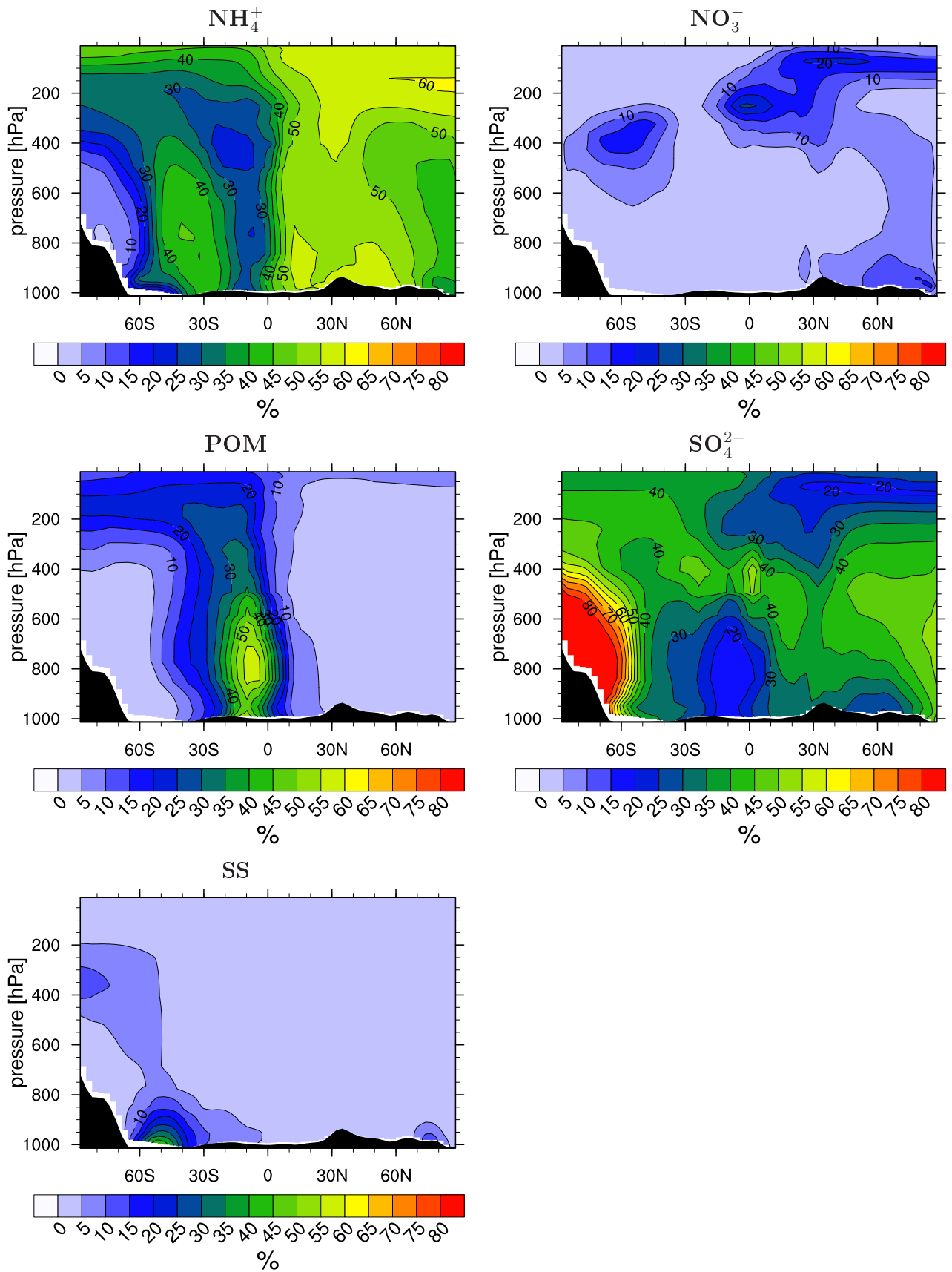


Figure 6.19: Vertical distribution of the annual zonal mean chemical composition of the dry mass of the coating present in the internally mixed BC and dust particles coating in the accumulation mode (acc_{mix}).

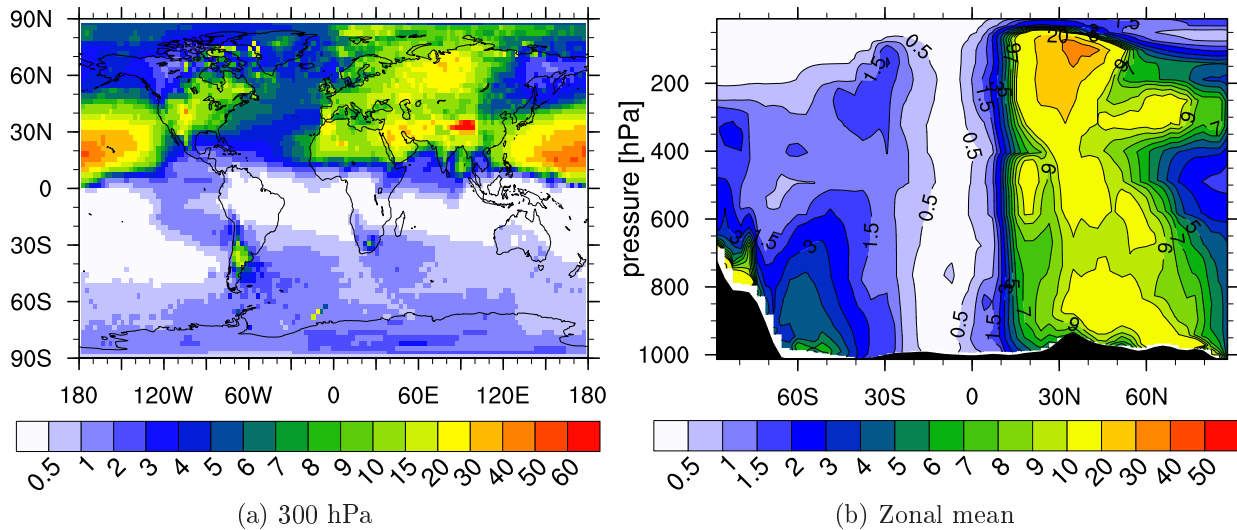


Figure 6.20: Annual mean horizontal distribution at 300 hPa (a) and zonal mean vertical distribution (b) of the ratio between the soluble and the insoluble mass in the internally mixed BC particles in the Aitken mode (akn_{mix}).

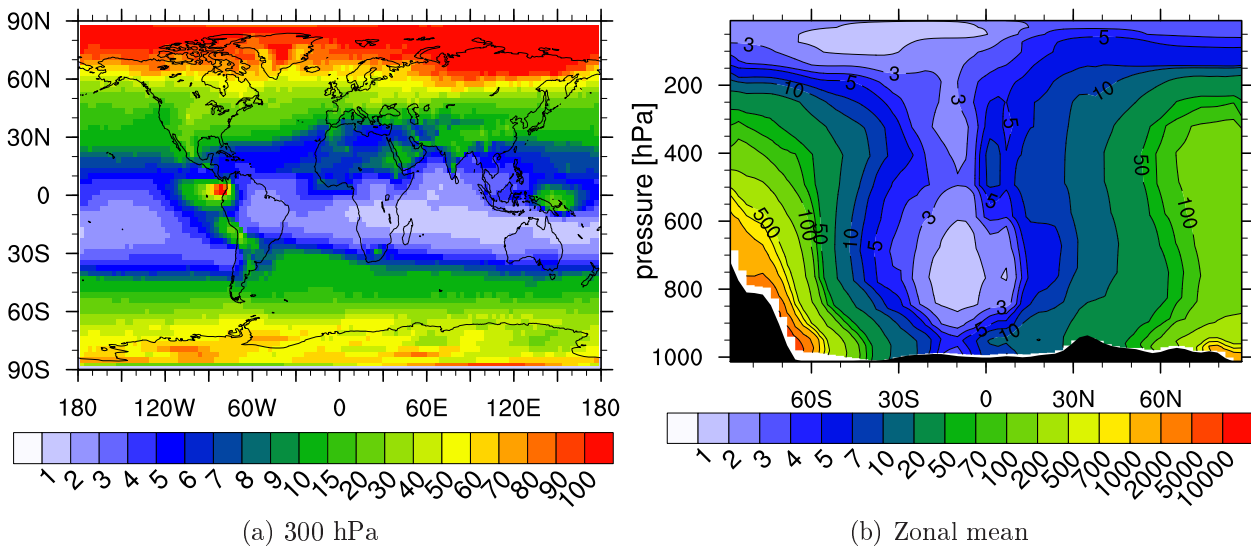


Figure 6.21: Annual mean horizontal distribution at 300 hPa (a) and zonal mean vertical distribution (b) of the ratio between the soluble and the insoluble mass in the internally mixed BC and dust particles in the accumulation mode (acc_{mix}).

dust particles. Externally mixed BC and dust particles scavenged by cloud particles are assigned to the externally mixed modes if the particle evaporates;

- COND: The condensation of sulfuric acid vapor is the only ageing process. The externally mixed modes do not take part in any coagulation process. Externally mixed BC and dust particles scavenged by cloud particles are assigned to the externally mixed modes if the particle evaporates;
- CLOUD: Cloud processing is the only ageing process. The condensation of sulfuric acid vapor takes place only on soluble particles and on internally mixed BC and dust particles. The externally mixed modes do not take part in any coagulation process.

The condensation of NO_3^- and NH_4^+ resulting from the gas/particle equilibrium is active in all three experiments. All other aspects of the simulations are exactly the same as for the reference run. The results shown in Fig. 6.22 and Fig. 6.23 represent annual means calculated over a 5 years period after one year of spin-up.

Fig. 6.22 and Fig. 6.23 show the fraction of accumulation mode dust and of total BC that is externally mixed. To estimate the effectiveness of each ageing process the area close to the sources has to be analyzed, moving away from the emission area horizontally for the horizontal distribution and vertically in the zonal mean. The analysis of the surface level alone would lead to a negative bias in the estimation of the effectiveness of cloud processing, since the cloud cover of the lowest model level is quite low.

Both in the case of dust and of BC, the experiment COND clearly shows the lowest fraction of externally mixed particles. In the case of dust the source regions are clearly defined. Looking at the Sahara in the horizontal distribution (but any other region where dust is emitted leads to the same conclusion), there is a very strong maximum over the desert where the fraction of externally mixed dust is over 90%. Moving west in the direction of the Archipelago Azores, the experiment COND (Fig. 6.23b) shows fractions between 40 % and 60 % of externally mixed dust where COAG (Fig. 6.23a) still shows more than 90 % externally mixed dust and CLOUD (Fig. 6.23c) more than 70 %. The analysis of the vertical distribution leads to the same conclusion. The ranking between coagulation and cloud processing depends on the region: While west of the Sahara desert and north of India cloud processing seems to be faster, the other emission areas seem to favor coagulation.

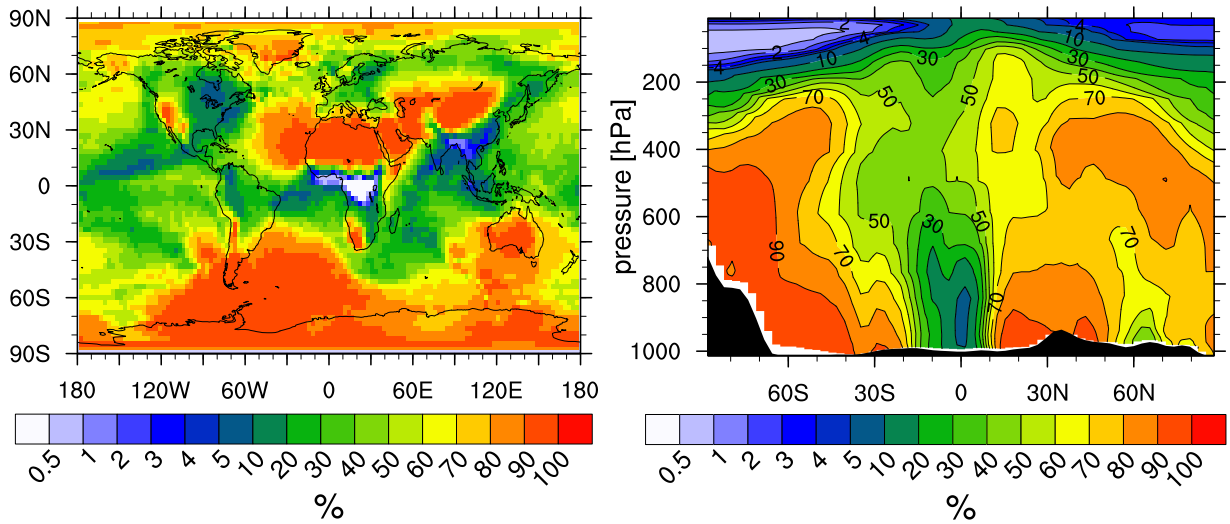
The larger efficiency of condensation is even clearer for BC (Fig. 6.23) than for dust, both in the horizontal distribution and in the vertical profile. The only region where coagulation and condensation are of similar importance is over the Gulf of Guinea, but the reason is more a lack of fresh emissions in the area, rather than a high efficiency of coagulation. The emissions from shipping can be recognized in that area, and BC from shipping emissions is more aged in the experiment COND than in COAG.

Globally, the efficiency of each process with respect to the others can be estimated from the global burden of the externally mixed BC and dust and their residence time calculated by means of Eq. [6.1], reported in Tab. 6.4. The residence time is a good indicator for comparing the effectiveness of the respective ageing processes, since ageing is the only sink of externally mixed BC and dust particles whose magnitude changes among the three test simulations (the other sinks are scavenging from impacting droplets, ice scavenging and dry deposition). On the global scale, condensation is the most efficient process, while cloud processing is the least for both BC and dust.

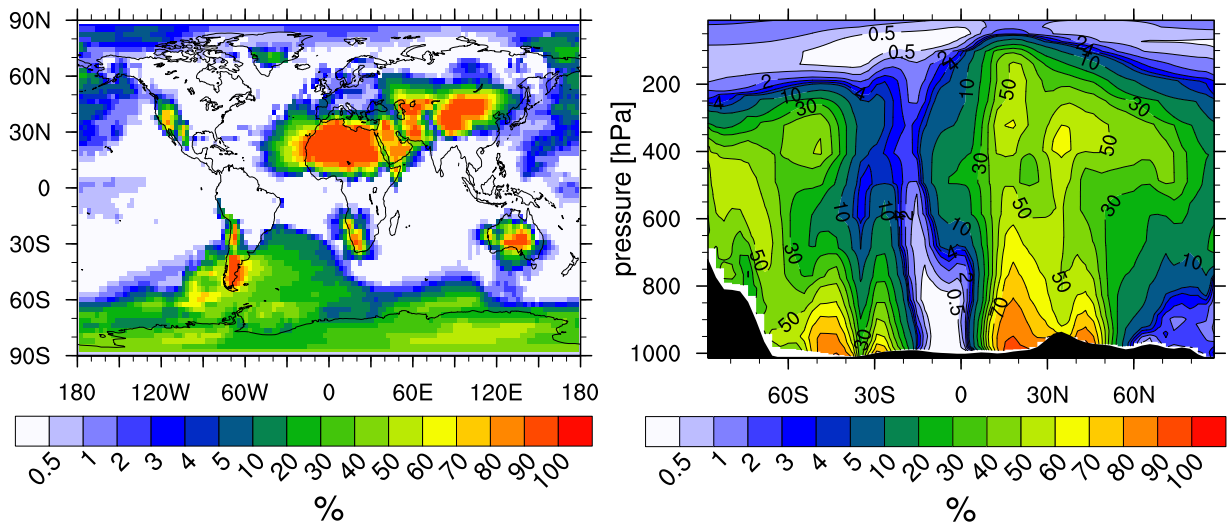
Note that what the three experiments show is not the absolute efficiency of each process, but only the efficiency relatively to the others. Coagulation, condensation and cloud processing are not independent from each other, therefore the comparison among the three experiments has to be interpreted only qualitatively.

	Total burden [$10^{-3} \cdot \text{Tg}$]			Residence time [days]		
	COAG	COND	CLOUD	COAG	COND	CLOUD
ext. mixed BC	10.9	6.00	58.6	0.61	0.33	3.26
ext. mixed dust	119	92.7	187	4.12	3.21	6.45

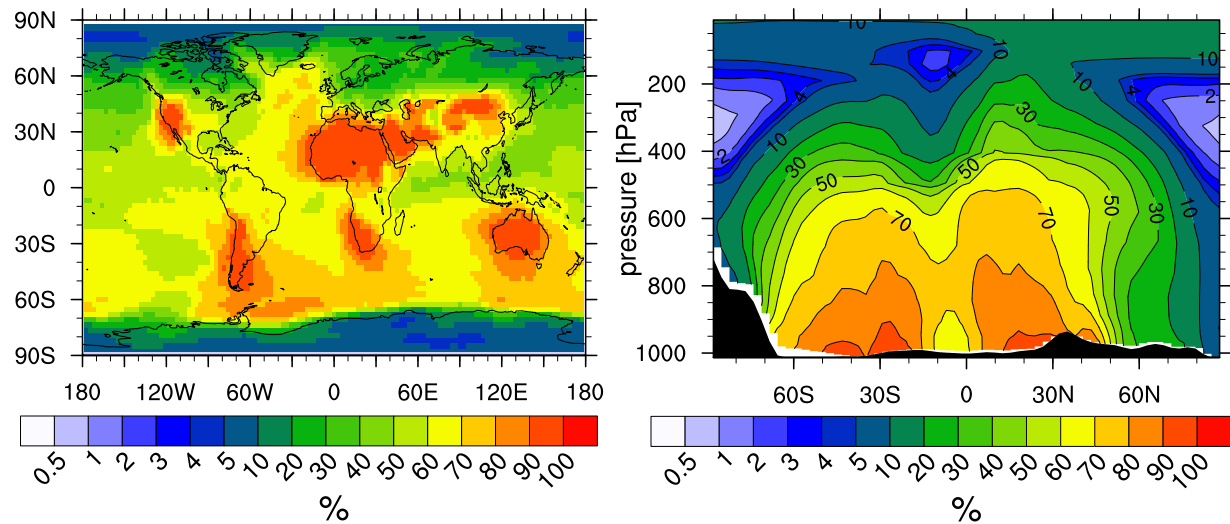
Table 6.4: Total burden and residence time of externally mixed BC and externally mixed accumulation mode dust in the three experiments COAG, COND and CLOUD.



(a) Exp. COAG: only ageing by coagulation.



(b) Exp. COND: only ageing by condensation.



(c) Exp. CLOUD: only ageing by cloud processing.

Figure 6.22: Annual mean horizontal distribution and zonal mean vertical distribution of the fraction of the accumulation mode dust that is externally mixed in the three experiments COAG (a), COND (b) and CLOUD (c).

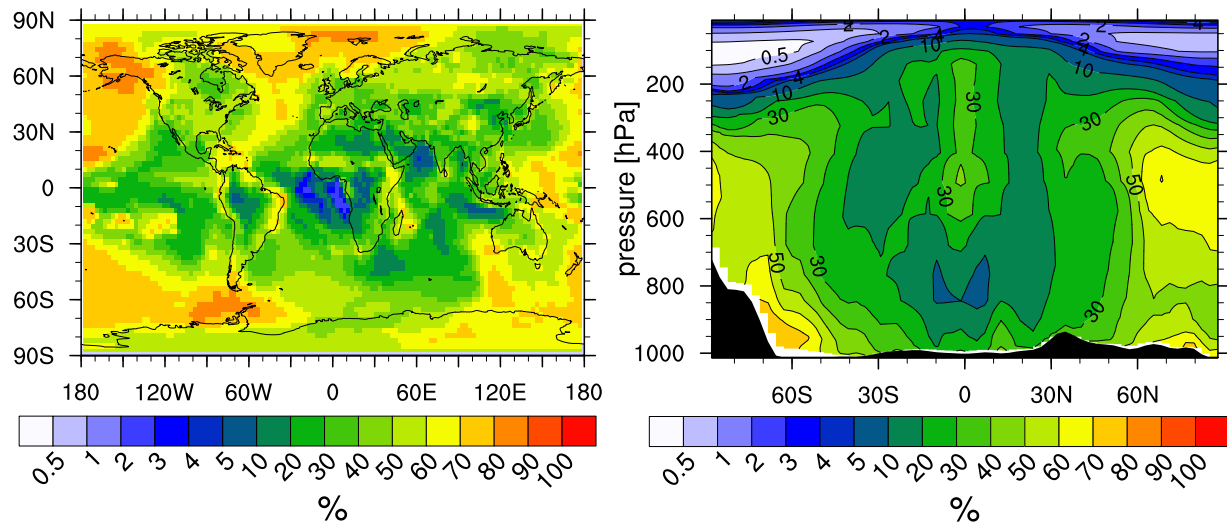
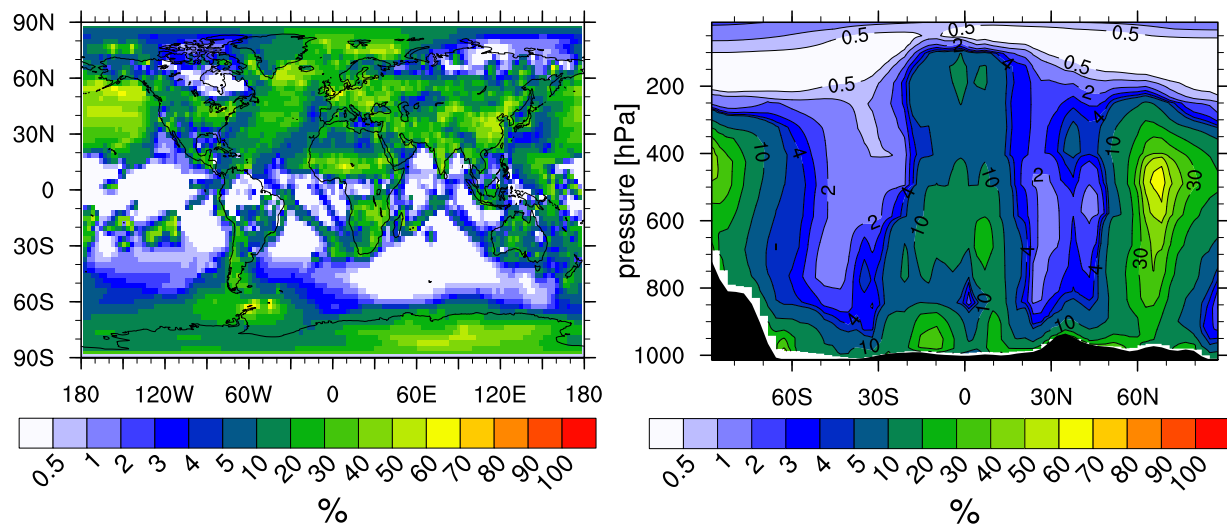
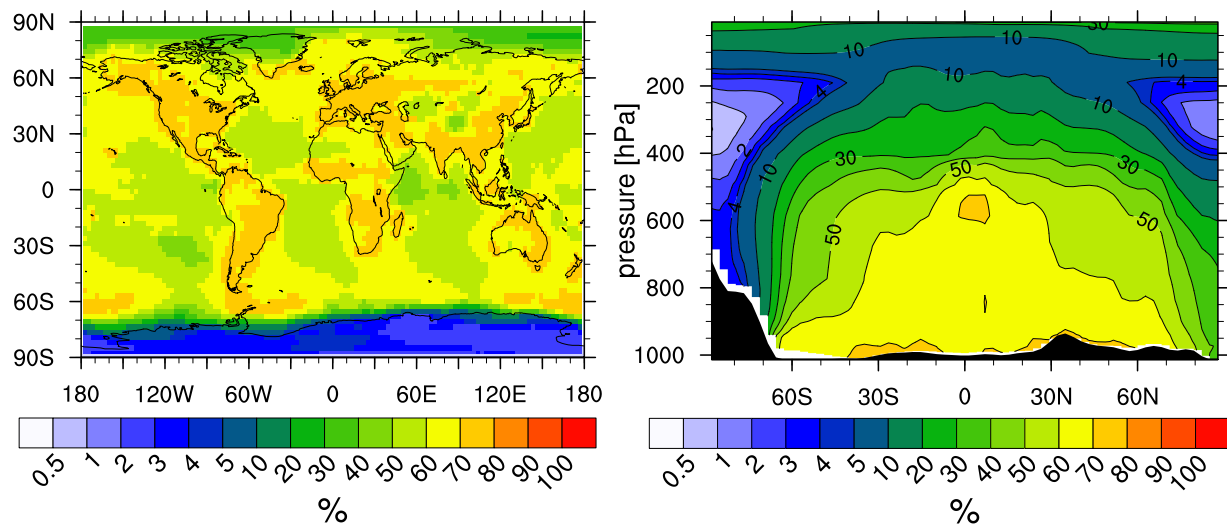
(a) **Exp. COAG**: only ageing by coagulation.(b) **Exp. COND**: only ageing by condensation.(c) **Exp. CLOUD**: only ageing by cloud processing.

Figure 6.23: Annual mean horizontal distribution and zonal mean vertical distribution of the fraction of the total BC that is externally mixed in the three experiments COAG (a), COND (b) and CLOUD (c).

6.3.2 Transformation time of externally mixed black carbon and dust

MADeSoot does not need any assumption as Eq. [6.2] on the ageing of BC, since this is explicitly simulated, hence MADeSoot allows for a direct calculation of the e-folding time τ . The so calculated τ can be used to evaluate the consistency of the assumption of $\tau = 1$ day, and could be used in future application of the aerosol sub-model MADE to reach a more precise representation of the mixing state of BC and dust. MADE is less detailed of MADeSoot in the description of aerosols but for this reason also computationally less expensive.

From Eq. [6.2], the e-folding time τ is in each model box equals to

$$\tau = \frac{c_{\text{ext BC}}(t_0)}{c_{\text{ext BC}}(t_0) - c_{\text{ext BC}}(t)} \cdot (t - t_0) \quad (6.3)$$

$$= \frac{\text{burden}(t_0)}{\text{loss}_{\Delta t}} \cdot \Delta t, \quad (6.4)$$

if no externally mixed BC and dust are emitted during the time Δt . Burden(t_0) is the burden of externally mixed BC or dust at the beginning of the time step, $\text{loss}_{\Delta t}$ the mass of externally mixed BC or dust that is transferred to an internal mixture during the time step and Δt the length of a time step. To ensure that the calculated τ corresponds only to ageing of BC and dust, all other possible sinks (dry and wet deposition, transport into other boxes) have to be excluded from the calculation. The burden is the amount of externally mixed BC or dust mass before the ageing process is implemented, i.e. before MADeSoot is executed, and the loss is the difference between the amount of externally mixed BC or dust before and after the execution of MADeSoot during the time step Δt . There are neither emissions nor transport sources of externally mixed BC and dust during the MADeSoot. Such a calculation excludes the cloud processing from the transformation time τ , even though it is present as ageing process: Given the results shown in Sec. 6.3.1, this approximation should not have a large influence on the estimation of τ .

On the global scale, integrating the burden and loss of BC and dust of Eq. 6.4 over the whole globe and averaging over the whole year, the transformation time τ is about 2 hours and a half for BC and 36 hours for dust. However, such a rough estimation of τ is misleading, since it is strongly dominated by the boundary layer, where the ageing process is much faster. This would lead to an overestimation of the efficiency of ageing for emissions, as for instance those from air traffic, injected in higher layers. Fig. 6.24 shows the vertical profile of the globally averaged tau for externally mixed BC and dust. The global transformation time τ_{BC} of externally mixed BC is below 4 hours up to 750 hPa. Above 750 hPa τ_{BC} grows to reach the value of 50 hours at 200 hPa. The global transformation time τ_{DU} of externally mixed dust is at no altitude lower than 20 hours, value which is reached between 500 hPa and 600 hPa. The lowest layers are strongly influenced by the high mass emissions over the desert. Fig. 6.22 shows at this altitude the lowest fraction of externally mixed dust particles both in the experiment COAG and in the experiment COND, excluding the region above 300 hPa. Above 300 hPa dust particles emitted at surface level have been transported over long distances and even slow ageing processes have had the time to act in the model layers below.

The vertical profiles of Fig. 6.24 provide only a very simplified picture of the time scale of the ageing of BC and dust, since τ shows also a very high geographical variability. Fig. 6.25 presents the transformation time for externally mixed BC in the lowermost model layer, i.e. up to about 100 m, in the 16th layer (~ 800 m), in the 11th (~ 5.5 km) and in the 8th (~ 10 km) layer. In the lowermost level (Fig. 6.25a) the minimum values of τ_{BC} , up to one hour,

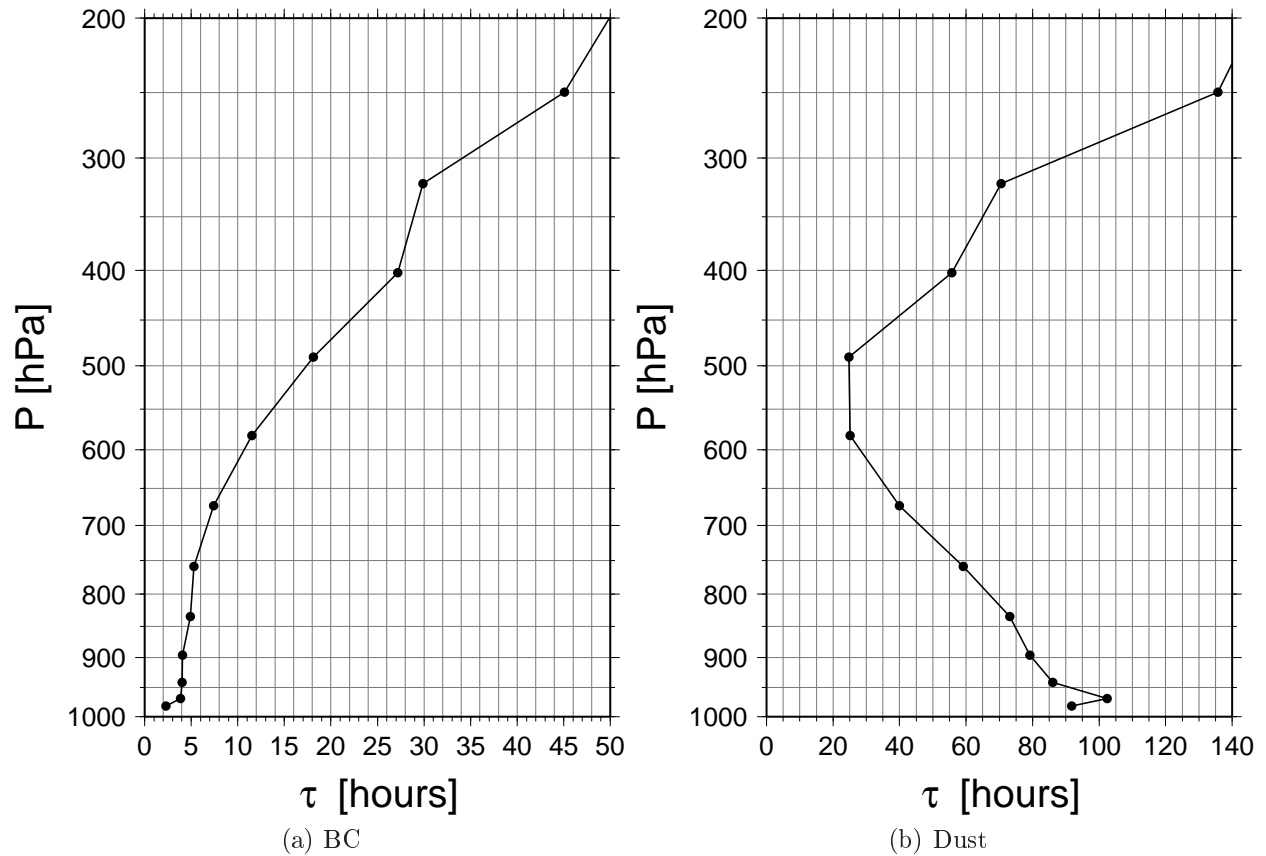


Figure 6.24: Vertical profile of the transformation time on the global scale of externally mixed BC and dust. The transformation time shown here is calculated from the annual mean of the burden and of the loss integrated in each layer over the whole globe.

occur over the areas where the main BC source is biomass burning. Biomass burning emits, together with larger BC particles, a high amount of POM, much higher than the amount emitted by fuel combustion (*Kloster et al.*, 2008). This may lead to the faster ageing of accumulation mode BC particles from biomass burning. *Schwarz et al.* (2008a) have arrived to the same conclusion by measuring freshly emitted black carbon with a SP2 in urban and biomass burning emissions. The maximum values are over the deserts and Antarctica, but they are not particularly significant because the concentrations of BC over those areas are low. Europe shows values of τ_{BC} between one and three hours. The values for the model layer around 500 m (Fig. 6.25b) are similar to the values calculated in the altitude range between 200 m and 3 km. Higher than 3 km the time scale of the ageing process grows quite fast, being nearly everywhere higher than 6 hours at 5.5 km (Fig. 6.25c) and than 12 hours at 10 km (Fig. 6.25d), the level at which aircraft emissions are injected in the atmosphere.

A comparison with the transformation time for BC calculated by *Riemer et al.* (2004) for the region of Karlsruhe has been performed. The model box where Karlsruhe is located covers the area between 47.4°N and 50.2°N and 7.0°E and 9.8°E in the T42 grid used by E5/M-MADEsoot. The τ in this model box has been calculated from the results of the simulation with $x = 5\%$, which is the threshold used by *Riemer et al.* (2004). They found that, during the day, τ_{BC} varies between 1 hour in the morning and 20 hours in the afternoon below 250 m, and is below 2 hours above 250 m up to 1.5 km. They calculated much higher values of τ_{BC} during night time. A vertical resolution as fine as the one of the regional model of *Riemer et al.* (2004) cannot be achieved with E5/M-MADEsoot, that divides the range between surface and 1.5 km in only 5 levels (0-65 m, 65 m-230 m, 230 m-540 m, 540

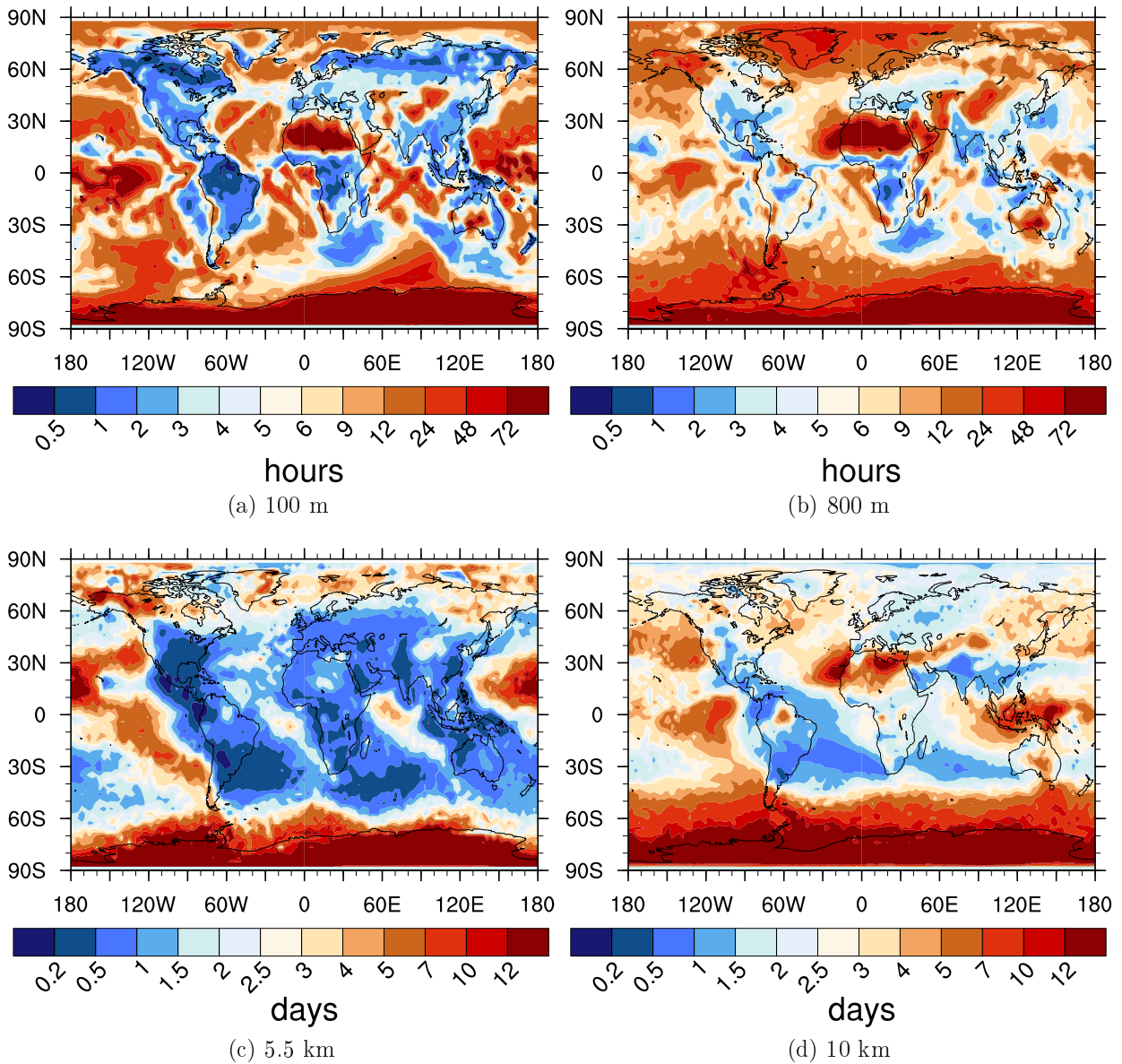


Figure 6.25: Horizontal distribution of the annual mean transformation time τ_{BC} of the externally mixed BC into an internal mixture at different altitudes.

m-1020 m, 1020 m-1680 m). It is also not possible to distinguish between day and night, because it would imply a more frequent output over the long simulation time that a global model needs, with a consequent very large need of disk space. The value of τ calculated with E5/M-MADEsoot is equal to 1.6 hour in the lowermost model layer, between 4 and 5 hours in the model layers between 65 m and 1020 m, and more than 6 hours in the highest level, with much shorter τ_{BC} in summer (below one hour in the lowermost level and up to two and a half hour in the higher levels) than in winter (between 5 hours in the lowermost level and up to 10 hours in the highest), in agreement with *Riemer et al. (2004)*. Taking into account the large differences between a regional and a global model, and the weakness of a global model to characterize regional effects, a direct comparison with *Riemer et al. (2004)* is difficult and would imply a more precise knowledge of the emissions and of the boundary conditions that they used in the model. Anyhow, both *Riemer et al. (2004)* and this study have found time scale of less than the one day assumed by MADE.

The pattern of the transformation time of dust τ_{DU} (Fig. 6.26) is similar to the one of BC. At surface level τ_{DU} reaches very high values over the deserts and decreases very fast

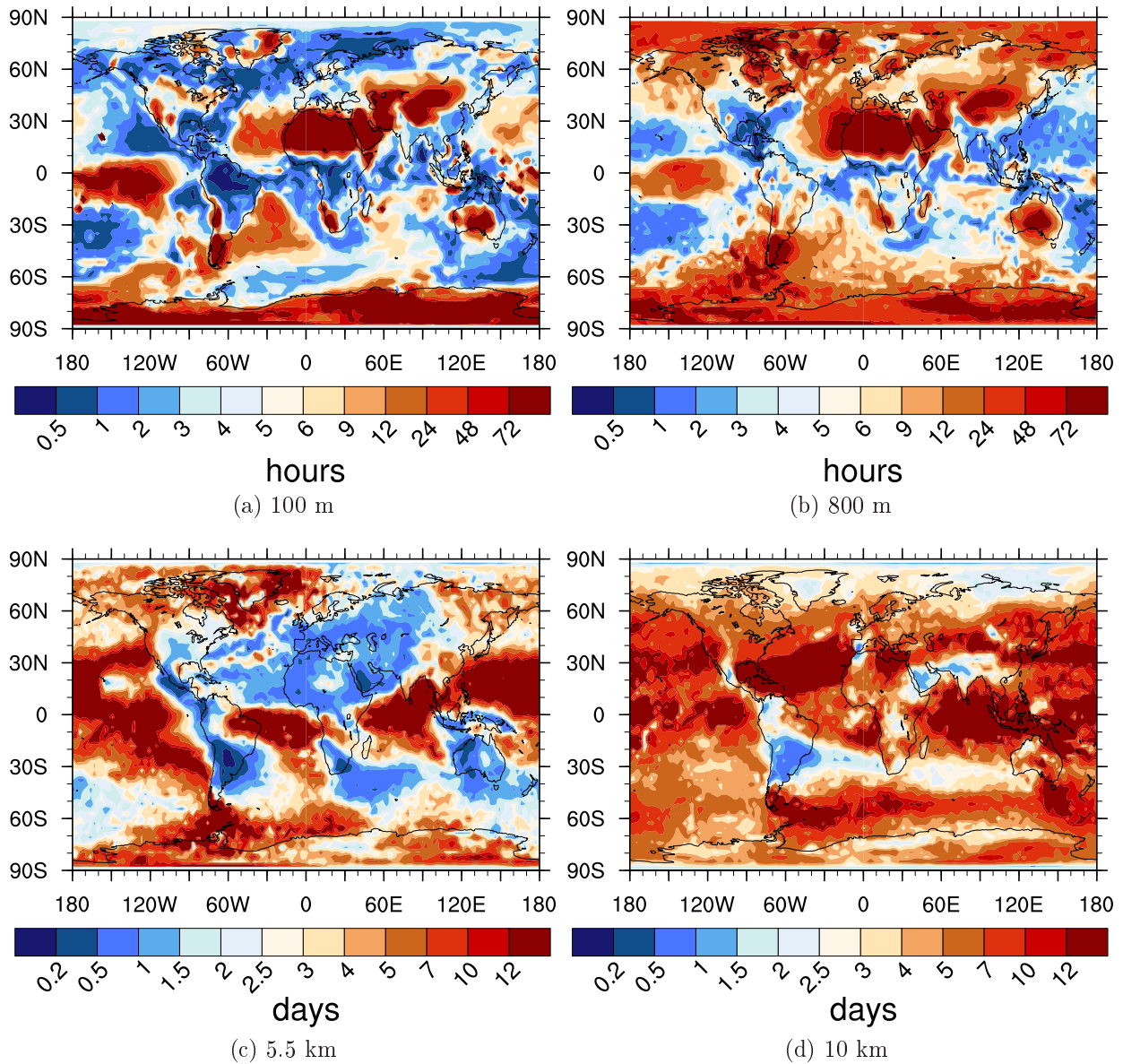


Figure 6.26: As Fig. 6.25, but for dust.

in the surrounding areas. From the deserts a high load of dust is risen in the atmosphere, making the burden of externally mixed dust very high. Additionally, no other species are emitted over deserts and the relative humidity, and therefore the aerosol water component, is low, making the loss of externally mixed dust close to zero. This causes in some grid boxes values of the transformation time of hundreds of days, that biases strongly the global mean of Fig. 6.24b in the lower layers. The minimum of τ_{DU} of Fig. 6.24b between 500 hPa and 600 hPa corresponds to the level at which τ_{DU} is not influenced anymore by the high values over the deserts. The dust emission regions are surrounded by areas where the transformation time has a strong descending gradient in the lowest level. Such a high transformation time indicates that nearly no dust particles are aged while they are close to the emission regions, but they have first to be transported to the neighboring areas, explaining the high global transformation time for dust as shown in Fig. 6.24.

The transformation time also shows a seasonal variability. Fig. 6.27 and Fig. 6.28 show the transformation time τ for BC and dust respectively in the lowermost model level during June, July, August (JJA) and December, January, February (DJF). τ has been calculated

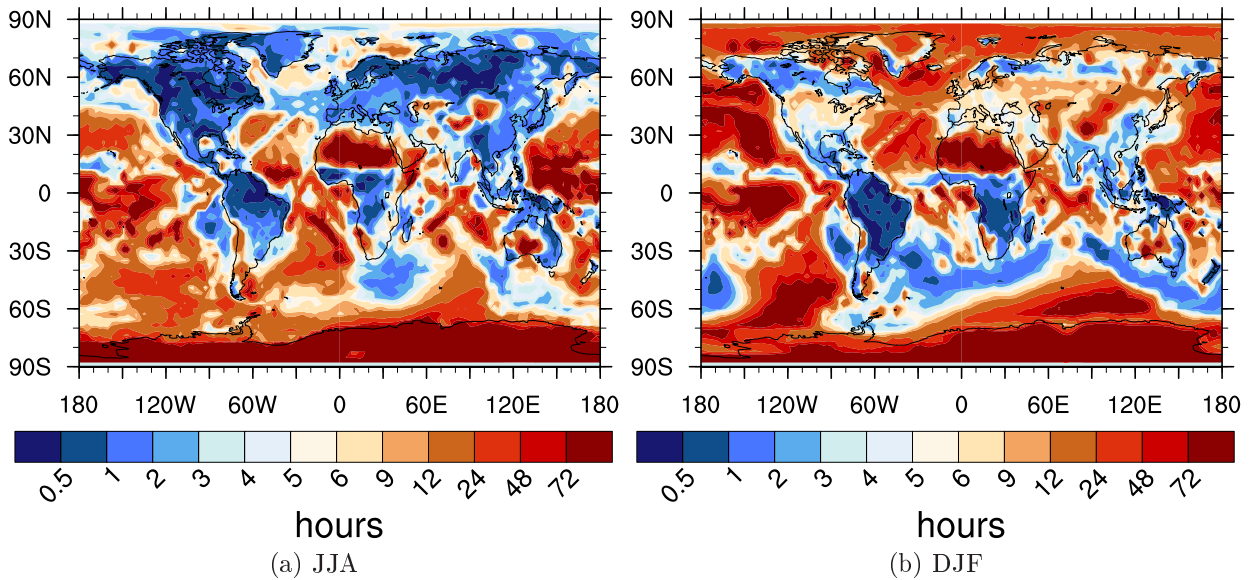


Figure 6.27: Transformation time of externally mixed BC into an internal mixture at surface level during summer (June, July, August) and during winter (December, January, February).

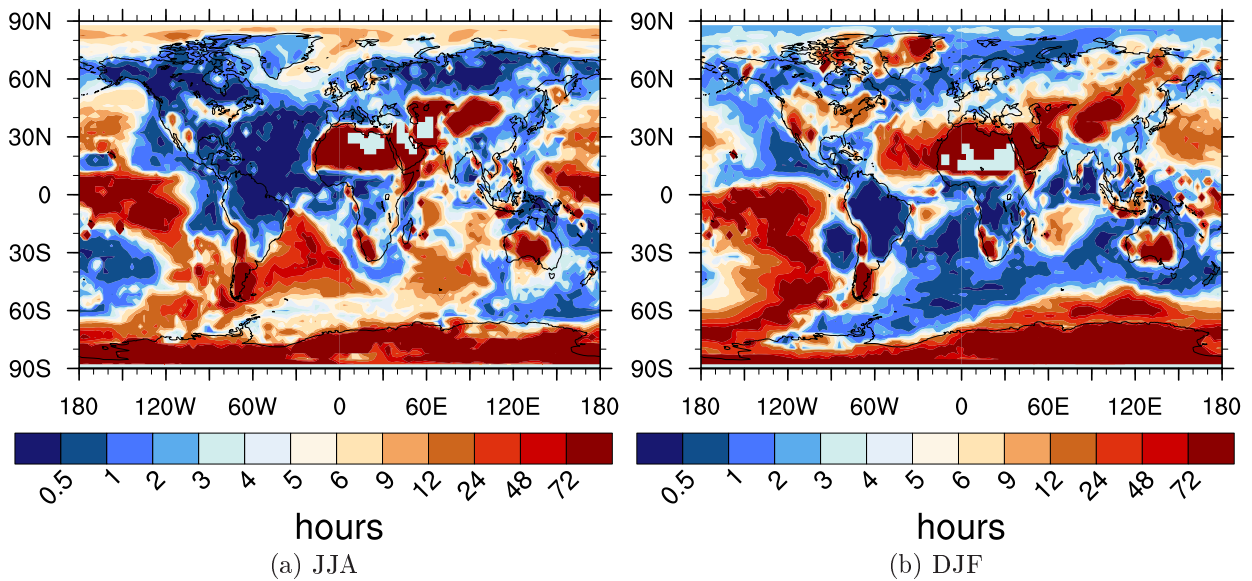


Figure 6.28: Transformation time of externally mixed dust into an internal mixture at surface level during summer (June, July, August) and during winter (December, January, February).

by means of Eq. [6.4] using the burden and sink of BC averaged over the whole analyzed period. North of 30° N and south of 30° S τ is shorter during the summer (JJA in the NH and DJF in the SH). This may be related to the higher production of sulfuric acid which characterizes summer. In the tropical region the variability between summer and winter is not as high as at mid-latitudes and in the Arctic region. The Antarctic region does not show any variability, since it is characterized by low aerosol concentrations during the whole year.

Overall, it appears clear that the simplification of a constant turnover rate for externally mixed BC is an excessive simplification. If the seasonal variability is not so large to be necessarily implemented in global models, the geographical dependence is very large and

should not be neglected in any model aiming to implement different mixing states of BC and dust. Globally, the assumption of an e-folding time of one day for the ageing of BC seems too high in the boundary layer, while it could represent a good approximation in the UTLS.

Chapter 7

Summary and outlook

A detailed investigation of the formation and climate impact of ice clouds requires a comprehensive characterization of potential ice nucleating aerosols. The aim of the present study is to investigate the properties and distribution of potential ice nuclei (PIN) on the global scale. In particular the number concentration, size distribution, chemical composition and mixing state were studied. This was realized by developing and applying the new global aerosol-chemistry model system ECHAM5/MESSy-MADEsoot. The newly developed ECHAM5/MESSy-MADEsoot is to date the only existing model which is able to resolve the mixing state of black carbon and dust particles and to keep track of the soot free particles, while providing a good description of aerosol in the upper troposphere and lowermost stratosphere (UTLS). Furthermore, in ECHAM5/MESSy-MADEsoot aerosol and chemistry are coupled: ECHAM5/MESSy provides MADEsoot with the concentrations of sulfate, nitrate and ammonia in the gas phase, and MADEsoot calculates the equilibrium between their gas and particulate phase. On the other hand MADEsoot provides ECHAM5/MESSy with the aerosol size distribution in order to calculate the heterogeneous reaction coefficients. The coupling between chemistry and aerosol is not a common feature of global aerosol model. All these characteristics make ECHAM5/MESSy-MADEsoot an appropriate tool to investigate the population of potential ice nuclei. In the following the different work steps as well as the achieved results are summarized.

MADEsoot as a box model. First the aerosol microphysical model MADEsoot has been developed as a box model, i.e. the microphysical core model not implemented in the global model. MADEsoot was developed starting from MADE, an aerosol microphysics model which describes the aerosol population by means of three log-normal modes. MADEsoot, instead, makes use of seven log-normal modes: two modes (an Aitken mode and an accumulation mode) are dedicated to externally mixed black carbon (BC) and dust particles, two to internally mixed BC and dust particles, and two to BC and dust free particles. The Aitken modes describe particles with diameter roughly between 10 nm and 100 nm and the accumulation modes particles between 100 nm and 1 μm . Additionally, particles larger than 1 μm are assigned to a coarse mode. MADEsoot simulates the partitioning between the gas and particulate state of water, nitric acid and ammonia, the condensation and the nucleation of sulfuric acid, and the coagulation between particles. Furthermore, the description of the state of mixing of BC and dust by means of different modes allows for an explicit simulation of their ageing process, i.e. the transformation from an external to an internal mixture.

Implementation of MADEsoot in the global climate model ECHAM5/MESSy. The box model of MADEsoot has been implemented in the ECHAM5/MESSy global climate model. In addition, ECHAM5/MESSy has been modified in order to provide a more reliable

description of the aerosol in the UTLS. The modifications introduced involve mainly the development of a more precise parameterization of aerosol scavenging in ice clouds. Furthermore, the parameterization of the aerosol scavenging has been modified in order to account also for the cloud processing as an ageing process. Externally mixed black carbon and dust particles are taken up by cloud particles and are transferred to an internal mixture when the cloud particles evaporate, since soluble matter aggregates with BC and dust inside the cloud droplet or ice crystal.

ECHAM5/MESSy-MADEsoot has been compared to surface and aircraft measurements and agrees well with the observations at all altitudes. ECHAM5/MESSy-MADEsoot was then applied to study the global sub-micrometer aerosol, with particular focus on potential ice nuclei in the UTLS.

Characterization of the total aerosol. The horizontal and vertical distribution of the total sub-micrometer aerosol mass and number concentration has been analyzed. The results are in agreement with the same studies conducted with other global aerosol models. The major results are the following:

- The highest number concentrations of the total sub-micrometer aerosol are reached at surface level over the industrialized areas by both the Aitken and the accumulation mode, and over the areas characterized by strong biomass burning by the accumulation mode. Additionally, the externally mixed accumulation mode particles shows high number concentrations over the Sahara desert, where strong dust emissions occur.
- The most abundant aerosols in the atmosphere are soluble particles. The highest number concentrations of purely soluble particles in the Aitken mode are reached between 30°N and 60°N in terms of annual and zonal means. These concentrations range between 200 and 500 particles/cm³ at 900 hPa and between 5000 and 7500 particles/cm³ around 300 hPa and 200 hPa, corresponding to the altitude of the UTLS. The high values in the UTLS are related to the efficient nucleation of small sulfuric acid particles. The soluble accumulation mode particles show the maximum number concentrations (between 500 and 1000 particles/cm³) in the tropical region at surface level and between 200 and 100 hPa. This is related to the high emissions from biomass burning and to the growth of the freshly nucleated Aitken mode particles into the accumulation mode, respectively.
- The horizontal distribution of the number concentration of the externally mixed BC and dust particles is strongly related to the location of the emission areas, since they can be emitted only as primary aerosol. Externally mixed BC particles in the Aitken mode show the highest annual mean concentrations of more than 1000 particles/cm³ over the industrialized areas of eastern China, India, north America and Europe. The corresponding accumulation mode shows high concentrations between 200 and 500 particles/cm³ over India and eastern China. Also over the Sahara desert high concentrations between 20 and 50 particles/cm³ occur. Above about 500 hPa the number concentration of externally mixed BC and dust particles becomes lower than 0.01 particles/cm³.
- The number concentration of the internally mixed BC and dust particles is similar for the Aitken and the accumulation mode. This is related to the fact that externally mixed Aitken mode BC particles frequently coagulate with accumulation mode particles, and the resulting internally mixed BC particle is assigned to the accumulation mode, so that even if the concentration of externally mixed BC and dust accumulation mode particles

is lower than the one of the externally mixed Aitken mode particles, the concentrations of the internally mixed modes are similar. The number concentrations of the internally mixed BC and dust particles both in the Aitken and in the accumulation mode show maximum values of more than 2000 particles/cm³ at surface level and decrease with altitude.

- The size distribution of the global aerosol is dominated by the soluble Aitken and accumulation modes. The median diameter of the soluble Aitken mode amounts to about 0.02 μm in the boundary layer and decreases with altitude. The decrease is related to the increasing contribution of small freshly nucleated particles to the number concentration.
- The most abundant species in the sub-micrometer range is SO₄²⁻, with a global burden of 1.4 Tg. The total burden of BC is 0.1 Tg and the burden of sub-micrometer dust is 0.2 Tg. While the concentration pattern of the primary aerosol species is strongly related to the emission areas, the pattern of secondary aerosol species is more spread, since the precursor gases can be transported over longer distances before they are transformed to particulate matter.
- The total burdens of all aerosol species calculated by ECHAM5/MESSy-MADEsoot are similar to those calculated by ECHAM5/MESSy-MADE and by ECHAM5/HAM. The total burdens of SO₄²⁻, POM and BC calculated by ECHAM5/MESSy-MADEsoot are smaller than those calculated by global model ensemble studies in the frame of the AeroCom project (*Textor et al.*, 2007). This is probably due to the simulation of the production of the precursor gases in the case of SO₄²⁻, to high scavenging coefficient in convective clouds in the case of POM and to the more efficient ageing simulated by ECHAM5/M-MADEsoot in the case of BC. The values calculated by *Textor et al.* (2007) are biased by some models which simulate very high aerosol burdens. On the other hand, when compared to experimental data the models based on the GCM ECHAM5 does not appear to simulate too low aerosol concentrations.

Characterization of the potential ice nuclei. The mass and number concentration, the composition and the size distribution of the population of potential ice nuclei (PIN) has been analyzed, both in terms of the horizontal distribution in the UTLS and of the vertical profile. Such a detailed characterization of the atmospheric potential ice nuclei is to date not present in literature.

- The annual mean zonally averaged PIN number concentration ranges from a maximum of more than 1000 particles/cm³ at surface level in the northern hemisphere to a minimum of less than 0.01 particles/cm³ in the Antarctic region. Excluding the Antarctic region, where also the concentration of total aerosol is very low, the minimum PIN number concentration is reached at the equator at altitudes between 250 hPa and 100 hPa, with annual and zonal mean values between 0.05 and 0.1 particles/cm³. At 300 hPa the highest number concentrations are reached at mid-latitudes in the northern hemisphere, with annual mean values between 5 and 10 particles/cm³ over eastern China.
- The potential ice nuclei represent only a small fraction of the total aerosol number concentration. In the UTLS, PIN represent nearly everywhere less than the 0.05% of the total aerosol number concentration. Only in areas characterized by strong emissions and fast convective updraft, PIN represent up to the 0.7% of the total aerosol number concentration in the UTLS. At surface level the fraction of the total aerosol that

contains BC or dust ranges between 10% and 50% at latitudes where the major emission areas are located.

- Nearly all PIN in the UTLS are internally mixed with soluble material. The contribution of externally mixed PIN to the total PIN number concentration is mainly lower than 3%. The regions with highest fractions of externally mixed PIN correspond to areas with low total PIN number concentration. This is related to the higher cloud scavenging efficiency for internally rather than for externally mixed PIN.
- The fraction of the total dust mass that is externally mixed is higher than the one of BC. Over the desert the fraction of externally mixed dust mass can reach 20% even in the UTLS, while the externally mixed BC fraction never exceed 5%. The longer transformation time of dust is caused by the larger size of the particles and by the lack of soluble aerosol over the deserts.
- The global size distribution of the externally mixed PIN is dominated by the Aitken mode and shows the maximum particle number concentration at diameters of 20-30 nm in the boundary layer, and around 10 nm at higher altitudes. The internally mixed BC and dust particles have a bimodal size distribution with maximum number concentrations at diameters between 30 and 40 nm for the Aitken mode and about 0.2 μm for the accumulation mode. The internally mixed PIN in the Aitken and in the accumulation mode show roughly the same number concentration, except in the tropopause region where the accumulation mode shows a higher number concentration, due to the higher age of the internally mixed BC and dust particles that reach that altitude.
- The coating of the internally mixed BC and dust particles in the troposphere is mainly composed of water. The relative importance of the other components has a large geographical variability. Globally, NH_4^+ and SO_4^{2-} represent the highest fraction of the dry mass of the coating, but also NO_3^- and POM are important in some areas. In the southern tropical region POM can represent up to 60% of the dry mass of the coating in the accumulation mode.
- The soluble to insoluble mass ratio in the internally mixed BC and dust modes is much higher in the accumulation mode than in the Aitken mode. This is due to the fact that the internally mixed Aitken mode particles result only from the condensation of gases or from the coagulation with the few other Aitken mode particles, that carry only a small amount of soluble mass. The accumulation mode shows the lowest ratio between 3 and 4 at the equator and the highest in the polar regions, where the soluble mass can be up to 10000 times the insoluble one. The highest ratios in the Aitken mode amount up to 50 and are located in the northern hemisphere.

The ageing of black carbon and dust particles. The efficiency of the individual ageing processes, i.e. condensation, coagulation and cloud processing as well as the time scale of the transformation of black carbon and dust from the external to the internal mixture have been investigated.

- The condensation of vapor onto externally mixed BC and dust particles is the most efficient ageing process. The ranking of coagulation and cloud processing varies spatially. From a global perspective, however, coagulation seems to be more effective than cloud processing.

- The transformation time scales of dust and BC amount to some hours at surface and several days in the upper troposphere. Hence the results of this study suggest that the e-folding time of one or two days assumed by most aerosol models for the ageing of BC is too long for the boundary layer, while it could be a good approximation for the upper troposphere.
- The transformation time scale shows a very high geographical variability, that makes a global generalization impossible. Furthermore, the transformation time scale shows a quite pronounced seasonal variability, probably related to the seasonal cycle of the production of condensable compounds.

Outlook

ECHAM5/MESSy-MADEsoot represents a highly appropriate tool for the investigation of the properties of global atmospheric aerosol and potential ice nuclei. The new features of MADEsoot can be used in the future to investigate the influence of particle emissions from specific sources, e.g. air traffic, on the atmospheric abundance of potential ice nuclei. The model can be applied in studies of aerosol-cirrus interaction and of their effects on climate. This study provides a detailed characterization of the background population of the potential ice nuclei, since aircraft emissions have not been included yet. With the implementation of aircraft emissions in the system, new simulations can be conducted to estimate the increase in the concentration of the potential ice nuclei due to air traffic with respect to the scenario described in this work. It is not clear whether the black carbon exhaust from aircraft have already aged in an internal mixture after the typical time step of a global climate model (*Kärcher et al.*, 2007). Therefore different scenarios should be considered, one where all aircraft-emitted black carbon is internally mixed, one where it is externally mixed, and additional scenarios with certain fractions of internally mixed BC could be considered.

The ability of MADEsoot of determining the number concentration of potential ice nuclei could be exploited by the coupling with a cirrus formation model. The estimation of the amount of soluble material in the internally mixed BC and dust modes can give indications about the mechanism of nucleation of ice crystals.

ECHAM5/MESSy-MADEsoot can also be used to investigate the influence of the mixing state on the aerosol radiative forcing. This can be achieved by comparing with simulations performed with ECHAM5/MESSy-MADE, which could not resolve the mixing state. Furthermore, the coupling between aerosol and radiation could be improved with the introduction of a core-shell parameterization for the absorption of solar radiation.

Even though the aerosol size distribution is in good agreement with the experimental data, its representation in MADEsoot could be further improved with the introduction of a nucleation mode for the freshly nucleated sulfuric acid particles.

Appendix A

Prognostic equations

The prognostic variables of MADE and MADEsoot are the number concentrations of each mode and the mass concentrations of the single species in each mode. The processes that play a role in the evolution of the prognostic variables are:

- gas/aerosol partitioning (*g/p*), i.e. the partitioning between nitric acid (HNO_3) and ammonia (NH_3), which are in the gas phase, and their particulate phase, nitrate (NO_3^-) and ammonium (NH_4^+), and between the gas and particulate phase of water.
- condensation (*cond*) of H_2SO_4 and organic material on preexisting aerosols;
- nucleation (*nucl*) of H_2SO_4 in fresh aerosol particles;
- intramodal coagulation (*coag i,i*) between aerosol particles belonging to the same mode. It acts only on the number concentration, not on the mass concentration;
- intermodal coagulation (*coag i,j*) between aerosol particles belonging to two different modes;
- particle *growth* from the Aitken modes into the accumulation modes;
- *aging* of BC and dust particles from externally to internally mixed (only in MADEsoot);
- all those processes which are simulated by other sub-models than MADE and MADEsoot, i.e. transport, emissions, wet and dry deposition for the number concentration and, additionally, chemistry for the mass concentrations. These processes are included in the term R .

The prognostic equations in E5/M-MADE and in E5/M-MADEsoot are here reported. In the prognostic equation of MADE the sign of each term is explicitly written. This is not possible in MADEsoot, since some terms can be positive, negative or equal to zero. Therefore the terms carrying a negative sign in the MADEsoot prognostic equations are those that can give only a negative contribution.

A.1 Prognostic equations in MADE

Prognostic equations for the number concentrations

$$\begin{aligned}\frac{\partial N_{\text{akn}}}{\partial t} &= R(N_{\text{akn}}) + \frac{\partial N_{\text{akn}}^{\text{nucl}}}{\partial t} - \frac{\partial N_{\text{akn}}^{\text{coag } i,i}}{\partial t} - \frac{\partial N_{\text{akn}}^{\text{coag } i,j}}{\partial t} - \frac{\partial N_{\text{akn}}^{\text{growth}}}{\partial t} \\ \frac{\partial N_{\text{acc}}}{\partial t} &= R(N_{\text{acc}}) - \frac{\partial N_{\text{acc}}^{\text{coag } i,i}}{\partial t} + \frac{\partial N_{\text{akn}}^{\text{growth}}}{\partial t} \\ \frac{\partial N_{\text{cor}}}{\partial t} &= R(N_{\text{cor}})\end{aligned}$$

Prognostic equations for the mass concentrations

- SO₄

$$\frac{\partial C_{\text{SO}_4, \text{akn}}}{\partial t} = R(C_{\text{SO}_4, \text{akn}}) + \frac{\partial C_{\text{SO}_4, \text{akn}}^{\text{cond}}}{\partial t} + \frac{\partial C_{\text{SO}_4, \text{akn}}^{\text{nucl}}}{\partial t} - \frac{\partial C_{\text{SO}_4, \text{akn}}^{\text{coag } i, j}}{\partial t} - \frac{\partial C_{\text{SO}_4, \text{akn}}^{\text{growth}}}{\partial t}$$

$$\frac{\partial C_{\text{SO}_4, \text{acc}}}{\partial t} = R(C_{\text{SO}_4, \text{acc}}) + \frac{\partial C_{\text{SO}_4, \text{akn}}^{\text{cond}}}{\partial t} + \frac{\partial C_{\text{SO}_4, \text{akn}}^{\text{coag } i, j}}{\partial t} + \frac{\partial C_{\text{SO}_4, \text{akn}}^{\text{growth}}}{\partial t}$$

- NO₃

$$\frac{\partial C_{\text{NO}_3, \text{akn}}}{\partial t} = R(C_{\text{NO}_3, \text{akn}}) + \frac{\partial C_{\text{NO}_3, \text{akn}}^{\text{g/p}}}{\partial t} - \frac{\partial C_{\text{NO}_3, \text{akn}}^{\text{coag } i, j}}{\partial t} - \frac{\partial C_{\text{NO}_3, \text{akn}}^{\text{growth}}}{\partial t}$$

$$\frac{\partial C_{\text{NO}_3, \text{acc}}}{\partial t} = R(C_{\text{NO}_3, \text{acc}}) + \frac{\partial C_{\text{NO}_3, \text{acc}}^{\text{g/p}}}{\partial t} + \frac{\partial C_{\text{NO}_3, \text{akn}}^{\text{coag } i, j}}{\partial t} + \frac{\partial C_{\text{NO}_3, \text{akn}}^{\text{growth}}}{\partial t}$$

- NH₄

$$\frac{\partial C_{\text{NH}_4, \text{akn}}}{\partial t} = R(C_{\text{NH}_4, \text{akn}}) + \frac{\partial C_{\text{NH}_4, \text{akn}}^{\text{g/p}}}{\partial t} - \frac{\partial C_{\text{NH}_4, \text{akn}}^{\text{coag } i, j}}{\partial t} - \frac{\partial C_{\text{NH}_4, \text{akn}}^{\text{growth}}}{\partial t}$$

$$\frac{\partial C_{\text{NH}_4, \text{acc}}}{\partial t} = R(C_{\text{NH}_4, \text{acc}}) + \frac{\partial C_{\text{NH}_4, \text{acc}}^{\text{g/p}}}{\partial t} + \frac{\partial C_{\text{NH}_4, \text{akn}}^{\text{coag } i, j}}{\partial t} + \frac{\partial C_{\text{NH}_4, \text{akn}}^{\text{growth}}}{\partial t}$$

- H₂O

$$\frac{\partial C_{\text{H}_2\text{O}, \text{akn}}}{\partial t} = R(C_{\text{H}_2\text{O}, \text{akn}}) + \frac{\partial C_{\text{H}_2\text{O}, \text{akn}}^{\text{g/p}}}{\partial t} - \frac{\partial C_{\text{H}_2\text{O}, \text{akn}}^{\text{coag } i, j}}{\partial t} - \frac{\partial C_{\text{H}_2\text{O}, \text{akn}}^{\text{growth}}}{\partial t}$$

$$\frac{\partial C_{\text{H}_2\text{O}, \text{acc}}}{\partial t} = R(C_{\text{H}_2\text{O}, \text{acc}}) + \frac{\partial C_{\text{H}_2\text{O}, \text{acc}}^{\text{g/p}}}{\partial t} + \frac{\partial C_{\text{H}_2\text{O}, \text{akn}}^{\text{coag } i, j}}{\partial t} + \frac{\partial C_{\text{H}_2\text{O}, \text{akn}}^{\text{growth}}}{\partial t}$$

$$\frac{\partial C_{\text{H}_2\text{O}, \text{cor}}}{\partial t} = R(C_{\text{H}_2\text{O}, \text{cor}})$$

- Particulate organic matter (POM)

$$\frac{\partial C_{\text{POM}, \text{akn}}}{\partial t} = R(C_{\text{POM}, \text{akn}}) + \frac{\partial C_{\text{POM}, \text{akn}}^{\text{cond}}}{\partial t} - \frac{\partial C_{\text{POM}, \text{akn}}^{\text{coag } i, j}}{\partial t} - \frac{\partial C_{\text{POM}, \text{akn}}^{\text{growth}}}{\partial t}$$

$$\frac{\partial C_{\text{POM}, \text{acc}}}{\partial t} = R(C_{\text{POM}, \text{acc}}) + \frac{\partial C_{\text{POM}, \text{acc}}^{\text{cond}}}{\partial t} + \frac{\partial C_{\text{POM}, \text{akn}}^{\text{coag } i, j}}{\partial t} + \frac{\partial C_{\text{POM}, \text{akn}}^{\text{growth}}}{\partial t}$$

- Sea salt (SS)

$$\frac{\partial C_{\text{SS}, \text{akn}}}{\partial t} = R(C_{\text{SS}, \text{akn}}) - \frac{\partial C_{\text{SS}, \text{akn}}^{\text{coag } i, j}}{\partial t} - \frac{\partial C_{\text{SS}, \text{akn}}^{\text{growth}}}{\partial t}$$

$$\frac{\partial C_{\text{SS}, \text{acc}}}{\partial t} = R(C_{\text{SS}, \text{acc}}) + \frac{\partial C_{\text{SS}, \text{akn}}^{\text{coag } i, j}}{\partial t} + \frac{\partial C_{\text{SS}, \text{akn}}^{\text{growth}}}{\partial t}$$

$$\frac{\partial C_{\text{SS}, \text{cor}}}{\partial t} = R(C_{\text{SS}, \text{cor}})$$

- Black carbon (BC)

$$\frac{\partial C_{\text{BC}, \text{akn}}}{\partial t} = R(C_{\text{BC}, \text{akn}}) - \frac{\partial C_{\text{BC}, \text{akn}}^{\text{coag } i, j}}{\partial t} - \frac{\partial C_{\text{BC}, \text{akn}}^{\text{growth}}}{\partial t}$$

$$\frac{\partial C_{\text{BC}, \text{acc}}}{\partial t} = R(C_{\text{BC}, \text{acc}}) + \frac{\partial C_{\text{BC}, \text{akn}}^{\text{coag } i, j}}{\partial t} + \frac{\partial C_{\text{BC}, \text{akn}}^{\text{growth}}}{\partial t}$$

- Dust (DU)

$$\frac{\partial C_{\text{DU, acc}}}{\partial t} = R(C_{\text{DU, acc}})$$

$$\frac{\partial C_{\text{DU, cor}}}{\partial t} = R(C_{\text{DU, cor}})$$

A.2 Prognostic equations in MADEsoot

Prognostic equations for the number concentrations

$$\begin{aligned} \frac{\partial N_{\text{akn}_{\text{sol}}}}{\partial t} &= R(N_{\text{akn}_{\text{sol}}}) + \frac{\partial N_{\text{akn}_{\text{sol}}}^{\text{nucl}}}{\partial t} - \frac{\partial N_{\text{akn}_{\text{sol}}}^{\text{coag } i,i}}{\partial t} - \frac{\partial N_{\text{akn}_{\text{sol}}}^{\text{coag } i,j}}{\partial t} - \frac{\partial N_{\text{akn}_{\text{sol}}}^{\text{growth}}}{\partial t} \\ \frac{\partial N_{\text{acc}_{\text{sol}}}}{\partial t} &= R(N_{\text{acc}_{\text{sol}}}) - \frac{\partial N_{\text{acc}_{\text{sol}}}^{\text{coag } i,i}}{\partial t} + \frac{\partial N_{\text{acc}_{\text{sol}}}^{\text{coag } i,j}}{\partial t} + \frac{\partial N_{\text{akn}_{\text{sol}}}^{\text{growth}}}{\partial t} \\ \frac{\partial N_{\text{akn}_{\text{ext}}}}{\partial t} &= R(N_{\text{akn}_{\text{ext}}}) - \frac{\partial N_{\text{akn}_{\text{ext}}}^{\text{coag } i,i}}{\partial t} + \frac{\partial N_{\text{akn}_{\text{ext}}}^{\text{coag } i,j}}{\partial t} - \frac{\partial N_{\text{akn}_{\text{ext}}}^{\text{growth}}}{\partial t} - \frac{\partial N_{\text{akn}_{\text{ext}}}^{\text{aging}}}{\partial t} \\ \frac{\partial N_{\text{acc}_{\text{ext}}}}{\partial t} &= R(N_{\text{acc}_{\text{ext}}}) - \frac{\partial N_{\text{acc}_{\text{ext}}}^{\text{coag } i,i}}{\partial t} + \frac{\partial N_{\text{acc}_{\text{ext}}}^{\text{coag } i,j}}{\partial t} + \frac{\partial N_{\text{akn}_{\text{ext}}}^{\text{growth}}}{\partial t} - \frac{\partial N_{\text{acc}_{\text{ext}}}^{\text{aging}}}{\partial t} \\ \frac{\partial N_{\text{akn}_{\text{mix}}}}{\partial t} &= R(N_{\text{akn}_{\text{mix}}}) - \frac{\partial N_{\text{akn}_{\text{mix}}}^{\text{coag } i,i}}{\partial t} + \frac{\partial N_{\text{akn}_{\text{mix}}}^{\text{coag } i,j}}{\partial t} - \frac{\partial N_{\text{akn}_{\text{mix}}}^{\text{growth}}}{\partial t} + \frac{\partial N_{\text{akn}_{\text{mix}}}^{\text{aging}}}{\partial t} \\ \frac{\partial N_{\text{acc}_{\text{mix}}}}{\partial t} &= R(N_{\text{acc}_{\text{mix}}}) - \frac{\partial N_{\text{acc}_{\text{mix}}}^{\text{coag } i,i}}{\partial t} + \frac{\partial N_{\text{acc}_{\text{mix}}}^{\text{coag } i,j}}{\partial t} + \frac{\partial N_{\text{akn}_{\text{mix}}}^{\text{growth}}}{\partial t} + \frac{\partial N_{\text{acc}_{\text{mix}}}^{\text{aging}}}{\partial t} \\ \frac{\partial N_{\text{cor}}}{\partial t} &= R(N_{\text{cor}}) \end{aligned}$$

Prognostic equations for the mass concentrations

- SO₄

$$\begin{aligned} \frac{\partial C_{\text{akn}_{\text{sol}}}^{\text{SO}_4}}{\partial t} &= R(C_{\text{akn}_{\text{sol}}}^{\text{SO}_4}) + \frac{\partial C_{\text{akn}_{\text{sol}}}^{\text{SO}_4 \text{ nucl}}}{\partial t} - \frac{\partial C_{\text{akn}_{\text{sol}}}^{\text{SO}_4 \text{ coag } i,j}}{\partial t} - \frac{\partial C_{\text{akn}_{\text{sol}}}^{\text{SO}_4 \text{ growth}}}{\partial t} \\ \frac{\partial C_{\text{acc}_{\text{sol}}}^{\text{SO}_4}}{\partial t} &= R(C_{\text{acc}_{\text{sol}}}^{\text{SO}_4}) + \frac{\partial C_{\text{acc}_{\text{sol}}}^{\text{SO}_4 \text{ coag } i,j}}{\partial t} + \frac{\partial C_{\text{akn}_{\text{sol}}}^{\text{SO}_4 \text{ growth}}}{\partial t} \\ \frac{\partial C_{\text{akn}_{\text{ext}}}^{\text{SO}_4}}{\partial t} &= R(C_{\text{akn}_{\text{ext}}}^{\text{SO}_4}) + \frac{\partial C_{\text{akn}_{\text{ext}}}^{\text{SO}_4 \text{ coag } i,j}}{\partial t} - \frac{\partial C_{\text{akn}_{\text{ext}}}^{\text{SO}_4 \text{ growth}}}{\partial t} - \frac{\partial C_{\text{akn}_{\text{ext}}}^{\text{SO}_4 \text{ aging}}}{\partial t} \\ \frac{\partial C_{\text{acc}_{\text{ext}}}^{\text{SO}_4}}{\partial t} &= R(C_{\text{acc}_{\text{ext}}}^{\text{SO}_4}) + \frac{\partial C_{\text{acc}_{\text{ext}}}^{\text{SO}_4 \text{ coag } i,j}}{\partial t} + \frac{\partial C_{\text{akn}_{\text{ext}}}^{\text{SO}_4 \text{ growth}}}{\partial t} - \frac{\partial C_{\text{acc}_{\text{ext}}}^{\text{SO}_4 \text{ aging}}}{\partial t} \\ \frac{\partial C_{\text{akn}_{\text{mix}}}^{\text{SO}_4}}{\partial t} &= R(C_{\text{akn}_{\text{mix}}}^{\text{SO}_4}) + \frac{\partial C_{\text{akn}_{\text{mix}}}^{\text{SO}_4 \text{ coag } i,j}}{\partial t} - \frac{\partial C_{\text{akn}_{\text{mix}}}^{\text{SO}_4 \text{ growth}}}{\partial t} + \frac{\partial C_{\text{akn}_{\text{mix}}}^{\text{SO}_4 \text{ aging}}}{\partial t} \\ \frac{\partial C_{\text{acc}_{\text{mix}}}^{\text{SO}_4}}{\partial t} &= R(C_{\text{acc}_{\text{mix}}}^{\text{SO}_4}) + \frac{\partial C_{\text{acc}_{\text{mix}}}^{\text{SO}_4 \text{ coag } i,j}}{\partial t} + \frac{\partial C_{\text{akn}_{\text{mix}}}^{\text{SO}_4 \text{ growth}}}{\partial t} + \frac{\partial C_{\text{acc}_{\text{mix}}}^{\text{SO}_4 \text{ aging}}}{\partial t} \end{aligned}$$

- Dust (DU)

$$\frac{\partial C_{\text{acc}_{\text{ext}}}^{\text{DU}}}{\partial t} = R(C_{\text{acc}_{\text{ext}}}^{\text{DU}}) + \frac{\partial C_{\text{acc}_{\text{ext}}}^{\text{DU}}}{\partial t} \text{ coag } i,j - \frac{\partial C_{\text{acc}_{\text{ext}}}^{\text{DU}}}{\partial t} \text{ aging}$$

$$\frac{\partial C_{\text{acc}_{\text{mix}}}^{\text{DU}}}{\partial t} = R(C_{\text{acc}_{\text{mix}}}^{\text{DU}}) + \frac{\partial C_{\text{acc}_{\text{mix}}}^{\text{DU}}}{\partial t} \text{ coag } i,j + \frac{\partial C_{\text{acc}_{\text{mix}}}^{\text{DU}}}{\partial t} \text{ aging}$$

$$\frac{\partial C_{\text{cor}}^{\text{DU}}}{\partial t} = R(C_{\text{cor}}^{\text{DU}})$$

Appendix B

Technical details

B.1 Calculation of the condensation coefficients

Condensation of sulfuric acid

The mass concentration of sulfuric acid gas evolves following the analytic solution of the equation

$$\frac{dC_{\text{H}_2\text{SO}_4}(t)}{dt} = P - L \cdot C_{\text{H}_2\text{SO}_4}(t), \quad (\text{B.1})$$

where P is the production rate of H_2SO_4 in the gas phase, which is given externally to the aerosol sub-model, and L is the loss due to condensation. The solution of Eq. [B.1] is

$$C_{\text{H}_2\text{SO}_4}(t) = \frac{P}{L} + \left(C_{\text{H}_2\text{SO}_4}(t_0) - \frac{P}{L} \right) e^{-L(t-t_0)}, \quad (\text{B.2})$$

assuming that P and L are constant during $\Delta t = t - t_0$. The change in the mass concentration of H_2SO_4 due solely to the condensation of gas ($\Delta C^{\text{cond.}}$) is

$$\begin{aligned} \Delta C^{\text{cond.}} &= \Delta C_{\text{H}_2\text{SO}_4} - \Delta C^{\text{production}} \\ &= \left(\frac{P}{L} - C_{\text{H}_2\text{SO}_4}(t_0) \right) (1 - e^{-L\Delta t}) - P\Delta t. \end{aligned} \quad (\text{B.3})$$

The loss coefficient L is calculated following *Whitby et al.* (1991). The loss of H_2SO_4 in the gas phase is equal to the gain of SO_4^{2-} mass in the aerosol modes. If $M_i^{(k)}$ is the k^{th} moment of the mode i and $G_i^{(k)}$ the corresponding growth coefficient, we have:

$$L = \sum_{i=1}^{N_{\text{modes}}} \frac{\partial C_{\text{SO}_4^{2-},i}}{\partial t} = \rho_{\text{SO}_4} \frac{\pi}{6} \sum_{i=1}^{N_{\text{modes}}} \frac{\partial M_i^{(3)}}{\partial t} \equiv \rho_{\text{SO}_4} \frac{\pi}{6} \sum_{i=1}^{N_{\text{modes}}} G_i^{(3)}, \quad (\text{B.4})$$

where the relation between mass and third moment from Eq. [3.10] is used. $G_i^{(3)}$ can be factorized in a size-dependent factor $\Psi(D)$, where D is the particle diameter, and in a size-independent factors Ψ_T (*Whitby and McMurry*, 1997)

$$G_i^{(3)} = \frac{6}{\pi} \Psi_T \int_0^\infty \Psi(D) n_i(D) dD. \quad (\text{B.5})$$

The size-independent component Ψ_T of the growth function is equal to

$$\Psi_T = \frac{M_w p_s (S_v - 1)}{\rho R T} \quad (\text{B.6})$$

where M_w is the molecular weight of the condensing gas, p_s the saturation vapour pressure, S_v the saturation ratio of the condensing species, ρ the density of the condensed substance, R the universal gas constant and T the temperature. The form size-dependent component $\Psi(D)$ depends on the regime of the gas, which is identified by the Knudsen number Kn (see Sec. 2.1.1). $\Psi(D)$ has two asymptotic forms for the free molecular ($Kn > 10$) and near continuum ($Kn < 1$) regimes:

$$\text{free-molecular: } Kn > 10 \rightarrow \Psi^{fm}(D) = \frac{\pi\alpha\bar{c}}{4}D^2 \quad (\text{B.7})$$

$$\text{near-continuum: } Kn < 1 \rightarrow \Psi^{nc}(D) = 2\pi D_v D \quad (\text{B.8})$$

where α is the accommodation coefficient, \bar{c} the mean molecular velocity and D_v the diffusion coefficient. The asymptotic expressions for the growth rate are:

$$G_i^{(3)fm} = \frac{6}{\pi}\Psi_T \frac{\pi\alpha\bar{c}}{4}M_i^{(2)} \quad (\text{B.9})$$

$$G_i^{(3)nc} = \frac{6}{\pi}\Psi_T 2\pi D_v M_i^{(1)} \quad (\text{B.10})$$

Whitby et al. (1991) shows how the harmonic mean between the free-molecular and the near-continuum expressions gives an expression of the growth rate that is computationally efficient and precise enough also in the transition phase between the two regimes:

$$G_i^{(3)} = \frac{G_i^{(3)fm} G_i^{(3)nc}}{G_i^{(3)fm} + G_i^{(3)nc}} \quad (\text{B.11})$$

The loss coefficient L is calculated substituting Eq. B.11 in Eq. B.4. The growth of SO_4^{2-} mass concentration in each mode i due to condensation of sulfuric acid ($M_{\text{SO}_4,i}^{\text{cond.}}$ in Eq. 3.14) is calculated through the non-dimensional coefficients Ω_i

$$\frac{\partial C_{\text{SO}_4^{2-},i}^{\text{cond}}}{\partial t} = \Omega_i \Delta C^{\text{cond.}} \quad (\text{B.12})$$

$$\Omega_i = \frac{G_i^{(3)}}{\sum_{i=1}^{N_{\text{modes}}} G_i^{(3)}}. \quad (\text{B.13})$$

The size-independent factor $\frac{6}{\pi}\Psi_T$ is cancelled in Eq. B.13.

Condensation of organic gases

The condensation of organic gases into secondary organic aerosol is calculated analogously to the condensation of sulfuric acid. The amount of condensing gas C_{SOA} , however, is not calculated, but given as an external field to the aerosol sub-model. Therefore

$$\frac{\partial C_{\text{POM},i}^{\text{cond}}}{\partial t} = \Omega_i^{\text{SOA}} C_{\text{SOA}} \quad (\text{B.14})$$

$$\Omega_i^{\text{SOA}} = \frac{G_{\text{SOA},i}^{(3)}}{\sum_{i=1}^{N_{\text{modes}}} G_{\text{SOA},i}^{(3)}}. \quad (\text{B.15})$$

B.2 Calculation of the coagulation rate

The rate of change of the k^{th} moment due to intermodal coagulation between particles belonging to the mode i and j is defined as

$$C_{k,ij} = \frac{\partial M_l^{(k)}}{\partial t}, \quad (\text{B.16})$$

where l is the mode to which the resulting particle is assigned. Following *Binkowski and Shankar* (1995), $C_{k,ij}$ is calculated as

$$C_{k,ij} = + \int_0^\infty \int_0^\infty D_1^k \beta(D_1, D_2) n_i(D_1) n_j(D_2) dD_1 dD_2, \quad (\text{B.17})$$

and the rate for intramodal coagulation is

$$C_{k,ii} = -\frac{1}{2} \int_0^\infty \int_0^\infty (D_1^3 + D_2^3)^{k/3} \beta(D_1, D_2) n_i(D_1) n_i(D_2) dD_1 dD_2 \quad (\text{B.18})$$

$$+ \int_0^\infty \int_0^\infty D_1^k \beta(D_1, D_2) n_i(D_1) n_i(D_2) dD_1 dD_2, \quad (\text{B.19})$$

where D_1 and D_2 are the diameters of the coagulation particles, $n_i(D)$ the number distribution of the mode and $\beta(D_1, D_2)$ the function describing the coagulation process, which depends on the regime of the gas. The asymptotic expressions of $\beta(D_1, D_2)$ for the near-continuum and in the free-molecular regime are, following *Friedlander* (2000),

$$\beta^{fm}(D_1, D_2) = \sqrt{\frac{3k_B T}{\rho} \left(\frac{1}{D_1^3} + \frac{1}{D_2^3} \right)} (D_1 + D_2)^2 \quad (\text{B.20})$$

$$\beta^{nc}(D_1, D_2) = 2\pi(D_{v,1} + D_{v,2})(D_1 + D_2) \quad (\text{B.21})$$

$$(\text{B.22})$$

where k_B is the Boltzmann constant, T the temperature, ρ the particle density and $D_{v,i}$ the diffusion coefficient of the particle i . As done for the calculation of the condensation coefficients (App. B.1), the coagulation rate can be calculated as the harmonic mean between the two asymptotic regimes

$$C_{k,ij} = \frac{C_{k,ij}^{fm} C_{k,ij}^{nc}}{C_{k,ij}^{fm} + C_{k,ij}^{nc}} \quad (\text{B.23})$$

$$C_{k,ii} = \frac{C_{k,ii}^{fm} C_{k,ii}^{nc}}{C_{k,ii}^{fm} + C_{k,ii}^{nc}} \quad (\text{B.24})$$

Appendix C

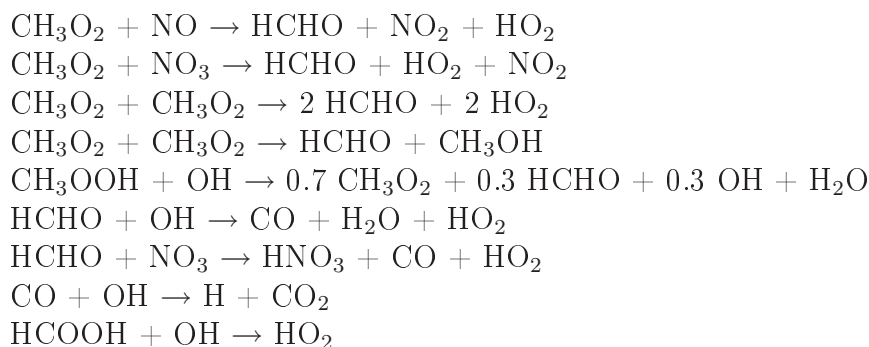
Chemical reactions

The reaction list does not report the reactants which are abundant in the atmosphere.

C.1 The chemical mechanism of MECCA

Gas phase reactions

- $O_2 + O^{1D} \rightarrow O^{3P} + O_2$
 $O_2 + O^{3P} \rightarrow O_3$
- $H + O_2 \rightarrow HO_2$
 $OH + O_3 \rightarrow HO_2$
 $OH + H_2 \rightarrow H_2O + H$
 $HO_2 + O_3 \rightarrow OH$
 $HO_2 + OH \rightarrow H_2O$
 $HO_2 + HO_2 \rightarrow H_2O_2$
 $H_2O + O^{1D} \rightarrow 2 OH$
 $H_2O_2 + OH \rightarrow H_2O + HO_2$
- $N_2 + O^{1D} \rightarrow O^{3P} + N_2$
 $NO + O_3 \rightarrow NO_2 + O_2$
 $NO_2 + O_3 \rightarrow NO_3 + O_2$
 $NO_3 + NO \rightarrow 2 NO_2$
 $NO_3 + NO_2 \rightarrow N_2O_5$
 $N_2O_5 \rightarrow NO_2 + NO_3$
 $NO + OH \rightarrow HONO$
 $NO + HO_2 \rightarrow NO_2 + OH$
 $NO_2 + OH \rightarrow HNO_3$
 $NO_2 + HO_2 \rightarrow HNO_4$
 $NO_3 + HO_2 \rightarrow NO_2 + OH + O_2$
 $HONO + OH \rightarrow NO_2 + H_2O$
 $HNO_3 + OH \rightarrow H_2O + NO_3$
 $HNO_4 \rightarrow NO_2 + HO_2$
 $HNO_4 + OH \rightarrow NO_2 + H_2O$
- $CH_4 + OH \rightarrow CH_3O_2 + H_2O$
 $CH_3OH + OH \rightarrow HCHO + HO_2$
 $CH_3O_2 + HO_2 \rightarrow CH_3OOH$
 $CH_3O_2 + HO_2 \rightarrow HCHO + H_2O + O_2$



- $\text{SO}_2 + \text{OH} \rightarrow \text{H}_2\text{SO}_4 + \text{HO}_2$
- $\text{DMS} + \text{OH} \rightarrow \text{CH}_3\text{SO}_2 + \text{HCHO}$
- $\text{DMS} + \text{OH} \rightarrow \text{DMSO} + \text{HO}_2$
- $\text{DMS} + \text{NO}_3 \rightarrow \text{CH}_3\text{SO}_2 + \text{HNO}_3 + \text{HCHO}$
- $\text{DMSO} + \text{OH} \rightarrow 0.6 \text{SO}_2 + \text{HCHO} + 0.6 \text{CH}_3\text{O}_2 + 0.4 \text{HO}_2 + 0.4 \text{CH}_3\text{SO}_3\text{H}$
- $\text{CH}_3\text{SO}_2 \rightarrow \text{SO}_2 + \text{CH}_3\text{O}_2$
- $\text{CH}_3\text{SO}_2 + \text{O}_3 \rightarrow \text{CH}_3\text{SO}_3$
- $\text{CH}_3\text{SO}_3 + \text{HO}_2 \rightarrow \text{CH}_3\text{SO}_3\text{H}$

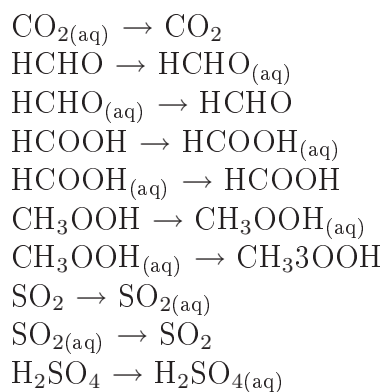
Photolysis reactions

- $\text{O}_3 + h\nu \rightarrow \text{O}^{1\text{D}}$
 $\text{O}_3 + h\nu \rightarrow \text{O}^{3\text{P}}$
- $\text{H}_2\text{O}_2 + h\nu \rightarrow 2 \text{OH}$
- $\text{NO}_2 + h\nu \rightarrow \text{NO} + \text{O}^{3\text{P}}$
 $\text{NO}_3 + h\nu \rightarrow \text{NO}_2 + \text{O}^{3\text{P}}$
 $\text{NO}_3 + h\nu \rightarrow \text{NO}$
 $\text{N}_2\text{O}_5 + h\nu \rightarrow \text{NO}_2 + \text{NO}_3$
 $\text{HONO} + h\nu \rightarrow \text{NO} + \text{OH}$
 $\text{HNO}_3 + h\nu \rightarrow \text{NO}_2 + \text{OH}$
 $\text{HNO}_4 + h\nu \rightarrow 0.7 \text{NO}_2 + 0.7 \text{HO}_2 + 0.3 \text{NO}_3 + 0.3 \text{OH}$
- $\text{CH}_3\text{OOH} + h\nu \rightarrow \text{HCHO} + \text{OH} + \text{HO}_2$
 $\text{HCHO} + h\nu \rightarrow \text{H}_2 + \text{CO}$
 $\text{HCHO} + h\nu \rightarrow \text{H} + \text{CO} + \text{HO}_2$

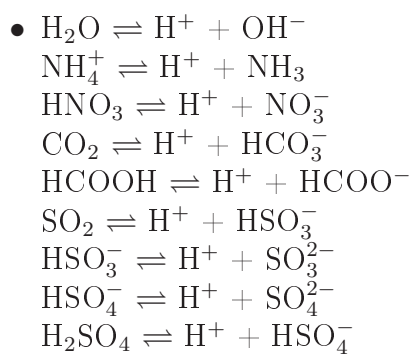
C.2 The chemical mechanism of SCAV

Heterogeneous reactions

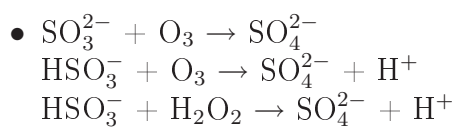
- $\text{O}_3 \rightarrow \text{O}_{3(\text{aq})}$
 $\text{O}_{3(\text{aq})} \rightarrow \text{O}_3$
 $\text{H}_2\text{O}_2 \rightarrow \text{H}_2\text{O}_{2(\text{aq})}$
 $\text{H}_2\text{O}_{2(\text{aq})} \rightarrow \text{H}_2\text{O}_2$
 $\text{NH}_3 \rightarrow \text{NH}_{3(\text{aq})}$
 $\text{NH}_{3(\text{aq})} \rightarrow \text{NH}_3$
 $\text{N}_2\text{O}_5 \rightarrow \text{HNO}_{3(\text{aq})} + \text{HNO}_{3(\text{aq})}$
 $\text{HNO}_3 \rightarrow \text{HNO}_{3(\text{aq})}$
 $\text{HNO}_{3(\text{aq})} \rightarrow \text{HNO}_3$
 $\text{CO}_2 \rightarrow \text{CO}_{2(\text{aq})}$



Equilibria



Liquid phase chemistry



Appendix D

Acronyms

MADE modes

akn	Aitken mode
acc	accumulation mode
cor	coarse mode (sea salt, dust, water)

MADEsoot modes

akn _{sol}	soluble Aitken mode
acc _{sol}	soluble accumulation mode
akn _{ext}	externally mixed black carbon and dust Aitken mode
acc _{ext}	externally mixed black carbon and dust accumulation mode
akn _{mix}	internally mixed Aitken mode with black carbon and dust
acc _{mix}	internally mixed accumulation mode with black carbon and dust
cor	coarse mode (sea salt, dust, water)

Chemical compounds

Cl ⁻	Chloride
DMS	Dimethylsulfide = (CH ₃) ₂ S
DMSO	Dimethylsulfoxid = (CH ₃) ₂ OS
HNO ₃	Nitric acid
H ₂ S	Hydrogen sulfide
H ₂ SO ₄	Sulfuric acid
Na	Sodium
NH ₃	Ammonia
NH ₄ ⁺	Ammonium
NO	Nitric oxide or nitrogen monoxide
NO ₂	Nitrogen dioxide
NO ₃ ⁻	Nitrate
NO _X	Nitrogen oxide (NO + NO ₂)
OH	Hydroxyl radical
SO ₂	Sulfur dioxide
SO ₄ ²⁻	Sulfate

Other acronyms

ACE-1	First Aerosol Characterization Experiment
AEROCOM	initiative for the comparison of aerosol models
bb	Biomass Burning
BC	Black Carbon
CFL	Courant-Friedrich-Levy (criterion)
CCN	Cloud Condensation Nuclei
CR-AVE	Costa Rica Aura Validation Experiment
DJF	December-January-February
DU	mineral DUst
E5/M	ECHAM5/MESSy Aerosol climate model
ECHAM	ECmwf model - HAMburg version
ECMWF	European Centre for Medium Range Weather Forecasts
EDGARv3.2 FT2000	Emission Database for Global Atmospheric Research version 3.2 Fast Track 2000
ERBE	Earth Radiation Budget Experiment
EURAD	European Air Pollution Dispersion model system
ff	fossil fuel
GEIA	Global Emissions Inventory Activity
GEOS DAS	NASA Goddard Earth Observing System Data Assimilation System
GCM	General Circulation Model
GFED	Global Fire Emission Database
GISS GCM	Goddard Institute for Space Studies General Circulation Model
GLOBE-2	Global Backscatter Experiment
GOCART	Georgia Tech/Goddard Global Ozone Chemistry Aerosol Radiation and Transport
GSG	Graphite Spark Generator
IMPROVE	Interagency Monitoring of Protected Visual Environments
IN	Ice Nuclei
INCA	Interhemispheric Differences in Cirrus properties from Anthro- pogenic Emissions
IPCC	Intergovernmental Panel on Climate Change
JJA	June-July-August
LACE	Lindenberg Aerosol Characterization Experiment
LCF	Long wave Cloud Forcing
MADE(soot)	Modal Aerosol Dynamics model for Europe (for soot)
MADRID-BC	Model of Aerosol Dynamics, Reaction, Ionization, and Dissolution for Black Carbon
MATRIX	Multiconfiguration Aerosol TRacker of mIXing state
MESSy	Modular Earth Submodel System
NH	Northern Hemisphere

NME	Normalized Mean Error
NMB	Normalized Mean Bias
OC	Organic Carbon
PEM-Tropics A/B	Pacific Exploratory Mission-Tropics A/B
PIN	Potential Ice Nuclei
PM _{2.5}	Particulate Matter with diameter smaller than 2.5 μ m
PM ₁₀	Particulate Matter with diameter smaller than 10 μ m
POM	Particulate Organic Matter
QMOM	Quadrature Method of Moments
RH	Relative Humidity
RHD	Relative Humidity of Deliquescence
RF	Radiative Forcing
SCF	Short wave Cloud Forcing
SH	Southern Hemisphere
SOA	Secondary Organic Aerosol
SP2	Single Particle Soot Photometer
SPEW	Speciated Particulate Emissions Wizard
SS	Sea Salt
TC4	Tropical Composition, Cloud and Climate Coupling campaign
UCN	Ultrafine Condensation Nuclei
UTLS	Upper Troposphere - Lowermost Stratosphere
VOC	Volatile Organic Compound
WHO	World Health Organization

Bibliography

- Abdul-Razzak, H., and S. Ghan (2000), A parameterization of aerosol activation. 2. Multiple aerosol types, *J. Geophys. Res.*, *105*(D5), 6837–6844.
- Ackerman, A., O. Toon, D. Stevens, A. Heymsfield, V. Ramanathan, and E. Welton (2000), Reduction of tropical cloudiness by soot, *Science*, *288*(5468), 1042 – 1047, doi:10.1126/science.288.5468.1042.
- Ackermann, I., H. Hass, M. Memmesheimer, A. Ebel, F. Binkowsky, and U. Shankar (1998), Modal aerosol dynamics model for Europe: development and first applications, *Atmosph. Env.*, *32*, 2971–2999, doi:10.1016/S1352-2310(98)00006-5.
- Adams, P. J., and J. H. Seinfeld (2002), Predicting global aerosol size distributions in general circulation models, *J. Geophys. Res.*, *107*(D19), 4370, doi:10.1029/2001JD001010.
- Adams, P. J., J. H. Seinfeld, and D. M. Koch (1999), Global concentrations of tropospheric sulfate, nitrate, and ammonium aerosol simulated in a general circulation model, *J. Geophys. Res.*, *104*(D11), 13791–13823.
- Albrecht, B. A. (1989), Aerosols, Cloud Microphysics, and Fractional Cloudiness, *Science*, *245*(4923), 1227–1230.
- Andreae, M., and D. Rosenfeld (2008), Aerosol-cloud-precipitation interactions. Part 1. The nature and sources of cloud-active aerosols, *Earth-Science Reviews*, *89*, 13–41.
- Andres, R., and A. Kasgnoc (1998), A time-averaged inventory of subaerial volcanic sulfur emissions, *J. Geophys. Res.*, *103*(19), 25251–25261.
- Ayash, T., S. L. Gong, C. Q. Jia, P. Huang, T. L. Zhao, and D. Lavoue (2008), Global modeling of multicomponent aerosol species: Aerosol optical parameters, *J. Geophys. Res.*, *113*, D12203, doi:10.1029/2007JD008968.
- Bauer, S. E., D. L. Wright, D. Koch, E. R. Lewis, R. McGraw, L.-S. Chang, S. E. Schwartz, and R. Ruedy (2008), MATRIX (Multiconfiguration Aerosol TRacker of mIXing state): an aerosol microphysical module for global atmospheric models, *Atmos. Chem. Phys.*, *8*, 6003–6035.
- Baumgardner, D., G. Kok, M. Kraemer, and F. Weidle (2008), Meridional gradients of light absorbing carbon over northern Europe, *Environ. Res. Lett.*, *3*, 025010, doi:doi:10.1088/1748-9326/3/2/025010.
- Binkowski, F., and U. Shankar (1995), The regional particulate matter model. Model description and preliminary results, *J. Geophys. Res.*, *100*, 26,191–26,206.
- Bond, T., D. Streets, K. Yarber, N. Nelson, J. H. Wo, and Z. Klimont (2004), A technology-based global inventory of black and organic carbon emissions from combustion, *J. Geophys. Res.*, *109*, D14203, doi:10.1029/2003JD003697.

- Bond, T. C., and R. W. Bergstrom (2006), Light Absorption by Carbonaceous Particles: An Investigative Review, *Aerosol Science and Technology*, *40*(1), 27–67, doi:10.1080/02786820500421521.
- Bond, T. C., G. Habib, and R. W. Bergstrom (2006), Limitations in the enhancement of visible light absorption due to mixing state, *J. Geophys. Res.*, *111*, D20211, doi:10.1029/2006JD007315.
- Chin, M., R. B. Rood, S.-J. Lin, J.-F. Müller, and A. M. Thompson (2000), Atmospheric sulfur cycle simulated in the global model GOCART: Model description and global properties, *J. Geophys. Res.*, *105*(D20), 24671–24687.
- Chin, M., R. A. Kahn, and S. E. Schwartz (2009), Atmospheric aerosol properties and climate impacts, *Final Report, Synthesis and Assessment Product 2.3*, NASA, Washington, D.C., USA.
- Chung, S. H., and J. H. Seinfeld (2002), Global distribution and climate forcing of carbonaceous aerosols, *J. Geophys. Res.*, *107*(D19), 4407, doi:10.1029/2001JD001397.
- Clarke, A., and V. Kapustin (2002), A Pacific Aerosol Survey - Part 1: A Decade of Data on Production, Transport, Evolution and Mixing in the Troposphere, *J. Atmos. Sci.*, *59*(3 PT 1), 363–382.
- Cofala, J., M. Amann, Z. Klimont, and W. Schöpp (2005), Scenarios of World Anthropogenic Emissions of SO₂, NO_x and CO up to 2030, *International report of the transboundary air pollution program*, International Institute for Applied Systems Analysis, Laxenburg, Austria.
- Cooke, W. F., C. Lioussé, H. Cachier, and J. Feichter (1999), Construction of a 1° × 1° fossil fuel emission data set for carbonaceous aerosol and implementation and radiative impact in the ECHAM4 model, *J. Geophys. Res.*, *104*(D18), 22137–22162.
- DeMott, P., Y. Chen, S. M. Kreidenweis, D. C. Rogers, and D. E. Sherman (1999), Ice formation by black carbon particles, *Geophys. Res. Lett.*, *26*, 2429–2432.
- DeMott, P. J., D. J. Cziczo, A. J. Prenni, D. M. Murphy, S. M. Kreidenweis, D. S. Thomson, R. Borys, and D. C. Rogers (2003), Measurements of the concentration and composition of nuclei for cirrus formation, *PNAS*, *100*(25), 14655–14660, doi:10.1073/pnas.2532677100.
- Dentener, F., S. Kinne, T. Bond, O. Boucher, J. Cofala, S. Generoso, P. Ginoux, S. Gong, J. J. Hoelzemann, A. Ito, L. Marelli, J. E. Penner, J.-P. Putaud, C. Textor, M. Schulz, G. R. van der Werf, and J. Wilson (2006), Emissions of primary aerosol and precursor gases in the years 2000 and 1750 prescribed data-sets for AeroCom, *Atmos. Chem. Phys.*, *6*, 4321–4344.
- Easter, R. C., S. J. Ghan, Y. Zhang, R. D. Saylor, E. G. Chapman, N. S. Laulainen, H. Abdul-Razzak, L. R. Leung, X. Bian, and R. A. Zaveri (2004), MIRAGE: Model description and evaluation of aerosols and trace gases, *J. Geophys. Res.*, *109*, D20210, doi:10.1029/2004JD004571.
- Ekman, A. M. L., C. Wang, J. Wilson, and J. Stroem (2004), Explicit simulations of aerosol physics in a cloud-resolving model: A sensitivity study based on an observed convective cloud, *Atmos. Chem. Phys.*, *4*, 773–791.

- Eyring, V., H. W. Köhler, J. van Aardenne, and A. Lauer (2005), Emissions from international shipping: 1. The last 50 years, *J. Geophys. Res.*, *110*, D17305.
- Feichter, J., E. Kjellström, H. Rodhe, F. Dentener, J. Lelieveld, and G. Roelofs (1996), Simulation of the tropospheric sulfur cycle in a global climate model, *Atmospheric Environment*, *30*, 1693–1707.
- Forster, P., V. Ramaswamy, P. Artaxo, T. Berntsen, R. Betts, D. Fahey, J. Haywood, J. Lean, D. Lowe, G. Myhre, J. Nganga, R. Prinn, G. Raga, M. Schulz, and R. V. Dorland (2007), *Climate Change 2007: The Physical Science Basis. Contribution of Working Group I to the Fourth Assessment Report of the Intergovernmental Panel on Climate Change*, chap. Changes in Atmospheric Constituents and in Radiative Forcing, pp. 129–234, Cambridge University Press, Cambridge, United Kingdom and New York, NY, USA.
- Friedlander, S. K. (2000), *Smoke, dust and haze. Fundamentals of aerosol dynamics*, Oxford University Press, New York, Oxford, 2nd edition.
- Ganzeveld, L. N., J. A. van Aardenne, T. M. Butler, M. G. Lawrence, S. M. Metzger, P. Stier, P. Zimmermann, and J. Lelieveld (2006), Technical Note: Anthropogenic and natural offline emissions and the online Emissions and dry DEPosition submodel EMDEP of the Modular Earth Submodel system (MESSy), *Atmos. Chem. Phys. Discuss.*, *6*, 5457–5483.
- Ghan, J. S., and E. S. Schwartz (2007), Aerosol Properties and Processes, *BAMS*, *88*, 1059–1083.
- Guelle, W., M. Schulz, Y. Balkanski, and F. Dentener (2001), Influence of the source formulation on modeling the atmospheric global distribution of sea salt aerosol, *J. Geophys. Res.*, *106*(D21), 27509–27524.
- Harvey, D., J. Gregory, M. Hoffert, A. Jain, M. Lal, R. Leemans, S. Raper, T. Wigley, and J. de Wolde (1997), An introduction to simple climate models used in the IPCC Second Assessment Report, *IPCC technical paper II*, IPCC, available at <http://www.ipcc.ch/pdf/technical-papers/paper-II-en.pdf>.
- Heintzenberg, J. (1989), Fine particles in the global troposphere - a review, *Tellus B*, *41*, 149–160.
- Hendricks, J., B. Kärcher, A. Döpelheuer, J. Feichter, U. Lohmann, and D. Baumgardner (2004), Simulating the global atmospheric black carbon cycle: a revisit to the contribution of aircraft emissions, *Atmos. Chem. Phys.*, *4* (SRef-ID: 1680-7324/acp/2004-4-2521), 2521–2541.
- Hendricks, J., B. Kärcher, U. Lohmann, and M. Ponater (2005), Do aircraft black carbon emission affect cirrus clouds on the global scale?, *Geophys. Res. Lett.*, *32*, L12814.
- Hitzenberger, R., A. Berner, H. Giebl, K. Drobesh, A. Kasper-Giebl, M. Loefflund, H. Urban, and H. Puxbaum (2001), Black carbon (BC) in alpine aerosols and cloud water-concentrations and scavenging efficiencies, *Atmos. Environ.*, *35*, 5135–5141.
- Hoose, C., U. Lohmann, R. Erdin, and I. Tegen (2008), The global influence of dust mineralogical composition on heterogeneous ice nucleation in mixed-phase clouds, *Environ. Res. Lett.*, *3*, 025003, doi:10.1088/1748-9326/3/2/025003.

- Jacobson, M. Z. (2001), Strong radiative heating due to the mixing state of black carbon in atmospheric aerosol, *Nature*, *409*, 695–697.
- Jöckel, P., R. Sander, A. Kerkweg, H. Tost, and J. Lelieveld (2005), Technical Note: The Modular Earth Submodel System (MESSy) - a new approach towards Earth System Modeling, *Atmos. Chem. Phys.*, *5*, 433–444.
- Jöckel, P., H. Tost, A. Pozzer, C. Brühl, J. Buchholz, L. Ganzeveld, P. Hoor, A. Kerkweg, M. G. Lawrence, R. Sander, B. Steil, G. Stiller, M. Tanarhte, D. Taraborrelli, J. van Aardenne, and J. Lelieveld (2006), The atmospheric chemistry general circulation model ECHAM5/MESSy1: consistent simulation of ozone from the surface to the mesosphere, *Atmos. Chem. Phys.*, *6*, 5067–5104.
- Kanji, Z., O. Florea, and J. P. D. Abbatt (2008), Ice formation via deposition nucleation on mineral dust and organics: dependence of onset relative humidity on total particulate surface area, *Environ. Res. Lett.*, *3*, 025004, doi:doi:10.1088/1748-9326/3/2/025004.
- Kerkweg, A., J. Buchholz, L. Ganzeveld, A. Pozzer, H. Tost, and P. Joeckel (2006a), Technical Note: An implementation of the dry removal processes DRY DEPosition and SEDimentation in the Modular Earth Submodel System (MESSy), *Atmos. Chem. Phys.*, *6*(12), 4617–4632.
- Kerkweg, A., R. Sander, H. Tost, and P. Joeckel (2006b), MESSy Emissions Users Manual, *Tech. rep.*, Air Chemistry Department, Max-Planck Institute of Chemistry, Air Chemistry Department Max-Planck Institute of Chemistry PO Box 3060, 55020 Mainz, Germany.
- Khalizov, A. F., R. Zhang, D. Zhang, H. Xue, J. Pagels, and P. H. McMurry (2009), Formation of highly hygroscopic soot aerosols upon internal mixing with sulfuric acid vapor, *J. Geophys. Res.*, *114*, D05208.
- Kiehl, J. T., and K. E. Trenberth (1997), Earth's Annual Global Mean Energy Budget, *B. Am. Meteorol. Soc.*, *78*, 197–208.
- Kloster, S., F. Dentener, J. Feichter, F. Raes, J. van Aardenne, E. Roeckner, U. Lohmann, P. Stier, and R. Swart (2008), Influence of future air pollution mitigation strategies on total aerosol radiative forcing, *Atmos. Chem. Phys.*, *6*, 6405–6437.
- Koch, D. (2001), Transport and direct radiative forcing of carbonaceous and sulfate aerosols in the GISS GCM, *J. Geophys. Res.*, *106*(D17), 20311–20332.
- Koch, D., D. Jacob, I. Tegen, D. Rind, and M. Chin (1999), Tropospheric sulfur simulation and sulfate direct radiative forcing in the Goddard Institute for Space Studies general circulation model, *J. Geophys. Res.*, *104*(D19), 23799–23822.
- Kotzick, R., and R. Niessner (1999), The effects of aging processes on critical supersaturation ratios of ultrafine carbon aerosols, *Atmos. Environ.*, *33*(17), 2669–2677, doi: 10.1016/S1352-2310(98)00315-X.
- Kärcher, B., Möhler, DeMott, Pechtl, and Yu (2007), Insights into the role of soot aerosols in cirrus cloud formation, *Atmos. Chem. Phys.*, *7*, 4203–4227.
- Köhler, I., M. Dameris, I. Ackermann, and H. Hass (2001), Contribution of road traffic emissions to the atmospheric black carbon burden in the mid-1990s, *J. Geophys. Res.*, *106*(D16), 17997–18014.

- Landgraf, J., and P. Crutzen (1998), An efficient method for online calculations of photolysis and heating rates, *J. Atmos. Sci.*, *55*(5), 863–878.
- Lauer, A. (2005), Untersuchung von Größenverteilung und Zusammensetzung des Troposphärischen Aerosols mit einem globalen Zirkulationsmodell, Ph.D. thesis, Institut für Meteorologie der Freien Universität Berlin.
- Lauer, A., and J. Hendricks (2006), Simulating aerosol microphysics with the ECHAM-MADE GCM - Part II: Results from a first multiannual integration, *Atmos. Chem. Phys.*, *6*, 7519–7562.
- Lauer, A., J. Hendricks, I. Ackermann, B. Schell, H. Hass, and S. Metzger (2005), Simulating aerosol microphysics with the ECHAM-MADE GCM - Part I: Model description and comparison with observations, *Atmos. Chem. Phys.*, *5*, 3251–3276.
- Lauer, A., V. Eyring, J. Hendricks, P. Jöckel, and U. Lohmann (2007), Global model simulations of the impact of ocean-going ships on aerosols, clouds, and the radiation budget, *Atmos. Chem. Phys.*, *7*, 5061–5079.
- Lelieveld, J., C. Brühl, P. Jöckel, B. Steil, P. Crutzen, H. Fischer, M. Giorgetta, P. Hoor, M. Lawrence, R. Sausen, and H. Tost (2007), Stratospheric dryness: Model simulations and satellite observations, *Atmos. Chem. Phys.*, *7*(5), 1313–1332.
- Liousse, C., J. E. Penner, C. Chuang, J. J. Walton, H. Eddleman, and H. Cachier (1996), A global three-dimensional model study of carbonaceous aerosols, *J. Geophys. Res.*, *101*(D14), 19411–19432.
- Lohmann, U. (2002a), Possible aerosol effects on ice clouds via contact nucleation, *J. Atmos. Sci.*, *59*, 647–656.
- Lohmann, U. (2002b), A glaciation indirect aerosol effect caused by soot aerosols, *Geophys. Res. Lett.*, *29*(4), 1052, doi:10.1029/2001GL014357.
- Lohmann, U., and J. Feichter (2005), Global indirect aerosol effect: a review, *Atmos. Chem. Phys.*, *5*, 715–737.
- Lohmann, U., and B. Kärcher (2002), First interactive simulations of cirrus clouds formed by homogeneous freezing in the ECHAM general circulation model, *J. Geophys. Res.*, *107*(D-10), 8–1, doi:10.1029/2001JD000767.
- Lohmann, U., J. Feichter, C. Chuang, and J. Penner (1999), Prediction of the number of cloud droplets in the ECHAM GCM, *J. Geophys. Res.*, *104*, 9169–9198.
- Lohmann, U., P. Stier, C. Hoose, S. Ferrachat, S. Kloster, E. Roeckner, and J. Zhang (2007), Cloud microphysics and aerosol indirect effects in the global climate model ECHAM5-HAM, *Atmos. Chem. Phys.*, *7*, 3425–3446.
- Mayer, B., and A. Kylling (2005), Technical note: The libRadtran software package for radiative transfer calculations - description and examples of use, *Atmos. Chem. Phys.*, *5*, 1855–1877.
- McGraw, R. (1997), Description of Aerosol Dynamics by the Quadrature Method of Moments, *Aerosol Sci. Technol.*, *27*(2), 255–265.
- Meng, Z., and J. Seinfeld (1996), Time scale to achieve atmospheric gas-aerosol equilibrium for volatile species, *Atmos. Environ.*, *30*, 2889–2900.

- Metzger, S., F. Dentener, M. Krol, A. Jeuken, and J. Lelieveld (2002a), Gas/aerosol partitioning: 2. Global modeling results, *J. Geophys. Res.*, *107*, D16.
- Metzger, S., F. Dentener, S. Pandis, and J. Lelieveld (2002b), Gas/aerosol partitioning: 1. A computationally efficient model, *J. Geophys. Res.*, *107*, D107.
- Minikin, A., A. Petzold, J. Stroem, R. Krejci, M. Seifert, P. van Velthoven, H. Schlager, and U. Schumann (2003), Aircraft observations of the upper tropospheric fine particle aerosol in the Northern and Southern Hemispheres at midlatitudes, *Geophys. Res. Lett.*, *30*(10), 1503.
- Minnis, P., J. . K. Ayers, R. Palikonda, and D. Phan (2004), Contrails, cirrus trend and climate, *J. Climate*, *17*, 1671–1685.
- Moteki, N., Y. Kondo, Y. Miyazaki, N. Takegawa, Y. Komazaki, G. Kurata, T. Shirai, D. R. Blake, T. Miyakawa, and M. Koike (2007), Evolution of mixing state of black carbon particles: Aircraft measurements over the western Pacific in March 2004, *Geophys. Res. Lett.*, *34*, L11803, doi:10.1029/2006GL028943.
- Möhler, O., S. Buettner, C. Linke, M. Schnaiter, H. Saathoff, O. Stetzer, R. Wagner, M. Kraemer, A. Mangold, V. Ebert, and U. Schurath (2005), Effect of sulfuric acid coating on heterogeneous ice nucleation by soot aerosol particles., *J. Geophys. res.*, *110*, D11210.
- Möhler, O., P. R. Field, P. Connolly, S. Benz, H. Saathoff, M. Schnaiter, R. Wagner, R. Cotton, M. Krämer, A. Mangold, and A. J. Heymsfield (2006), Efficiency of the deposition mode ice nucleation on mineral dust particles, *Atmos. Chem. Phys.*, *6*, 3007–3021.
- Möhler, O., S. Benz, H. Saathoff, M. Schnaiter, R. Wagner, J. Schneider, S. Walter, V. Ebert, and S. Wagner (2008), The effect of organic coating on the heterogeneous ice nucleation efficiency of mineral dust aerosols, *Environ. Res. Lett.*, *3*, 025007, doi:10.1088/1748-9326/3/2/025007.
- Naoe, H., S. Hasegawa, J. Heintzenberg, K. Okada, A. Uchiyama, Y. Zaizen, E. Kobayashi, and A. Yamazakia (2009), State of mixture of atmospheric submicrometer black carbon particles and its effect on particulate light absorption, *Atmos. Environ.*, *43*(6), 1296–1301.
- Nordeng, T. (1994), Extended versions of the convective parametrization scheme at ECMWF and their impact on the mean and transient activity of the model in the tropics, *Tech. rep.*, ECWMF.
- Okada, K., M. Ikegami, Y. Zaizen, Y. Tsutsumi, Y. Makino, J. Jensen, and J. Gras (2005), Soot particles in the free troposphere over Australia, *Atmos. Environ.*, *39*(28), 5079–5089.
- Olivier, J., J. Berdowski, J. Peters, J. Bakker, A. Visschedijk, and J.-P. Bloos (2002), Applications of EDGAR. Including a description of EDGAR 3.0: reference database with trend data for 1970-1995, *NOP-NRP report 410200051*, RIVM, Bilthoven, The Netherlands.
- Olivier, J. G. H., J. A. van Aardenne, F. Dentener, L. Ganzeveld, and J. A. H. W. Peters (2005), Recent trends in global greenhouse gas emissions: regional trends and spatial distribution of sources, *Env. Sci.*, *2*, 81–99, doi:10.1080/15693430500400345.
- Oshima, N., M. Koike, Y. Zhang, Y. Kondo, N. Moteki, N. Takegawa, and Y. Miyazaki (2009), Aging of black carbon in outflow from anthropogenic sources using a mixing state resolved model: Model development and evaluation, *J. Geophys. Res.*, *114*, D06210.

- Ouimette, J., and R. Flagan (1982), The extinction coefficient of multicomponent aerosols, *Atmos. Env.*, *16*, 2405–2419.
- Penner, J., D. Lister, D. Griggs, D. Dokken, and M. McFarland (1999), IPCC Report - Aviation and the global atmosphere - Summary for policymakers, *Tech. rep.*, IPCC.
- Petzold, A., M. Fiebig, H. Flentje, A. Keil, U. Leiterer, F. Schröder, A. Stifter, M. Wendisch, and P. Wendling (2002), Vertical variability of aerosol properties observed at a continental site during the Lindenberg Aerosol Characterization Experiment (LACE 98), *J. Geophys. Res.*, *107*(D21), 8128, doi:doi:10.1029/2001JD001043.
- Pincus, R., and M. B. Baker (1994), Effect of precipitation on the albedo susceptibility of clouds in the marine boundary layer, *Nature*, *372*, 250–252, doi:10.1038/372250a0.
- Price, C., and D. Rind (1992), A simple lightning parameterization for calculating global lightning distributions, *J. Geophys. Res.*, *97*(D9), 9919–9933.
- Pruppacher, H., and J. Klett (2000), *Microphysics of clouds and precipitation*, Kluwer Academic Publishers.
- Rayner, N. A., D. E. Parker, E. B. Horton, C. K. Folland, L. V. Alexander, D. P. Rowell, E. C. Kent, and A. Kaplan (2003), Global analyses of sea surface temperature, sea ice, and night marine air temperature since the late nineteenth century, *J. Geophys. Res.*, *108*(D14), 4407, doi:10.1029/2002JD002670.
- Riemer, N., Vogel, Vogel, and Fiedler (2003), Modeling aerosol on the mesoscale- γ : treatment of soot aerosol and its radiative effects, *J. Geophys. Res.*, *108*, 4601, doi:10.1029/2003JD003448.
- Riemer, N., H. Vogel, and B. Vogel (2004), Soot aging time scales in polluted regions during day and night, *Atmos. Chem. Phys.*, *4*, 1885–1893.
- Roeckner, E., K. Arpe, L. Bengtsson, M. Christoph, M. Claussen, L. Dümenil, M. Esch, M. Giorgetta, U. Schlese, and U. Schulzweida (1996), The atmospheric general circulation model ECHAM4: Model description and simulation of present-day climate, *Report 218*, Max Planck Institut für Meteorologie, Hamburg, Germany.
- Roeckner, E., G. Bäuml, L. Bonaventura, R. Brokopf, M. Esch, M. Giorgetta, S. Hagemann, I. Kirchner, L. Kornbluh, E. Manzini, A. Rhodin, U. Schlese, U. Schulzweida, and A. Tompkins (2003), The atmospheric general circulation model ECHAM5: Part 1. Model description, *Report 349*, Max-Plan-Institut fuer Meteorologie.
- Rosenfeld, D., and W. L. Woodley (2000), Deep convective clouds with sustained supercooled liquid water down to -37.5 °C, *Nature*, *405*, 440–442, doi:10.1038/35013030.
- Saathoff, H., K.-H. Naumann, M. Schnaiter, W. Schöck, O. Möhler, U. Schurath, E. Weingartner, M. Gysel, and U. Baltensperger (2003), Coating of soot and $(\text{NH}_4)_2\text{SO}_4$ particles by ozonolysis products of α -pinene, *J. Aer. Sci.*, *34*, 1297–1321, doi:10.1016/S0021-8502(03)00364-1.
- Sander, R., A. Kerckweg, P. Jöckel, and J. Lelieveld (2005), Technical Note: The new comprehensive atmospheric chemistry module MECCA., *Atmos. Chem. Phys.*, *5*, 445–450.
- Sassen, K., P. J. DeMott, J. M. Prospero, and M. R. Poellot (2003), Saharan dust storms and indirect aerosol effects on clouds: CRYSTAL-FACE results, *Geophys. Res. Lett.*, *30*(12), 1633, doi:10.1029/2003GL017371.

- Sausen, R., I. Isaksen, V. Grewe, D. Hauglustaine, D. S. Lee, G. Myhre, M. O. Köhlers, G. Pitari, U. Schumann, F. Stordal, and C. Zerefos (2005), Aviation radiative forcing in 2000: An update on IPCC (1999), *Meteorol. Z.*, *14*(4), 555–561.
- Schmitt, A., and B. Brunner (1997), Emissions from aviation and their development over time, in pollutants from air traffic - results of atmospheric research 1992-1997, *Mitteilung 97-4, 37-52*, DLR, Köln, Germany, eds. Schumann et al.
- Schnaiter, M., C. Linke, O. Möhler, K.-H. Naumann, H. Saathoff, R. Wagner, U. Schurath, and B. Wehner (2005), Absorption amplification of black carbon internally mixed with secondary organic aerosol, *J. Geophys. Res.*, *110*, D19204, doi:10.1029/2005JD006046.
- Schwarz, J., R. S. Gao, D. W. Fahey, D. S. Thomson, L. A. Watts, J. C. Wilson, J. M. Reeves, M. Darbeheshti, D. G. Bamgardner, G. L. Kok, S. H. Chung, M. Schulz, J. Hendricks, A. Lauer, B. Kärcher, J. G. Slowik, K. H. Rosenlof, T. L. Thompson, A. O. Langford, M. Loewenstein, and K. C. Aikin (2006), Single-particle measurements of midlatitude black carbon and light-scattering aerosols from the boundary layer to the lower stratosphere., *J. Geophys. Res.*, *111*, D16207, doi:10.1029/2006JD007076.
- Schwarz, J. P., R. S. Gao, J. R. Spackman, L. A. Watts, D. S. Thomson, D. W. Fahey, T. B. Ryerson, J. Peischl, J. S. Holloway, M. Trainer, G. J. Frost, T. Baynard, D. A. Lack, J. A. de Gouw, C. Warneke, and L. D. Negro (2008a), Measurement of the mixing state, mass, and optical size of individual black carbon particles in urban and biomass burning emissions, *Geophys. Res. Lett.*, *35*, L13810.
- Schwarz, J. P., J. Spackman, D. W. Fahey, R. S. Gao, U. Lohmann, P. Stier, L. A. Watts, D. S. Thomson, D. A. Lack, L. Pfister, M. J. Mahoney, D. Baumgardner, J. Wilson, and J. M. Reeves (2008b), Coatings and their enhancement of black-carbon light absorption in the tropical atmosphere, *J. Geophys. Res.*, *113*, D03203.
- Scott, N. A., A. Chedin, R. Armante, J. Francis, C. Stubenrauch, J. P. Chaboureaud, F. Chevallier, C. Claud, and F. Cheruy (1999), Characteristics of the TOVS Pathfinder Path-B dataset, *B. Am. Meteorol. Soc.*, *80*, 2679–2701.
- Seinfeld, J. H., and S. N. Pandis (2006), *Atmospheric Chemistry and Physics.*, Wiley, 2nd edition.
- Shiraiwa, M., Y. Kondo, N. Moteki, N. Takegawa, L. K. Sahu, A. Takami, S. Hatakeyama, S. Yonemura, and D. R. Blake (2008), Radiative impact of mixing state of black carbon aerosol in Asian outflow, *J. Geophys. Res.*, *113*, D24210.
- Spiro, P. A., D. J. Jacob, and J. A. Logan (1992), Global inventory of sulfur emissions with $1^\circ \times 1^\circ$ resolution, *J. Geophys. Res.*, *97*, 6023–6036.
- Stier, P., J. Feichter, S. Kinne, S. Kloster, E. Vignati, J. Wilson, L. Ganzeveld, I. Tegen, M. Werner, Y. Balkauski, M. Schulz, O. Boucher, A. Minikin, and A. Petzold (2005), The aerosol-climate model ECHAM5-HAM, *Atmos. Chem. Phys.*, *5*, 1125–1156.
- Susskind, J., P. Piraino, L. Rokke, T. Iredell, and A. Mehta (1997), Characteristics of the TOVS Pathfinder Path-A dataset, *B. Am. Meteorol. Soc.*, *78*, 1449–1472.
- Takemura, T., H. Okamoto, Y. Maruyama, A. Numaguti, A. Higurashi, and T. Nakajima (2000), Global three-dimensional simulation of aerosol optical thickness distribution of various origins, *J. Geophys. Res.*, *105*(D14), 17853–17873.

- Textor, C., M. Schulz, S. Guibert, S. Kinne, Y. Balkanski, S. Bauer, T. Berntsen, T. Berglen, O. Boucher, M. Chin, F. Dentener, T. Diehl, R. Easter, H. Feichter, D. Fillmore, S. Ghan, P. Ginoux, S. Gong, A. Grini, J. Hendricks, L. Horowitz, P. Huang, I. Isaksen, T. Iversen, S. Kloster, D. Koch, A. Kirkevåg, J. Kristjansson, M. Krol, A. Lauer, J. Lamarque, X. Liu, V. Montanaro, G. Myhre, J. Penner, G. Pitari, S. Reddy, Ø. Seland, P. Stier, T. Takemura, and X. Tie (2006), Analysis and quantification of the diversities of aerosol life cycles within AeroCom, *Atmos. Chem. Phys.*, *6*, 1777–1813.
- Textor, C., M. Schulz, S. Guibert, S. Kinne, Y. Balkanski, S. Bauer, T. Berntsen, T. Berglen, O. Boucher, M. Chin, F. Dentener, T. Diehl, R. Easter, H. Feichter, D. Fillmore, S. Ghan, P. Ginoux, S. Gong, A. Grini, J. Hendricks, L. Horowitz, P. Huang, I. Isaksen, T. Iversen, S. Kloster, D. Koch, A. Kirkevåg, J. Kristjansson, M. Krol, A. Lauer, J. Lamarque, X. Liu, V. Montanaro, G. Myhre, J. Penner, G. Pitari, S. Reddy, Ø. Seland, P. Stier, T. Takemura, and X. Tie (2007), The effect of harmonized emissions on aerosol properties in global models - an AeroCom experiment, *Atmos. Chem. Phys.*, *7*, 4489–4501.
- Tiedtke, M. (1989), A comprehensive mass flux scheme for cumulus parameterization in large-scale models, *Monthly Weather Review*, *117*(8), 1779–1800.
- Tost, H. (2006), Global Modelling of Cloud, Convection and Precipitation Influences on Trace Gases and Aerosols, Ph.D. thesis, Rheinischen Friedrich-Wilhelms-Universität Bonn.
- Tost, H., P. Jöckel, A. Kerckweg, R. Sander, and J. Lelieveld (2006), Technical note: A new comprehensive SCAVenging submodel for global atmospheric chemistry modelling, *Atmos. Chem. Phys.*, *6*, 565–574.
- Twomey, S. (1977), The influence of pollution on the shortwave albedo of clouds, *J. Atmos. Sci.*, *34*, 1149–1152.
- UNEP (2006), Handbook for the Montreal Protocol on Substances that Deplete the Ozone Layer - 7th edition, *Tech. rep.*, The Vienna Convention for the Protection of the Ozone Layer and The Montreal Protocol on Substances that Deplete the Ozone Layer, available at http://ozone.unep.org/Publications/MP_Handbook.
- UNFCCC (2008), Kyoto protocol reference manual, *Tech. rep.*, United Nation Framework Convention on Climate Change, Bonn, Germany, available at http://unfccc.int/resource/docs/publications/08_unfccc_kp_ref_manual.pdf.
- van der Werf, G. R., J. T. Randerson, G. C. Collatz, L. Giglio, p. S. Kasibhatla, A. F. Arellano, S. C. Olsen, and E. S. Kasischke (2004), Continental-scale partitioning of fire emissions during the 1997 to 2001 El Nino/La Nina period, *Science*, *303*(5654), 73–76.
- Vehkamäki, H., M. Kulmala, I. Napari, K. E. J. Lehtinen, C. Timmreck, M. Noppel, and A. Laaksonen (2002), An improved parameterization for sulfuric acid-water nucleation rates for tropospheric and stratospheric conditions, *J. Geophys. Res.*, *107*(D22), 4622, doi:10.1029/2002JD002184.
- Verheggen, B., J. Cozic, E. Weingartner, K. Bower, S. Mertes, P. Connolly, M. Gallagher, M. Flynn, T. Choulaton, and U. Baltensperger (2007), Aerosol partitioning between the interstitial and the condensed phase in mixed-phase clouds, *J. Geophys. Res.*, *112*, D23202, doi:doi:10.1029/2007JD008714.
- Vignati, and Wilson (2004), M7: An efficient size-resolved aerosol microphysical module for large-scale aerosol transport models, *J. Geophys. Res.*, *109*, D22202.

- Weber, R. J., J. J. Marti, P. H. McMurry, F. L. Eisele, D. J. Tanner, and A. Jefferson (1997), Measurements of new particle formation and ultrafine particle growth rates at a clean continental site, *J. Geophys. Res.*, *102*(D4), 4375–4385.
- Weingartner, E., H. Burtscher, and H. Baltensperger (1997), Hygroscopic properties of carbon and diesel soot particles, *Atmos. Environ.*, *31*, 2311 – 2327.
- Weingartner, E., H. Saathoff, N. Streit, V. Lavanchy, M. Schnaiter, U. Matter, and U. Baltensperger (2000), Hicroscopic Behaviour of soot particles coated with oxidation products of α -pinene, *J. Aerosol Sci.*, *31* (Suppl. 1), S987–S988.
- Whitby, E., and P. McMurry (1997), Modal aerosol dynamics modelling, *Aerosol Science and Technology*, *27*, 673–688, printed.
- Whitby, E. R., P. McMurray, U. Shankar, and F. Binkowsky (1991), Modal aerosol dynamics modeling, *Tech. Rep. 600/3-91/020*, Atmospheric Research and Exposure Assess. Lab., U.S. Environmental Protection Agency, Research Triangle Park, available as NTIS PB91-161729/AS.
- Whitby, K. (1978), The physical characteristics of aerosol, *Atmosph. Env.*, *12*, 135–159.
- WHO (2003), Health aspects of air pollution with particulate matter, ozone and nitrogen, *Report on a WHO Working Group 13-15*, WHO Regional Office for Europe, Bonn, Germany.
- Zhang, D., J. Zang, G. Shi, Y. Iwasaka, A. Matsuki, and D. Trochkin (2003), Mixture state of individual Asian dust particles at a coastal site of Qingdao, China, *Atmos. Environ.*, *37*(28), 3895–3901, doi:10.1016/S1352-2310(03)00506-5.
- Zhang, R., A. Khalizov, J. Pagels, D. Zhang, H. Xue, and P. McMurry (2008), Variability in morphology, hygroscopicity, and optical properties of soot aerosols during atmospheric processing, *PNAS*, *105*(30), 10291–10296.
- Zuberi, B., K. S. Johnson, G. K. Aleks, L. T. Molina, M. J. Molina, and A. Laskin (2005), Hydrophilic properties of aged soot, *Geophys. Res. Lett.*, *32*, L01807, doi: 10.1029/2004GL021496.

Acknowledgments

I would like to thank Prof. Dr. Robert Sausen for giving me the opportunity of writing my PhD thesis in his group at the Deutsches Zentrum für Luft- und Raumfahrt, Oberpfaffenhofen, Germany. The confidence he showed in me has been a strong motivation for my work. I also want to thank Prof. Dr. George Craig for his availability as a second corrector and for the good ideas to make this work clearer.

I want to especially thank Dr. Johannes Hendricks for the extraordinary supervision. It has been great to know I can always find his door open for help and discussions. A huge thanks to Dr. Axel Lauer, for sharing his work and his knowledge with me at any time. After moving to the other side of the world, he kept helping me as if he was still sitting two door away from my office.

I thank Prof. Dr. Ulrich Schumann for the useful suggestion about my work. Many thanks to Dr. Andrea Stenke and Dr. Volker Grewe for their technical help with the model and for listening to me while I was trying to get things clear. Thanks to Prof. Dr. Bernd Kärcher for the helpful discussions and suggestions and for the enthusiasm he showed in my work. Thanks to Dr. Mattia Righi and Dr. Irene Cionni for their the huge help with NCL and with a lot of other things, not only about science. The long discussions about MADE and MADEsoot with Mattia rose my motivation even when it was very low. Thanks to Dr. Veronika Eyring and Prof. Dr. Martin Dameris for the advices about my thesis and thanks to them and to Prof. Dr. Michael Ponater for the advices about my future too. A special thank you to Winfried Beer, the friendliest system administrator ever.

I thank the whole MESSy-Team for the development of the model. In particular I thank Dr. Patrick Jöckel and Dr. Holger Tost for the prompt and uncomplicated support with MESSy and SCAV, and Dr. Swen Metzger for the clarifications about EQSAM. I kindly acknowledge the provision of MADE by the University of Cologne, Germany (RIU/EURAD-project) and the provision of MADEsoot by the Institut für Meteorologie und Klimaforschung, Forschungszentrum Karlsruhe, Germany, and in particular Dr. Nicole Riemer, Dr. Heike Vogel and Dr. Bernhard Vogel. I also thank Dr. Nicole Riemer for the useful and motivating discussions. I acknowledge Prof. Dr. Ulrike Lohmann for the provision of the cloud microphysics model. I would like to thank Dr. David Fahey, Dr. Joshua Schwarz, Dr. Ryan Spackman and Dr. Darrel Baumgardner for making their measurements available for the evaluation of the model and for their help in interpreting the data, and Dr. Andreas Petzold and Dr. Michael Esselborn for the clarifications about experimental methods.

Thanks to the whole Dynamics of the Atmosphere Department at the Institut für Physik der Atmosphäre at the DLR Oberpfaffenhofen and in particular to my long term room mates Christine Fichter, Simone Dietmüller, Katrin Dahlmann and Rudi Deckert.

A very special thanks to my family, because they relieve me from any worry and assure me the calm I need to enjoy my work. Thanks for giving me the opportunity of steering my life the way that makes me feel satisfied.

All the simulations here contained were performed at the Leibniz-Rechenzentrum der Bayerischen Akademie der Wissenschaften, Garching bei München. This work was supported by the DLR projects PAZI and CATS.

Lebenslauf

PERSÖNLICHE DATEN

Name: Valentina Aquila
Geburtsdatum: 30. Juli 1980
Geburtsort: Genua, Italien

SCHULAUSBILDUNG

09/1986 – 06/1991 Scuola elementare C. Palli, Genua
09/1991 – 06/1994 Scuola media inferiore B. Strozzi, Genua
09/1994 – 06/1999 Liceo scientifico statale M. L. King, Genua
Naturwissenschaftliches Gymnasium

STUDIUM

11/1999 – 09/2004 Studium in Physik an der Università di Genova, Genua
Thema der Diplomarbeit: *Semileptonic B meson decays*
12/2004 – 04/2006 Stipendium in der Graduiertenkolleg
Particle Physics at the Energy Frontier of New Phenomena
an der Ludwig-Maximilians-Universität München
seit 05/2006 Doktorandin in Meteorologie
Wissenschaftliche Mitarbeiterin am Institut für Physik der Atmosphäre,
Deutsches Zentrum für Luft- und Raumfahrt e.V., Oberpfaffenhofen.

München, 15. Dezember 2009